



# Stereoselective Ring-Opening Polymerizations of Racemic Lactide by Organocatalysis

Beste Orhan

## ► To cite this version:

Beste Orhan. Stereoselective Ring-Opening Polymerizations of Racemic Lactide by Organocatalysis. Polymers. Université de Bordeaux; Université de Mons, 2019. English. NNT : 2019BORD0361 . tel-03533729

**HAL Id: tel-03533729**

**<https://theses.hal.science/tel-03533729>**

Submitted on 19 Jan 2022

**HAL** is a multi-disciplinary open access archive for the deposit and dissemination of scientific research documents, whether they are published or not. The documents may come from teaching and research institutions in France or abroad, or from public or private research centers.

L'archive ouverte pluridisciplinaire **HAL**, est destinée au dépôt et à la diffusion de documents scientifiques de niveau recherche, publiés ou non, émanant des établissements d'enseignement et de recherche français ou étrangers, des laboratoires publics ou privés.

THÈSE EN COTUTELLE PRÉSENTÉE

POUR OBTENIR LE GRADE DE

**DOCTEUR DE**  
**L'UNIVERSITÉ DE BORDEAUX**  
**ET DE L'UNIVERSITÉ DE MONS**

ÉCOLE DOCTORALE DES SCIENCES CHIMIQUES (UBX)

FACULTE DES SCIENCES (UMons)

SPÉCIALITÉ POLYMERES

Par Beste ORHAN

**STEREOSELECTIVE RING-OPENING POLYMERIZATIONS  
OF RACEMIC LACTIDE BY ORGANOCATALYSIS**

Sous la direction de Pr. Daniel TATON  
et du Dr. Olivier COULEMBIER

Soutenue le 17 décembre 2019

Membres du jury :

M. GUICHARD, Gilles  
M. RAYNAL, Matthieu  
Mme CAMMAS-MARION, Sandrine  
M. RAQUEZ, Jean-Marie  
M. ZINCK, Philippe  
M. TATON, Daniel  
M. COULEMBIER, Olivier

Directeur de Recherche, Université de Bordeaux, Bordeaux  
Chargé de Recherche CNRS, Sorbonne Université, Paris  
Chargé de Recherche CNRS, Université De Rennes 1, Rennes  
Chercheur Qualifié FNRS, Université de Mons, Mons  
Professeur, Université Lille, Lille  
Professeur, Université de Bordeaux, Bordeaux  
Chercheur Qualifié FNRS, Université de Mons, Mons

Président  
Rapporteur  
Rapporteur  
Examineur  
Examineur  
Directeur de thèse  
Invité







## Acknowledgement

The thesis work described in this manuscript was carried out in co-tutelle agreement between the Laboratoire de Chimie des Polymères Organiques (LCPO) in University of Bordeaux and Laboratory of Polymeric and Composite Materials (SMPC) in University of Mons, under the supervision of Pr. Daniel Taton and Dr. Olivier Coulembier. The work of this thesis financially supported through SUSPOL-EJD project which is the European Union's Horizon 2020 research and innovation programme under the Marie Skłodowska-Curie action with a grant agreement No. 64267.

First of all, I would like to thank Ms. Sandrine Cammas-Marion from University of Rennes 1, Mr. Matthieu Raynal from Sorbonne University, Mr. Philippe Zinck from University of Lille and Mr. Jean-Marie Raquez from University of Mons for having accepted to evaluate this manuscript. Thanks also to Pr. Gilles Guichard from University of Bordeaux, for having accepted to participate in my thesis jury and chair in this viva.

I would like to thank Pr. Sébastien Lecommandoux who is director of LCPO and Pr. Philippe Dubois who is director of SMPC, to welcome me in your great laboratories and for allowed me to conduct my research under optimal conditions.

I would like to express my sincere gratitude to my supervisors Pr. Daniel Taton and Dr. Olivier Coulembier, for giving me the wonderful opportunity of working on this project and conducting my PhD research under their supervision. Their continuous support and guidance throughout helped me in all times of research and writing of the thesis. Their patience, motivation and helpfulness were invaluable.

I would like to express my gratitude to Dr. Sirus Zarbakhsh and Dr. Vinit Chilekar for welcoming me in BASF in Germany for my secondment work under the SUSPOL project. They provided me a very nice and comfortable work zone in their laboratory, and supervised me during a month, I appreciate their precious help. I also would like to thank Pr. Andrew P. Dove from University of Birmingham and Dr. Mathieu Tschan as a postdoctoral researcher in his group, for their invaluable collaborations and welcoming me in their laboratory for a week.

I would like to thank the all LCPO and SMPC members, permanent staff, doctoral students, postdoctoral fellows and interns for making these laboratories warmer and social. I wish to thank first to the technical staff of the laboratories (Dominique, Corinne, Claud,

## Acknowledgement

Severine, and Loïc from LCPO, Nathalie, Sébastien and Laura from SMPC) for their precious help, time and making the laboratory conditions more comfortable. I also would deeply like to thank all the engineers of the two laboratories for their invaluable help and making our research more meaningful. Firstly, Amélie and Anne-Laure a very big thanks to you for your time, effort, briefly everything you've done for me. For the thermal analysis, I would like to thank to Gerard and Cédric from LCPO, Antoniya and Samira from SMPC for their trainings and time.

I would also like to thank past and present members of DT Team. Ana, Anne-Laure, Romain, Sofiem, Amaury, and Mathilde, I am grateful that you've welcomed me and trained me. Stéphanie, Jana and Daniela thanks a lot for your warm friendship, and for the great time we spent together. Thanks a lot for the good moments in the lab, in the office and scientific discussions. Thanks also to Samir and Amélie for good times spent together.

I would like to thank all members of the SUSPOL network for creating the best teamwork and for fruitful collaborations.

A very special thanks to my amazing friends Emin, Esra, Amélie, Damla, Anne-Laure, Andere, Ali, Stéphanie, Mariana and Sofiem to made my life very much enjoyable, more tolerable and way much easier during my PhD. Your endless support, always being next to me during the good and bad times, and our shared moments is so much invaluable to me. I feel so lucky that you're with me. Another special thanks to my precious friends in Turkey, they were always with me supporting, I cannot thank enough to them. Also, I very much thank to Ana, Chiara, Elena, Jana, Daniela, Estelle, Gladys, Rana and Vangelis for their nice friendship, our good conversations and the good time we've spent together. I also would like to thank to all the lab mates from LCPO and SMPC that we worked together and had some chats.

To my wonderful family, words fail to describe how valuable you are to me. I would most probably lose this most challenging part of my life without you. Thanks to your presence, I am feeling like the luckiest person in the world. Emin, my spouse, you know that you are one of the most important people in my life. Without your support, I can't even imagine how this journey would end up. You're meaning everything to me, life, love, soul, color...just so magical. The one simple « thank you » would never have been enough, so I am grateful to have you just next to me. My father, namely « babam » in Turkish, the biggest supporter of me. Thanks to his insistence, I started this journey. He believes that I can be successful in everything like I am a super girl. He made me believe in myself too. Thankfully you are my father and so glad that I have you. My mother, « annem », you're the strongest

## Acknowledgement

woman in this world and I am so lucky that I'm your daughter. You are my precious. I know that our personalities are so similar, kind of a « like mother, like daughter ». So, you always knew that I am going to overcome challenges, thus you made me believe that too. Thank you mom, I love you. And here comes the big boy is my elder brother Ozan, for him there are no difficulties in the world, we create our own difficulties. I sort of started to believe that a bit late but better late than never. You are the stubbornest person I've ever known, and thanks to you I've learnt how to make something out of nothing. Thanks a lot to all of you, who created my character, my personality.

Finally, I would like to thank everybody that are not mentioned here, who has been part of this journey and who has been important to the successful realization.



# Table of Contents

<b>Acknowledgement .....</b>	<b>5</b>
<b>Table of Contents .....</b>	<b>2</b>
<b>List of Tables.....</b>	<b>6</b>
<b>List of Schemes .....</b>	<b>7</b>
<b>List of Figures .....</b>	<b>8</b>
<b>List of Abbreviations.....</b>	<b>14</b>
<b>General Introduction .....</b>	<b>16</b>
References .....	23
<b>Chapter 1. Stereoselective Ring-Opening Polymerization Involving Racemic Lactide... 24</b>	
1.1. Introduction.....	26
1.2. Chiral polymers.....	28
1.3. Stereoregularity and tacticity in polymers .....	28
1.4. Asymmetric polymerizations .....	31
1.5. Synthesis of polyesters: some generalities.....	35
1.5.1. Step growth polymerization .....	36
1.5.2. Ring-Opening Polymerization .....	36
1.5.2.1. Anionic Ring-Opening Polymerization.....	37
1.5.2.2. Cationic Ring-Opening Polymerization .....	38
1.5.2.3. Organocatalyzed and Enzymatic ROPs.....	39
1.5.2.4. Coordination- Insertion Ring-Opening Polymerization .....	42
1.6. Polylactide .....	45
1.6.1. Generalities on PLA .....	45
1.6.2. Stereochemistry and microstructures of PLA .....	46
1.6.3. Stereoselective ROP of LA .....	50
1.6.3.1. Mechanism of stereocontrol polymerization of lactide .....	51
1.6.3.2. Mesotacticity analysis .....	52
1.6.3.3. Catalytic systems for stereoselective ROP of <i>rac</i> -LA.....	53
1.6.3.3.1. Organometallic catalysts.....	53
1.6.3.3.2. Organic catalysts.....	66
1.7. Concluding remarks and objectives of this PhD thesis.....	69
1.8. References.....	71
<b>Chapter 2. Stereoselective Ring-Opening Polymerization of <i>rac</i>-Lactide initiated by Chiral Thiourea-Amine Organocatalyst: Elucidation of Stereocontrol Mechanism..... 77</b>	
2.1. Introduction.....	79
2.2. Results and Discussion .....	83
2.2.1. Polymerization procedure .....	83
2.2.2. Polymer Characterization.....	85
2.2.3. Analysis of the microstructure of PLA derived from chiral TUC's..	90
2.2.3.1. DSC Analysis .....	90
2.2.3.2. Homonuclear decoupled <sup>1</sup> H NMR and quantitative <sup>13</sup> C NMR analysis	94

2.2.4. Kinetics of the ring-opening polymerization's of <i>rac</i> -LA from chiral thiourea .....	101
2.3. Conclusions and outlooks .....	103
2.4. Experimental and supporting information .....	104
2.5. References.....	108
<b>Chapter 3. Stereoselective Ring-Opening Polymerization of <i>rac</i>-Lactide Catalyzed by Chiral <i>N</i>-Heterocyclic Carbene Organocatalysts .....</b>	<b>111</b>
3.1. Introduction.....	113
3.2. Generalities on <i>N</i> -heterocyclic carbenes (NHCs) and their use as organic catalysts in (macro)molecular chemistry .....	116
3.3. Stereoselective ROP of <i>rac</i> -LA using chiral NHCs as organocatalysts .....	125
3.3.1. Polymerization procedure .....	125
3.3.2. Characterization of chiral NHC-derived PLAs .....	129
3.3.3. Analysis of the stereoselectivity of NHC-derived PLA materials ..	135
3.3.3.1. DSC Analysis .....	135
3.3.3.2. Homonuclear decoupled <sup>1</sup> H NMR and quantitative <sup>13</sup> C NMR analysis ..	137
3.3.4. Kinetic studies of the ROP of <i>rac</i> -LA.....	142
3.4. Conclusions and perspectives .....	146
3.5. Experimental and supporting information .....	148
3.6. References.....	160
<b>Chapter 4. Chiral Unimolecular Bifunctional Urea Organocatalyst for the Stereoselective Ring-Opening Polymerization of <i>rac</i>-Lactide.....</b>	<b>164</b>
4.1. Introduction.....	166
4.2. Results and Discussion .....	174
4.2.1. Polymerization procedure .....	174
4.2.2. Polymer Characterization.....	176
4.2.3. Microstructure analysis of PLA derived from chiral ( <i>S,S</i> )-UC.....	181
4.2.3.1. DSC Analysis .....	181
4.2.3.2. Homonuclear decoupled <sup>1</sup> H NMR and quantitative <sup>13</sup> C NMR analysis ..	182
4.2.4. Polymerization Kinetics .....	187
4.3. Conclusions and perspectives .....	189
4.4. Experimental and supporting informations.....	190
4.5. References.....	193
<b>Chapter 5. Selective ROP of <i>rac</i>- and <i>meso</i>-Lactides from TBD under Cryogenic Conditions: A Tripartite Tetris Interaction Explanation.....</b>	<b>196</b>
5.1. Introduction.....	198
5.2. Results and Discussion .....	200
5.2.1. Polymerization procedure .....	200
5.2.2. Polymer Characterization.....	202
5.2.3. Analysis of the microstructure of PLA derived from achiral TBD. ....	202
5.2.4. Theoretical Investigations .....	204
5.3. Conclusions and perspectives .....	208

5.4. Experimental and supporting informations.....	210
5.5. References.....	217
<b>General Conclusion .....</b>	<b>218</b>





## List of Tables

<b>Table 1.1.</b> Thermal properties of common industrial, non- or biodegradable, petroleum- or bio-based polymers in different tacticities. ( $T_g$ = Glass transition temperature, $T_m$ = Melting temperature) .....	35
<b>Table 1.2.</b> Thermal properties of PLA polymers of different tacticities (Adapted from reference 123).....	47
<b>Table 1.3.</b> Possible tacticities of PLA in the presence of chain-end and enantiomorphic-site stereocontrol mechanisms during stereoselective ROP of <i>rac</i> - or <i>meso</i> -LA. (The reverse monomer sequencing is also possible considering to opposite enantioface of the catalyst used.)	
<b>Table 1.4.</b> Tetrad probabilities of ESC and CEC mechanisms based on non-Bernoullian and Bernoullian statistics .....	53
<b>Table 2.1.</b> Stereoselective ring-opening polymerizations of <i>rac</i> -LA catalyzed by ( <i>S,S</i> )-TUC and ( <i>R,R</i> )-TUC. ....	84
<b>Table 2.2.</b> Tetrad probabilities of ESC and CEC mechanisms based on non-Bernoullian and Bernoullian statistics. ....	96
<b>Table 2.3.</b> Probabilities of tetrad mesodyads based on ESC and CEC statistics. ....	96
<b>Table 2.4.</b> Chiral HPLC results of residual monomer which is recovered from hexane/isopropanol.....	100
<b>Table 3.1.</b> Possible tacticities of PLA in the presence of chain-end and enantiomorphic-site stereocontrol mechanisms during stereoselective ROP of <i>rac</i> - or <i>meso</i> -LA. (The reverse monomer sequencing is also possible considering to opposite enantioface of the catalyst used.) .....	114
<b>Table 3.2.</b> Stereoselective ring-opening polymerizations of <i>rac</i> -LA catalyzed by chiral NHC precursors. ....	128
<b>Table 3.3.</b> Stereoselective ring-opening polymerizations of <i>D</i> -, and <i>L</i> - catalyzed by chiral NHC precursors.....	147
<b>Table 4.1.</b> Stereoselective ring-opening polymerizations of <i>rac</i> -LA catalyzed by ( <i>S,S</i> )-UC. ....	175
<b>Table 4.2.</b> Tetrad probabilities of ESC and CEC mechanisms based on non-Bernoullian and Bernoullian statistics. ....	183
<b>Table 4.3.</b> Probabilities of tetrad mesodyads based on ESC and CEC statistics. ....	183
<b>Table 5.1.</b> Ring-opening polymerizations of <i>rac</i> -LA in toluene at -75°C .....	201
<b>Table 5.2.</b> Calculated Hansen solubility parameters ( $\delta_p$ , $\delta_d$ , $\delta_h$ ; p, d, and h stand for polar (electrostatic), dispersion (van der Waals) and h-bond, respectively) for <i>L</i> -LA, <i>D</i> -LA and toluene. ....	<b>Hata! Yer işareti tanımlanmamış.</b>
<b>Table S5.1.</b> Summary of the chirality of the molecules involved in the simulated ROP processes (column 2 and 3) together with those of the resulting growing polymer chains (column 4). Column 5 corresponds to the DFT-calculated ( $\omega$ B97XD/6-31G**) relative energies (in kcal/mol) of the transition states.....	

## List of Schemes

<b>Scheme 1.1.</b> Synthesis of aliphatic polyesters by step growth polycondensation. ....	36
<b>Scheme 1.2.</b> ROP of unsubstituted lactones, lactides and glycolides. ....	37
<b>Scheme 1.3.</b> ROP Mechanism. ....	38
<b>Scheme 1.4.</b> Proposed pathway for cationic ROP of lactide. ....	38
<b>Scheme 1.5.</b> Proposed activated monomer pathway for cationic ROP of lactide. ....	39
<b>Scheme 1.6.</b> Bifunctional activated mechanism using hydrogen bonding (thio)urea catalyst. ....	40
<b>Scheme 1.7.</b> Plausible mechanism for the nucleophilic ROP of lactide. ....	41
<b>Scheme 1.8.</b> Polymerization steps of lactones using lipase as a catalyst. ....	42
<b>Scheme 1.9.</b> Coordination-insertion mechanism for lactide polymerization using metal alkoxide catalyst. ....	43
<b>Scheme 1.10.</b> Schematic representations for the transesterification side reactions. ....	44
<b>Scheme 1.11.</b> Enantiopure PLLA and PDLA and corresponding stereocomplex. ....	48
<b>Scheme 1.12.</b> Microstructures of PLA obtained by stereoselective ROPs of <i>rac</i> - and <i>meso</i> -LA. (Adapted from reference 39). ....	50
<b>Scheme 1.13.</b> Synthesis of stereoblock PLA using <i>rac</i> -(SalBinap)AlO <sup>i</sup> Pr. ....	54
<b>Scheme 1.14.</b> Synthesis of PLLA-PDLA stereoblock copolymer through a ligand exchange mechanism. (Adapted from reference 134). ....	55
<b>Scheme 2.1.</b> Stereoselective organocatalyzed ROP of <i>rac</i> -LA catalyzed by chiral ( <i>S,S</i> )-TUC. ....	83
<b>Scheme 2.2.</b> Proposed activation mechanism for ROP of LA catalyzed by TUC <b>Hata!</b> <b>Yer</b> <b>işareti tanımlanmamış.</b>	
<b>Scheme 3.1.</b> Possible generation routes to NHCs. ....	117
<b>Scheme 3.2.</b> (a) Nucleophilic monomer activated mechanism for the ROP of LA in the presence of alcoholic initiator (b) Nucleophilic mechanism for the zwitterionic ROP of LA in the absence of initiator (Adapted from reference 52). ....	120
<b>Scheme 3.3.</b> Basic mechanism for ROP of LA conducted by NHC. ....	121
<b>Scheme 3.4.</b> <i>In situ</i> generation of <b>NHC1</b> salt with an appropriate base and nucleophilic ROP mechanism of <i>rac</i> -LA using generated <b>NHC1</b> . ....	126
<b>Scheme 3.5.</b> Nucleophilic <i>versus</i> basic mechanism in competition, here for the NHC-ROP of <i>rac</i> -LA. ....	127
<b>Scheme 4.1.</b> Neutral versus imidate mediated ROP of LA (adapted from reference 53). ....	171
<b>Scheme 4.2.</b> Proposed bifunctional activation mechanism for ROP of LA using ( <i>S,S</i> )-UC. ....	174
<b>Scheme 5.1.</b> Ring-Opening Polymerization of <i>rac</i> -LA through dual activation by TBD. ....	200
<b>Scheme 5.2.</b> Ring-opening products obtained from complexes I and II formed between <i>meso</i> -LA, methyl (L)-lactate and TBD. ....	206

## List of Figures

<b>Figure 1.1.</b> The distinct forms of lactide .....	27
<b>Figure 1.2.</b> Examples of naturally occurring chiral four-nucleotide segment of DNA with an adenine-cytosine-guadine-thymine sequence segment and cellulose .....	28
<b>Figure 1.3.</b> Isotactic, syndiotactic and atactic forms of PP .....	29
<b>Figure 1.4.</b> Primary structure of polymers.....	29
<b>Figure 1.5.</b> The illustrations of polymer stereoregularities (Adapted from reference 55) .....	30
<b>Figure 1.6.</b> Organizational chart of asymmetric polymerization.....	31
<b>Figure 1.7.</b> Representative structures of static helical polymers (Adapted from reference 75) .....	33
<b>Figure 1.8.</b> Tacticity of common industrial polymers. ....	34
<b>Figure 1.9.</b> Structure of $\epsilon$ -caprolactone, Lactide and Glycolide.....	35
<b>Figure 1.10.</b> Structure of tin(II)octanoate, aluminum(III)isopropoxide, zinc(II)lactate. ....	42
<b>Figure 1.11.</b> Representation of the single site catalysis of the form $\text{LnM-OR}$ .....	45
<b>Figure 1.12.</b> Life cycle of PLA.....	46
<b>Figure 1.13.</b> Stereoisomers of LA .....	46
<b>Figure 1.14.</b> Schematic diagrams to show chemical shifts (in ppm) of the tetrads for PLA in (a) homonuclear decoupled $^1\text{H}$ NMR of PLA from <i>rac</i> -lactide (Adapted from reference 39) .....	49
<b>Figure 1.15.</b> Tetradentate (imino- and amino-phenolato) aluminum complexes for stereoselective lactide ROP.....	57
<b>Figure 1.16.</b> Tetradentate and Tridentate Schiff base metal complexes for stereoselective lactide ROP. ....	59
<b>Figure 1.17.</b> ( $\beta$ -Diketiminato) metal complexes for catalysis of stereospecific lactide ROP. ....	60
<b>Figure 1.18.</b> Tetradentate amino (bis- and tris-phenolato) complexes for stereospecific lactide ROP .....	63
<b>Figure 1.19.</b> Miscellaneous catalysts for the stereocontrolled ROP of lactide.....	65
<b>Figure 1.20.</b> Organic catalysts for the stereoregular ROP of lactide.....	67
<b>Figure 2.1.</b> Stereoselective organocatalyzed ROP of <i>rac</i> -LA leading to metal-free and semi-crystalline PLA.....	80
<b>Figure 2.2.</b> Organic catalysts for the stereoregular ROP of lactide.....	81
<b>Figure 2.3.</b> The two enantiomeric structures of the thiourea-amino catalyst .....	82
<b>Figure 2.4.</b> $^1\text{H}$ NMR spectrum (400 MHz, $\text{CDCl}_3$ ) of PLA prepared with ( <i>S,S</i> )-TUC/ <i>rac</i> -LA at 25 °C Inset 1: Methine region of PLA and methyl region of PLA.....	85
<b>Figure 2.5.</b> $M_{n,\text{SEC}}$ and dispersity ( $D_M$ ) vs. monomer conversion for PLA synthesized from ( <i>S,S</i> )-TUC at RT. ....	86
<b>Figure 2.6.</b> Size exclusion chromatograms of PLA during ROP of <i>rac</i> -LA using ( <i>S,S</i> )-TUC at 25°C (Table 2.1, entry 3) .....	87
<b>Figure 2.7.</b> MALDI-ToF mass spectrum of PLA prepared with ( <i>S,S</i> )-TUC/ <i>rac</i> -LA at 25 °C (Table 2.1, entry 3).....	88

<b>Figure 2.8.</b> MALDI-ToF mass spectrum of PLA prepared with ( <i>S,S</i> )-TUC/ <i>rac</i> -LA at 85 °C (Table 2.1, entry 6).....	89
<b>Figure 2.9.</b> NMR spectra (400 MHz, CDCl <sub>3</sub> ) of the methyl region of PLA (A) obtained at 25 °C (B) obtained at 45 °C (C) obtained at 85 °C indicates epimerization reaction from <i>rac</i> -LA and to <i>meso</i> -LA in the presence of ( <i>S,S</i> )-TUC.....	90
<b>Figure 2.10.</b> <sup>1</sup> H NMR spectra (400 MHz, CDCl <sub>3</sub> ) of the methyl region of PLA indicates epimerization reaction from (A) <i>rac</i> -LA (B) <i>D</i> - and (C) <i>L</i> -LA and to <i>meso</i> -LA in the presence of ( <i>S,S</i> )-TUC.....	90
<b>Figure 2.11.</b> DSC thermograms (1 <sup>st</sup> scan; 10 °C/min) of (A) atactic PLA (B) isotactic PLA obtained by ( <i>S,S</i> )-TUC at 25 °C. ....	91
<b>Figure 2.12.</b> DSC thermogram (1 <sup>st</sup> scan; 10 °C/min) of the PLA obtained by ( <i>S,S</i> )-TUC at 25 °C (Table 2.1, entry 2).....	92
<b>Figure 2.13.</b> DSC thermogram (1 <sup>st</sup> scan; 10 °C/min) of the PLA obtained by ( <i>S,S</i> )-TUC at 45 °C (Table 2.1, entry 5).....	92_Toc21778523
<b>Figure 2.14.</b> DSC thermogram (1 <sup>st</sup> scan; 10 °C/min) of the PLA obtained by ( <i>S,S</i> )-TUC at 85 °C (Table 2.1, entry 7).....	93
<b>Figure 2.15.</b> DSC thermogram (1 <sup>st</sup> scan; 10 °C/min) of the (A) initial and annealed PLAs obtained at 25 °C (Table 2.1, entry 2) (B) initial and annealed PLAs obtained at 85 °C (Table 2.1, entry 7). ....	94
<b>Figure 2.16.</b> Deconvoluted <sup>1</sup> H { <sup>1</sup> H} NMR spectra (400 MHz, CDCl <sub>3</sub> ) of the methine region of (A) atactic PLA (B) completely isotactic PLA. ....	95
<b>Figure 2.17.</b> Quantitative <sup>13</sup> C NMR spectra (in CDCl <sub>3</sub> ) of (A) an atactic (B) a completely isotactic PLA. ....	95
<b>Figure 2.18.</b> Deconvoluted <sup>1</sup> H { <sup>1</sup> H} NMR spectra (400 MHz, CDCl <sub>3</sub> ) of the methine region of PLAs prepared by the catalysis of (A) ( <i>S,S</i> )-TUC inset: <sup>13</sup> C NMR spectrum (B) ( <i>R,R</i> )-TUC inset: <sup>13</sup> C NMR spectrum at 25 °C (Table 2.3, entry 1 and 8). ....	97
<b>Figure 2.19.</b> Deconvoluted <sup>1</sup> H { <sup>1</sup> H} NMR spectra (400 MHz, CDCl <sub>3</sub> ) of the methine region of PLA prepared by the catalysis of ( <i>S,S</i> )-TUC at 45 °C inset: <sup>13</sup> C NMR spectrum (Table 2.3, entry 3) ....	98
<b>Figure 2. 20.</b> Deconvoluted <sup>1</sup> H { <sup>1</sup> H} NMR spectra (400 MHz, CDCl <sub>3</sub> ) of the methine region of PLAs prepared by the catalysis of (A) ( <i>S,S</i> )-TUC inset: <sup>13</sup> C NMR spectrum (B) ( <i>R,R</i> )-TUC inset: <sup>13</sup> C NMR spectrum at 85 °C (Table 2.3, entry 5 and 11). ....	98
<b>Figure 2. 21.</b> Mechanisms of stereocontrol forming stereoerrors. ....	99
<b>Figure 2.22.</b> Kinetic plots of the ROP of <i>rac</i> -LA, <i>D</i> -LA and <i>L</i> -LA catalyzed by ( <i>S,S</i> )-TUC and ( <i>R,R</i> )-TUC in CH <sub>2</sub> Cl <sub>2</sub> at RT in the presence of BnOH as a initiator: [LA] <sub>0</sub> : [TUC]: [BnOH]=200:5:1, deceleration point is highlighted with yellow circle.....	102
<b>Figure S2.1.</b> Illustrated binary Schlenk system used in polymerizations.....	106
<b>Figure 3.1.</b> (a) Ground-state electronic structure of imidazol-2-ylidenes (NHCs) (Adapted from reference 30) (b) The most common types of NHCs.....	116
<b>Figure 3.3.</b> Some examples of masked NHCs used for ROP of cyclic esters. ....	119

<b>Figure 3.4.</b> Triazolo-oxazinium derivative chiral <i>N</i> -heterocyclic carbenes studied (a) saturated with tetrafluoroborate salts (b) saturated with chloride salts.....	124
<b>Figure 3.5.</b> Representative $^1\text{H}$ NMR spectrum (400 MHz, $\text{CDCl}_3$ ) of PLA prepared with <b>NHC1</b> / <i>rac</i> -LA at 25 °C: inset 1(navy colored): Methine region of PLA, inset 2 (dark blue colored): methyl region of PLA and inset 3 (light blue colored): $\omega$ -hydroxy proton of terminal methine group.....	130
<b>Figure 3.6.</b> Evolution of corrected $M_{n,\text{SEC}}$ (■) and dispersity $D_M$ (●) vs. monomer conversion for PLA synthesized from (a) <b>NHC1</b> (b) <b>NHC2</b> (c) <b>NHC3</b> and (4) <b>NHC4</b> at RT.; $[\text{LA}]_0 / [\text{BnOH}]_0 = 50 : 1$ (entries 2,8,14 and 20, Table 3.2).....	131
<b>Figure 3.7.</b> Normalized monomodal SEC traces of PLAs obtained by (a) <b>NHC1</b> (entry 2, Table 3.2), (b) <b>NHC2</b> (entry 6, Table 3.2), (c) <b>NHC3</b> (entry 10, Table 3.2) and (d) <b>NHC4</b> (entry 14, Table 3.2) catalysis at in $\text{CH}_2\text{Cl}_2$ at R.T; $[\text{LA}]_0 / [\text{BnOH}]_0 = 50 : 1$ .....	132
<b>Figure 3.8.</b> MALDI-ToF mass spectrum of PLA prepared using (a) <b>NHC1</b> (b) <b>NHC2</b> (c) <b>NHC3</b> and (d) <b>NHC4</b> in $\text{CH}_2\text{Cl}_2$ at 25 °C (entry 2, 8, 14 and 20, Table 3.2) respectively ...	134
<b>Figure 3.9.</b> DSC thermograms (1 <sup>st</sup> scan; 10 °C/min) of PLA prepared with (a) <b>NHC1</b> , (b) <b>NHC2</b> , (c) <b>NHC3</b> and (d) <b>NHC4</b> at both 25 and -50 °C. ....	136
<b>Figure 3.10.</b> $^1\text{H}$ { $^1\text{H}$ } NMR spectra (400 MHz, $\text{CDCl}_3$ ) of the methine region of PLA obtained from: (a) $\text{K}_2\text{CO}_3$ -activated <b>NHC1</b> at 25 °C (entry 2, Table 3.2); (b) $\text{K}_2\text{CO}_3$ -activated <b>NHC2</b> at 25 °C (entry 6, Table 3.2); (c) $\text{K}_2\text{CO}_3$ -activated <b>NHC3</b> at 25 °C (entry 10, Table 3.2); (d) $\text{K}_2\text{CO}_3$ -activated <b>NHC4</b> at 25 °C (entry 14, Table 3.2); Inset: quantitative $^{13}\text{C}$ NMR spectra.....	138
<b>Figure 3.11.</b> $^1\text{H}$ { $^1\text{H}$ } NMR spectra (400 MHz, $\text{CDCl}_3$ ) of the methine region of PLA obtained from: (a) $\text{K}_2\text{CO}_3$ -activated <b>NHC1</b> at -50 °C (entry 1, Table 3.2); (b) $\text{K}_2\text{CO}_3$ -activated <b>NHC2</b> at -50 °C (entry 5, Table 3.2); (c) $\text{K}_2\text{CO}_3$ -activated <b>NHC3</b> at -50 °C (entry 9, Table 3.2); (d) $\text{K}_2\text{CO}_3$ -activated <b>NHC4</b> at -50 °C (entry 13, Table 3.2); Inset: quantitative $^{13}\text{C}$ NMR spectra.....	140
<b>Figure 3.12.</b> Semi-logarithmic plots of the ROP of <i>rac</i> -LA, <i>D</i> -LA and <i>L</i> -LA catalyzed by <b>NHC1</b> and <b>NHC2</b> (entries 2, 5, 6, 8, 11 and 12, Table 3.2) in $\text{CH}_2\text{Cl}_2$ at RT in the presence of BnOH as a $[\text{LA}]/[\text{Cat.}]/[\text{K}_2\text{CO}_3]/[\text{BnOH}] = 50:0.5:0.5:1$ .....	142
<b>Figure 3.13.</b> Semi-logarithmic kinetic plots of the ROP of <i>rac</i> -LA, <i>D</i> -LA and <i>L</i> -LA catalyzed by (a) <b>NHC3</b> (entries 14, 17 and 18, Table 3.2,) and (b) <b>NHC4</b> (entries 20, 23 and 24, Table 3.2,) in $\text{CH}_2\text{Cl}_2$ at R.T in the presence of BnOH as a initiator: $[\text{LA}]_0 : [\text{BnOH}]_0=50 : 1$ .....	144
<b>Figure S3.1.</b> $^1\text{H}$ NMR spectrum (400 MHz, $\text{CDCl}_3$ ) of PLA prepared with <b>NHC2</b> / <i>rac</i> -LA at 25 °C Inset 1(navy colored): Methine region of PLA, inset 2 (dark blue colored): methyl region of PLA and inset 3 (light blue colored): $\omega$ -hydroxy proton of terminal methine group .....	151
<b>Figure S3.2.</b> $^1\text{H}$ NMR spectrum (400 MHz, $\text{CDCl}_3$ ) of PLA prepared with <b>NHC3</b> / <i>rac</i> -LA at 25 °C Inset 1(navy colored): Methine region of PLA, inset 2 (dark blue colored): methyl region of PLA and inset 3 (light blue colored): $\omega$ -hydroxy proton of terminal methine group .....	151

<b>Figure S3.3.</b> $^1\text{H}$ NMR spectrum (400 MHz, $\text{CDCl}_3$ ) of PLA prepared with <b>NHC4</b> / <i>rac</i> -LA at 25 °C Inset 1(navy colored): Methine region of PLA, inset 2 (dark blue colored): methyl region of PLA and inset 3 (light blue colored): $\omega$ -hydroxy proton of terminal methine group .....	152
<b>Figure S3.4.</b> MALDI-ToF mass spectrum of PLA obtained $\text{K}_2\text{CO}_3$ -activated <b>NHC1</b> at -50 °C (entry 1, Table 3.2).....	152
<b>Figure S3.5.</b> MALDI-ToF mass spectrum of PLA obtained by <b>NHC1</b> / <i>t</i> -BuOK (entry 3, Table 3.2).....	153
<b>Figure S3.6.</b> MALDI-ToF mass spectrum of PLA obtained by <b>NHC1</b> /DBU (entry 4, Table 3.2).....	153
<b>Figure S3.7.</b> MALDI-ToF mass spectrum of PLA obtained by $\text{K}_2\text{CO}_3$ -activated <b>NHC2</b> at -50 °C (entry 5, Table 3.2).....	154
<b>Figure S3.8.</b> MALDI-ToF mass spectrum of PLA obtained by <b>NHC2</b> / <i>t</i> -BuOK (entry 7, Table 3.2).....	154
<b>Figure S3.9.</b> MALDI-ToF mass spectrum of PLA obtained by <b>NHC2</b> /DBU (entry 8, Table 3.2).....	155
<b>Figure S3.10.</b> MALDI-ToF mass spectrum of PLA obtained by $\text{K}_2\text{CO}_3$ -activated <b>NHC3</b> at -50 °C (entry 9, Table 3.2).....	155
<b>Figure S3.11.</b> MALDI-ToF mass spectrum of PLA obtained by <b>NHC3</b> /DBU catalysis (entry 12, Table 3.2) .....	156
<b>Figure S3.12.</b> MALDI-ToF mass spectrum of PLA obtained by $\text{K}_2\text{CO}_3$ -activated <b>NHC4</b> catalysis at -50 °C (entry 13, Table 3.2).....	156
<b>Figure S3.13.</b> MALDI-ToF mass spectrum of PLA obtained by <b>NHC4</b> / <i>t</i> -BuOK catalysis (entry 15, Table 3.2).....	157
<b>Figure S3.14.</b> MALDI-ToF mass spectrum of PLA obtained by <b>NHC4</b> /DBU catalysis (entry 16, Table 3.2) .....	157
<b>Figure S3.15.</b> Deconvoluted $^1\text{H}$ { $^1\text{H}$ } NMR spectra (400 MHz, $\text{CDCl}_3$ ) of the methine region of PLA prepared at 25 °C by the catalysis of (A) <b>NHC1</b> / <i>t</i> -BuOK inset: Q. $^{13}\text{C}$ NMR spectrum (B) <b>NHC1</b> /DBU inset: Q. $^{13}\text{C}$ NMR spectrum (entries 3 & 4, Table 3.2).....	158
<b>Figure S3.16.</b> Deconvoluted $^1\text{H}$ { $^1\text{H}$ } NMR spectra (400 MHz, $\text{CDCl}_3$ ) of the methine region of PLA prepared at 25 °C by the catalysis of (A) <b>NHC2</b> / <i>t</i> -BuOK inset: Q. $^{13}\text{C}$ NMR spectrum (B) <b>NHC2</b> /DBU inset: Q. $^{13}\text{C}$ NMR spectrum (entries 9 & 10, Table 3.2).....	158
<b>Figure S3.17.</b> Deconvoluted $^1\text{H}$ { $^1\text{H}$ } NMR spectra (400 MHz, $\text{CDCl}_3$ ) of the methine region of PLA prepared at 25 °C by the catalysis of (A) <b>NHC3</b> / <i>t</i> -BuOK inset: Q. $^{13}\text{C}$ NMR spectrum (B) <b>NHC3</b> /DBU inset: Q. $^{13}\text{C}$ NMR spectrum (entries 15 & 16, Table 3.2).....	159
<b>Figure S3.18.</b> Deconvoluted $^1\text{H}$ { $^1\text{H}$ } NMR spectra (400 MHz, $\text{CDCl}_3$ ) of the methine region of PLA prepared at 25 °C by the catalysis of (A) <b>NHC4</b> / <i>t</i> -BuOK inset: Q. $^{13}\text{C}$ NMR spectrum (B) <b>NHC4</b> /DBU inset: Q. $^{13}\text{C}$ NMR spectrum (entries 21 & 22, Table 3.2).....	159
<b>Figure 4.1.</b> Some representative H-bond donor (thio)ureas for organocatalytic transformations.....	168

<b>Figure 4.2.</b> Pioneering bifunctional amine-thiourea organocatalyst and its general structure.....	170
<b>Figure 4.3.</b> Representatives of bifunctional organocatalysts; (a) unimolecular proton donor/proton acceptor type and (b) proton donor + external proton acceptor type.....	170
<b>Figure 4.4.</b> Chemical structures of catalysts employed in this thesis and their $pK_a$ values...	173
<b>Figure 4.5.</b> $^1\text{H}$ NMR spectrum (400 MHz, $\text{CDCl}_3$ ) of PLA prepared with ( <i>S,S</i> )-UC/ <i>rac</i> -LA at 25 °C Inset 1: Methine region of PLA (blue), methyl region of PLA (green) and $\omega$ -methine hydroxyl proton of terminated group (red). ....	176
<b>Figure 4.6.</b> $M_{n,\text{SEC}}$ and dispersity ( $D_M$ ) vs. monomer conversion for PLA synthesized from ( <i>S,S</i> )-UC at RT. ....	177
<b>Figure 4.7.</b> Size exclusion chromatograms of PLA during ROP of <i>rac</i> -LA using ( <i>S,S</i> )-UC at 25°C.....	178
<b>Figure 4.8.</b> MALDI-ToF mass spectrum of PLA obtained at 25 °C using ( <i>S,S</i> )-UC (Table 4.1, entry 1) .....	179
<b>Figure 4.9.</b> MALDI-ToF mass spectrum of PLA obtained at 45 °C using ( <i>S,S</i> )-UC (Table 4.1, entry 3) .....	179
<b>Figure 4.10.</b> MALDI-ToF mass spectrum of PLA obtained at 85 °C (Table 4.1, entry 5) ...	180
<b>Figure 4.11.</b> NMR spectra (400 MHz, $\text{CDCl}_3$ ) zoomed in the methyl region of PLA obtained at (A) 25 °C, (B) 45 °C and (C) 85 °C. Those indicate epimerization reactions from <i>rac</i> -LA and to <i>meso</i> -LA in the presence of ( <i>S,S</i> )-UC .....	181
<b>Figure 4.12.</b> DSC thermogram (1 <sup>st</sup> scan; 10 °C/min) of the initial and annealed PLAs obtained at 25 °C (Table 4.1, entry 1).....	181
<b>Figure 4.13.</b> DSC thermograms (1 <sup>st</sup> scan; 10 °C/min) of PLAs obtained by ( <i>S,S</i> )-UC at (A) 45 °C, and (B) 85 °C (Table 4.1, entries 3 & 5) .....	182
<b>Figure 4.14.</b> Deconvoluted $^1\text{H}$ { $^1\text{H}$ } NMR spectra (400 MHz, $\text{CDCl}_3$ ) of the methine region of PLAs prepared by the catalysis of ( <i>S,S</i> )-UC. Inset: Q. $^{13}\text{C}$ NMR spectrum at 25 °C (Table 4.3, entry 1). ....	184
<b>Figure 4.15.</b> Deconvoluted $^1\text{H}$ { $^1\text{H}$ } NMR spectra (400 MHz, $\text{CDCl}_3$ ) of the methine region of PLA prepared by the catalysis of ( <i>S,S</i> )-UC at 45 °C inset: Q. $^{13}\text{C}$ NMR spectrum (Table 4.3, entry 3) .....	185
<b>Figure 4.16.</b> Deconvoluted $^1\text{H}$ { $^1\text{H}$ } NMR spectra (400 MHz, $\text{CDCl}_3$ ) of the methine region of PLAs prepared by the catalysis of ( <i>S,S</i> )-UC. Inset: Q. $^{13}\text{C}$ NMR spectrum at 85 °C (Table 4.3, entry 5). ....	186
<b>Figure 4.17.</b> Kinetic plots of the ROP of <i>rac</i> -LA, <i>D</i> -LA and <i>L</i> -LA catalyzed by ( <i>S,S</i> )-UC and in $\text{CH}_2\text{Cl}_2$ at RT in the presence of BnOH as a initiator: $[\text{LA}]_0:[\text{UC}]:[\text{BnOH}]=200:5:1$ . ....	187
<b>Figure 5.1.</b> Structures of chiral and achiral catalysts employed for the stereoselective ROP of <i>rac</i> -LA.....	199
<b>Figure 5.2.</b> Methine region of homonuclear decoupled $^1\text{H}$ -NMR spectra of poly( <i>rac</i> -LA) obtained at different polymerization temperatures using TBD as catalyst. ....	203
<b>Figure 5.3.</b> DSC thermogram of the PLA obtained by TBD at -75 oC (Table 5.1, entry 1).205	

<b>Figure 5.4.</b> DFT-calculated ( $\square$ B97XD/6-31G**) energy profiles corresponding to the nucleophilic attack of the oxygen of the alcohol on the carbonyl carbon for complexes I-II (top panel) and III-IV (bottom panel). All the energies (in kcal/mol) are relative to the complex I reactant energy. The optimized transition state geometries of all the complexes are also displayed.....	208
<b>Figure S5.1.</b> Mixture of <i>L</i> - and <i>D</i> -LA (1/1 molar ratio) at 23°C ( $[rac\text{-}LA]_0 = 0.22\text{ M}$ ) .....	211
<b>Figure S5.2.</b> Mixture of <i>L</i> - and <i>D</i> -LA (1/1 molar ratio) after a) 10 and b) 20 and c) 30 minutes of polymerization at -75°C .....	211
<b>Figure S5.3.</b> DSC thermogram of the PLA obtained by TBD at -75 °C (entry 2, Table 5.1)	214
<b>Figure S5.4.</b> DSC thermogram of the PLA obtained by TBD at -75 °C (entry 3, Table 5.1)	215
<b>Figure S5.5.</b> DSC thermogram of the PLA obtained by TBD at -75 °C (entry 4, Table 5.1)	215



## List of Abbreviations

$^1\text{H}$  NMR: Proton nuclear magnetic resonance  
 $^1\text{H} \{^1\text{H}\}$  NMR: Homonuclear decoupled proton nuclear magnetic resonance  
 $^{13}\text{C}$  NMR: Carbon nuclear magnetic resonance  
Q.  $^{13}\text{C}$  NMR: Quantitative carbon nuclear magnetic resonance  
ACEM: Active chain end mechanism  
AMM: Activated monomer mechanism  
AROP: Anionic ring-opening polymerization  
 $\beta$ -BL:  $\beta$ -butyrolactone  
BnOH: Benzyl alcohol  
CEC: Chain-end control  
DEC: Cohesive Energy Density  
CROP: Cationic ring-opening polymerization  
*D*: Dispersity  
 $\Delta H_m$ : Melting enthalpy  
DFT: Density functional theory  
*D*-LA: *D*-lactide  
*DL*-LA: racemic lactide  
DNA: Deoxyribonucleic acid  
DP<sub>n</sub> : Degree of polymerization  
dRI: differential refractive index detector  
DSC: differential scanning calorimetry  
ESC: Enantiomorphic-site control  
FTIR: Fourier-transform infrared spectroscopy  
GTP: Group transfer polymerization  
HDPE: High density polyethylene  
HOMO: Highest occupied molecular orbital  
*It*-PLA: Isotactic PLA  
LA: Lactide  
LDPE: Low density polyethylene  
*L*-LA: *L*-lactide  
LLDPE: Linear low density polyethylene  
LPs: Lewis pairs  
LUMO: Lowest unoccupied molecular orbital  
MALDI-ToF: matrix-assisted laser desorption/ionization - time-of-flight mass spectrometer  
MALS: Multi-angles light scattering detector  
MD: Molecular dynamics  
*Meso*-LA: *meso* lactide  
MeOH: Methyl alcohol  
MeOTf: Methyl triflate  
MM: Molecular mechanics  
MMA: Methyl methacrylate  
 $M_n$ : Number average molar mass  
 $M_w$ : Weight average molar mass  
NMR: Nuclear magnetic resonance  
NHCs: *N*-Heterocyclic carbenes  
OROP: Organocatalyzed ring-opening polymerization  
PBL: Polybutyrolactone

PCL: Polycaprolactone  
 PEO: Poly(ethylene oxide)  
 PET: Polyethyleneterephthalate  
 PGA: Poly(glycolic acid)  
 $P_i$ : Probability of isodyad  
 $pK_a$ : Acid dissociation constant at logarithmic scale  
 PLA: Polylactide  
 $P_m$ : Probability of mesodyad  
 PMMA: Poly(methyl methacrylate)  
 PO: Propylene oxide  
 PPO: Poly(propylene oxide)  
 $P_r$ : Probability of racemodyad  
 $P_s$ : Probability of syndiodiad  
 PS: Poly(styrene)  
 PU: Polyurethane  
 PVC: Polyvinylchloride  
 PVL: Polyvalerolactone  
*rac*-LA: Racemic lactide  
 RED: Relative energy difference  
 ROP: Ring-opening polymerization  
 RT: room temperature  
 (*R,R*)-TUC: (*R,R*)-thiourea catalyst  
 (*S,S*)-TUC: (*S,S*)-thiourea catalyst  
 (*S,S*)-UC: (*S,S*)-urea catalyst  
 SEC: Size exclusion chromatography  
 $T_g$ : Glass transition temperature  
 $T_m$ : Melting temperature  
 TUC: Thiourea catalyst  
 UC: Urea catalyst  
 ZROP: Zwitterionic ring-opening polymerization

## **General Introduction**



Nowadays, rapidly growing ecological consciousness necessitates an update and improvement in the field of chemical and biochemical industries. It has become mandatory to develop alternative natural resources instead of the petrochemical ones. The use of petrochemical resources in chemical industry is numerous. In 2008, more than 280 Mt of polymers were produced worldwide. However, only 0.1% of them was produced from natural resources. The expected annual growth rate is 37% in the use of natural resources, and the production capacity of biorenewable polymers will reach 3.45 Mt in 2020.<sup>1</sup> To date, the most widely produced common plastics are represented by polyethylene, polypropylene, polystyrene and polyvinyl chloride. In 2004, the consummation of high density polyethylene (HDPE), linear low density polyethylene (LLDPE) and low density polyethylene (LDPE) are 18.4, 17.4 and 12.1% in United States, Canada and Mexico, respectively. However, some challenges are encountered by the production of these commonly used polymers: (i) they are produced from non-renewable fossil fuels and (ii) they are not readily degradable nor recyclable.<sup>2</sup> Also, non-degradable plastics accumulate at a rate of 25 million ton/year in the environment and more than 400 years are needed for their degradation thus creating serious pollution issues.<sup>3</sup> Large-scaled consummation of non-biodegradable plastics and their accumulation in the environment highlights the importance of replaceable other biodegradable polymer variations or to find a smart solutions instead. Herein, some innovations or developments can be offered: (i) Replacing the petroleum-based polymers with the bio-based polymers (ii), enhancing the biodegradability of non-biodegradable with blending with the natural polymers such as starch or cellulose and (iii) improving the microorganisms for biodegradation process.

The most prominent representatives of biodegradable polyesters are polycaprolactone (PCL), polylactide (PLA) and their copolymers. Their inherent properties as well as their biodegradable aspect make them suitable for both biomedical and pharmaceutical applications.<sup>4-6</sup> Moreover, PLA can be produced from 100% renewable resources (corn, sugar beets, etc.). Thus, many companies are started to commercialize PLA, such as Futerro, Tokyo Chemical, Polysciences, Corbion and NatureWorks are the top five PLA producers in the world. Very recently, Corbion (NL) and Total (FR) started a joint venture for PLA manufacturing, and in their statements, they've mentioned that PLA as a first renewable polymer, creates a fast-growing polymer market with an estimated annual growth rate of 10-15% to 2025. Within a unique functional properties as transparency, gloss and stiffness, it can be used in a broad range markets including food packaging, single-use tableware, textiles,

electronics and 3D printing.<sup>7</sup> PLA can be produced either by polycondensation of lactic acid or by a ring-opening polymerization (ROP) process of lactide (LA, cyclic dimer of lactic acid). The method of polycondensation suffers from difficulties of water separation providing only moderate control over the molar mass and the microstructure of the as-produced polymer. So, the ROP of LA comes to the fore by offering a well better control of polymerization in terms of molar masses, end-groups diversity and tacticity.<sup>8</sup> PLA also gets attraction because the sourced monomer of LA possesses three different stereoisomers, *RR*, *SS* as homoenantiomers and *RS* as diastereomer thus provides to obtain unique PLA chains in different stereoregularities. In the presence of different stereoregularities, variety of polymer tacticities can be obtained, namely, atactic, isotactic, heterotactic and syndiotactic. Depending on the tacticity, thermal and the mechanical properties of PLA can be changed. In other words, while atactic PLA is amorphous, both heterotactic and isotactic PLAs exhibit semi-crystalline properties, with a melting temperature ( $T_m$ ) around 120 °C and 170 °C and high, respectively, isotactic PLA showing an improved mechanical strength. Very interestingly, *L*-PLA and *D*-PLA enantiomers can co-crystallize when blended in a 1:1 molar ratio, forming a stereocomplex that has an even higher  $T_m$  up to 230 °C. Thus, tailor made stereo-di- or multi-block copolymers can be achievable within different catalytic systems.

Due to a precise molar mass control and a high end-group fidelity, ROP of LA is the most preferred technique of PLA synthesis. However, LA exists in three different isomers: (*R,R*)-LA (*D*-LA), (*S,S*)-LA (*L*-LA) and (*R,S*)-LA (*meso*-LA). In addition, a commercially available racemic lactide (*rac*-LA) can be found as an equally mixture *D*- and *L*-LA. The tacticity of PLA is the most important factor affecting the chemical and physical polymer properties, and which can be controlled by compatible catalytic systems. The great majority of studies reported for this purpose concern metal-salts or coordination complexes operating via the coordination-insertion mechanism. While great advances have been made in organometallic catalysts for stereoselective ROP, organocatalysts generate convenient alternatives. They can indeed offer different mechanistic pathways in addition to providing PLAs free of residual metal contaminants that could compromise the polymer performance in biomedical and microelectronic applications.

Metallic ligands, organic compounds or enzymes used in specifically designed catalytic systems enable to trigger the stereoselective ROP of *rac*-LA. Until only recently, only transition metal complexes and enzymes could be used for such asymmetric catalysis. In the general context of organic chemistry, however, there have been endless of small organic

molecules used for asymmetric catalysis. Many organic catalysts are simple, commercially available molecules that are typically easily purified and, as a consequence of insensitivity to water and oxygen, have long shelf lives.<sup>9</sup> Furthermore, organic catalysts are well suited to a range of reaction conditions, solvents, and monomers and, as a consequence of their acidic or basic nature, are typically very easy to remove from the resultant polymers by simple washing or trapping in resin beads.

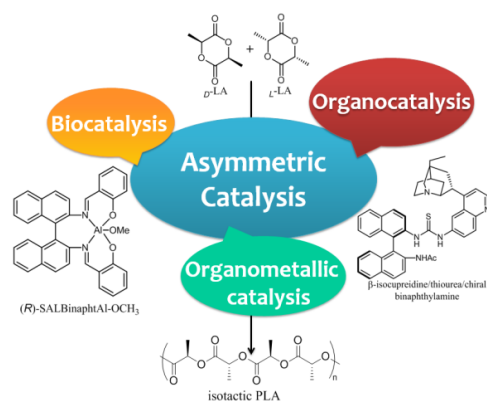
This PhD work relates to a developing field in polymer chemistry that is the use of organocatalysts in polymerization reactions, a topic that is at the interface of polymer chemistry, organic chemistry, catalysis and materials science. The diverse reactivity of organic catalysts found in organocatalyzed reactions of molecular chemistry has been successfully applied to polymer synthesis. Organic catalysts have thus grown significantly in organopolymerization in the past 15 years, through the activation of a wide range of monomer substrates, and involving various reaction mechanisms, including anionic-like and zwitterionic chain-growth processes and step-growth reactions as well. Subtle changes in chemical catalyst structure sometimes cause dramatic differences in reaction with specific substrates.

By far, cyclic esters, such as lactones and lactides, have been the most investigated as monomer substrates *via* the chain-growth ROP, but the scope of monomer substrates amenable to ROP has been extended to cyclic carbonates, cyclic siloxanes, *N*-carboxyanhydrides or epoxides.

Among organocatalysts, only few of them have been reported for the organic asymmetric ROP. By asymmetric polymerizations of *rac*-LA, tailor-made PLA formations could be obtained in the presence of chiral catalytic systems. Starting from the homomonomers (*D*- or *L*-LA), only homo-stereoregular PLA formation can be monitored, and those crystalline polymer chain shows  $T_m = 160\text{--}180\text{ }^{\circ}\text{C}$ , as mentioned above. However, stereoselective ROP of *rac*-LA provides stereodi- or multi-block copolymers (PDLA-*co*-PLLA) which introduces highly enhanced thermal properties of PLA within  $T_m = 220\text{--}240\text{ }^{\circ}\text{C}$  in the presence of appropriate catalytic systems. However, surprisingly, investigations of novel organic catalysts remained relatively low, although their quite comparable catalytic activities both in reaction and stereo-control in terms of the high polymerization control, low molar mass distribution, good end-group fidelity and high stereoselectivity. Organocatalysts which spreaded among the Brønsted/Lewis acids or bases, amines, NHCs, phosphazenes, guanidines, (thio)urea derivatives are mainly investigated for the ring-opening polymerization

of *rac*-LA, and only few of them was reported for the asymmetric polymerizations of *rac*-LA such as; *L*-proline, oxazolidinone, NHCs, cinchona alkaloids and (thio)urea derivatives. Considering very few numbers of reports, the new organic catalysts that catalyze cyclic dimer lactide polymerization via asymmetric pathway have to be investigated for both industry and academia.

**Thesis Overview:** To date, only a handful of studies of stereocontrolled ROPs of *rac*-LA using either chiral or achiral organo-based catalysts have been reported. Such limited amount of research stimulated us to investigate and elaborate new chiral organic catalysts useful in the isoselective ROP of *rac*-LA. Our main motivations were addressed to the use of chiral (thio)urea and *N*-heterocyclic carbene molecules able to transfer their chirality to the polymer backbone during the polymerization.

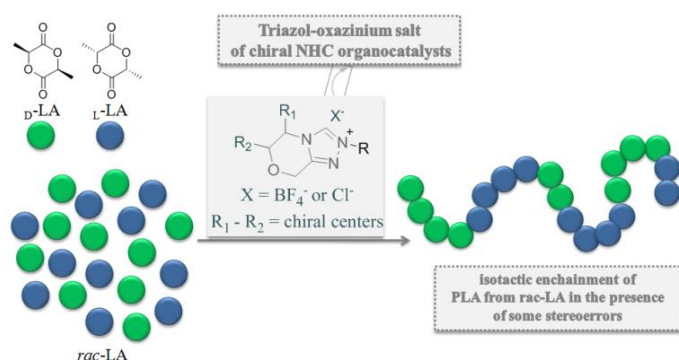
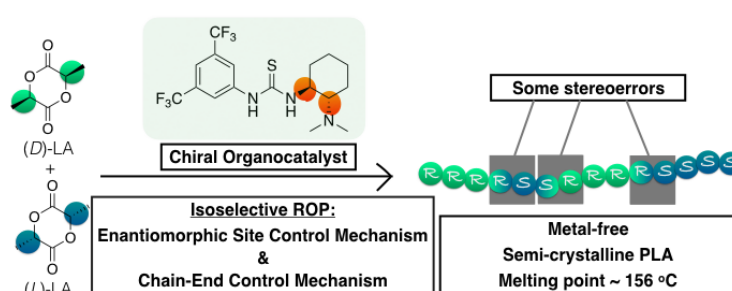


This dissertation is divided into five chapters and organized as shown below.

The first chapter presents a literature overview of different biodegradable and biosourced monomers readily used in stereoselective polymerizations. A special emphasize on the very attractive properties of the lactide monomer as well as the available polymerization techniques which could be applied for its stereospecific polymerization will be presented.

In the chapter 2, the stereocontrol ring-opening polymerization of *rac*-LA using chiral thiourea-amine Takemoto's organocatalyst in (*R,R*)- and (*S,S*)-enantiofaces is

described. Efficient control and high isoselectivity are demonstrated by kinetic resolution, yielding highly isotactic and semi-crystalline polylactide at room temperature.

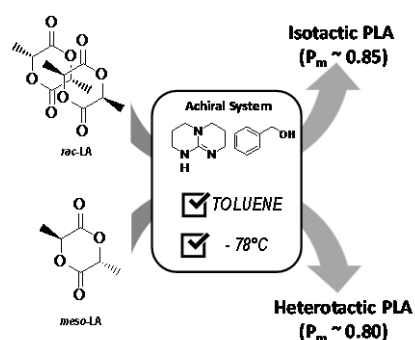
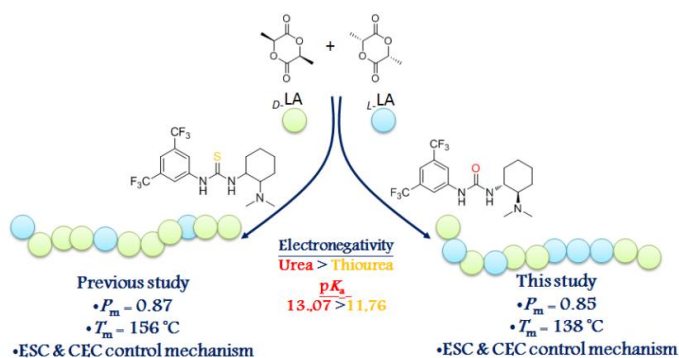


Chapter 3 presents novel chiral *N*-heterocyclic carbene (NHC) molecules as efficient organocatalytic systems to provide a high stereoselectivity during



the ROP of *rac*-LA. The generation of those NHC carbenes has been realized by basic treatments of their corresponding salts for different temperatures. Effect of those NHCs on the controlled or uncontrolled polymerizations is discussed.

Chapter 4 introduces the comparison study of the thiourea which has been discussed in the 2<sup>nd</sup> chapter, to its urea homologue in terms of stereoselectivity imposed during the ROP of *rac*-LA. The electronegative atom effect on the catalytic activity will be described as well as the stereoregulation of polymer chain.



Finally, Chapter 5 presents stereoselective ROP of *rac*- and *meso*-LA using achiral TBD catalyst under cryogenic (at  $-75\text{ °C}$ ) conditions.

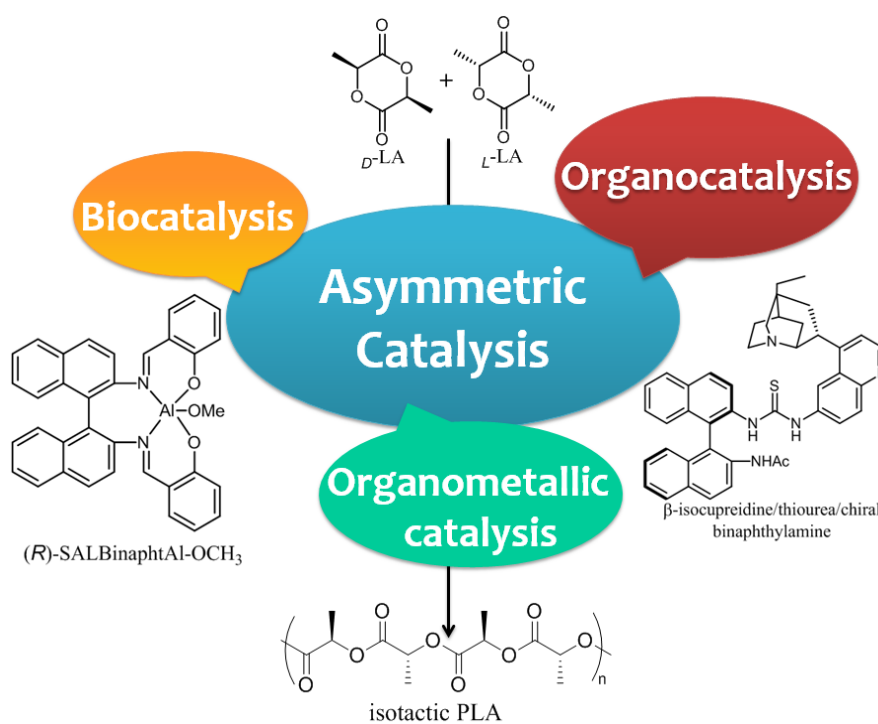
This project is funded by the European Union grant agreement No 64267. This project has been coordinated by Dr. Haritz Sardon from the University of the Basque Country, with Prof. Daniel Taton as the scientific coordinator.

## References

- [1] L. Shen, J. Haufe, M. K. Patel, *PRO-BIP 2009, Final Rep.* **2009**.
- [2] B. G. G. Lohmeijer, R. C. Pratt, F. Leibfarth, J. W. Logan, D. A. Long, A. P. Dove, F. Nederberg, J. Choi, C. Wade, R. M. Waymouth, J. L. Hedrick, *Macromolecules* **2006**, 39, 8574.
- [3] L. S. Nair, C. T. Laurencin, *Prog. Polym. Sci.* **2007**, 32, 762.
- [4] M. A. Woodruff, D. W. Hutmacher, *Prog. Polym. Sci.* **2010**, 35, 1217.
- [5] E. Chiellini, R. Solaro, *Adv. Mater. (Weinheim, Ger.) F. Full J. TitleAdvanced Mater. (Weinheim, Ger.* **1996**, 8, 305.
- [6] C. K. Williams, M. A. Hillmyer, *Polym. Rev.* **2008**, 48, 1.
- [7] P. Dubois, O. Coulembier, J. Raquez, *Handbook of Ring-Opening Polymerization*; 2009.
- [8] M. Fèvre, J. Vignolle, Y. Gnanou, D. Taton, *Organocatalyzed Ring-Opening Polymerizations*; Elsevier B.V., 2012; Vol. 4.
- [9] W. N. Ottou, H. Sardon, D. Mecerreyes, J. Vignolle, D. Taton, *Prog. Polym. Sci.* **2016**, 56, 64.

## Chapter 1.

### Stereoselective Ring-Opening Polymerization Involving Racemic Lactide



**Keywords:** Stereoselective • Lactide • Organocatalysis • Ring-Opening Polymerization

# Chapter 1.

## Stereoselective Ring-Opening Polymerization Involving Racemic Lactide

### Contents

<b>Chapter 1. Stereoselective Ring-Opening Polymerization Involving Racemic Lactide...</b>	<b>24</b>
1.1. Introduction.....	26
1.2. Chiral polymers .....	28
1.3. Stereoregularity and tacticity in polymers.....	28
1.4. Asymmetric polymerizations.....	31
1.5. Synthesis of polyesters: some generalities .....	35
1.5.1. Step growth polymerization .....	36
1.5.2. Ring-Opening Polymerization .....	36
1.5.2.1. Anionic Ring-Opening Polymerization.....	37
1.5.2.2. Cationic Ring-Opening Polymerization .....	38
1.5.2.3. Organocatalyzed and Enzymatic ROPs .....	39
1.5.2.4. Coordination- Insertion Ring-Opening Polymerization.....	42
1.6. Polylactide .....	45
1.6.1. Generalities on PLA.....	45
1.6.2. Stereochemistry and microstructures of PLA .....	46
1.6.3. Stereoselective ROP of LA.....	50
1.6.3.1. Mechanism of stereocontrol polymerization of lactide.....	51
1.6.3.2. Mesotacticity analysis .....	52
1.6.3.3. Catalytic systems for stereoselective ROP of <i>rac</i> -LA .....	53
1.6.3.3.1. Organometallic catalysts .....	53
1.6.3.3.1.1. Tri- and tetra-dentate iminophenolato- and aminophenolato- (salen and salan) complexes.....	53
1.6.3.3.1.2. $\beta$ -Diketiminato (BDI) complexes .....	59
1.6.3.3.1.3. Tetradentate amino (bis- and tris-phenolato) complexes..	61
1.6.3.3.1.4. Miscellaneous ligands.....	64
1.6.3.3.2. Organic catalysts .....	66
1.7. Concluding remarks and objectives of this PhD thesis .....	69
1.8. References.....	71

## 1.1. Introduction

Among commercial synthetic polymers, polyolefins represent by far the most important class of materials, owing to various factors including monomer availability and cost, synthetic ease and excellent properties.<sup>[1]</sup> Despite the numerous advantages of these polymers, two drawbacks remain to be solved, namely, the need for non-renewable petrol-based resources for their production and the ultimate fate of these large scale commodity polymers. Disposal of these nondegradable materials has indeed led to serious environmental issues. Since 2015, approximately 6300 million tons of plastic waste have been generated, a significant proportion of which has found its way to the environment as a result of uncontrolled dumping of wastes.<sup>[2]</sup>

There are at least three potential ways to solve this environmental problem, which includes recycling, incineration, and biodegradation.<sup>[3]</sup> Re-processing of waste plastics and their transformation into their initial monomer, followed by a re-use of the latter refers to as *the tertiary recycling*.<sup>[4]</sup> In Europe, the potential for recycling plastic wastes remains largely unexploited: around 25.8 million tons of plastic wastes are generated, but less than 30% are truly collected for recycling.<sup>[5]</sup>

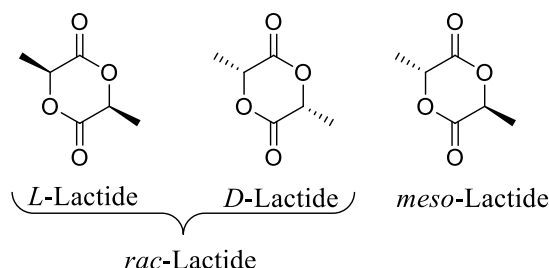
Secondly, many plastics can be burned and transformed to gases as energy sources. Plastic incineration is however limited as it produces carcinogenic dioxins, unless burned at very high temperatures. It has been estimated that plastic production and incineration of plastic wastes give rise to approximately 400 million tons of CO<sub>2</sub> per year.<sup>[5]</sup>

The third -and likely the most promising solution- is the production of sustainable biodegradable polymers. Naturally occurring polymers are potentially biodegradable. In addition, many of them are chiral in essence, as a key-component of their function of recognition, binding and catalytic activities.<sup>[6]</sup> Polysaccharides such as starch and cellulose are representative examples of naturally occurring polymers exhibiting biodegradable properties.<sup>[7]</sup> In order to produce biopolymers such as proteins, DNA or polysaccharides, nature uses readily available enantiopure amino acids and sugars, through enzyme-catalyzed pathways. Based on these grounds, synthetic chiral polymers have been conceived to mimic some of the properties of natural polymers.<sup>[8]</sup> Inspired by such concepts found in nature, chiral polymer synthesis relying on the repetition of optically active monomer units has received a great deal of attention. In the context of molecular chemistry, the design of chiral molecules

showing specific properties (e.g. biological or catalytic activities) by asymmetric synthesis is a very productive area.<sup>[9–11]</sup>

In the field of nature-mimic enantioselective polymers, particular interest has been paid to polylactide (PLA), which is probably the synthetic biodegradable and biocompatible polymer the most investigated.<sup>[12–14]</sup> PLA is manufactured from biorenewable sources, such as corn starch or sugar cane. These features make PLA suitable for several applications, for instance, in the pharmaceutical and micro-electronics fields, or as a biodegradable plastic in packaging.<sup>[15–18]</sup>

Lactide possesses two chiral centers. As such, it can exist in three distinct diastereoisomers, namely, *D*-, *L*- (commonly used as a racemic mixture, *rac*-LA) and *DL*- (*meso*-LA) (Figure 1.1).



**Figure 1.1.** The distinct forms of lactide

Control over stereoselectivity (stereocontrol) in some polymerization reactions is of paramount importance, as the resulting tacticity of the polymer drastically affects the physical and mechanical properties of the final material.<sup>[19–24]</sup> In the past decades, many catalysts and/or initiators, such as enzymatic<sup>[25]</sup>, metal-based<sup>[26–35]</sup> and organic catalysts,<sup>[36,37]</sup> have been reported for the ring-opening polymerization (ROP) of LA<sup>[38]</sup>. Only a few of them, however, have been shown to achieve highly stereoregular PLA from racemic LA.<sup>[39–41]</sup>

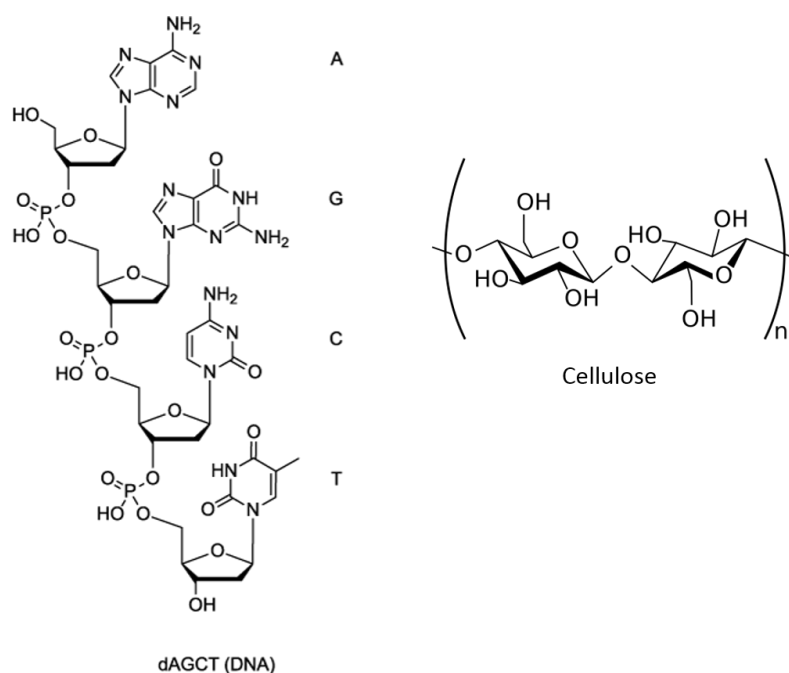
Salen-Al metal complexes and the derivatives reported by Spassky *et al.* and others<sup>[12,14,33,42–47]</sup> have attracted the most attention in the last two decades. In very recent years, attempts to conduct the stereoselective ROP of *rac*-LA using organocatalysts have also emerged in the literature.<sup>[48,49]</sup>

A great deal of research has been focused on stereochemical control in PLA synthesis. A large number of investigations has been directed towards designing efficient metal-based and organic catalysts/initiators and studying their reactivities. In the following chapter, these efforts will be summarized. In the first section, are discussed the synthetic strategies to biodegradable PLAs, with a special emphasis on the different ROP reaction mechanisms. In

many cases, a quite good control over the molecular features of PLA can be achieved, *i.e.* PLAs can be obtained with a predictable molar mass and narrow molar mass distribution. Then, asymmetric polymerization enabling the synthesis of highly crystalline PLAs from the racemic monomer by stereoselective ROP of lactide will be presented. Main organometallic and organic catalysts that have been investigated for this purpose will be covered.

## 1.2. Chiral polymers

Interest in chiral polymers has originally focused on naturally occurring polymers, with emphasis on the modelling and interpretation of the conformational properties of these polymers in solution. As mentioned, a vast majority of naturally occurring polymers are chiral in essence, as nature takes advantage of the presence of chiral monomers, such as amino acids and sugars to construct proteins, nucleic acids and polysaccharides (Figure 1.2). As a means to mimic Nature, polymerization of chiral monomers has been successfully achieved, but the number of enantiomerically pure monomers remains limited.

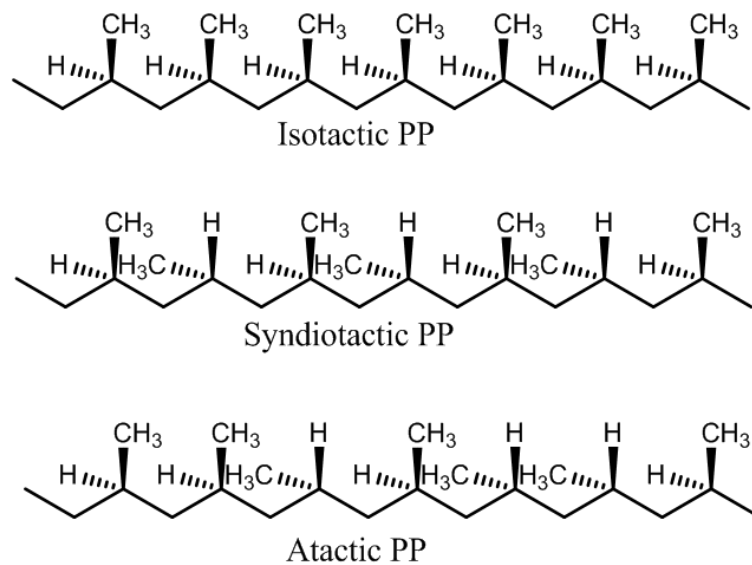


**Figure 1.2.** Examples of naturally occurring chiral four-nucleotide segment of DNA with an adenine-cytosine-guanine-thymine sequence segment and cellulose

## 1.3. Stereoregularity and tacticity in polymers

Synthesis of stereoregular polymers has been extensively studied since the discovery of the Ziegler-Natta catalysts.<sup>[50,51]</sup> The correlation between the *modus operandi* of these catalysts and the polymer chain configuration has also been extensively investigated.<sup>[52,53]</sup> The

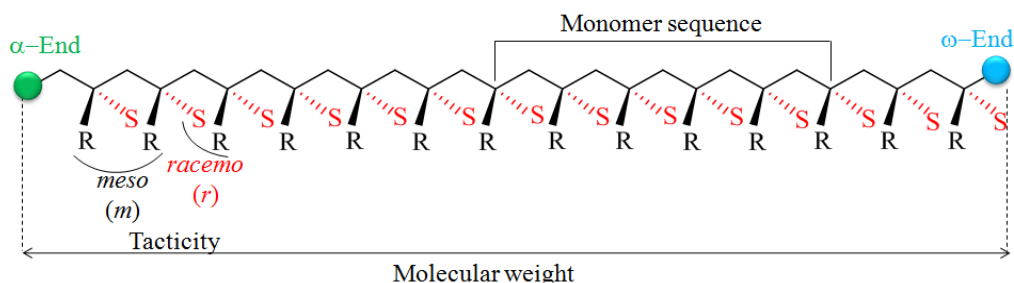
most representative examples of stereoregular polymers are polyvinyl chloride (PVC) and polypropylene (PP), as depicted in Figure 1.3.



**Figure 1.3.** Isotactic, syndiotactic and atactic forms of PP

The discovery of the polymerization processes and the foundation of macromolecular stereochemistry have represented major breakthroughs in polymer chemistry in the 20<sup>th</sup> century. The study of macromolecular compounds has introduced a new dimension in organic stereochemistry. Among the points that distinguish macromolecules from low molar mass compounds are the non-homogeneity of their molecular dimension and structure. Main factors affecting the primary structure of polymers include monomer sequences, terminal groups, stereoregularity and polymer chain length, or molar mass (Figure 1.4).

Stereoregularity is one of the most important factors, with a dramatic influence on the morphological aspects, affecting the physical, thermal and mechanical properties of the final polymeric material.<sup>[54]</sup>



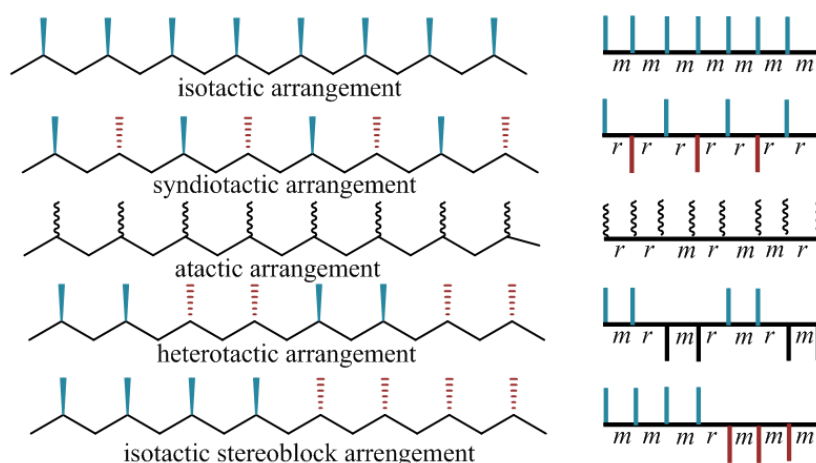
**Figure 1.4.** Primary structure of polymers

Stereoregularity provides crystallinity, *i.e.* stereoregular polymers are usually high-strength materials, as a result of the uniform structure that leads to a close packing of the



polymer chains and a high degree of crystallinity. The ability for a polymer to crystallize is obviously correlated to its stereoregularity, as crystalline regions are formed by the stereoregular blocks. In general, differences in stereoregularity of polymeric materials cause drastic differences in microstructures, morphology, crystallinity and physical/mechanical properties. For example, commercially available polypropylene is typically a mixture of tactic forms in a ratio of 75% isotactic and 25% atactic, which provides a material with a high molar mass and high tensile strength, stiffness.<sup>[4]</sup>

The steric configurations of a polypropylene chain can be best represented by drawing the chain in its extended-chain or in its planar zigzag conformation, as illustrated in Figure 1.5. Several arrangements of the substituent group, -CH<sub>3</sub>, are possible. In one configuration, all the methyl groups may lie on the same side of the plane formed by the extended-chain backbone. Such polymers are qualified as *isotactic*.<sup>[4]</sup> If the substituent group regularly alternates from one side of the plane to the other, the polymer is *syndiotactic*. Polymers with no preferred configuration are referred to as *atactic*.



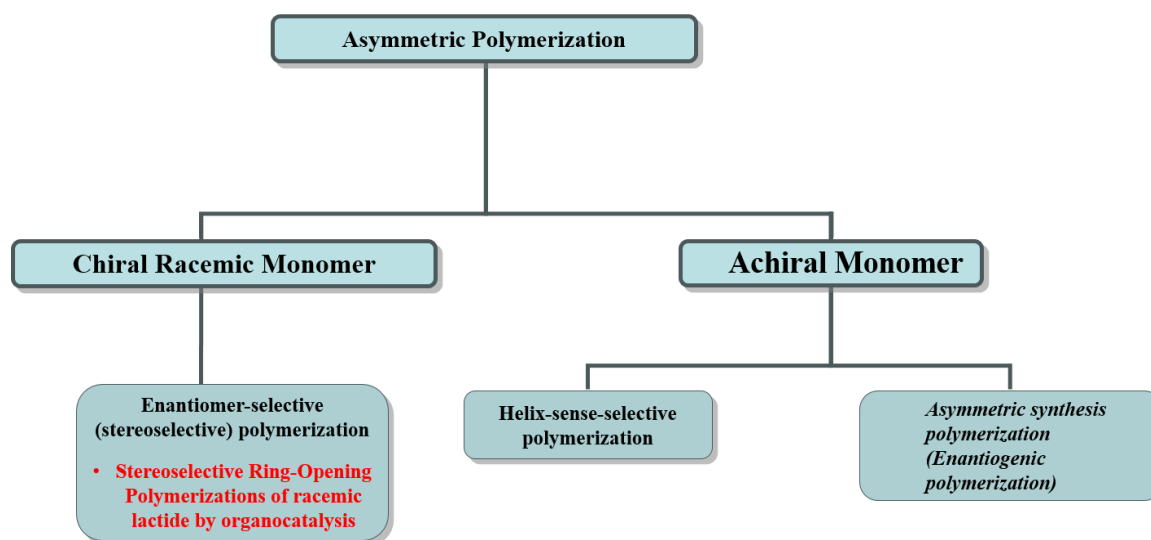
**Figure 1.5.** The illustrations of polymer stereoregularities (Adapted from reference 55).

Two adjacent units in a polymer chain constitute a dyad, and if the dyad consists of two identical configurations, it is called a *meso* dyad, abbreviated as “*m*”. An alternated order of (*R*) and (*S*) configuration will form a racemic dyad, abbreviated as “*r*”.<sup>[55]</sup> Triads, tetrads and pentads can be assigned to three, four and five repeating monomer units, respectively. Isotacticity refers to a non-changing regulation of monomer units in a polymer backbone, *i.e.* –*RRRR*– or –*SSSS*– which exhibits the term of tetrad and referred as “*mmm*”. In comparison, the alternate monomer configuration of syndiotacticity, *i.e.* –*RSRS*– is basically abbreviated by “*rrr*”.<sup>[56]</sup>

#### 1.4. Asymmetric polymerizations

As mentioned above, chiral polymer synthesis utilizing optically active monomers has received a great deal of attention.<sup>[8,57]</sup> Maybe a more versatile route in generating chirality during polymer synthesis utilizes cheap and readily available achiral monomers, using the so-called **asymmetric polymerization** (*vide infra*). Modern asymmetric polymerizations mainly rely on metal-catalyzed chain polymerization processes, starting from achiral (but prochiral) monomers. The Ziegler-Natta/metallocene olefin polymerizations<sup>[58–62]</sup> are prototypical examples of asymmetric chain growth polymerization of prochiral monomers. However, the resulting polymers are generally not optically active.

Achiral, prochiral as well as racemic monomers represent a much broader source of polymer precursors. One can then distinguish three main strategies of asymmetric polymerization from such monomers, but only a few of them eventually lead to chiral polymers *stricto sensu* (Figure 1.6).



**Figure 1.6.** Organizational chart of asymmetric polymerization

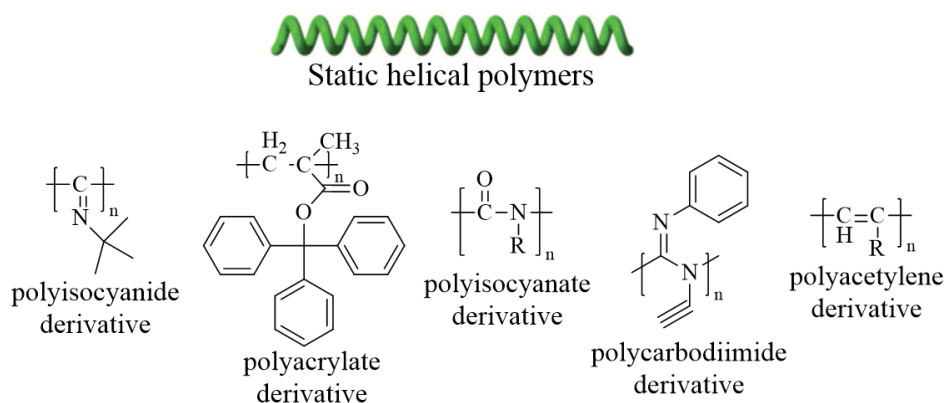
Asymmetric polymerization can be achieved either i) by polymerization of achiral monomers through the use of optically active catalysts or initiators that convey chirality in the polymer main chain, ii) or by polymerization of chiral monomers. Modern asymmetric polymerizations mainly rely on metal-catalyzed chain polymerization processes, starting from achiral -but prochiral- monomers, or from racemic monomers possessing a chiral center. The latter route can be sub-divided into two distinct pathways, namely, asymmetric synthesis polymerization and helix-sense-selective polymerization, as summarized in Figure 1.6.

### 1. Asymmetric Polymerization

In this case, an optically inactive (prochiral) monomer featuring an optically active auxiliary, is polymerized to give a polymer presenting a configurational main chain chirality. This usually involves attack of only one specific enantio-face of the monomer by the reactive growing species during propagation steps. Various types of olefinic compounds and dienes, such as 1,3-pentadiene,<sup>[63]</sup> (*R*), 2-3, pentadiene,<sup>[64]</sup> benzofuran<sup>[65]</sup> and *N*-phenylmaleimide<sup>[66]</sup> have been reported to operate through this type of polymerization mechanism.

### 2. Helix-sense-selective polymerization

Helix-sense-selective polymerization, also referred to as atropogenic polymerization, leads to optically active polymers the chirality of which is based on a helical conformation with an excess of single-screw sense. Since the right- and left-handed helices are mirror images –called atropisomers, if one enantiomer is preferentially achieved, the polymer will exhibit an optical activity. The rigidity of the polymer backbone or sterical hindrance of the side groups enable to avoid the random regulation. In addition, the chirality of the initiator/catalyst can provide an optically active helical conformation. Some representative examples of synthetic helical polymers include sterically restricted polyacrylates<sup>[67,68]</sup>, polyisocyanides,<sup>[69–71]</sup> polyisocyanates,<sup>[72]</sup> polycarbodiimide,<sup>[73]</sup> and polyacetylenes<sup>[74]</sup> (Figure 1.7).<sup>[75]</sup>

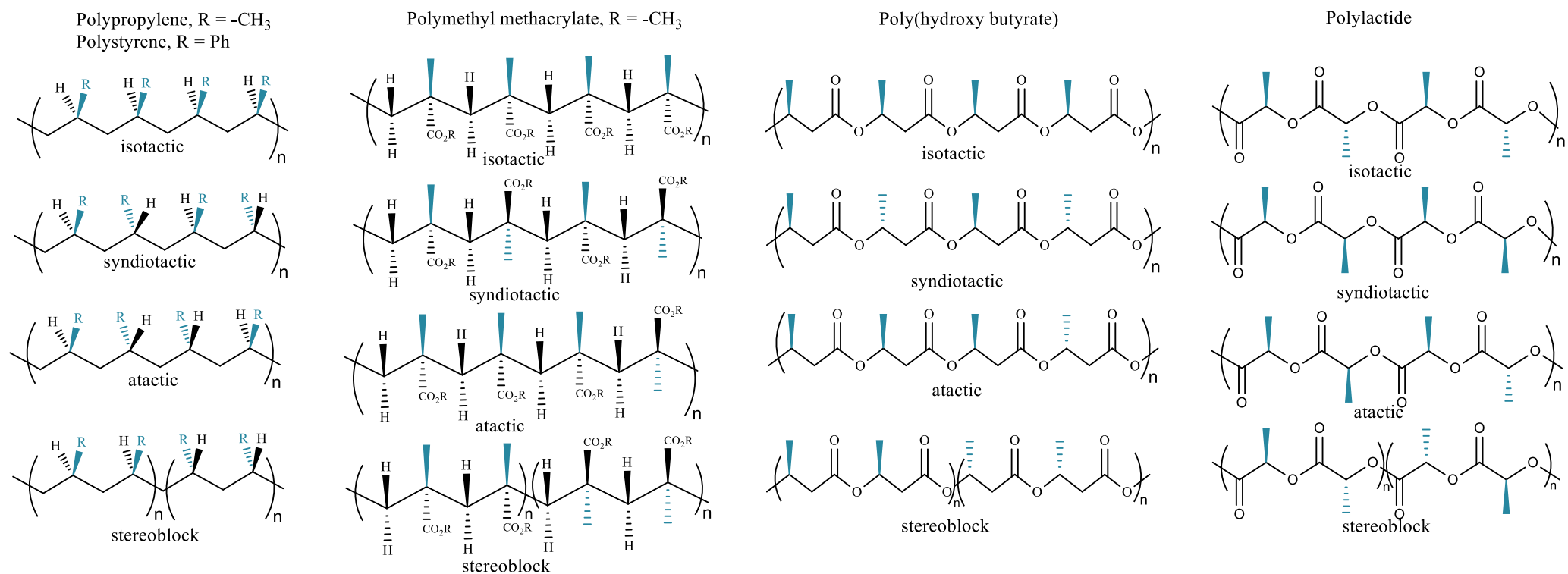


**Figure 1.7.** Representative structures of static helical polymers (Adapted from reference 75).

### 3. Enantiomer-selective (enantioasymmetric or stereoselective) polymerization

Enantiomer-selective polymerization refers to a polymerization reaction involving the preferential incorporation of one enantiomer from a racemic mixture of the two monomers, affording an optically active polymer. This is very similar to the kinetic resolution of enantiomers occurring in many reactions in organic chemistry.<sup>[76]</sup> Enantiomer-selective polymerization has been developed using optically active catalysts/initiators. The degree of enantiomer selection is generally evaluated through the determination of the enantiomeric excess (*e.e.*) of the starting monomer, as well as that of the resulting polymers (see further). It should be noted that a racemic mixture of monomers can be converted either into a mixture of polymers of opposite configuration or to so-called stereoblock copolymers, with the aid of a catalyst/initiator in its racemic form.

For instance, enantiomer-selective polymerization of propylene oxide has been reported by Inoue *et al.* in 1962.<sup>[77]</sup> Monomers subjected to this polymerization mode include  $\alpha$ -olefins,<sup>[78]</sup> propylene sulfide,<sup>[79]</sup> lactide,<sup>[80]</sup> methacrylates,<sup>[81]</sup>  $\alpha$ -amino acids<sup>[82]</sup> and *N*-carboxy anhydrides<sup>[83,84]</sup> (Figure 1.8). Polymer chains synthesized resulting from the enantiomer-selective polymerization may exhibit drastic differences in terms of mechanical, physical and thermal properties (melting temperature, crystallinity, and mechanical strength) depending on the stereocontrol (see Table 1.1).

**Figure 1.8.** Tacticity of common industrial polymers.

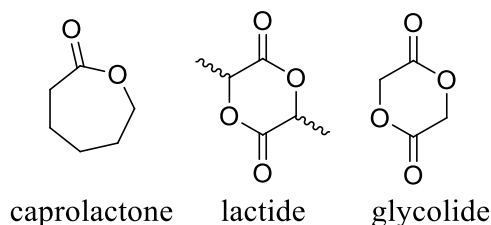
**Table 1.1.** Thermal properties of common industrial, non- or biodegradable, petroleum- or bio-based polymers in different tacticities. ( $T_g$  = Glass transition temperature,  $T_m$  = Melting temperature)

	Semi-crystalline Stereoblock	Crystalline Isotactic	Semi-crystalline Isotactic	Semi-crystalline Syndiotactic	Amorphous Atactic
<b>Polypropylene</b> <b>Petroleum based</b> <b>nonbiodegradable</b>	$T_g = -10 - 0^\circ\text{C}$ $T_m = 140-180^\circ\text{C}$	$T_g = -$ $T_m = 180-200^\circ\text{C}$	$T_g = -10 - 10^\circ\text{C}$ $T_m = 170-190^\circ\text{C}$	$T_g = -10 - 10^\circ\text{C}$ $T_m = 170-190^\circ\text{C}$	$T_g = -10^\circ\text{C}$ $T_m = -$
<b>Polystyrene</b> <b>Petroleum based</b> <b>nonbiodegradable</b>	$T_g = 100-120^\circ\text{C}$ $T_m = 250-280^\circ\text{C}$	$T_g = -$ $T_m = 210-250^\circ\text{C}$	$T_g = 110-130^\circ\text{C}$ $T_m = 210-250^\circ\text{C}$	$T_g = 120-130^\circ\text{C}$ $T_m = 265-270^\circ\text{C}$	$T_g = 116^\circ\text{C}$ $T_m = -$
<b>Poly(methyl methacrylate)</b> <b>Biobased</b> <b>nonbiodegradable</b>	$T_g = 30-50^\circ\text{C}$ $T_m = 160-180^\circ\text{C}$	$T_g = -$ $T_m = 140-160^\circ\text{C}$	$T_g = 40-60^\circ\text{C}$ $T_m = 140-160^\circ\text{C}$	$T_g = 110-130^\circ\text{C}$ $T_m = 200-220^\circ\text{C}$	$T_g = 100^\circ\text{C}$ $T_m = -$
<b>Poly(hydroxybutyrate)</b> <b>Biobased-biodegradable</b>	$T_g = -10 - (-5)^\circ\text{C}$ $T_m = 180-210^\circ\text{C}$	$T_g = -$ $T_m = 170-190^\circ\text{C}$	$T_g = 0-10^\circ\text{C}$ $T_m = 140-180^\circ\text{C}$	$T_g = -10 - (-5)^\circ\text{C}$ $T_m = 90-100^\circ\text{C}$	$T_g = 0-10^\circ\text{C}$ $T_m = -$
<b>Poly(lactide)</b> <b>Biobased-biodegradable</b>	$T_g = 40-60^\circ\text{C}$ $T_m = 240-270^\circ\text{C}$	$T_g = -$ $T_m = 140-170^\circ\text{C}$	$T_g = 40-60^\circ\text{C}$ $T_m = 130-170^\circ\text{C}$	$T_g = 40-60^\circ\text{C}$ $T_m = 130-170^\circ\text{C}$	$T_g = 40-60^\circ\text{C}$ $T_m = -$

### 1.5. Synthesis of polyesters: some generalities

Aliphatic polyesters, such as polylactide (PLA),<sup>[20,38,85]</sup> polyglycolic acid (PGA), polycaprolactone (PCL)<sup>[85-87]</sup> and their associated copolymers, are well known as biodegradable polymers used in miscellaneous applications, in particular in the biomedical field.<sup>[86,88]</sup> Synthesis of these polymers can be achieved following by two major pathways.

- (i) Step growth polymerization or polycondensation
- (ii) Ring-Opening Polymerization (ROP) of lactones, lactide and glycolide (Figure 1.9).

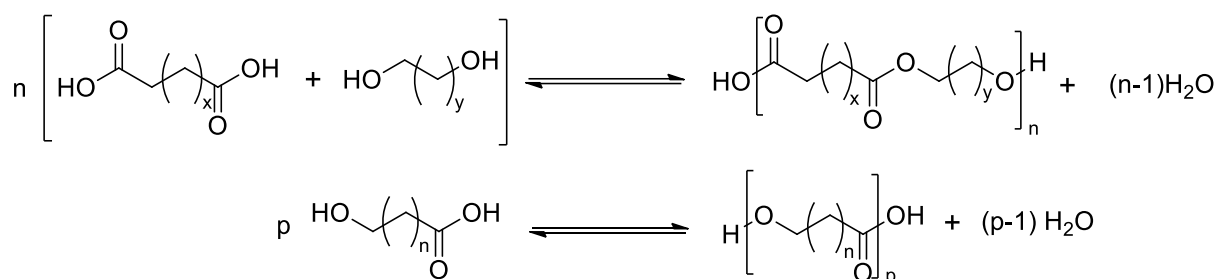


**Figure 1.9.** Structure of  $\epsilon$ -caprolactone, lactide and glycolide.

### 1.5.1. Step growth polymerization

The step growth polymerization technique relies on the reaction -in fact a condensation reaction- of hydroxy acids (AB-type monomers) or mixtures of diacids and diols (AA- + BB-type monomers). (Scheme 1.1). Although these polycondensation techniques allow synthesizing a wide range of polyesters compared to ROP with an easier access of the monomers involved, they exhibit some drawbacks:

- Conversion may be limited due to formation of the volatile side-product ( $\text{H}_2\text{O}$ ,  $\text{HCl}$ ,  $\text{MeOH}$ , ...) giving rise to an equilibrium, which is typical of esterification reactions. Consequently, high temperatures are required in order to eliminate this side-product, and thus reach high conversions and high molar mass polyester.
- In the case of (AA + BB) monomers, if the stoichiometry is not perfect, conversion will also decrease and oligomers only will be achieved



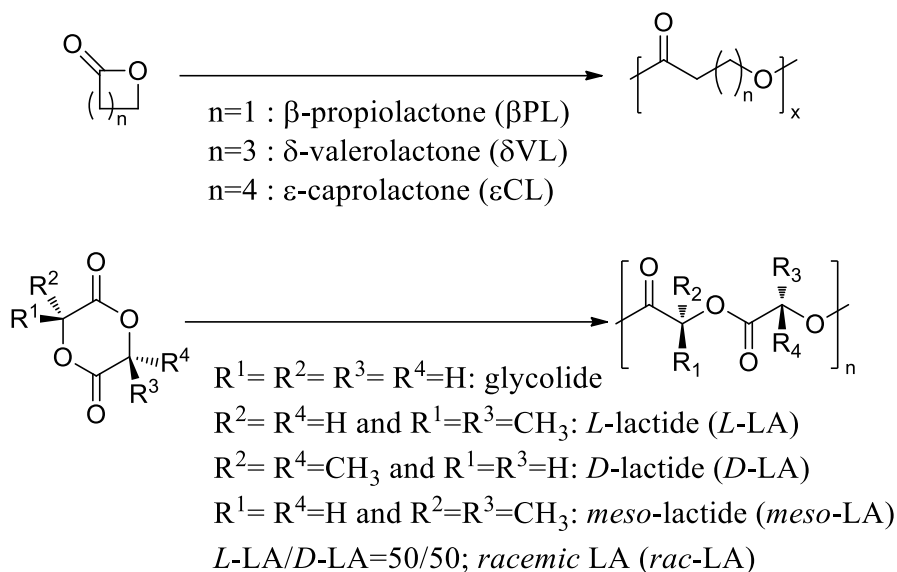
**Scheme 1.1.** Synthesis of aliphatic polyesters by step growth polycondensation.

### 1.5.2. Ring-Opening Polymerization

The polymerization of lactide and lactones by ring-opening polymerization (ROP) overcomes some of the limitations pertaining to step growth polymerization. In particular, ROP is more convenient to access polyesters with a better control over molar masses, dispersity, polymer chain ends and, possibly tacticity. High molar mass polyesters can be synthesized under mild conditions from lactide and lactones of different ring sizes, substituted or not by functional groups (Scheme 1.2).<sup>[89–91]</sup>

Ring strain is the most important factor affecting the ROP of cyclic esters.<sup>[92]</sup> For the lactone series, ring strain and thermodynamic polymerizability increases with increasing the ring size, *i.e.* from five to seven. The ROP of lactones and lactides can occur through five polymerization methods, namely, anionic, cationic, organocatalytic, enzymatic and “coordination-insertion” polymerizations. Polyesters thus formed can be readily chain-end

functionalized using either a functional termination agent and/or a functional initiator. By altering the catalyst or initiator and the termination reaction, the nature of the functional groups can be varied to fit the application of the final polymer.



**Scheme 1.2.** ROP of unsubstituted lactones, lactides and glycolides.

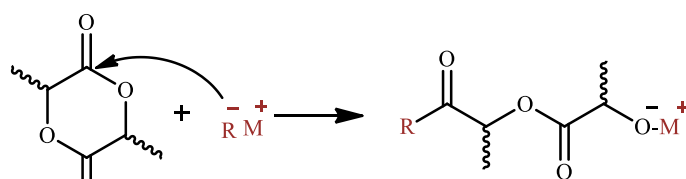
#### 1.5.2.1. Anionic Ring-Opening Polymerization

From a mechanistic point of view, anionic ROP of cyclic esters has been demonstrated to occur *via* acyl-oxygen cleavage except for  $\beta$ -lactones.<sup>[38]</sup> The initiation step can occur either by the nucleophilic attack of a negatively charged initiator on the carbon of the carbonyl function, or by attack of anionic species (initiator) on the carbon atom (deprotonation) adjacent to the acyl-oxygen. The propagating species is negatively charged and is counter balanced with a positive ion. These two different initiation steps are easily differentiated by the end group analysis by NMR analysis, since the deprotonation pathway can be easily identified by the absence of initiator fragments, whereas the acyl-oxygen cleavage pathway can be identified from the ester end groups derived from the alkoxide initiators (Scheme 1.3, same for lactones).

One shortcoming associated to this method is the occurrence of side reactions, such as intramolecular transesterification or epimerization also referred to as “back biting”, which generally occurs at the latter stages of polymerization. As a consequence, polymerizations have to be stopped before completion to avoid these side reactions.

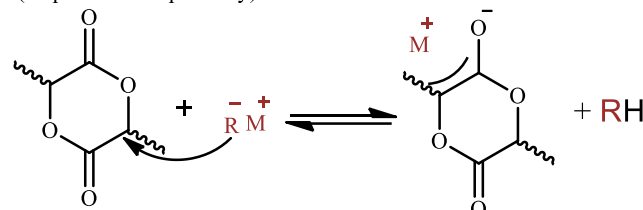


Nucleophilic attack (acyl-oxygen bond cleavage)



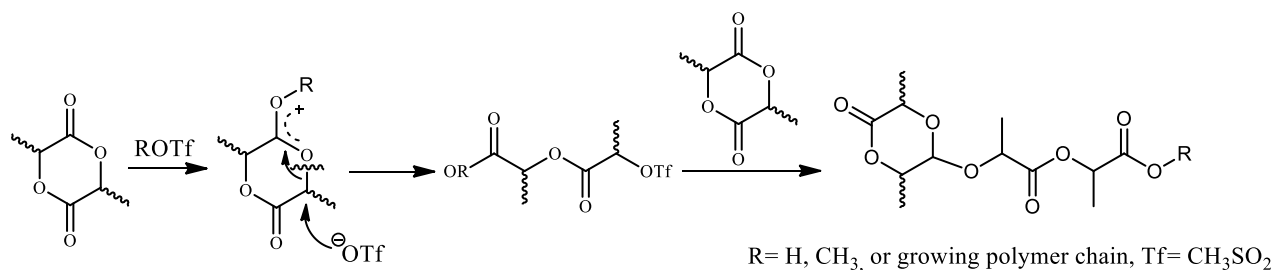
R = alkyl, alkoxy and M= Li, K, Mg

(Deprotonation pathway)

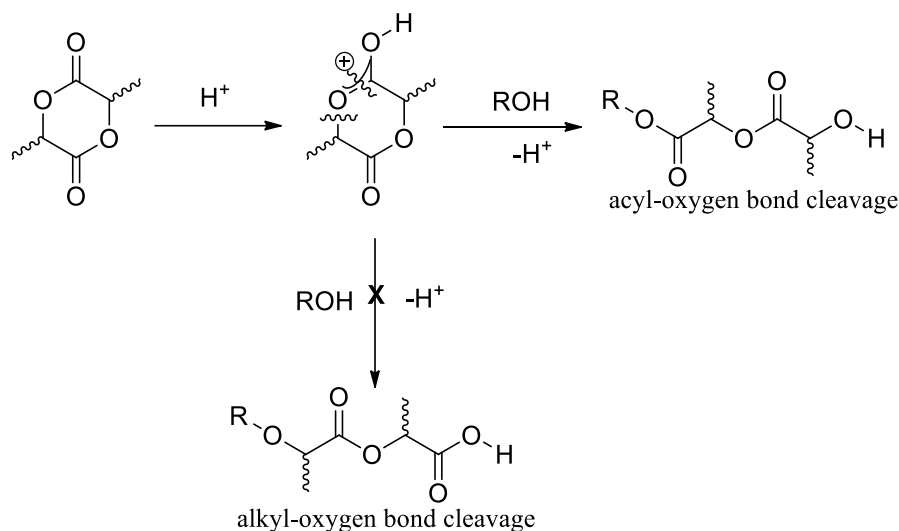
**Scheme 1.3.** ROP Mechanism.**1.5.2.2. Cationic Ring-Opening Polymerization**

The cationic ROP of lactides and lactones has been achieved using alkylating agents, acylating agents, Lewis acids, and Brønsted acids.<sup>[48]</sup> Kricheldorf *et al.* screened a variety of acidic compounds. Among them, trifluoromethane sulfonic acid (triflic acid, HOTf) and methyl triflate (MeOTf) proved to be useful initiators for the cationic ROP of LA.<sup>[93,94]</sup> End group analysis by <sup>1</sup>H NMR spectroscopy of the resulting PLAs indicated the presence of methyl ester end groups when MeOTf was used as the initiator, suggesting that the polymerization occurs *via* cleavage of alkyl-oxygen bond rather than the acyl-oxygen bond.

A two-step propagation mechanism was proposed involving activation of the monomer by methylation with (MeOTf) followed by S<sub>N</sub>2 attack on the triflate anion on the positively charged LA with inversion of configuration. Propagation was proposed to proceed by nucleophilic attack by LA on the activated cationic chain end with inversion in configuration, leading to net retention of the configuration (Scheme 1.4). Similar mechanism was proposed for the ROP of  $\epsilon$ -caprolactone by Khanna *et al.*<sup>[95]</sup> and Stridsberg *et al.*<sup>[96]</sup>

**Scheme 1.4.** Proposed pathway for cationic ROP of lactide.

More recently, Bourissou *et al.* reported on the controlled cationic polymerization of LA using a combination of the triflic acid as catalyst, and a protic reagent –typically water or an alcohol– as the initiator.<sup>[97]</sup> The polymerization proceeds *via* an “activated cationic polymerization mechanism” as originally proposed by Penczek,<sup>[98]</sup> where the acid would activate the cyclic ester monomer and the alcohol would be the initiator of the polymerization. Polymerization is therefore, thought to proceed by protonation of LA by triflic acid followed by nucleophilic attack of the initiating alcohol or that of the growing polymer chain, as shown in Scheme 1.5. Analysis of the polymer by <sup>1</sup>H NMR indicated isopropyl ester chain ends, suggesting that ring-opening proceeds by acyl bond cleavage and not by alkyl bond cleavage. Kim *et al.*<sup>[99]</sup> and Endo *et al.*<sup>[100]</sup> postulated for the same mechanism for the ROP of  $\epsilon$ -caprolactone.



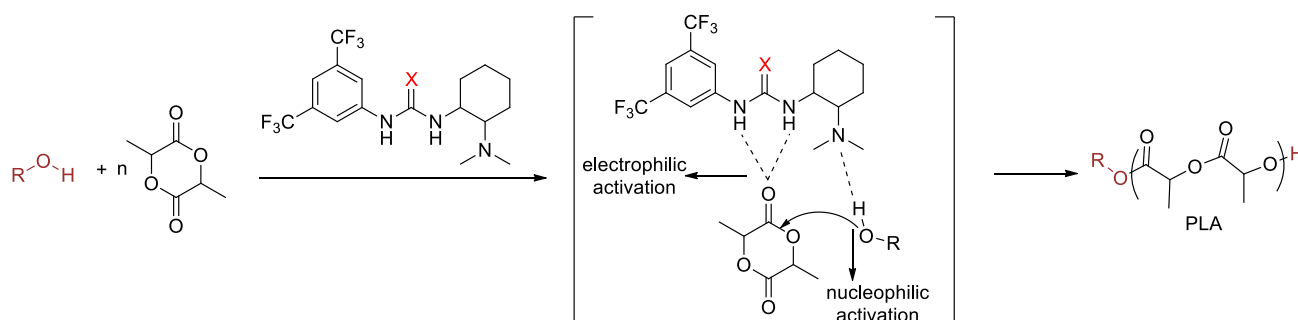
**Scheme 1.5.** Proposed activated monomer pathway for cationic ROP of lactide.

### 1.5.2.3. Organocatalyzed and Enzymatic ROPs

In recent years, organic catalysts have been successfully applied to the ROP of many heterocyclic monomers providing polymers free of metallic residue, which is particularly interesting in sensitive applications, for instance in the biomedical field or for microelectronics. In these approaches, the organic catalyst, e.g. amines, a phosphine, a carbene, an amino-thiourea, acts as an activator of the initiating/propagating species and/or of the monomer substrate (Scheme 1.6).<sup>[48,49]</sup>

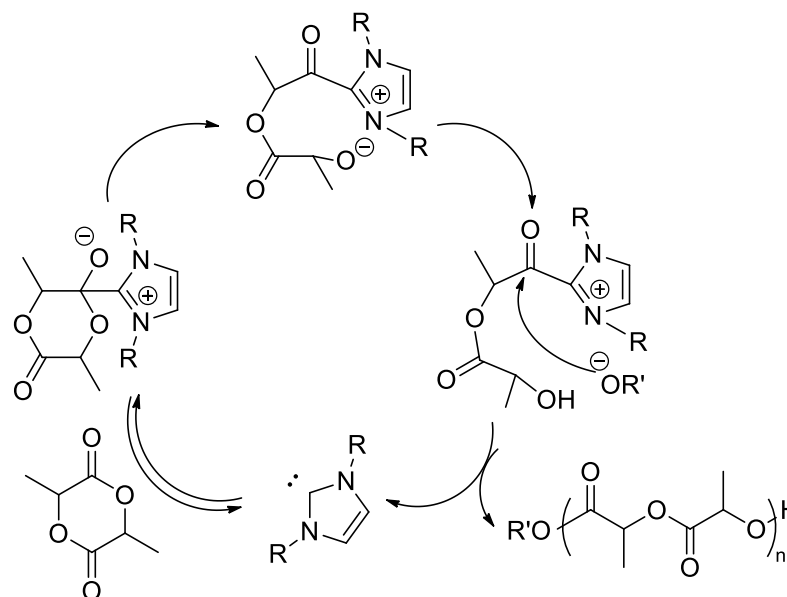
In this context, the bifunctional mechanism involving activation of both the monomer and the initiator/chain end is a very effective strategy for the controlled ROP of cyclic esters. One particular example for the ROP of lactide utilizes a thiourea-based bifunctional catalyst

consisting of both an electrophilic activating thiourea and a nucleophilic activating amine. Related mechanistic and theoretical studies have established the occurrence of hydrogen-bonding of the thiourea and the amine moieties.<sup>[101]</sup>



**Scheme 1.6.** Bifunctional activated mechanism using hydrogen bonding (thio)urea catalyst.

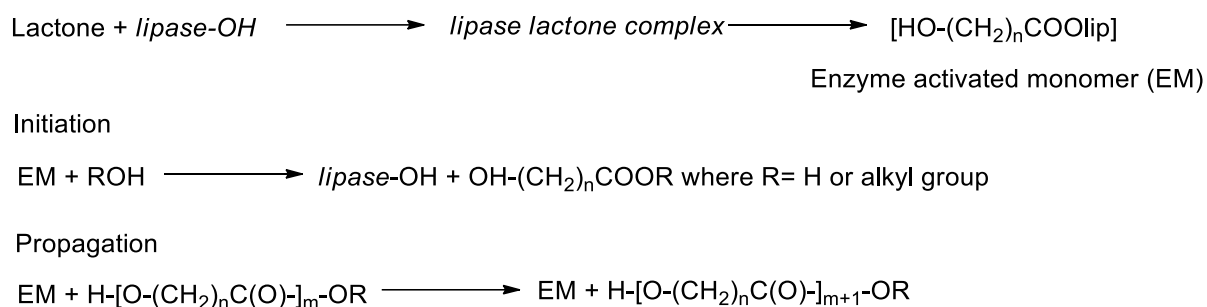
*N*-Heterocyclic carbenes (NHCs) represent another class of potent neutral organic catalysts, acting either as bases or as nucleophiles, for the ROP of lactide and lactones.<sup>[48,102–104]</sup> The polymerization has been initially proposed to proceed *via* a “Monomer Activated Mechanism” involving the formation of zwitterionic intermediates by the attack of the nucleophile (NHCs) on the carbonyl carbon of the lactide and lactones, followed by ring-opening of the tetrahedral intermediate to generate the acylimidazolium alkoxide zwitterions. Protonation of the alkoxide of the zwitterion by the initiating or chain-end terminated alcohol generates an alkoxide that esterifies the acylimidazolium to generate the open chain ester and the carbene (Scheme 1.7). Compelling evidence of nucleophilic mechanism in the ROP of LA has been provided in an attempt to generate zwitterionic ring-opening polymerization of lactide from the NHCs in the absence of alcohol initiator. These mechanistic studies led to the new strategy to generate cyclic polylactides.



**Scheme 1.7.** Plausible mechanism for the nucleophilic ROP of lactide.

Enzymatic polymerizations also appear as an alternative technique for producing metal-free polyesters. Kobayashi,<sup>[105]</sup> and Knani<sup>[106]</sup> first reported in 1993 the enzymatic bulk and solution ROPs of  $\epsilon$ -CL with the enzyme *Candida Antarctica* Lipase B. Generally, enzymes catalyze reactions with high enantio- and regio-selectivity and even under mild reaction conditions (*i.e.* temperature, pressure, pH, etc.)

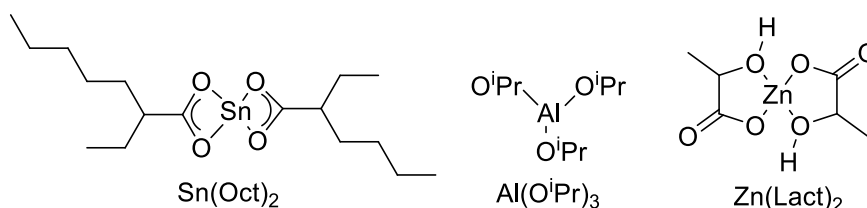
The lipase catalyzed polymerization of lactones is believed to proceed by an activated monomer mechanism. The key step is the reaction of the catalytic active serine residue of the enzyme with the cyclic ester leading to the formation of the acyl-enzyme intermediate. This intermediate reacts with water or alcohol to regenerate the enzyme and a  $\omega$ -hydroxycarboxylic acid or ester (Scheme 1.8). In the next propagation step, nucleophilic attack of the terminal hydroxyl group of the propagating polymer on the acyl-enzyme intermediate leads to the addition of one more unit to the chain and regeneration of the enzyme. More insights into the mechanism of lipase- catalyzed ROP of lactones are discussed in details in the review by Kobayashi *et al.*<sup>[107]</sup> Further advances in enzymatic ROP have been made and the polymerization of different monomers has been studied and reviewed.<sup>[48,108–110]</sup>



**Scheme 1.8.** Polymerization steps of lactones using lipase as a catalyst.

#### 1.5.2.4. Coordination- Insertion Ring-Opening Polymerization

Coordination-insertion ring-opening polymerization has been extensively used for the preparation of aliphatic polyesters with well-defined microstructure and architecture. The covalent metal alkoxides and carboxylates with vacant “d” orbitals act as coordination initiators and not as anionic initiators in this polymerization. The first generations of metal initiators are mainly constituted by simple homoleptic metal complexes. Tin(II)octanoate [Sn(Oct)<sub>2</sub>] as an active species precursor, aluminum(III)isopropoxide Al(O<sup>*i*</sup>Pr)<sub>3</sub> as an initiator, and zinc(II)lactate [Zn(Lact)<sub>2</sub>] are the most widely used complexes (Figure 1.10).<sup>[111]</sup>

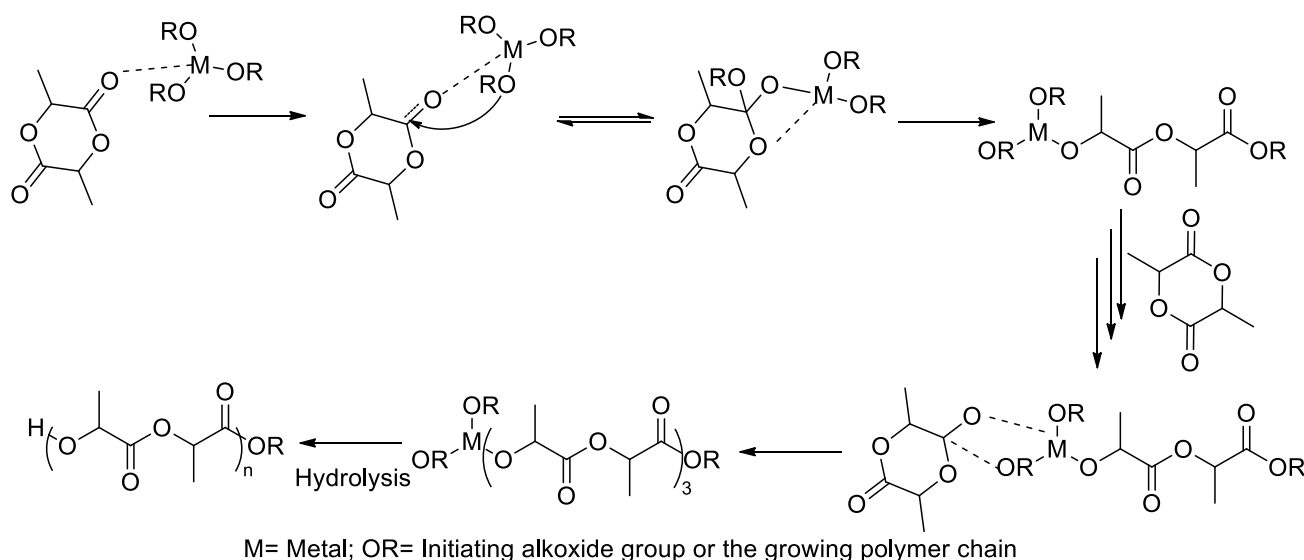


**Figure 1.10.** Structure of tin(II)octanoate, aluminum(III)isopropoxide, zinc(II)lactate.

Sn(Oct)<sub>2</sub> is commercially available, easy to handle, soluble in most of the organic solvents. It activates exogenous alcohols by *in situ* generation. It is highly active under melt polymerization conditions, *i.e.* in a range of temperatures of 140-180 °C. Typical reaction times require a few minutes to hours. Al(O<sup>*i*</sup>Pr)<sub>3</sub> also proves to be an efficient initiator and has been mostly used for mechanistic studies, its activity being less than that of Sn(Oct)<sub>2</sub> due to some kind of aggregation phenomenon, *i.e.* due to the presence of equilibrium between the tetramer and trimer structure of Al(O<sup>*i*</sup>Pr)<sub>3</sub>.<sup>[112]</sup> Zinc(II)lactate is a potential nontoxic catalyst, commercially available, and its activity is in the range of Al(O<sup>*i*</sup>Pr)<sub>3</sub>.<sup>[113]</sup> These first generations of metal catalysts/initiators have been widely used for the controlled ROP of cyclic esters and have brought important contributions for the mechanism understanding.

In 1971, Dittrich and Schulz were the first to suggest a three-step coordination-insertion mechanism for the ROP of cyclic esters.<sup>[114]</sup> Kricheldorf *et al.*<sup>[115]</sup> and Teyssie *et al.*<sup>[116]</sup> demonstrated the first experimental proof for such a mechanism in the  $\text{Al}(\text{OiPr})_3$  initiated polymerization of lactide.

The coordination-insertion mechanism of lactide polymerization involves the coordination of the monomer to the Lewis-acidic metal center (Scheme 1.9), which enhances the electrophilicity of the carbonyl group and the nucleophilicity of the alkoxide (OR) group. The monomer is then inserted into one of the metal alkoxide bonds *via* nucleophilic addition of OR group on the carbonyl carbon, followed by ring-opening *via* acyl oxygen cleavage. The chain propagation continues by the subsequent monomer addition. Hydrolysis of the metal alkoxide bonds leads to a polymer chain having a hydroxyl end group.



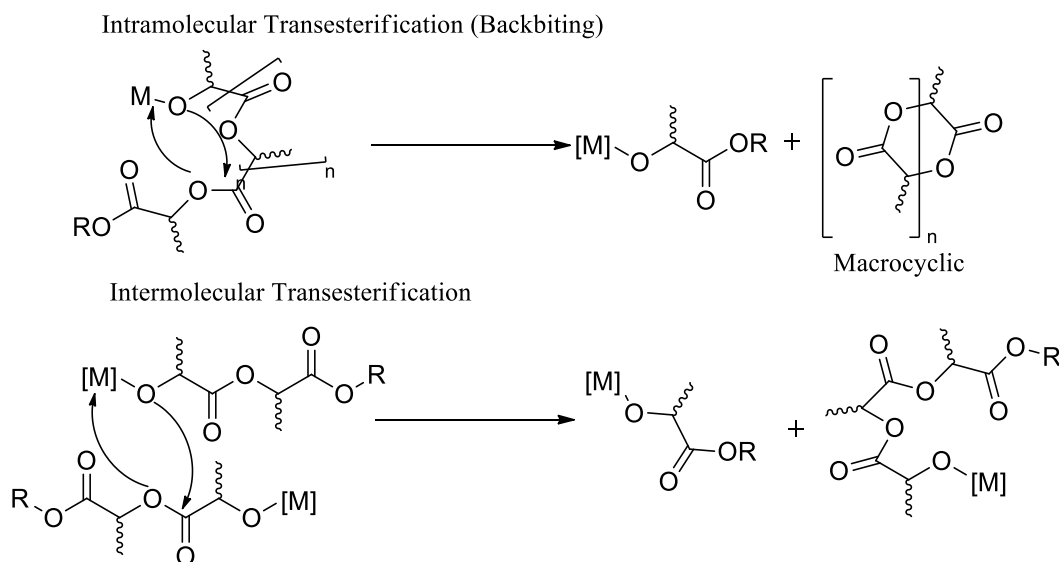
**Scheme 1.9.** Coordination-insertion mechanism for lactide polymerization using metal alkoxide catalyst.

However, although tin-, aluminum- and zinc-based catalytic systems proved to be quite convenient -in terms of activity, polymerization control and mechanism- for the ROP of cyclic esters, such homoleptic metal alkoxide complexes,<sup>[38]</sup> may sometimes present some drawbacks:

- **Multiple nuclearities:** The presence of multiple active metal sites present in the catalyst structure can initiate more than one growing polymer chain from each metallic center and the control of molar mass distribution is complicated by the clustered form of these active

species, *i.e.* the exact nature of active site is not always very well-known because of possible aggregation.

- Homoleptic nature of these species results in detrimental side reactions such as transesterification that can occur both intramolecularly (also called backbiting, leading to macrocyclic structure and shorter chains) and intermolecularly (chain redistributions; see Scheme 1.10). These side reactions lead to polymer with broader molar mass distributions and unpredictable molar mass. The extent of these transesterification reactions depends on the polymerization temperature and the type of metallic initiator.<sup>[115,117]</sup> For example with  $\text{Sn}(\text{Oct})_2$ , these side reactions occur at the very beginning of the polymerization leading to broad molar mass distributions, ( $M_w/M_n = \bar{D}$  values around 2) whereas these side reactions occur at high or even complete monomer conversion with  $\text{Al}(\text{OiPr})_3$  leading to lower  $\bar{D}$  (less than 1.5).



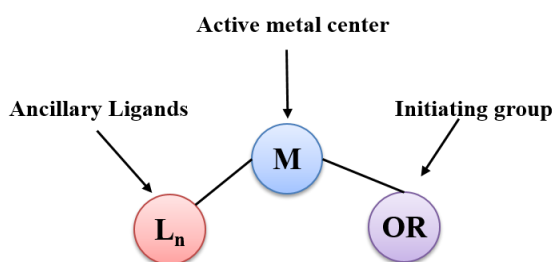
**Scheme 1.10.** Schematic representations for the transesterification side reactions.

In order to overcome these problems, well defined catalysts bearing supporting ligands were developed to control the structure of the corresponding heteroleptic complexes. This second generation of catalytic systems, namely, so-called single site catalysts, attracted interests as a means to achieve better control, activity, and selectivity of the polymerization.

Single-site metal catalysts for olefin polymerizations have provided some of the most spectacular advances in controlled polymerization in recent years and have made available a plethora of new materials.<sup>[118]</sup> Thereby some of these catalysts lead to controlled polymerization, namely, a process involving minimal chain transfer, combined with fast initiation. Such process may be defined as a “living” polymerization that lead to polymers of

predetermined molar mass (achieved by the specific monomer/catalyst ratio chosen) and narrow molar mass distributions ( $\bar{D}$  approaching 1.0).

Single-site catalysts dedicated to cyclic esters ROP are of the form  $L_nM-OR$ , where the alkoxide group (OR) is capable of propagation, M is the active metal center, and  $L_n$  are ancillary ligands that are not directly involved in the polymerization but can tune the properties of the metal center and minimize the aggregation process and side reactions (Figure 1.11). These catalysts are conceptually different from typical homoleptic catalysts of the form  $M(OR)_n$ , which do not possess a permanent ancillary ligand.



**Figure 1.11.** Representation of the single site catalysis of the form  $L_nM-OR$ .

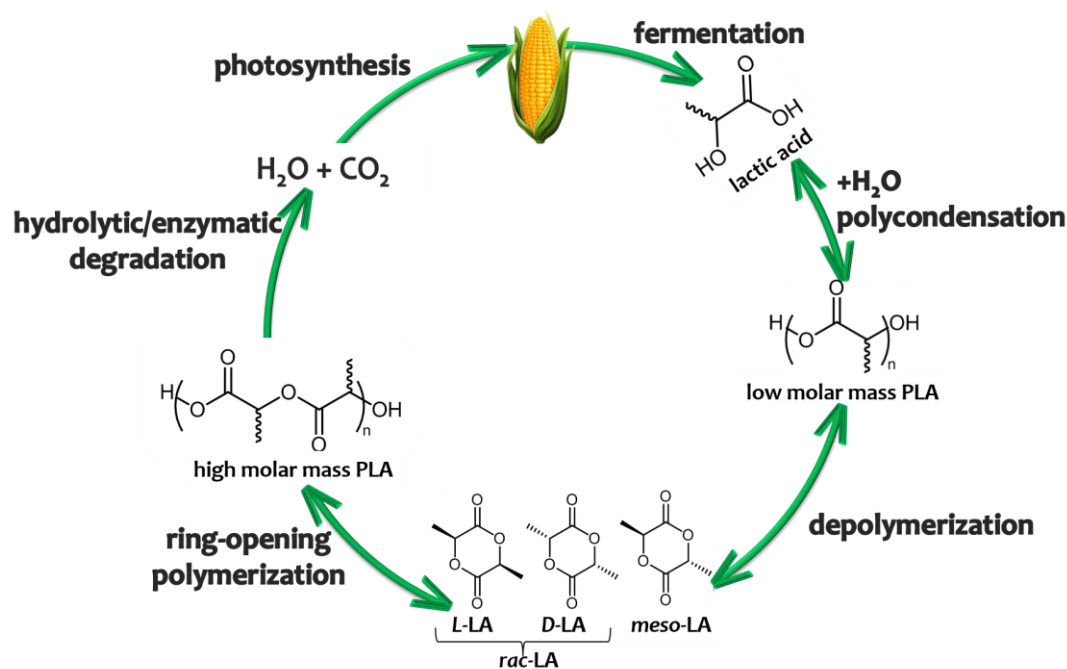
## 1.6. Polylactide

### 1.6.1. Generalities on PLA

Poly (lactic acid) or Polylactide (PLA) is a biodegradable, biocompatible, thermoplastic, aliphatic polyester derived from 100% renewable resources such as corn, sugar beets, and dairy products. As PLA is biodegradable and its degradation products ( $H_2O$  and  $CO_2$ ) are non-toxic, it has found numerous applications in the biomedical field, such as absorbable stitches, resorbable medical implants, disposable degradable plastic articles, scaffolds for tissue engineering,<sup>[119]</sup> and matrixes for controlled drug release of pharmaceuticals.<sup>[120]</sup>

More recently, applications of PLA as a substitute for the traditional thermoplastics derived from fossil fuels, e.g., in packaging films, are being developed.<sup>[111]</sup> Large scale manufacturers are very keen to PLA because of its renewable and easy biodegradable properties. Life cycle of PLA is shown in Figure 1.12.<sup>[88]</sup> Copolymerization of lactide with other monomers like glycolide or lactones can significantly enhance the properties and broaden the use of polylactide.<sup>[121,122]</sup> A wide range of degradation rates, physical and mechanical properties, can be reached by varying its molar masses and composition in the copolymers.

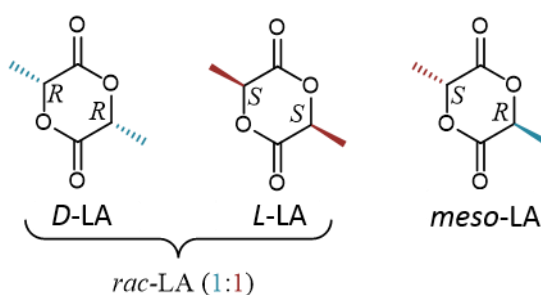




**Figure 1.12.** Life cycle of PLA

### 1.6.2. Stereochemistry and microstructures of PLA

PLA materials prepared by ROP of lactide can exhibit different microstructures. The lactide (LA) monomer, indeed, exists in the form of different stereoisomers, *RR*, *SS*, and *RS*. An *RR* configuration is referred to as *D*-lactide, *SS* is referred to as *L*-lactide, and *RS* is referred to as *meso*-lactide, as shown in Figure 1.13. A mixture of equal amounts of *D* and *L*-lactide is referred to as the *racemic* or *DL*-lactide.



**Figure 1.13.** Stereoisomers of LA

Control of the polymer microstructure has been demonstrated to significantly affect the physical properties of PLA. Differences in tacticity have for instance been shown to result in altered polymer melting ( $T_m$ ) and glass transition ( $T_g$ ) temperatures such that heterotactic PLA displays a  $T_m$  of 130 °C, enantiopure PLLA possesses a  $T_g$  of ~50 °C and  $T_m$  = 180 °C and a 50:50 mixtures of PLLA and PDLA displays a comparable  $T_g$  to PLLA but a significantly

increased  $T_m$  of *ca.* 230 °C (Table 1.2). This increased melting point is attributed to the formation of a stereocomplex,<sup>[123]</sup> most significant in a 1:1 mix of polymer chains (*ca.* 50 °C). Stereocomplexation is also observed in stereoblock copolymers and therefore can be accessed through the application of *rac*-lactide as a feedstock. The formation of the stereocomplex is related to the increase in crystallinity when the opposite chains of PLLA and PDLA come together and form a much more stable structure than pure chains of either enantiopure component.

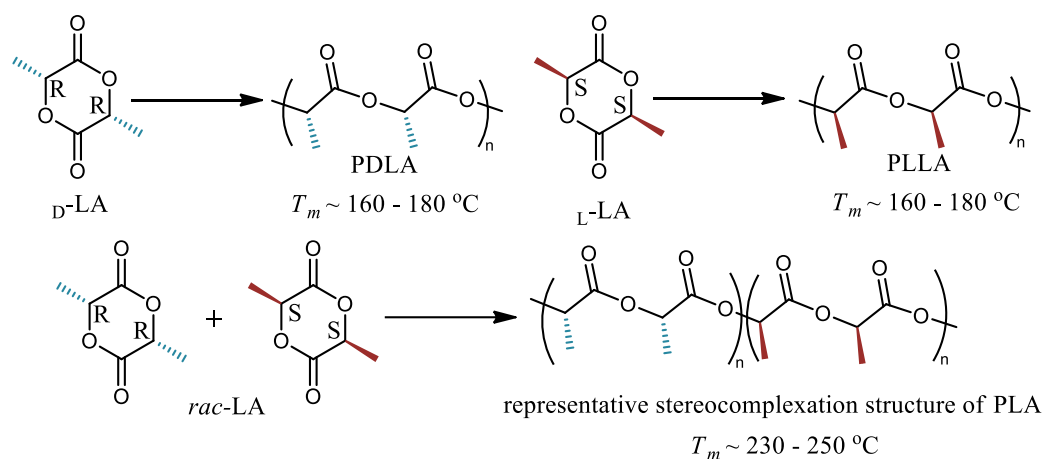
**Table 1.2.** Thermal properties of PLA polymers of different tacticities (Adapted from reference 123).

	$T_g$ (°C)	$T_m$ (°C)	Solid phase
Atactic (PDLLA)	50 - 60	-	Amorphous
Syndiotactic (PDLLA)	35	150	Semi-crystalline
Isotactic (PLLA or PDLA)	-	160 - 180	Semi-Crystalline
Stereoblock (PLLA- <i>co</i> -PDLA)	50 - 60	180 - 210	Semi-crystalline
Stereocomplex (PLLA + PDLA)	65 - 72	230 - 250	Semi-crystalline

Microstructures of ROP-derived PLAs are thus highly dependent on the type of monomer employed, and obviously on the overall polymerization conditions as well (Scheme 1.12).<sup>[124]</sup>

- Isotactic polylactides either poly(*L*-LA) or poly(*D*-LA), containing sequential stereocenters of the same relative configuration are prepared from enantiomerically pure *L*- and *D*-LA, respectively.
- Syndiotactic polymers namely poly(*meso*-lactide) contains sequential stereocenters of opposite configuration prepared from the *meso*-lactide by using a stereoselective catalyst.

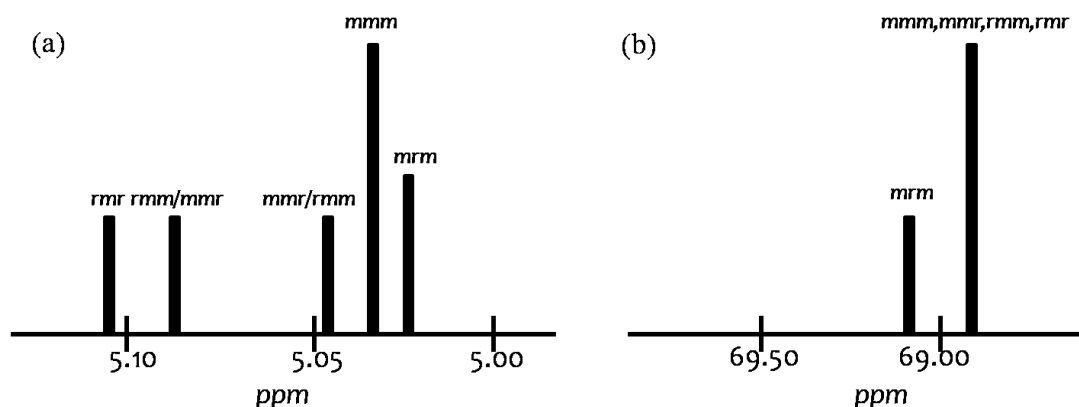
- Heterotactic polylactides contain regular alternation of *L*- and *D*-lactidyl units along the polymer chain afforded from the ROP of *rac*-lactide or *meso*-lactide.
- Stereoblock PLA contains alternating blocks of *D*- and *L*-lactides in the main chain afforded from the *rac*-lactide by using stereoselective catalyst.<sup>[44]</sup>



**Scheme 1.11.** Enantiopure PLLA and PDLA and corresponding stereocomplex

- Amorphous atactic polymers are afforded from the ROP of *rac*-lactide or *meso*-lactide with non stereoselective catalysts/initiators aluminum tris-(alkoxide)<sup>[112,116]</sup> or tin bis(carboxylate).<sup>[125]</sup> Atactic PLA thus features random placements of  $-RR-$  and  $-SS-$  stereosequences for *rac*-lactide and  $-RS-$  and  $-SR-$  stereosequences for *meso*-lactide.

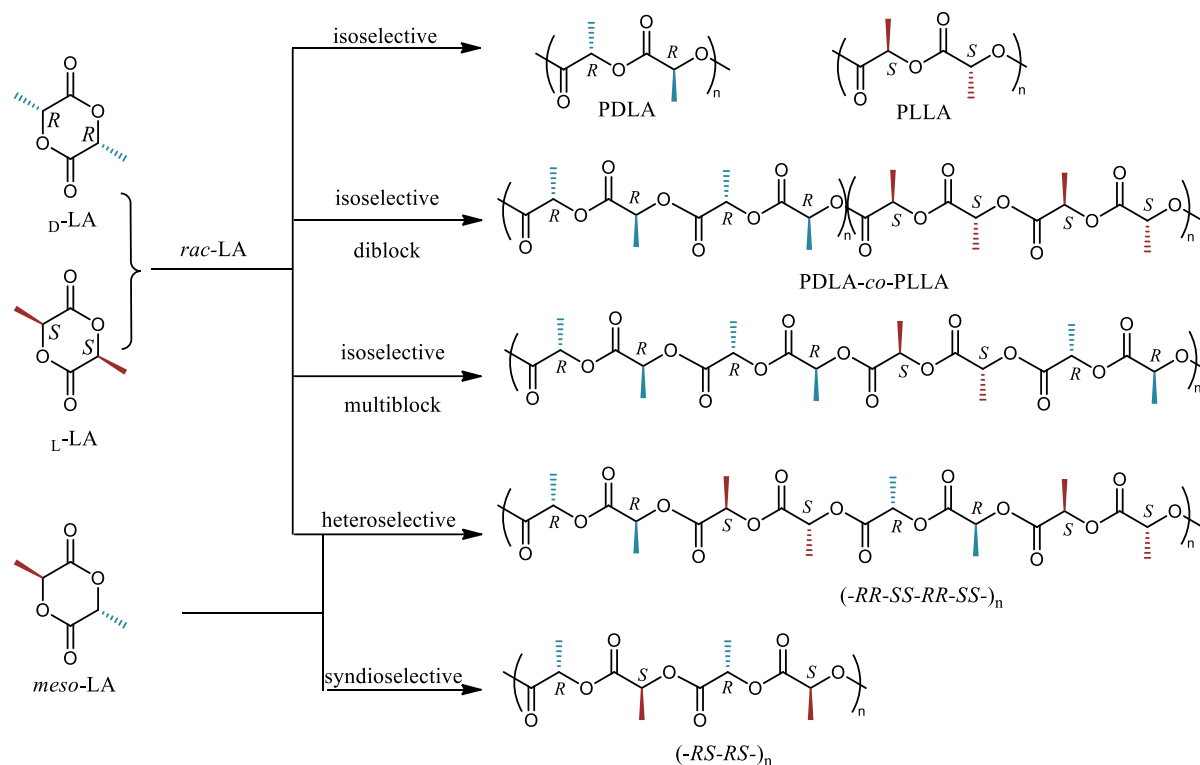
Stereosequence distribution in polylactide is most often determined by NMR spectroscopy, through inspection of the methine and / or carbonyl regions, namely, by  $^{13}\text{C}$  NMR and homonuclear decoupled  $^1\text{H}$  NMR. In order to decouple the effect of splitting between the methyl and methine protons, homonuclear decoupling of the methyl signal is carried out resulting in singlet resonances in the methine region ( $\delta = 5.15\text{--}5.25\text{ ppm}$ ). Adaptation of the Bovey formalism such that '*m*' describes a *meso* and '*r*' a *racemic* relationship between adjacent stereocenters provides a method for describing the tacticities of the polymer. At the tetrad level this is a three-letter sequence such that a chain of pure poly(*L*-lactide) will have a repeating tetrad of *LLLL* which would be represented by *mmm* whereas a pure heterotactic PLA would contain tetrads of both *LLDD* and *LDDL*, or *mrm* and *rmr*, respectively. It is worthy to note that in the absence of epimerization and transesterification the ROPs of *rac*- and *meso*-lactide result in different possible tetrad sequences (Figure 1.14).



**Figure 1.14.** Schematic diagrams to show chemical shifts (in ppm) of the tetrads for PLA in (a) homonuclear decoupled <sup>1</sup>H NMR of PLA from *rac*-lactide (Adapted from reference 39).

The degree of stereoregularity is expressed as the probability of racemic or meso enchainment (probability of forming a new racemic (syndiotactic) or meso (isotactic) dyad),  $P_r$  and  $P_m$ , respectively. These parameters can be directly calculated from the deconvoluted homonuclear decoupled <sup>1</sup>H NMR spectra<sup>[126,127]</sup> (see reference and section 1.5.3.2 for calculation). For both the ROP of *rac*- and *meso*-lactide,  $P_r$  or  $P_m = 0.50$  describes a completely atactic polymer. In the case of *rac*-lactide  $P_r = 1.00$  ( $P_m = 0.00$ ) and  $P_m = 1.00$  ( $P_r = 0.00$ ) describe perfect heterotactic and isotactic polymers, respectively, whereas for the ROP of *meso*-lactide  $P_r = 1.00$  ( $P_m = 0.00$ ) and  $P_m = 1.00$  ( $P_r = 0.00$ ) describe perfect syndiotactic ((-RSRSRS-)<sub>n</sub>) and heterotactic ((-RR-SS-RR-SS)<sub>n</sub>) polymers, respectively.<sup>[39]</sup>

- These types of stereoregular polymers should be achievable using well characterized, discrete single site catalytic systems. Several groups have reported the formation of both heterotactic ((RRSS)<sub>n</sub>) and isotactic stereoblock ((RR)<sub>n</sub>(SS)<sub>m</sub>) by well controlled metal alkoxide catalyzed ROP of *rac*-lactide.<sup>[40]</sup>



**Scheme 1.12.** Microstructures of PLA obtained by stereoselective ROPs of *rac*- and *meso*-LA. (Adapted from reference 39)

### 1.6.3. Stereoselective ROP of LA

The stereoselective ROP of racemic lactide (*rac*-LA) has received a considerable attention, because this can lead to semi-crystalline PLAs with improved mechanical properties and biodegradability.<sup>[112]</sup> For instance, enantiopure PLAs can form stereocomplexes upon mixing enantiomeric PLA chains at stoichiometry.<sup>125</sup> Such stereocomplexation allows enhancing both thermal properties, and the hydrolytic stability of PLA as well. Stereocomplex form of PLA shows a melting temperature as high as 230 °C, that is, higher of 50 °C compared to the homochiral crystals of either PLLA or PDLA.<sup>19</sup>

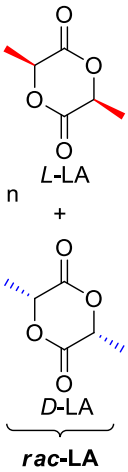
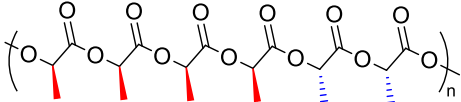
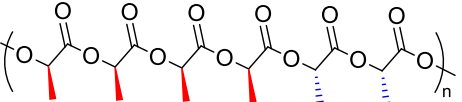
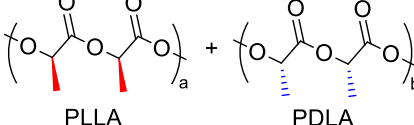
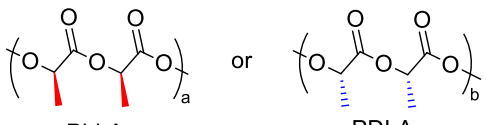
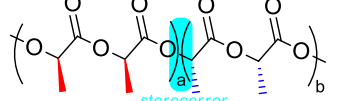
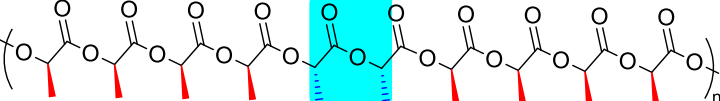

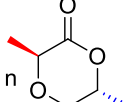
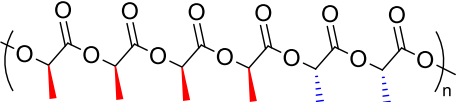
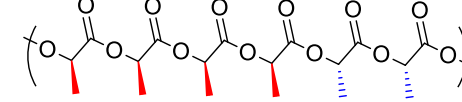
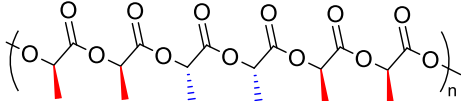
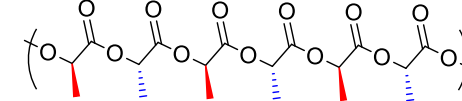
Isotactic PLA can be obtained by sequential polymerization of (*R,R*)-lactide or (*S,S*)-lactide with an achiral, living initiator. An alternative approach is to employ a more selective catalyst to affect the kinetic resolution of *rac*-lactide, *i.e.* a catalyst with a propagation rate constant for the preferred enantiomer that is much higher than the corresponding rate constant for the unpreferred enantiomer.

In the following sections, mechanisms that regulate the stereoselectivity are presented. Results pertaining to the synthesis of stereocontrolled PLAs will be summarized.

### 1.6.3.1. Mechanism of stereocontrol polymerization of lactide

Stereocontrolled ROP of *rac*-LA can operate following two distinct mechanisms, namely, the enantiomorphic site control mechanism (ESC) and the chain end control (CEC) mechanism. In the ESC mechanism, the chirality of the catalyst defines the stereochemistry of the subsequent monomer insertion during chain propagation. In the CEC mechanism, the stereochemistry of the last inserted monomer in the growing polymer chain influences which enantiomeric form of the monomer is incorporated next. There may happen undesired stereoerrors in the growing chain, which will reduce the tacticity when instead of inserting the new monomer in the same stereoregularity, it does reverse, disrupting the same regularity. Side reactions, such as epimerization or transesterification, can be the principal causes of stereoerrors, rather than the wrong enantiofacial selection at the insertion step. However, stereoerrors result in a stereoblock copolymer in preference to enantiopure polymer chains are a result of insertion stereoerrors rather than chain transfer. Although, the formation of enantiopure PDLA and PLLA chains is possible under perfect kinetic resolution conditions, the degree of selectivity, chain exchange and insertion of stereoerrors will influence the polymer microstructure. In this way multiblock (stereoblock) copolymers can be synthesized, in the case of large numbers of stereoerrors or significant chain transfer events.<sup>39</sup> In the case of enantiomorphic-site control mechanism, stereoerrors cause the shortening of the isotactic polymer chains, while resulting in the formation of stereoblocks in the case of chain-end control mechanism.

**Table 1.3.** Possible tacticities of PLA in the presence of chain-end and enantiomorph-site stereocontrol mechanisms during stereoselective ROP of *rac*- or *meso*-LA. (The reverse monomer sequencing is also possible considering to opposite enantioface of the catalyst used.)

	Chain-end Control Mechanism	Enantiomorph-site Control Mechanism
 $n$ L-LA + $n$ D-LA <i>rac</i> -LA	 atactic PLA	 atactic PLA
	 PLLA + PDLA	 PLLA or PDLA
	 isotactic diblock PLLA- <i>b</i> -PDLA (in the presence of a stereoerror)	 isotactic PDLA in the presence of a stereoerror
	 isotactic multiblock PLLA-co-PDLA (in the presence of multiple stereoerrors)	
 $n$ meso-LA	 atactic PLA	 atactic PLA
	 heterotactic PLA	 syndiotactic PLA

### 1.6.3.2. Mesotacticity analysis

As mentioned above, mesotacticity ratios can be analyzed using quantitative  $^{13}\text{C}$  NMR or homonuclear decoupled  $^1\text{H}$  NMR ( $^1\text{H}\{^1\text{H}\}$  NMR) techniques. The expression of the different tetrad ratios of PLA, as obtained by ROP of *rac*-LA, *D*-LA and *L*-LA, is summarized in the Table 1.3. below as a result of quantitative  $^{13}\text{C}$  NMR and homonuclear decoupled  $^1\text{H}$  NMR spectra (Figure 1.14).

According to Bernoullan and non-Bernoullan statistics (Table 1.3), it is usually assumed that *mmr* and *rmm* tetrad ratios are equal for poly(*DL*-lactide). Under the control of the CEC mechanism, Bernoullan statistics can be applied onto the mesotactic tetrad ratio. In this case, tetrad ratios are expressed as follows  $mmr = rmm \neq rmr$ . However, in case of

enantiomorphic-site control mechanism (ESC), non-Bernoullan statistics are applied and the tetrad ratios can be written as:  $rmr = mmr = rmm = mrm/2$ .<sup>[44]</sup>

**Table 1.4.** Tetrad probabilities of ESC and CEC mechanisms based on non-Bernoullan and Bernoullan statistics

tetrad	Probability of ESC (non-Bernoullan)	Probability of CEC (Bernoullan)
<i>mmm</i>	$[P_m^2 + (1 - P_m)^2 + P_m^3 + (1 - P_m)^3]/2$	$P_m^2 + 0.5 P_m P_r$
<i>mmr</i>	$[P_m^2(1 - P_m) + P_m(1 - P_m)^2]/2$	$0.5 P_m P_r$
<i>rmm</i>	$[P_m^2(1 - P_m) + P_m(1 - P_m)^2]/2$	$0.5 P_m P_r$
<i>rmr</i>	$[P_m^2(1 - P_m) + P_m(1 - P_m)^2]/2$	$0.5 P_r^2$
<i>mrmm</i>	$[P_m(1 - P_m)]$	$0.5 (P_m^2 + P_m P_r)$

### 1.6.3.3. Catalytic systems for stereoselective ROP of *rac*-LA

Stereoselective polymerizations achieving semi-crystalline polymers require highly effective and selective catalysts/initiators. Despite such major successes in the stereoselective ROP of LA by metal catalysts, inevitable contamination of the polymer product by metal trace residue can have non-negligible to even significant impacts on the overall quality of the final product, especially when it is applied to biomedical or microelectronic fields. Such considerations have provided a strong incentive for intensified research in utilizing metal-free organocatalysts in the ROP of cyclic esters, especially lactide and  $\epsilon$ -caprolactone.<sup>[36,49]</sup>

#### 1.6.3.3.1. Organometallic catalysts

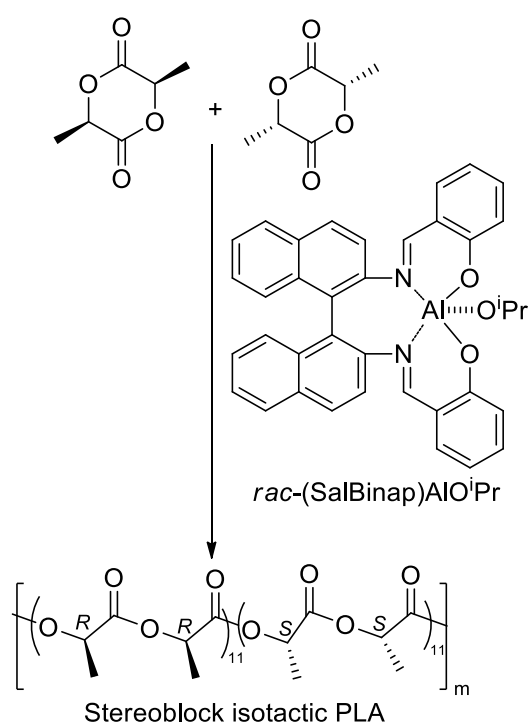
##### 1.5.3.3.1.1. Tri- and tetra-dentate iminophenolato- and aminophenolato- (salen and salan) complexes

Tetradentate iminophenolates (salicaldimine or salen) and aminophenolates (salicaldamine or salan) have been widely applied as ligands in the area of stereocontrolled ROP of lactide.<sup>[39]</sup> Initial works in 1993 by Spassky *et al.* employed a single (+)-enantiomer of a chiral BINAP-derived salen–aluminum complex, (+)**1**, (Figure 1.15a) to mediate the ROP of *rac*-LA.<sup>[128]</sup> At low monomer conversion, it was identified that the growing polymer chain consisted of almost exclusively *D*-lactide (up to 88% enantiomeric enrichment at 19% conversion), although at higher conversion both enantiomers of the monomer were incorporated. An increase in the melting point of these polymers was observed when high



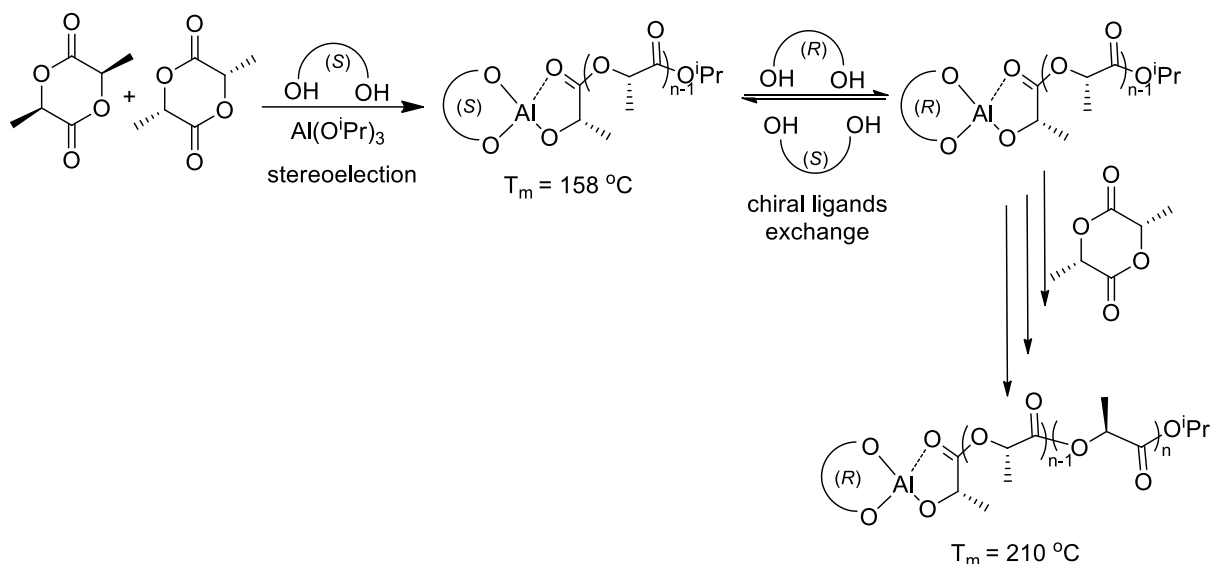
conversion was reached, suggesting that stereocomplexation was occurring by formation of a tapered stereoblock microstructure.<sup>[22,129]</sup>

Later on the same catalyst was shown by Ovitt and Coates to produce syndiotactic PLA from *meso*-lactide.<sup>[130]</sup> Radano *et al.* further identified that, through the application of both enantiomers of the catalyst, it was possible to produce stereocomplex PLA simultaneously in the polymerization ( $T_m = 179\text{ }^{\circ}\text{C}$ ).<sup>[42]</sup> This catalytic system was thought to achieve pure PDLA and PLLA from *rac*-LA using different catalyst enantiomers. However, Ovitt and Coates *et al.* demonstrated that the polymer produced was actually a stereoblock copolymer with an average block length of 11 lactide monomer units (Scheme 1.13).<sup>[131]</sup>



**Scheme 1.13.** Synthesis of stereoblock PLA using *rac*-(SalBinap)AlOiPr.

Due to the presence of chiral ligands, these catalysts were postulated to provide stereocontrol by the ESC mechanism. Majerska and Duda *et al.* demonstrated that the same catalyst system could be utilized to synthesize a true PLLA–PDLA stereoblock copolymer through a ligand exchange mechanism (Scheme 1.14).



**Scheme 1.14.** Synthesis of PLLA-PDLA stereoblock copolymer through a ligand exchange mechanism. (Adapted from reference 134)

Such a mechanism involves initiation from one enantiomer of the catalyst with addition of the opposite enantiomer at 50% lactide conversion, enabling the synthesis of a stereoblock copolymer through chain transfer. The polymer synthesized in this way exhibited a melting point of  $210\text{ }^\circ\text{C}$ , indicative of a stereocomplexation behavior very similar to that of a 50:50 mixture of pure PLLA and PDLA.<sup>[46]</sup> It was recognized that the ligand chirality, polymer chain end and even the solvent played a crucial role in the stereocontrol.<sup>[132]</sup>

Subtle changes in the backbone of the salen ligands were postulated to result in a complex adopting different stereoisomers in response to a chiral chain end, greatly influencing the outcome of the stereocontrol. Feijen *et al.* thus investigated the application of comparable, more simply derived catalysts (Figure 1.15b) based around the cyclohexyl backbone and commercially available Jacobsen's ligand, **2** (both *R,R*- and *rac*-derivatives).<sup>[12,45]</sup> Application of the enantiopure *R,R*-**2**, kinetic differences in the insertion rates of the *L*- and *D*-lactide monomers into the PLA chain were observed and resulted in high levels of isotactic enchainment, with a  $P_m$  equal to 0.92.

Notably, high levels of stereocontrol were reported for the first time ( $P_m = 0.88$ ) under melt polymerization conditions ( $130\text{ }^\circ\text{C}$ ). Such bulk conditions not only suppress the need for a solvent, but also overcome initiator solubility issues and decreased reaction times. The chirality of this Jacobsen-type catalyst was demonstrated to exert minimal control during the initial ring-opening event. Solvent played a key role, such that the opposite enantiomer of lactide to the last inserted stereocenters in the propagating polymer chain was found to be

inserted in chloroform and toluene suggesting that the high levels of stereocontrol are exerted by a chain end control mechanism.<sup>[133]</sup> Transesterification side reactions and epimerization forming *meso*-LA were found negligible with this catalytic system. Transesterification reactions were noticeable only after significant prolonged reaction times. These observations suggested that, the main reason for obtaining stereoblock copolymers instead of enantiopure PLA chains using enantiopure catalysts is stereoerrors rather than chain transfer.

Several achiral salen-based catalysts were also demonstrated to display very high levels of stereocontrol in the ROP of *rac*-LA. By application of a sterically hindered ligand, **3**, (Figure 1.15c) Nomura *et al.* succeeded in synthesizing stereoregular heterotactic PLA with a  $P_r = 0.81$ .<sup>[14]</sup> These achiral catalysts are postulated to provide stereocontrol *via* a CEC mechanism. While the high levels of steric hindrance around the active metal center resulted in reduced rates of the polymerization, the concurrent increase in the energy barrier of lactide coordination to the metal enabled excellent stereocontrol.

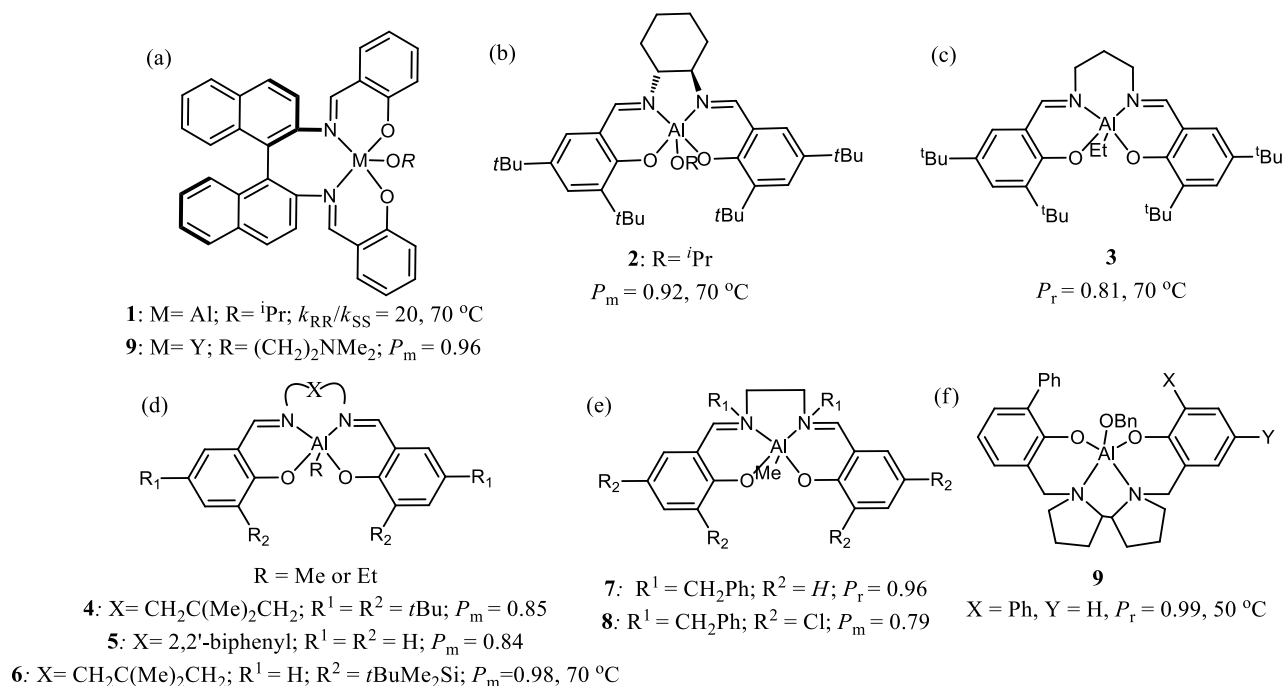
More recently, Nomura *et al.* and Hormnirun *et al.* independently reported the application of a wide range of differently substituted (salen)aluminum catalysts for the stereocontrolled ROP of *rac*-LA. In both cases, the aluminum alkoxide initiators were *in situ* generated from the corresponding aluminum alkyl and alcohol.

Gibson *et al.* reported extensive studies of the effect of variation of both backbone and phenoxy substituent of (salen) aluminum complexes on the kinetics and stereocontrol of the polymerization of *rac*-LA. In general, the increase in steric hindrance offered by bulky *o*-phenoxy substituents led to greater levels of stereocontrol, although the effect of imine linker unit (X, Figure 1.15d) was not so clear, such that  $-\text{CH}_2\text{C}(\text{R}_2)\text{CH}_2-$ , **4**, and 2,2'-biphenyl, **5**, groups led to the highest levels of isotactic enchainment ( $P_m = 0.85$  and  $P_m = 0.84$ , respectively).<sup>[47]</sup>

Nomura *et al.* subsequently reported their investigations of a wide range of differently substituted salen ligands, varying the imine spacer to examine ethyl and a range of substituted propyl ( $-\text{CH}_2\text{C}(\text{R}_2)\text{CH}_2-$ ) groups as well as the *o*- ( $\text{R}^1$ , Figure 1.15d) and *p*-phenoxy ( $\text{R}^2$ , Figure 1.15d) substituents. The longer and the less rigid units led to the highest stereocontrol in combination with the most sterically hindering ortho-substituents (para-substituents had indeed little effect on the stereocontrol). In this way a ligand structure with a  $-\text{CH}_2\text{C}(\text{R}_2)\text{CH}_2-$  imine linker and a *t*-BuMeSi *o*-phenoxy substituent, **6**, (Figure 1.15d) resulted in very high levels of stereo- selectivity ( $P_m = 0.98$ ) for the ROP of *rac*-LA in toluene solution at 70 °C, reducing to  $P_m = 0.92$  under bulk polymerization conditions at 210 °C.<sup>[43]</sup>

Gibson *et al.* also extensively investigated the effect of a variation of salen ligands on the stereocontrol of the ROP of *rac*-LA (Figure 1.15e).<sup>[134]</sup> By a careful manipulation of the ligand substituents, both the nature of the stereoselectivity (*meso* vs. *racemo*) and the magnitude of that selection could be manipulated, such that a range of PLA tacticities (for *rac*-LA ROP) from  $P_r = 0.96$  to  $P_m = 0.79$  (with catalyst **7** and **8**, respectively) could be achieved. In all of these studies, the electron withdrawing phenoxy substituents generally increased the rate of the ROP reactions, while sterically encumbering groups in ortho-position resulted in slower rates but allowed reaching a higher stereoselectivity.

Stereocontrol was also generally improved through increased backbone flexibility, possibly due to the ease with which the sterically hindered process, such as monomer approach could be facilitated. Tang *et al.* further demonstrated the importance of this linker by making use of extended ligand backbones to achieve  $P_m = 0.90$ .<sup>[135]</sup>



**Figure 1.15.** Tetradentate (imino- and amino-phenolato) aluminum complexes for stereoselective lactide ROP.

Yttrium-based salen and salan supported complexes were also shown to mediate the stereoselective ROP of *rac*-LA. While Ovitt, Coates *et al.* showed that a (salen)-yttrium complex, **9**, demonstrated no effect on stereocontrol in the polymerization<sup>[44]</sup> (the analogous aluminum catalyst results in high levels of isotacticity,  $P_m = 0.96$ ), Liu *et al.* could polymerize *rac*-LA with modest heteroselectivity ( $P_r = 0.69$ ) with both salen and salan based yttrium complexes.<sup>[136]</sup>

Phophalen indium complexes were reported as highly selective sterically hindered achiral organometallic catalysts to favor the CEC mechanism, leading to  $P_m = 0.85 - 0.92$  at 25 °C.<sup>[137]</sup>

The large amount of research in this area resulted in a significant library of catalysts with a broad array of ligand structures allowing for a complete range of PLA microstructures to be synthesized by judicious catalyst selection. Salen–salan aluminum-based complexes also have the advantage that the active species, namely, the aluminum alkoxide, can be generated *in situ* from the appropriate alkyl aluminum complex and alcohol. Recent reports indeed showed that this facilitated control over the PLA chain end and the chain topology, *i.e.* linear, telechelic and star-shaped PLAs could be readily achieved.<sup>[138]</sup>

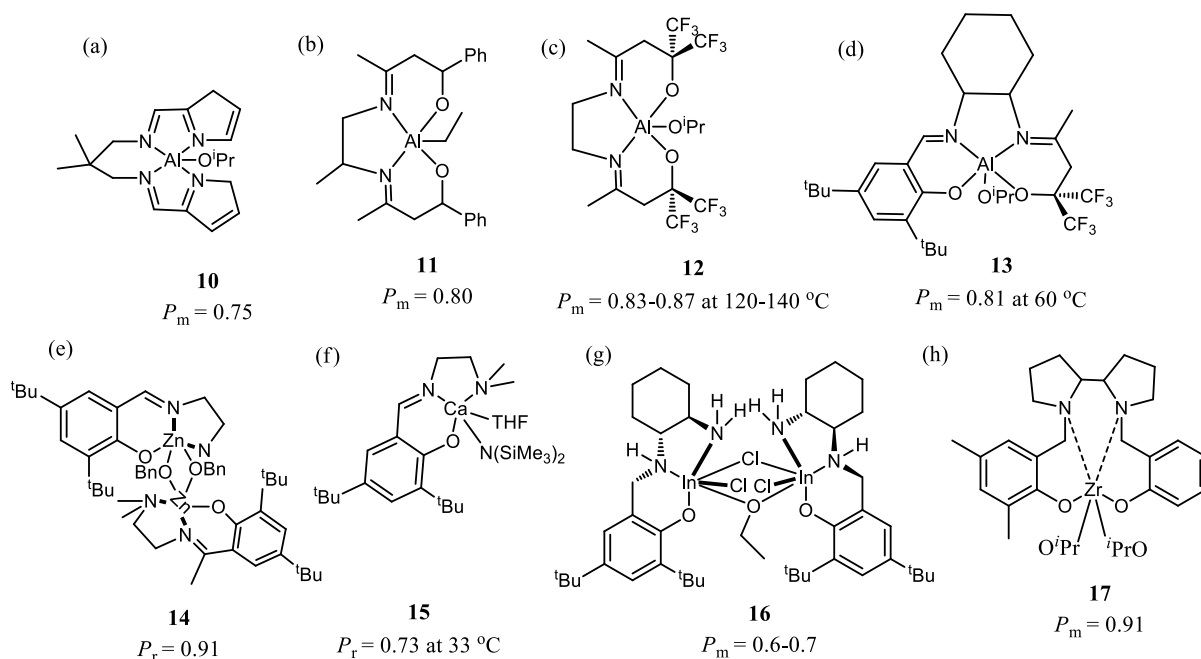
Several other tetradentate and tridentate Schiff base ligands were also applied as catalysts for the ROP of *rac*-LA. Achiral bis(pyrroline) Schiff base aluminum alkoxides, **10**, (Figure 1.16a) mediated a moderately isospecific ROP of *rac*-LA ( $P_m = 0.75$ ).<sup>[139]</sup> Notably, these catalysts showed very little stereocontrol ( $P_r = 0.59$ ) for the ROP of *meso*-LA, with no correlation between ligand substituents and stereocontrol.

Enolic tetradentate Schiff base aluminum catalysts, **11**, (Figure 1.16b) were also employed for the ROP of *rac*-LA, resulting in appreciable stereocontrol ( $P_m = 0.80$ ).<sup>[140]</sup> A similar system was employed by Carpentier *et al.* in which electron withdrawing trifluoromethyl groups were located adjacent to the alkoxides, **12**, (Figure 1.16c).<sup>[141]</sup> No difference in PLA tacticity was noted when either chiral or achiral ligands were applied, suggesting that stereocontrol was again determined by a CEC mechanism ( $P_m = 0.83\text{--}0.87$  under melt conditions of 120–140 °C). The same authors also examined the application of a mixed fluororous alkoxy–phenolate Schiff base ligand, **13**, (Figure 1.16d) that also led to isotactic PLA at 60 °C in toluene solution ( $P_m = 0.81$ ).<sup>[142]</sup>

Tridentate Schiff base ligands (NNO) with hindered substituents were demonstrated to provide high stereocontrol with zinc-, calcium- and indium-based catalysts. The zinc analogues (Figure 1.16e) produced highly heterotactic PLA from the ROP of *rac*-LA ( $P_r = 0.91$ ).<sup>[143]</sup> Reduction in hetero-specificity was observed with reduction of steric hindrance ( $P_r = 0.59\text{--}0.65$ ) and presence of both monomeric and dimeric species in solution, as indicated by <sup>1</sup>H NMR studies at ambient temperature.

Calcium-based analogues (Figure 1.16f) were also shown to enable stereocontrol in THF at 33 °C ( $P_r = 0.73$ ).<sup>[144]</sup> Mehrkhodavandi *et al.* employed a tridentate Schiff base indium

catalyst, **16**, that formed a dimeric initiating species through a single bridging ethoxido and chlorido ligands (Figure 1.16g).<sup>[145]</sup> The mechanism was thought to involve an equilibrium between an active monomeric lactate species and the inactive dimeric form of the catalyst (**16**) and results in modest stereocontrol ( $P_r = 0.6$ – $0.7$ ). Tridentate Schiff base ligands (NNO) within zirconium (Figure 1.16h,  $P_r = 0.91$ )<sup>[146,147]</sup> and calcium ( $P_r = 0.73$ ) metals also demonstrated as highly efficient for the stereoselective ROP of *rac*-LA.<sup>[144,145,148]</sup>



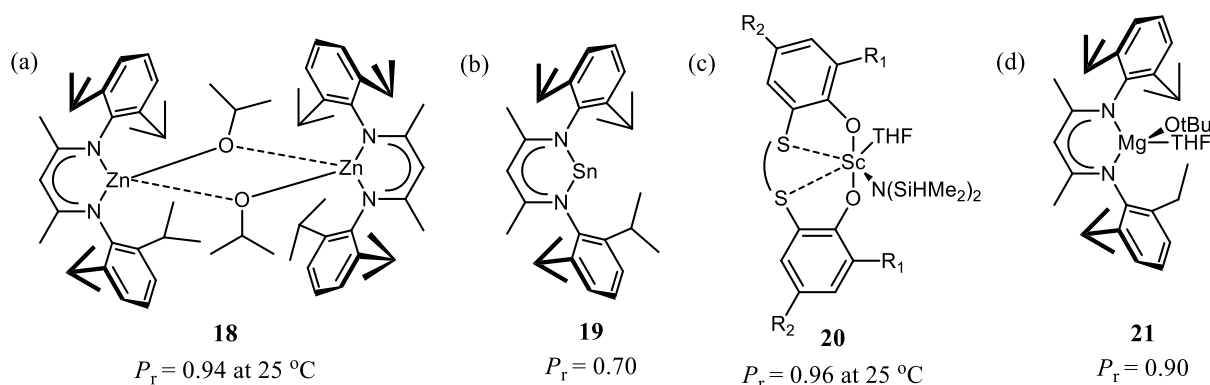
**Figure 1.16.** Tetradentate and Tridentate Schiff base metal complexes for stereoselective lactide ROP.

Very recently, racemic mixture of alkoxo-aluminum catalysts of chiral bipyrrrolidine-based salan ligands were described for synthesis of highly heterotactic PLA from *rac*-LA and syndiotactic PLA from *meso*-LA following exchange mechanism of CEC and ESC. *Meso*-LA insertions led to syndiotactic PLAs reaching a syndiotacticity degree of 0.96. This polymer featured a  $T_m$  of 153 °C matching the highest reported value, and the highest crystallinity ( $\Delta H_m = 56$  J/g) ever reported for syndiotactic PLA (Figure 1.15f).<sup>[149]</sup>

#### 1.5.3.3.1.2. $\beta$ -Diketiminato (BDI) complexes

$\beta$ -Diketiminato metal complexes were shown to provide powerful catalysts for the stereospecific ROP of *rac*-LA. Cheng *et al.* demonstrated that a ( $\beta$ -diketiminato) zinc isopropoxide species, **18** (Figure 1.17a) was able to mediate the highly heterospecific ROP of *rac*-LA ( $P_r = 0.94$ ) at ambient temperature, also providing a high activity (complete within 20 minutes for a targeted DP = 200).<sup>[150]</sup> Variation of the initiating group revealed that

polymerization could be initiated using alkoxide, acetate, alkyl, lactate and amide species although only alkoxide and lactate afforded controlled polymers with narrow dispersity, a consequence of their analogous nature to the putative chain end of the growing polymer.<sup>[151]</sup> Subsequent research showed that control of the substituents in the  $\beta$ -diketiminato (BDI) system combined both good stereocontrol and high rate of polymerization.<sup>[56,151]</sup> Decrease of the steric hindrance of the ortho-substituents on the aromatic rings of the ligand, to ethyl and *n*-propyl groups, decreased the extent of stereocontrol ( $P_r = 0.79$  and  $0.76$ , respectively) suggesting that the ROP took place *via* a CEC mechanism, as also supported by the increased levels of heterotacticity at lower temperature ( $P_r = 0.94$  at  $0^\circ\text{C}$ ).



**Figure 1.17.** ( $\beta$ -Diketiminato) metal complexes for catalysis of stereospecific lactide ROP.

BDI-based complexes based on tin(II) and magnesium also proved to lead to notable levels of stereocontrol ROP of *rac*-LA. DBI-tin(II) isopropoxide, **19**, (Figure 1.17b) and dimethylamide complexes were reported as first examples of stereoregular ROP of *rac*-LA by a tin complex, although a low heterotactic behavior is shown ( $P_r = 0.70$ ),<sup>[152]</sup> believed to be a consequence of the stereochemically active part on the tin.<sup>[153]</sup>

Scandium complexes<sup>[154]</sup> were also investigated as ligands for the ROP of *rac*-LA, as reported by Ma *et al.* The resultant PLAs proved to be heterotactic with  $P_r = 0.96$  at ambient temperature (Figure 1.17c).<sup>[155]</sup> DBI-magnesium complexes were also shown to be highly active catalysts. Notably, stereocontrol was only observed for (BDI)Mg complexes (Figure 1.17d) when the polymerization was carried out in THF, resulting in a highly heterotactic polymers ( $P_r = 0.90$ ). In otherwise identical conditions, polymerizations in either dichloromethane or benzene resulted in atactic PLA.<sup>[156,157]</sup> These results actually contrasted the analogous zinc complexes that exhibited high levels of stereocontrol in the three solvents.

Through low temperature  $^1\text{H}$  NMR studies, Chisholm *et al.* observed notable differences between the zinc- and magnesium-type complexes in the binding of THF to the metal center. In the former case, THF was rapidly dissociated in solution, and even at 80 °C, rapid exchange was observed. In the analogous magnesium complexes, both free and bound THF molecules were observed at low temperature, maintaining a high level of symmetry above and below the plane of the BDI backbone. This led the authors to postulate that incorporation of THF into the active magnesium catalytic species might generate a more coordinately hindered metal center that was more discriminatory to the incoming lactide.<sup>[133]</sup> Computational studies showed that for both zinc and magnesium catalysts, the BDI ligand enabled stereocontrol through a CEC mechanism resulting from the high level of steric hindrance at the active site, with the approach of the monomer reported to be governed by both electrostatic and stereoelectronic interactions.<sup>[158]</sup> In the case of magnesium, the rate and stereocontrol determining step were calculated to be the minimization of the steric interactions forming a transition state in which ring opening of a ligated monomer with THF could stabilize a monomeric lactate propagating (resting) species.

#### 1.5.3.3.1.3. Tetradentate amino (bis- and tris-phenolato) complexes

A wide range of metal complexes bearing tetradentate amino(bisphenolato) and amino(trisphenolato) ligands were employed for the stereocontrolled ROP of *rac*-LA. Chmura *et al.* applied amine(trisphenolato) ligands to titanium, zirconium, and hafnium as well as to germanium to mediate the stereospecific ROP of *rac*-LA (Figure 1.18a).<sup>[159,160]</sup> Zr-, Hf- and Ge-based complexes were employed both under melt conditions at 130 °C and in solution at ambient temperature, producing similar levels of stereocontrol (**22** (Zr):  $P_r = 0.96$ ; **23** (Hf):  $P_r = 0.88$  and **24** (Ge):  $P_r = 0.80$ ). Unlike the other group 4 metals, titanium mediated polymerizations do not result in any stereocontrol, producing atactic polymer ( $P_r = 0.50$ ). This was proposed to be a consequence of chelation of the growing polymer chain being less favored, leading to a large amount of chain transfer and hence poor stereocontrol.

Zirconium- and hafnium-based catalysts provided more comparable stereocontrol, producing heterotactic PLA from *rac*-LA with  $P_r = 0.98$  and 0.97, respectively, in solution at ambient temperature, and  $P_r = 0.96$  and 0.88, respectively, under melt conditions (130 °C).

Davidson *et al.* further demonstrated that, upon using diamine-(bisphenolato) ligands around group 4 metal centers (Figure 1.18b and c), a reduction in stereocontrol was noted, such that a maximum  $P_m = 0.75$  was obtained with complex **25**.<sup>[161]</sup> This difference was

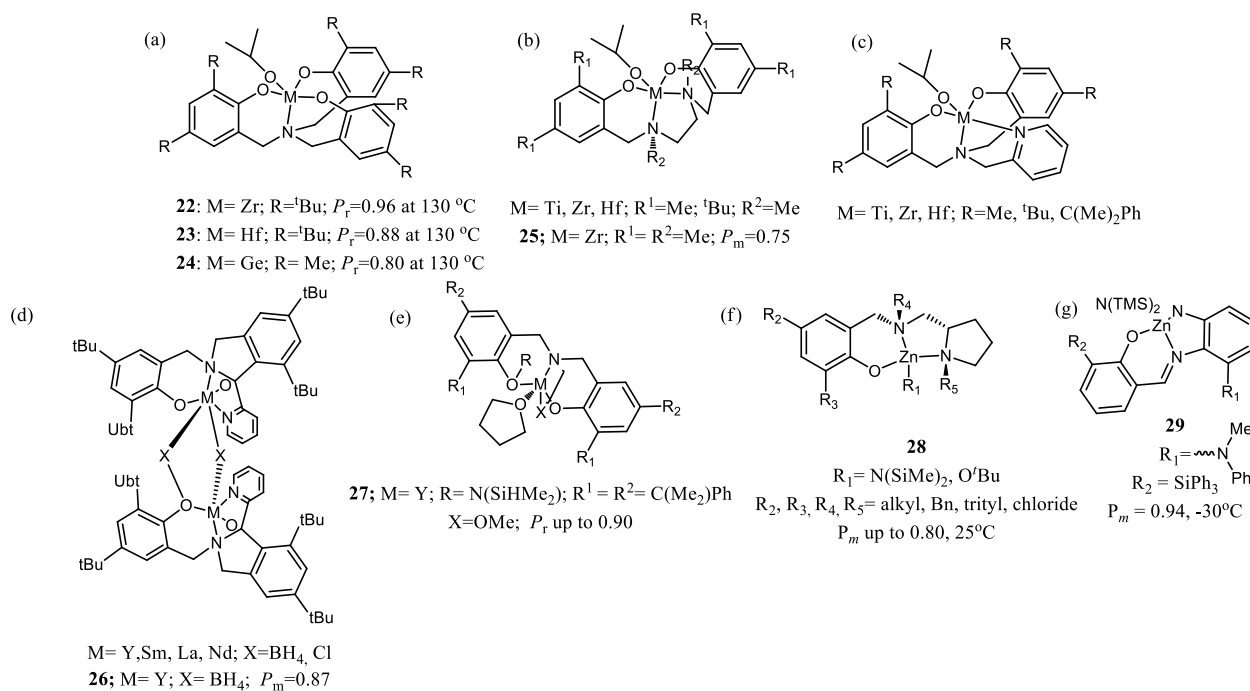


attributed to the structural differences in the catalysts, resulting from the formation of C<sub>2</sub>-symmetric chiral complexes such as **22**, in contrast to achiral C<sub>s</sub>-symmetric complexes such as **25**. Given the comparable steric demands placed on the active site by both ligand sets, an ESC mechanism was postulated.

Mountford *et al.* employed a range of rare earth metals with diaminobis(phenoxide) ligands to form dimeric boro-hydride complexes.<sup>[162]</sup> ROP of *rac*-LA by yttrium-, samarium- and neodymium-based complexes in THF all produce heterotactic enrichment to some degree with the yttrium complex, **26** (Figure 1.18d), resulting in the highest level of heterotactic enrichment (**26** (Y):  $P_r = 0.87$ , Sm:  $P_r = 0.72$ , and Nd:  $P_r = 0.64$ ).

A similar, achiral, tetradentate alkoxyaminobis(phenolate) ligand (Figure 1.18e) was used to synthesize heterotactic PLA from *rac*-LA with a variety of group 3 metals.<sup>[163]</sup> Cai *et al.* explored the use of lanthanum, yttrium and neodymium with varying degrees of success. Yttrium-based catalysts resulted in the highest levels of stereocontrol with  $P_r$  of up to 0.90 possible with tailoring of the ligand system (complex **27**), initiating species and solvent. Indeed, the need to carry out polymerization in THF was evidenced by a reduction of  $P_r$  from 0.80 to 0.60 upon moving to toluene as a solvent. The significantly decreased stereocontrol of lanthanum and neodymium when compared to yttrium strongly suggested that the metal center had a direct influence in the ROP process. The ionic radius of the metal center was postulated to be influential with the small size of yttrium resulting in better selectivity during the approach of the monomer. Aggregation of group 3 metal isopropoxides was also proposed to be involved in LA coordination and hence stereoselection process.<sup>[164]</sup> The steric bulk of the substituents on the aromatic rings, in particular the ortho-position, significantly affected the stereocontrol.<sup>[165]</sup> Increasing the steric hindrance of these groups also reduced the rate of polymerization, although these catalysts enabled fast ROP reactions, completing a DP = 200 polymers in 20 minutes at ambient temperature. ROP of *meso*-lactide resulted in modestly syndiotactic polymer ( $P_r = 0.76$ ), indicative of a CEC mechanism.

In an analogous fashion to the (salen/salan) aluminum-based catalysts, **27**, the metal alkoxide could be derived *in situ*. Carpentier *et al.* employed this *in situ* alkoxide generation and established that such catalysts could trigger the “immortal” polymerization of lactide.<sup>[166]</sup> Typically, a single catalytic species enabled to produce up to 50 polymer chains in presence of 50 equivalents of the alcohol initiator with respect to catalyst. The PLA synthesized in this manner exhibited a highly heterotactic microstructure ( $P_r = 0.90$ ) and a high level of control over the polymerization ( $\bar{D} = 1.08$ ).



**Figure 1.18.** Tetradentate amino (bis- and tris-phenolato) complexes for stereospecific lactide ROP

In 2013, Ma *et al.* designed an enantiomerically pure zinc-based complex featuring a highly isoselective bis(amino) phenolate ligand (Figure 1.18f,  $P_m$  = 0.84). The ROP of *rac*-LA was found to be controlled, providing monodisperse PLA ( $\bar{D} < 1.24$ ), with a slight decrease in tacticity ( $P_m$  = 0.80) in the presence of an equivalent of *i*PrOH. The system proved robust, able to polymerize 1000 eq. of *rac*-LA in 6 hours at room temperature, in toluene, with [*rac*-LA] = 1 M, maintaining a high stereoregularity. This confirmed the higher activity of this Zn-based catalyst over the Al-Salen systems.<sup>[167]</sup> Without any co-initiator, the amide group was found capable of initiating the ROP, albeit in a less efficient manner ( $\bar{D}$  = 1.66, and observation of a slower kinetics), but without any significant decrease in isoselectivity. Kinetic analysis showed a polymerization rate of *D*-LA four times higher than that of *L*-LA, supporting a chain growth by the ESC mechanism. Though, the microstructural analysis of the resulting PLA proved to be more in favor of the ESC mechanism. Lastly, Li *et al.* reported a series of zinc complexes bearing a bulky triphenylsilyl substituent which exhibited good stereochemical control during the ROP of *rac*-LA to produce highly heterotactic PLAs at ambient temperature ( $P_r$  = 0.90) as well as low temperature (-30 °C,  $P_r$  = 0.94) with narrow molar mass distributions ( $\bar{D} < 1.2$ ) (Figure 1.18g).<sup>[168]</sup>

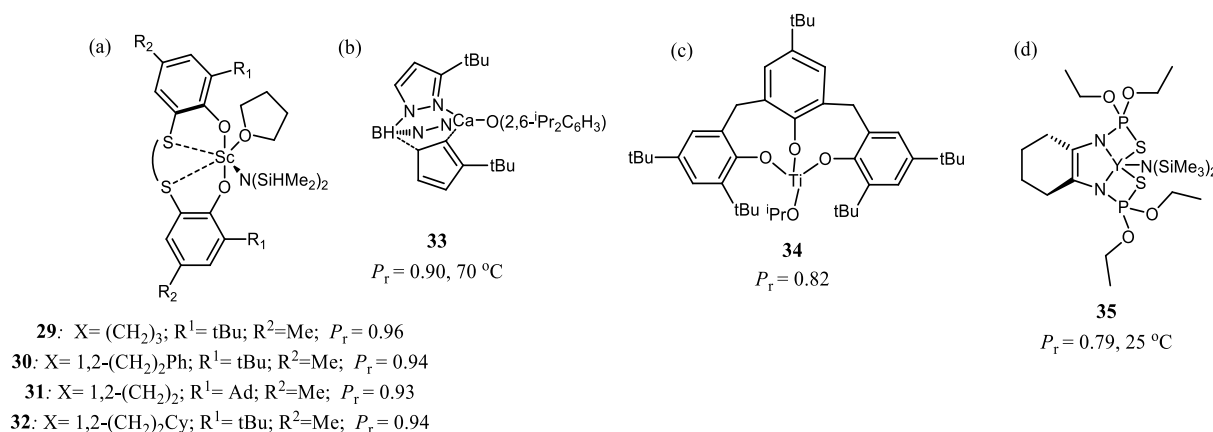
## 1.5.3.3.1.4. Miscellaneous ligands

A range of other catalytic metal complexes demonstrate high levels of stereocontrol in ROP of LA, but do not fit into the broad categories outlined above. For instance, Ma *et al.* applied (dithia-alkanediyl-bridged bisphenolato)scandium complexes (Figure 1.19a), which enabled a highly heterospecific ROP of *rac*-LA at ambient temperature ( $P_r = 0.67\text{--}0.96$ ).<sup>[155]</sup> A range of these (OSSO)-type ligands were also reported to result in varying activity and selectivity, based around the length of the S–S spacer unit. Thus, more flexible thiolate linkers provided the highest heteroselectivities in combination with sterically bulky *o*-phenoxy substituents (**29**:  $P_r = 0.96$ ; **30**:  $P_r = 0.94$ ; **31**:  $P_r = 0.93$ ; **32**:  $P_r = 0.94$ ). In common with the yttrium and lutetium analogues of these complexes, which were also demonstrated to result in stereoregular polymers,<sup>[169]</sup> increased heteroselectivities were observed by increasing the steric bulk around the phenolate rings. A mechanism involving a “dynamic monomer recognition” was proposed to explain the stereoselectivity control, based on the fluxionality and interconversion of the ancillary ligand configuration; this was coined as an enantiomorphic site control mechanism.

Metal complexes bearing tris-pyrazolyl- and tris-indazolyl-borate ancillary ligands (Figure 1.19b) were also employed for the ROP of LA.<sup>[157]</sup> Chisholm *et al.* reported that zinc complexes had no enantiomeric preference whereas magnesium derivatives demonstrated a slight propensity to form syndiotactic PLA from *meso*-LA. In contrast, calcium centered complexes, such as **33**, resulted in highly heterotactic polymer ( $P_r \sim 0.90$ ).

The calcium species was also significantly more reactive than either the magnesium or zinc, reaching high levels of monomer conversion in the polymerization of *rac*-LA (target DP = 100) in 1 min compared to 1 h and 6 days for Mg and Zn, respectively. These catalysts also demonstrated anomalous behavior in copolymerizations of 1:1 *meso*–*rac*-lactide. The zinc catalyst, despite its modest stereocontrol, preferentially polymerized *L*-LA from this mixture whereas the Mg and Ca systems preferentially incorporated *meso*-LA, suggesting that the stereocontrol results from an ESC mechanism imposed by the achiral catalyst.<sup>[170]</sup>

(Trisphenolate)titanium alkoxide complexes, **34**, (Figure 1.19c) were shown to result in heteroselective polymerization of *rac*-LA ( $P_r = 0.82$ ).<sup>[171]</sup> Despite significantly higher heteroselectivity compared to titanium-based catalysts,<sup>171</sup> an induction period of up to 30 minutes was observed, which was attributed to the steric bulk of the para-substituent of the phenoxy rings interfering with the conformational isomerization of the trisphenolate ligand.



**Figure 1.19.** Miscellaneous catalysts for the stereocontrolled ROP of lactide.

A series of bis(thiophosphonic amido)yttrium catalysts (Figure 1.19d) were reported for the stereocontrolled ROP of LA, such that despite modest activities, complex **35** displayed good heteroselectivities ( $P_r = 0.79$ ) in the ROP of *rac*-LA at ambient temperature.<sup>[172]</sup> However, a high extent of transesterification of PLA chain inevitably led to scrambling of the stereochemistry, hence to a reduction in stereocontrol of the polymerization.

Interestingly, metal salts that did not feature any bulky or chiral ancillary ligands could also mediate the stereospecific ROP of LA. Alkoxychloridotitanium(IV) complexes of the general formula  $\text{TiCl}_x(\text{OiPr})_{4-x}$  provided moderate levels of stereocontrol in the ROP of *rac*-LA.<sup>[173]</sup> In both solution polymerization at  $70^\circ\text{C}$  and bulk polymerization at  $130^\circ\text{C}$ , a heterotacticity of  $P_r \sim 0.7$  was noted. However, increasing the number of chloro ligands improved the stereocontrol. A recent investigation by Pietrangelo *et al.* demonstrated that in absence of a complex ancillary ligand, the combination of indium(III) chloride and triethylamine with a benzyl alcohol initiator resulted in the synthesis of highly heterotactic PLA from *rac*-LA ( $P_r = 0.90$ ).<sup>[13]</sup> Notably, ROP of *meso*-LA led to atactic PLA being formed. The stereocontrol in this system was postulated to be the result of the formation of complex species in which LA is bound to the metal center as an ancillary ligand.

Although the degree of stereoselectivity ( $P_m$ ) can easily exceed 0.9, there are still several problems for catalytic systems: (1) they are often characterized by a low catalytic activity and need hours or even days to achieve high conversions<sup>[134]</sup>; (2) their synthesis are tedious adding to the final cost of the resulting material<sup>[174]</sup>; (3) their structures are hard to modify and tune the catalytic properties<sup>[175]</sup>; (4) conditions of ROP for these systems are usually stringent (low or high temperature).<sup>[175,176]</sup>

Polymer chemists have thus devoted many efforts to develop new catalytic systems that could combine a high catalytic activity, high selectivity, and ease of preparation.<sup>[177,178]</sup>

### 1.6.3.3.2. Organic catalysts

The replacement of metal catalysts with organic catalysts has emerged for the synthesis of plastics, especially for those used in biomedical and microelectronic applications. Since the pioneering work of Hedrick in 2001,<sup>[179]</sup> the application of organic catalysts to ROP has witnessed significant progress in the last 15 years. This field has grown to the point that it now provides a powerful and, in some cases, better alternative to the use of traditional metal-based catalysts.<sup>[48,49]</sup> Several attributes of organic catalysts, including their low cost and wide availability, easy removal from polymers, low toxicity, and versatile catalytic mechanisms, make possible a greener and more versatile synthesis of polyesters and polycarbonates. Depending on the nature of the catalyst, organocatalysts can operate through a variety of mechanisms.<sup>[49]</sup>

Organic bases such as *N*-heterocyclic carbenes (NHCs) and amidines can activate the alcohol initiator/chain ends through hydrogen bonding interactions. Alternatively, they can activate the monomer through nucleophilic addition. This has led to the development of zwitterionic ring-opening polymerization for the synthesis of high molar mass polyesters<sup>[180]</sup> and polycarbonates<sup>[181]</sup> with cyclic topology.

Organic acids such as sulfonic or phosphoric acid can catalyze the polymerization through electrophilic activation of monomers. Catalytic systems combining both H-bond donor and H-bond acceptor moieties, such as thiourea/amine, can simultaneously activate the monomer and alcohol initiator/chain end. These systems have proven especially selective for chain propagation over transesterification, affording narrowly dispersed polyesters and polycarbonates. The diversity in mechanistic pathways not only provides new opportunities for enhancing the rate and selectivity of polymerization but also enables the synthesis of polymer architectures that are difficult to access by metal-mediated processes. Many review articles have covered different aspects of this topic.<sup>[37,48,49,100,180,182–184]</sup>

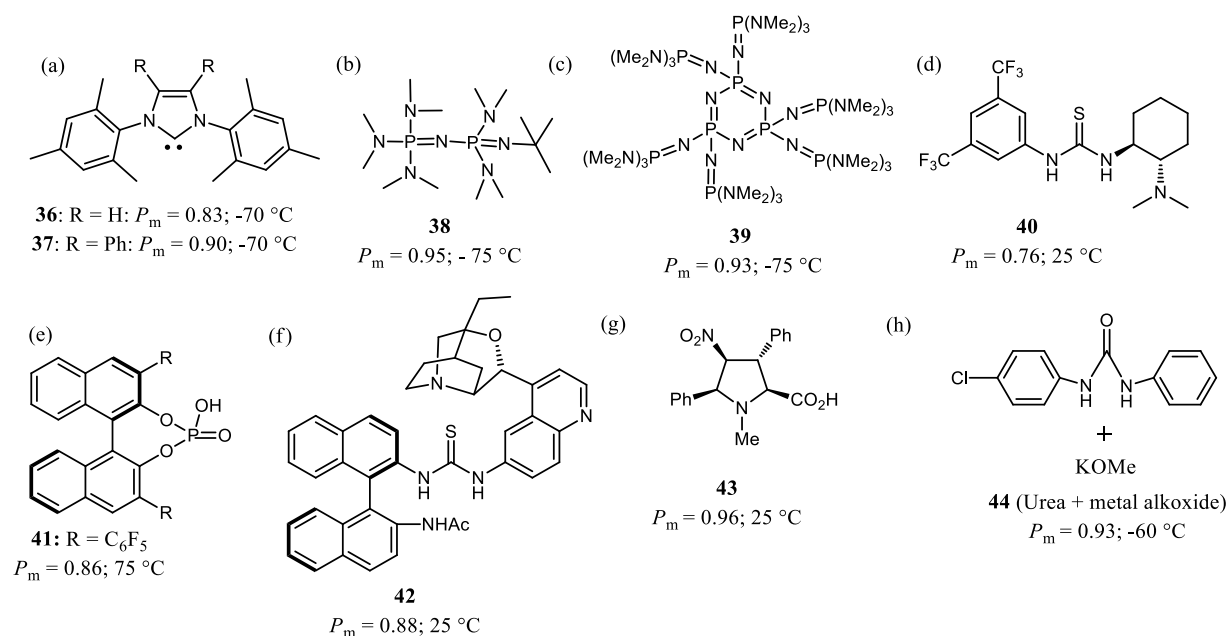
While low stereocontrol at ambient temperature has been a long-standing problem for organocatalytic ROP, recent advances in catalyst design have demonstrated the potential of organocatalysts to rival the state-of-the-art metal catalysts.

The first successful report on the use of achiral and sterically hindered *N*-heterocyclic carbene derivative allowed producing PLA with a  $P_m$  of 0.83, under cryogenic conditions

(Figure 1.20a, Temp. = -70 °C). Thereafter, mesotacticity has been enhanced to 0.90 using more sterically hindered NHC catalyst<sup>[176]</sup> **36** (Figure 1.20a).

Another example was reported by Wade *et al.* who employed a dimeric phosphazene organic base, **38**, (P<sub>2</sub>-*t*Bu, Figure 1.20b). A very high stereoselectivity was reported despite harsh experimental conditions were implemented ( $P_m = 0.95$  at -75 °C).<sup>[175]</sup> Later on, Li *et al.* have investigated the cyclic trimeric phosphazene organocatalyst **39** (Figure 1.20c), which enabled the stereoselective ROP of *rac*-LA with a  $P_m = 0.93$  at -75 °C.<sup>[185]</sup>

In 2006, Pratt *et al.* have investigated the chiral mono-component thiourea-amine catalyst (**40**, (*R,R*)-TUC), known as Takemoto's catalyst<sup>[186]</sup>, for stereoselective ROP of *rac*-LA ( $P_m = 0.76$ ) at room temperature.<sup>[187]</sup> However, the mechanism by which the catalyst was able to stereoselect was not determined. After that, Orhan *et al.* investigated the stereocontrol mechanism of chiral TUC catalysts, which eventually involves both ESC and CEC, by kinetic investigations and combined analyses.<sup>[188]</sup>



**Figure 1.20.** Organic catalysts for the stereoregular ROP of lactide.

Later on, Terada and Satoh reported a binaphthol-derived chiral phosphates (**41**, Figure 1.20e) for the enantioselective polymerization of *rac*-LA ( $k_D/k_L$  up to 28) at 75 °C to generate isotactic PLAs ( $P_m = 0.86$ ) at 49% conversion.<sup>[189]</sup>

Chen developed a bifunctional catalyst that combines  $\beta$ -isocupreidine, a previously reported chiral ROP catalyst with low enantioselectivity ( $k_L/k_D = 4.4$ ),<sup>[190]</sup> and a chiral thiourea based on the binaphthyl scaffold.<sup>[191]</sup> This catalyst exerts double stereo-

differentiation for the ROP of *rac*-LA with  $k_L/k_D$  up to 53 (**42**, Figure 1.20f). The ROP of *rac*-LA mediated by TU-ICD generated isotactic PLAs ( $P_m = 0.88$ ) at 25 °C and 50% conversion. Mecerreyes and Cossío found that a cocatalytic system consisted of a densely substituted proline (**43**, Figure 1.20g), and DBU was able to kinetically resolve racemic lactide. Exo-PRO exhibited a strong preference for *L*-LA, and the ROP of *rac*-LA by this catalyst at 50% conversion generates a highly isotactic PLAs with  $P_m$  up to 0.96 at 25 °C.<sup>[174]</sup> Kan *et al.* have investigated the binary urea/MOR catalytic system, **44**, for stereoselective ROP of *rac*-LA for the first time. They reported that the ROP of *rac*-LA with fast rate (90% conversion within 1 min) and high stereoselectivity ( $P_m = 0.87$ ) was achieved at room temperature and stereoselectivity was even increased up to 0.93 at lower temperature (Figure 1.20h).<sup>[192]</sup> Recently, Lim *et al.* reported achiral rotaxanes providing high isoselectivity ( $P_m = 0.8$  at r.t) by a chain end control mechanism. They described a new method to control tacticity by exploiting rotaxane sterical hindrance.<sup>[193]</sup>

### 1.7. Concluding remarks and objectives of this PhD thesis

The stereoselective ROP is an important aspect for the controlled synthesis of sustainable polymers. Among all chiral monomers, the stereoselective ROP of lactide has been most extensively studied because of the important application of PLAs. PLAs with different types of stereosequences (isotactic, heterotactic, syndiotactic, and stereocomplex) have been successfully synthesized by metal-based catalysts. Studies of the resulting polymers have shown a strong correlation between the thermal and mechanical properties of PLAs and their stereosequences. However, the replacement of metal catalysts with organic catalysts has emerged for the synthesis of plastics, especially for those used in biomedical and microelectronic applications. While a variety of active and selective catalysts are available for converting renewable monomers into well-defined polymers, data to assess their environmental impacts or sustainability are incomplete. Several attributes of organic catalysts, including their low cost and wide availability, easy removal from polymers, low toxicity, and versatile catalytic mechanisms, make possible a greener and more versatile synthesis of polyesters and polycarbonates. While metal-based catalysts are in general more competent in tackling the aforementioned challenges, organocatalysts have emerged as an efficient alternative. Surprisingly, the small number of investigated chiral organic small molecules as a stereoselective organocatalyst motivated us to investigate more about them.

The objective of the thesis was to expand the scope and limitations of the organocatalyzed stereoselective ROP of lactide. For achieving a stereocontrol LA polymerization, we resorted to mono-component catalytic systems showing excellent enantioselectivity in organic asymmetric transformations, including chiral (thio)urea and *N*-heterocyclic carbene derivatives. In addition, stereocontrol mechanisms were investigated in detail for these catalysts. While the following chapter is going to be focused more on the re-investigation of chiral thiourea-amine catalyst namely Takemoto's catalyst and the interesting conducted mechanism, in third chapter, chiral organic *N*-heterocyclic carbene precursors will be reported for the stereoselective ROP of *rac*-LA. The fourth chapter is going to introduce the chiral urea-amine organocatalysts which is a counterpart of the one that discussed in second chapter, its stereoselectivity properties and the differences between thiourea and urea groups on stereoselectivity is going to be debated. Finally, in the last chapter, non-sterically encumbered and achiral triazabicyclo[4.4.0]dec-5-ene (TBD) will be reported for the stereoselective ROP of *rac*-LA at cryogenic temperatures in toluene. The research on isoselectivity of TBD and its



correlation with solubility and the energy, which is associated with the coordination of TBD, LA isomer, and the propagating chain end, will be presented.

## 1.8. References

- [1] B. Heurtefeu, C. Bouilhac, É. Cloutet, D. Taton, A. Deffieux, H. Cramail, *Prog. Polym. Sci.* **2011**, *36*, 89.
- [2] R. Geyer, J. R. Jambeck, K. L. Law, *Sci. Adv.* **2017**, *3*, e1700782.
- [3] R. Smith, *Biodegradable polymers for industrial applications*; Smith, R., Ed.; Woodhead Publishing: Cambridge.
- [4] C. B. Crawford, B. Quinn, *Microplastic Pollutants*; Elsevier.
- [5] A. E. Strategy, *Plastics, A European Strategy For Plastics In A Circular Economy 2018*.
- [6] S. Itsuno, *Prog. Polym. Sci.* **2005**, *30*, 540.
- [7] A. Gandini, T. M. Lacerda, A. J. F. Carvalho, E. Trovatti, *Chem. Rev.* **2016**, *116*, 1637.
- [8] J. W. Kramer, D. S. Treitler, E. W. Dunn, P. M. Castro, T. Roisnel, C. M. Thomas, G. W. Coates, *J. Am. Chem. Soc.* **2009**, *131*, 16042.
- [9] T. P. Yoon, E. N. Jacobsen, *Angew. Chemie - Int. Ed.* **2005**, *44*, 466.
- [10] S. Chen, Y. Wang, Z. Zhou, *J. Org. Chem.* **2016**, *81*, 11432.
- [11] M. S. Taylor, E. N. Jacobsen, *J. Am. Chem. Soc.* **2004**, *126*, 10558.
- [12] Z. Zhong, P. J. Dijkstra, J. Feijen, *J. Am. Chem. Soc.* **2003**, *125*, 11291.
- [13] A. Pietrangelo, M. A. Hillmyer, W. B. Tolman, *Chem. Commun.* **2009**, 2736.
- [14] N. Nomura, R. Ishii, M. Akakura, K. Aoi, *J. Am. Chem. Soc.* **2002**, *124*, 5938.
- [15] C. Li, T. Jiang, J. Wang, H. Wu, S. Guo, X. Zhang, J. Li, J. Shen, R. Chen, Y. Xiong, *ACS Appl. Mater. Interfaces* **2017**, *9*, 25818.
- [16] J. Wang, Y. Liu, Y. Ma, C. Sun, W. Tao, Y. Wang, X. Yang, J. Wang, *Adv. Funct. Mater.* **2016**, *26*, 7516.
- [17] L. Tang, R. Tong, V. J. Coyle, Q. Yin, H. Pondenis, L. B. Borst, J. Cheng, T. M. Fan, *ACS Nano* **2015**, *9*, 5072.
- [18] X. Wu, Y. Ma, G. Zhang, Y. Chu, J. Du, Y. Zhang, Z. Li, Y. Duan, Z. Fan, J. Huang, *Adv. Funct. Mater.* **2015**, *25*, 2138.
- [19] H. Tsuji, *Macromol. Biosci.* **2005**, *5*, 569.
- [20] D. Garlotta, *J. Polym. Environ.* **2002**, *9*, 63.
- [21] D. Arbeiter, K. Schümann, O. Sahmel, T. Eickner, K.-P. Schmitz, N. Grabow, *Curr. Dir. Biomed. Eng.* **2016**, *2*, 27.
- [22] M. Wisniewski, A. Le Borgne, N. Spassky, *Macromol. Chem. Phys.* **1997**, *198*, 1227.
- [23] H. Tsuji, S. H. Hyon, Y. Ikada, *Macromolecules* **1991**, *24*, 5657.
- [24] H. Tsuji, Y. Ikada, F. Horii, M. Nakagawa, H. Odani, R. Kitamaru, *Macromolecules* **1992**, *25*, 4114.
- [25] H. Ö. Düşkünkörur, A. Bégué, E. Pollet, V. Phalip, Y. Güvenilir, L. Avérous, *J. Mol. Catal. B Enzym.* **2015**, *115*, 20.
- [26] B. J. O. Keefe, M. A. Hillmyer, W. B. Tolman, *Dalt. Perspect.* **2001**, 2215.
- [27] T. R. Jensen, L. E. Breyfogle, M. a Hillmyer, W. B. Tolman, *Chem. Commun. (Camb)*. **2004**, 0135, 2504.
- [28] A. Arbaoui, C. Redshaw, D. L. Hughes, *Chem. Commun.* **2008**, *0*, 4717.
- [29] A. Arbaoui, C. Redshaw, *Polym. Chem.* **2009**, *1*, 801.
- [30] J.-F. Carpentier, *Macromol. Rapid Commun.* **2010**, *31*, 1696.
- [31] A. Sauer, A. Kapelski, C. Fliedel, S. Dagorne, M. Kol, J. Okuda, *Dalt. Trans.* **2013**, *42*, 9007.
- [32] M. J. Walton, S. J. Lancaster, C. Redshaw, *ChemCatChem* **2014**, *6*, 1892.
- [33] W. Luo, T. Shi, S. Liu, W. Zuo, Z. Li, *Organometallics* **2017**, *36*, 1736.
- [34] A. C. Redshaw, X. Wang, K. Zhao, Y. Al-khafaji, *Eur. J. Inorg. Chem.* **2017**, 1951.
- [35] T. Q. Xu, G. W. Yang, C. Liu, X. B. Lu, *Macromolecules* **2017**, *50*, 515.

- [36] N. E. Kamber, W. Jeong, R. M. Waymouth, R. C. Pratt, B. G. G. Lohmeijer, J. L. Hedrick, *Chem. Rev.* **2007**, *107*, 5813.
- [37] W. N. Ottou, H. Sardon, D. Mecerreyes, J. Vignolle, D. Taton, *Prog. Polym. Sci.* **2016**, *56*, 64.
- [38] O. Dechy-Cabaret, B. Martin-Vaca, D. Bourissou, *Chem. Rev.* **2004**, *104*, 6147.
- [39] M. J. Stanford, A. P. Dove, *Chem. Soc. Rev.* **2010**, *39*, 486.
- [40] C. M. Thomas, *Chem. Soc. Rev.* **2010**, *39*, 165.
- [41] P. J. Dijkstra, H. Du, J. Feijen, *Polym. Chem.* **2011**, *2*, 520.
- [42] C. P. Radano, G. L. Baker, M. R. Smith, *J. Am. Chem. Soc.* **2000**, *122*, 1552.
- [43] N. Nomura, R. Ishii, Y. Yamamoto, T. Kondo, *Chem. - A Eur. J.* **2007**, *13*, 4433.
- [44] T. M. Ovitt, G. W. Coates, *J. Am. Chem. Soc.* **2002**, *124*, 1316.
- [45] Z. Zhong, P. J. Dijkstra, J. Feijen, *Angew. Chem. Int. Ed.* **2002**, *41*, 4510.
- [46] K. Majerska, A. Duda, *J. Am. Chem. Soc.* **2004**, *126*, 1026.
- [47] P. Hormnirun, E. L. Marshall, V. C. Gibson, A. J. P. White, D. J. Williams, *J. Am. Chem. Soc.* **2004**, *126*, 2688.
- [48] N. E. Kamber, W. Jeong, R. M. Waymouth, R. C. Pratt, B. G. G. Lohmeijer, J. L. Hedrick, *Chem. Rev.* **2007**, *107*, 5813.
- [49] M. K. Kiesewetter, E. J. Shin, J. L. Hedrick, R. M. Waymouth, *Macromolecules* **2010**, *43*, 2093.
- [50] K. Ziegler, *Angew. Chem.* **1964**, *76*, 545.
- [51] G. Natta, *Angew. Chemie* **1964**, *76*, 553.
- [52] S. H. Wilen, E. L. Eliel, *Topics in Stereochemistry*; 1987; Vol. 17.
- [53] Y. Okamoto, T. Nakano, *Chem. Rev.* **1994**, *94*, 349.
- [54] S. Hu, J. Zhao, G. Zhang, H. Schlaad, *Prog. Polym. Sci.* **2017**, *74*, 34.
- [55] M. J. Miri, B. P. Pritchard, H. N. Cheng, *J. Mol. Model.* **2011**, *17*, 1767.
- [56] B. M. Chamberlain, M. Cheng, D. R. Moore, T. M. Ovitt, E. B. Lobkovsky, G. W. Coates, *J. Am. Chem. Soc.* **2001**, *123*, 3229.
- [57] E. N. Jacobsen, A. Pfaltz, H. Yamamoto, *Comprehensive Asymmetric Catalysis*; Springer-Verlag Berlin Heidelberg, 1999; Vol. Chapter 36.
- [58] P. Pino, M. Galimberti, P. Prada, G. Consiglio, *Makromol. Chem.* **1990**, *191*, 1677.
- [59] G. W. Coates, R. M. Waymouth, *J. Am. Chem. Soc.* **1991**, *113*, 6270.
- [60] G. W. Coates, R. M. Waymouth, *J. Am. Chem. Soc.* **1993**, 91.
- [61] G. W. Coates, R. M. Waymouth, *J. Mol. Catal.* **1992**, *76*, 189.
- [62] H. H. Brintzinger, D. Fischer, R. Mülhaupt, B. Rieger, R. M. Waymouth, *Angew. Chemie Int. Ed. English* **1995**, *34*, 1143.
- [63] G. Cytidine, *Macromolecules* **1973**, *6*, 652.
- [64] L. Porri, R. Rossi, G. Ingrosso, *Tetrahedron Lett.* **1971**, *16*, 1083.
- [65] G. Natta, M. Farina, *Tetrahedron Lett.* **1963**, *11*, 703.
- [66] Y. Okamoto, T. Nakano, H. Kobayashi, K. Hatada, *Polym. Bull.* **1991**, *25*, 5.
- [67] G. M. Miyake, W. R. Mariott, E. Y. X. Chen, *J. Am. Chem. Soc.* **2007**, *129*, 6724.
- [68] S. Jiang, Y. Zhao, L. Wang, L. Yin, Z. Zhang, J. Zhu, W. Zhang, X. Zhu, *Polym. Chem.* **2015**, *6*, 4230.
- [69] R. J. M. Nolte, *Chem. Soc. Rev.* **1994**, *23*, 11.
- [70] E. Yashima, K. Maeda, Y. Furusho, *Acc. Chem. Res.* **2008**, *41*, 6102.
- [71] W. Makiguchi, S. Kobayashi, Y. Furusho, E. Yashima, *Angew. Chemie - Int. Ed.* **2013**, *52*, 5275.
- [72] M. M. Green, N. C. Peterson, T. Sato, A. Teramoto, R. Cook, S. Lifson, *Science (80-. )*. **1995**, *268*, 1860.
- [73] J. F. Reuther, J. D. Desousa, B. M. Novak, *Macromolecules* **2012**, *45*, 7719.
- [74] R. Nomura, J. Tabei, T. Masuda, *J. Am. Chem. Soc.* **2001**, *123*, 8430.

- [75] Z. P. Yu, N. Liu, Y. L. Lin, J. Huang, H. Q. Wang, Z. Q. Wu, *J. Polym. Sci. Part A Polym. Chem.* **2017**, *55*, 2227.
- [76] I. Ojima, *Catalytic asymmetric synthesis*; Ojima, I., Ed.; Wiley-VCH Verlag, 2010.
- [77] S. Inoue, T. Tsuruta, J. Furukawa, *Macromol. Chem. Phys.* **1962**, *53*, 215.
- [78] N. Nakata, K. Nakamura, A. Ishii, *Organometallics* **2018**.
- [79] N. Spassky, A. Leborgne, A. Momtaz, M. Sepulchre, **1980**, *18*, 3089.
- [80] R. Ligny, M. M. Hänninen, S. M. Guillaume, J. F. Carpentier, *Angew. Chemie - Int. Ed.* **2017**, *56*, 10388.
- [81] F. Vidal, L. Falivene, L. Caporaso, L. Cavallo, E. Y. X. Chen, *J. Am. Chem. Soc.* **2016**, *138*, 9533.
- [82] A. V. Soloshonok, K. Izawa, *Asymmetric Synthesis and Application of  $\alpha$ -Amino Acids*; 2009; Vol. 136.
- [83] Y. Imanishi, Y. Hashimoto, *J. Macromol. Sci. Part A - Chem.* **1979**, *13*, 673.
- [84] Q. Feng, L. Yang, Y. Zhong, D. Guo, G. Liu, L. Xie, W. Huang, R. Tong, *Nat. Commun.* **2018**, *9*, 1.
- [85] E. S. Place, J. H. George, C. K. Williams, M. M. Stevens, *Chem. Soc. Rev.* **2009**, *38*, 1139.
- [86] A. C. Albertsson, I. K. Varma, *Aliphatic Polyesters: Synthesis, Properties and Applications*; 2002.
- [87] D. Goldberg, *J. Environ. Polym. Degrad.* **1995**, *3*, 61.
- [88] Y. Ikada, H. Tsuji, *Macromol. Rapid Commun.* **2000**, *21*, 117.
- [89] C. Jérôme, P. Lecomte, *Adv. Drug Deliv. Rev.* **2008**, *60*, 1056.
- [90] X. Lou, C. Detrembleur, R. Jérôme, *Macromol. Rapid Commun.* **2003**, *24*, 161.
- [91] C. K. Williams, *Chem. Soc. Rev.* **2007**, *36*, 1573.
- [92] W. Saiyasombat, R. Molloy, T. M. Nicholson, A. F. Johnson, I. M. Ward, S. Poshyachinda, *Polymer (Guildf)*. **1998**, *39*, 5581.
- [93] H. R. Kricheldorf, I. Kreiser, *Makromol. Chem.* **1987**, *188*, 1861.
- [94] R. Dunsing, H. R. Kricheldorf, *Makromol. Chem.* **1986**, *187*, 1611.
- [95] A. Khanna, Y. S. Sudha, S. Pillai, S. S. Rath, *J. Mol. Model.* **2008**, *14*, 367.
- [96] K. Stridsberg, M. Ryner, A.-C. Albertsson, *Advances in Polymer Science*; 2002.
- [97] D. Bourissou, B. Martin-Vaca, A. Dumitrescu, M. Graullier, F. Lacombe, *Macromolecules* **2005**, *38*, 9993.
- [98] S. Penczek, *J. Polym. Sci. Part A Polym. Chem.* **2000**, *38*, 1919.
- [99] M. S. Kim, K. S. Seo, G. Khang, H. B. Lee, *Macromol. Rapid Commun.* **2005**, *26*, 643.
- [100] P. Dubois, O. Coulembier, J. Raquez, *Handbook of Ring-Opening Polymerization*; 2009.
- [101] A. P. Dove, R. C. Pratt, B. G. G. Lohmeijer, R. M. Waymouth, J. L. Hedrick, *J. Am. Chem. Soc.* **2005**, *127*, 13798.
- [102] E. F. Connor, G. W. Nyce, M. Myers, A. Möck, J. L. Hedrick, *J. Am. Chem. Soc.* **2002**, *124*, 914.
- [103] G. Nyce, T. Glauser, E. F. Connor, A. Möck, R. M. Waymouth, J. L. Hedrick, *J. Am. Chem. Soc.* **2003**, *125*, 3046.
- [104] A. P. Dove, R. C. Pratt, B. G. G. Lohmeijer, D. A. Culkin, E. C. Hagberg, G. W. Nyce, R. M. Waymouth, J. L. Hedrick, *Polymer (Guildf)*. **2006**, *47*, 4018.
- [105] H. Uyama, S. Kobayashi, Enzymatic Ring-Opening Polymerization of Lactones Catalyzed by Lipase. *Chem. Lett.* **1993**, *22*, 1149–1150.
- [106] D. Knani, A. L. Gutman, D. H. Kohn, *J. Polym. Sci. Part A Polym. Chem.* **1993**, *31*, 1221.
- [107] S. Kobayashi, *Macromol. Symp.* **2006**, *240*, 178.
- [108] A. C. Albertsson, I. K. Varma, *Biomacromolecules* **2003**, *4*, 1466.

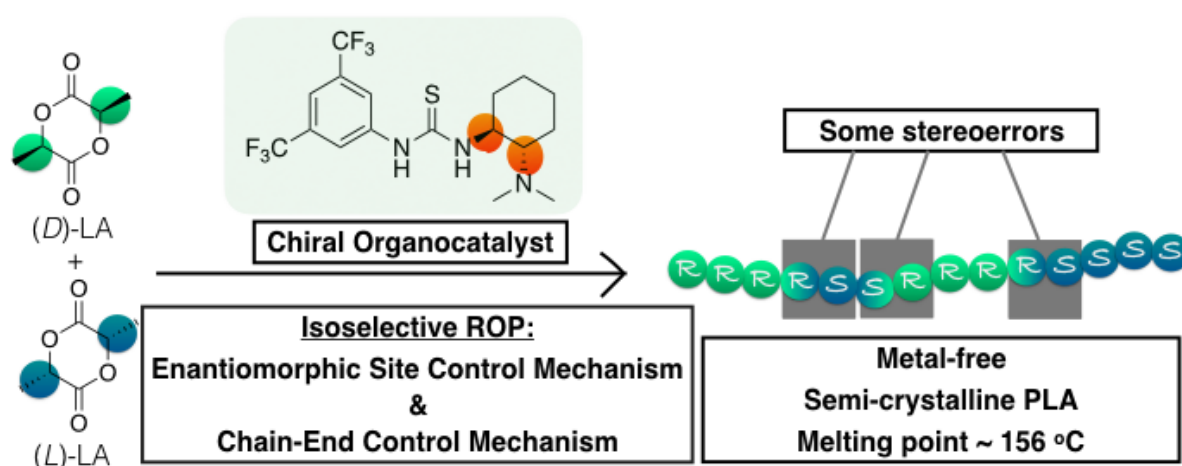
- [109] I. K. Varma, A. C. Albertsson, R. Rajkhowa, R. K. Srivastava, *Prog. Polym. Sci.* **2005**, *30*, 949.
- [110] R. A. Gross, A. Kumar, B. Kalra, *Chem. Rev.* **2001**, *101*, 2097.
- [111] D. E. Henton, P. Gruber, J. Lunt, J. Randall, *Adv. Mater.* **2000**, *12*, 1841.
- [112] A. Duda, A. Kowalski, S. Penczek, *Macromolecules* **1998**, *31*, 9297, 2114.
- [113] H. R. Kricheldorf, D. O. Damrau, *Macromol. Chem. Phys.* **1997**, *198*, 1753.
- [114] V. W. Dittrich, R. C. Schulz, *Die Angew. Makromol. Chemie* **1971**, *15*, 109.
- [115] M. Berl, H. R. Kricheldorf, N. Scharnagl, *Macromolecules* **1988**, *21*, 286.
- [116] P. Dubois, C. Jacobs, R. Jérôme, P. Teysssté, *Macromolecules* **1991**, *24*, 2266.
- [117] J. Baran, A. Duda, A. Kowalski, R. Szymanski, S. Penczek, *Macromol. Symp.* **1997**, *123*, 93.
- [118] G. J. Domski, J. M. Rose, G. W. Coates, A. D. Bolig, M. Brookhart, *Prog. Polym. Sci.* **2007**, *32*, 30.
- [119] J. R. Dorgan, H. J. Lehermeier, L.-I. Palade, John Cicero, *Macromol. Symp.* **2001**, *175*, 55.
- [120] M. Vert, *Macromol. Symp.* **2000**, *153*, 96.
- [121] X. Chen, S. P. McCarthy, R. A. Gross, *Macromolecules* **1998**, *31*, 662.
- [122] C. D. Xiong, L. M. Cheng, R. P. Xu, X. M. Deng, *J. Appl. Polym. Sci.* **1995**, *55*, 865.
- [123] K. Fukushima, Y. Kimura, *Polym. Int.* **2006**, *55*, 626.
- [124] T. Biela, A. Duda, S. Penczek, *Macromolecules* **2006**, *39*, 3710.
- [125] A. Kowalski, A. Duda, S. Penczek, *Macromolecules* **2000**, *33*, 7359.
- [126] J. Belleney, M. Wisniewski, A. Le Borgne, *Eur. Polym. J.* **2004**, *40*, 523.
- [127] J. Coudane, C. Ustariz-Peyret, G. Schwach, M. Vert, *J. Polym. Sci. Part A Polym. Chem.* **1997**, *35*, 1651.
- [128] A. L. E. Borgne, V. Vincens, M. Jouglard, N. Spassky, **1993**, *73*, 37.
- [129] N. Spassky, M. Wisniewski, C. Pluta, A. Le, *Macromol. Chem. Phys.* **1996**, *196*, 2637, 2627.
- [130] T. M. Ovitt, G. W. Coates, *J. Am. Chem. Soc.* **1999**, *121*, 4072.
- [131] T. M. Ovitt, G. W. Coates, *J. Polym. Sci. Part A Polym. Chem.* **2000**, *38*, 4686.
- [132] M. H. Chisholm, N. J. Patmore, Z. Zhou, *Chem. Commun.* **2005**, 127.
- [133] M. H. Chisholm, J. C. Gallucci, K. T. Quisenberry, Z. Zhou, *Inorg. Chem.* **2008**, *47*, 2613.
- [134] P. Hormnirun, E. L. Marshall, V. C. Gibson, R. I. Pugh, A. J. P. White, *Proc. Natl. Acad. Sci.* **2006**, *103*, 15343.
- [135] Z. Tang, X. Chen, X. Pang, Y. Yang, X. Zhang, X. Jing, *Biomacromolecules* **2004**, *5*, 965.
- [136] X. Liu, X. Shang, T. Tang, N. Hu, F. Pei, D. Cui, X. Chen, X. Jing, *Organometallics* **2007**, *26*, 2747.
- [137] D. Myers, A. J. P. White, C. M. Forsyth, M. Bown, C. K. Williams, *Angew. Chemie - Int. Ed.* **2017**, *56*, 5277.
- [138] M. J. Stanford, A. P. Dove, *Macromolecules* **2009**, *42*, 141.
- [139] H. Du, A. H. Velders, P. J. Dijkstra, Z. Zhong, X. Chen, J. Feijen, *Macromolecules* **2009**, *42*, 1058.
- [140] M. K. Samantaray, V. Katiyar, K. Pang, H. Nanavati, P. Ghosh, *J. Organomet. Chem.* **2007**, *692*, 1672.
- [141] M. Bouyahyi, N. Ajellal, E. Kirillov, C. M. Thomas, J. F. Carpentier, *Chem. - A Eur. J.* **2011**, *17*, 1872.
- [142] N. Ajellal, M. Bouyahyi, A. Amgoune, C. M. Thomas, A. Bondon, I. Pillin, Y. Grohens, J. F. Carpentier, *Macromolecules* **2009**, *42*, 987.
- [143] H. Y. Chen, H. Y. Tang, C. C. Lin, *Macromolecules* **2006**, *39*, 3745.

- [144] D. J. Darensbourg, W. Choi, O. Karroonnirun, N. Bhuvanesh, *Macromolecules* **2008**, *41*, 3493.
- [145] A. F. Douglas, B. O. Patrick, P. Mehrkhodavandi, *Angew. Chemie - Int. Ed.* **2008**, *47*, 2290.
- [146] S. Kernbichl, M. Reiter, D. H. Bucalon, P. J. Altmann, A. Kronast, B. Rieger, *Inorg. Chem.* **2018**, acs.inorgchem.8b01060.
- [147] D. E. Stasiw, A. M. Luke, T. Rosen, A. B. League, M. Mandal, B. D. Neisen, C. J. Cramer, M. Kol, W. B. Tolman, *Inorg. Chem.* **2017**, *56*, 14366.
- [148] M. Honrado, A. Otero, J. Ferna, L. F. Sa, U. Rey, J. Carlos, *Organometallics* **2014**, *33*, 1859.
- [149] R. Hador, A. Botta, V. Venditto, S. Lipstman, I. Goldberg, M. Kol, *Angew. Chemie Int. Ed.* **2019**.
- [150] M. Cheng, A. B. Attygalle, E. B. Lobkovsky, G. W. Coates, *J. Am. Chem. Soc.* **1999**, *121*, 11583.
- [151] S. D. Allen, D. R. Moore, E. B. Lobkovsky, G. W. Coates, *J. Organomet. Chem.* **2003**, *683*, 137.
- [152] A. P. Dove, V. C. Gibson, E. L. Marshall, A. J. P. White, D. J. Williams, *Chem. Commun.* **2001**, 283.
- [153] A. P. Dove, V. C. Gibson, E. L. Marshall, H. S. Rzepa, A. J. P. White, D. J. Williams, *J. Am. Chem. Soc.* **2006**, *128*, 9834.
- [154] T. P. Seifert, T. S. Brunner, T. S. Fischer, C. Barner-kowollik, P. W. Roesky, *Organometallics* **2018**, A.
- [155] H. Ma, T. P. Spaniol, J. Okuda, *Angew. Chemie - Int. Ed.* **2006**, *45*, 7818.
- [156] M. H. Chisholm, J. Gallucci, K. Phomphrai, *Inorg. Chem.* **2002**, *41*, 2785.
- [157] M. H. Chisholm, K. Phomphrai, *Inorganica Chim. Acta* **2003**, *350*, 121.
- [158] E. L. Marshall, V. C. Gibson, H. S. Rzepa, *J. Am. Chem. Soc.* **2005**, *127*, 6048.
- [159] A. J. Chmura, M. G. Davidson, C. J. Frankis, M. D. Jones, M. D. Lunn, *Chem. Commun.* **2008**, 944, 1293.
- [160] A. J. Chmura, C. J. Chuck, M. G. Davidson, M. D. Jones, M. D. Lunn, S. D. Bull, M. F. Mahon, *Angew. Chemie - Int. Ed.* **2007**, *46*, 2280.
- [161] A. J. Chmura, M. G. Davidson, M. D. Jones, M. D. Lunn, M. F. Mahon, *J. Chem. Soc. Dalt. Trans.* **2006**, *60*, 887887.
- [162] F. Bonnet, A. R. Cowley, P. Mountford, *Inorg. Chem.* **2005**, *44*, 9046.
- [163] C. X. Cai, A. Amgoune, C. W. Lehmann, J. F. Carpentier, *Chem. Commun.* **2004**, *4*, 330.
- [164] H. Ma, J. Okuda, *Macromolecules* **2005**, *38*, 2665.
- [165] A. Amgoune, C. M. Thomas, S. Ilinca, T. Roisnel, J. F. Carpentier, *Angew. Chemie - Int. Ed.* **2006**, *45*, 2782.
- [166] A. Amgoune, C. M. Thomas, J. F. Carpentier, *Macromol. Rapid Commun.* **2007**, *28*, 693.
- [167] Y. Wang, H. Ma, *J. Organomet. Chem.* **2013**, *731*, 23.
- [168] M. Li, S. Behzadi, M. Chen, W. Pang, F. Wang, C. Tan, *Organometallics* **2019**, *38*, 461.
- [169] H. Ma, T. P. Spaniol, J. Okuda, *Inorg. Chem.* **2008**, *47*, 3328.
- [170] J. C. Huffman, K. Phomphrai, N. W. Eilerts, M. H. Chisholm, S. S. Iyer, M. Pacold, *J. Am. Chem. Soc.* **2000**, *122*, 11845.
- [171] S. K. Russell, C. L. Gamble, K. J. Gibbins, K. C. S. Juhl, W. S. Mitchell, A. J. Tumas, G. E. Hofmeister, *Macromolecules* **2005**, *38*, 10336.
- [172] L. M. Hodgson, R. H. Platel, A. J. P. White, C. K. Williams, *Macromolecules* **2008**, *41*, 8603.

- [173] Y. Kim, G. K. Jnaneshwara, J. G. Verkade, *Inorg. Chem.* **2003**, 42, 1437.
- [174] A. Sanchez-Sanchez, I. Rivilla, M. Agirre, A. Basterretxea, A. Etxeberria, A. Veloso, H. Sardon, D. Mecerreyes, F. P. Cossío, *J. Am. Chem. Soc.* **2017**, 139, 4805.
- [175] L. Zhang, F. Nederberg, J. M. Messman, R. C. Pratt, J. L. Hedrick, C. G. Wade, *J. Am. Chem. Soc.* **2007**, 129, 12610.
- [176] A. P. Dove, H. Li, R. C. Pratt, B. G. G. Lohmeijer, D. A. Culkin, R. M. Waymouth, J. L. Hedrick, *Chem. Commun.* **2006**, 2881.
- [177] X. Zhang, G. O. Jones, J. L. Hedrick, R. M. Waymouth, *Nat. Chem.* **2016**, 8, 1047.
- [178] B. Lin, R. M. Waymouth, *J. Am. Chem. Soc.* **2017**, 139, 1645.
- [179] F. Nederberg, E. F. Connor, M. Möller, T. Glauser, J. L. Hedrick, *Angew. Chem. Int. Ed. Engl.* **2001**, 40, 2712.
- [180] H. A. Brown, R. M. Waymouth, *Acc. Chem. Res.* **2013**, 46, 2585.
- [181] Y. A. Chang, A. E. Rudenko, R. M. Waymouth, *ACS Macro Lett.* **2016**, 5, 1162.
- [182] C. Thomas, B. Bibal, *Green Chem.* **2014**, 16, 1687.
- [183] A. P. Dove, *ACS Macro Lett.* **2012**, 1, 1409.
- [184] F. Suriano, O. Coulembier, J. L. Hedrick, P. Dubois, *Polym. Chem.* **2011**, 2, 528.
- [185] S. Liu, H. Li, N. Zhao, Z. Li, *ACS Macro Lett.* **2018**, 7, 624.
- [186] T. Okino, Y. Hoashi, Y. Takemoto, *J. Am. Chem. Soc.* **2003**, 125, 12672.
- [187] R. C. Pratt, B. G. G. Lohmeijer, D. A. Long, P. N. P. Lundberg, A. P. Dove, H. Li, C. G. Wade, R. M. Waymouth, J. L. Hedrick, *Macromolecules* **2006**, 39, 7863.
- [188] B. Orhan, M. J.-L. Tschan, A.-L. Wirotius, A. P. Dove, O. Coulembier, D. Taton, *ACS Macro Lett.* **2018**, 1413.
- [189] K. Makiguchi, T. Yamanaka, T. Kakuchi, M. Terada, T. Satoh, *Chem. Commun.* **2014**, 50, 2883.
- [190] G. M. Miyake, E. Y. X. Chen, *Macromolecules* **2011**, 44, 4116.
- [191] J. B. Zhu, E. Y. X. Chen, *J. Am. Chem. Soc.* **2015**, 137, 12506.
- [192] Z. Kan, W. Luo, T. Shi, C. Wei, B. Han, D. Zheng, S. Liu, *Front. Chem.* **2018**, 6, 1.
- [193] J. Y. C. Lim, N. Yuntawattana, P. D. Beer, C. K. Williams, *Angew. Chemie - Int. Ed.* **2019**, 58, 6007.

## Chapter 2.

# Stereoselective Ring-Opening Polymerization of *rac*-Lactide initiated by Chiral Thiourea-Amine Organocatalyst: Elucidation of Stereocontrol Mechanism



**Keywords:** Stereoselective • Lactide • Thiourea • Ring-Opening Polymerization



## Chapter 2.

# Stereoselective Ring-Opening Polymerization of *rac*-Lactide initiated by Chiral Thiourea-Amine Organocatalyst: Elucidation of Stereocontrol Mechanism

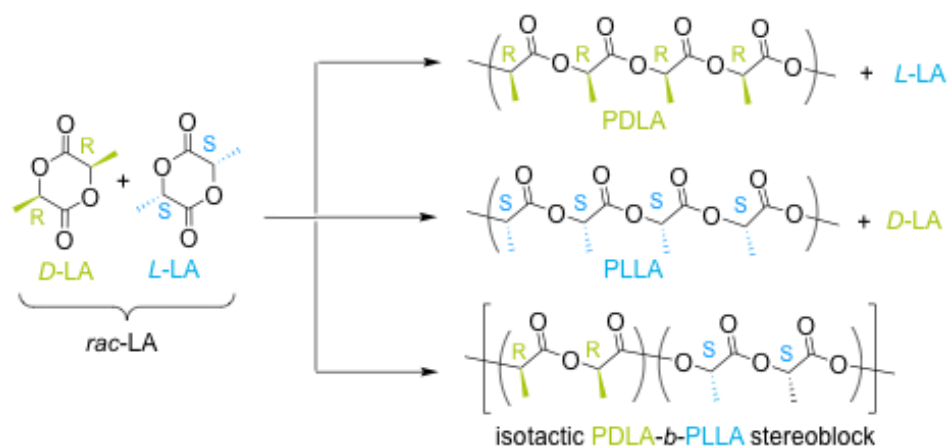
### Contents

<b>Chapter 2. Stereoselective Ring-Opening Polymerization of <i>rac</i>-Lactide initiated by Chiral Thiourea-Amine Organocatalyst: Elucidation of Stereocontrol Mechanism.....</b>	<b>77</b>
2.1. Introduction.....	79
2.2. Results and Discussion .....	83
2.2.1. Polymerization procedure .....	83
2.2.2. Polymer Characterization.....	85
2.2.3. Analysis of the microstructure of PLA derived from chiral TUC's ....	90
2.2.3.1 DSC Analysis .....	90
2.2.3.2 Homonuclear decoupled <sup>1</sup> H NMR and quantitative <sup>13</sup> C NMR analysis .....	90
2.2.4. Kinetics of the ring-opening polymerization's of <i>rac</i> -LA from chiral TU .....	100
2.3. Conclusions and outlooks .....	103
2.4. Experimental and supporting information .....	107
2.5. References.....	108

## 2.1. Introduction

Tremendous developments have been made in the past two decades to employ organocatalysts in a variety of transformations. Mainly focused on asymmetric reactions, small organic catalysts operate under mild reaction conditions, without some of the shortcomings of biocatalysts, such as a complex structure/conformation/function relationship or lack of robustness.<sup>[1–6]</sup> Organocatalysts have also been introduced in macromolecular synthesis.<sup>[3,7–11]</sup> Their often lower toxicity in comparison to many metal-based catalysts is driving their development in, for instance, biomedical, personal beauty care, microelectronic device, and food packaging applications.<sup>[12–14]</sup>

The possibility to transfer the chirality from an organocatalyst to the polymer backbone, *i.e.* stereoselective organocatalyzed polymerization, remains underexplored. This is perhaps surprising given the numerous chiral organic catalysts that are easily accessible. Control over stereoselectivity (stereocontrol) in some polymerization reactions is of paramount importance as the resulting tacticity of the polymer drastically affects the physical and mechanical properties of the final material.<sup>[15–21]</sup> Differences in tacticity lead to major differences in both the melting ( $T_m$ ) and the glass transition ( $T_g$ ) temperatures. An archetypal example of stereocontrolled polymer synthesis is ROP of LA.<sup>[22]</sup> Polylactide (PLA) is not only a biocompatible and biodegradable polymer but also manufactured from biorenewable sources such as corn starch or sugar cane. These features make PLA suitable for several applications, for instance, in the pharmaceutical and microelectronics fields or as a biodegradable plastic in packaging.<sup>[23–26]</sup> LA possesses two chiral centers. As such, it can exist in three distinct diastereoisomers, namely, DD-, LL- (commonly used as a racemic mixture, *rac*-LA), and DL- (*meso*-LA). With appropriate catalysts/initiators, stereospecific ROP enables a controlled insertion of monomers into the polymer backbone based on their stereochemistry.<sup>[27,28]</sup> While ROP of either enantiomer yields isotactic PLA, stereocontrolled ROP of *rac*- and *meso*-LA forms different microstructures (Figure 2.1) with different properties. Poly(*L*-LA) (PLLA) exhibits a  $T_m$  around 160–180 °C, whereas atactic PLA is amorphous and brittle. The  $T_m$  value can be dramatically increased up to 230–240 °C when mixing equimolar amounts of PLLA and PDLA, owing to the formation of a stereocomplex.<sup>[15,18,20]</sup>

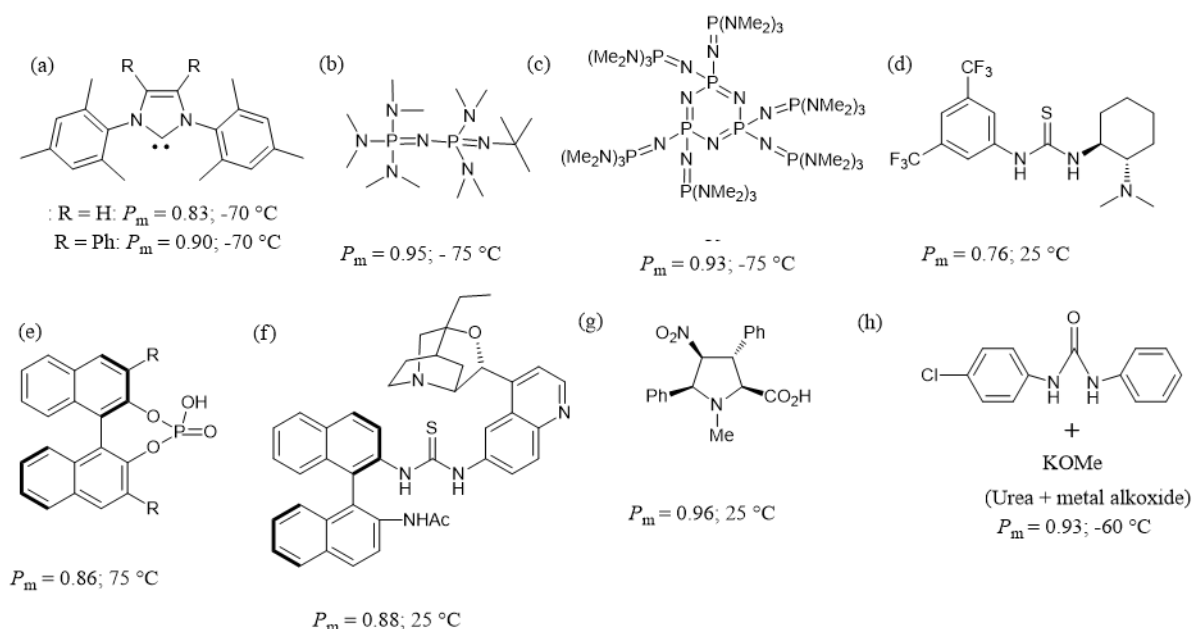


**Figure 2.1.** Stereoselective organocatalyzed ROP of *rac*-LA leading to metal-free and semi-crystalline PLA

As discussed in the previous chapter, stereocontrolled polymerization can be mediated by two distinct mechanisms, namely, chain end control (CEC) or enantiomorphic site control (ESC).<sup>[27,28]</sup> In the former case, control of the chirality is associated with the propagating chain end that in the transition state of the next monomer insertion defines the chirality of the next monomer unit to be inserted. Such control is most commonly achieved using sterically hindered catalysts that reinforce a chiral environment. In contrast, in polymerizations mediated through an ESC mechanism, the chirality of the catalyst determines the chirality of the next monomer unit. In particular, the enantioasymmetric, *i.e.*, by kinetic resolution, ROP of *rac*-LA involves the reaction of only one enantiomer to provide a chiral PLA, leaving the other enantiomer unchanged (Figure 2.1). Organometallic catalysts typically based on aluminum or rare earths that induce a “coordination–insertion” mechanism have been by far the most investigated for the stereocontrolled ROP of LA. Beyond these few examples, stereocontrol in the ROP of LA is more commonly achieved by CEC, even if the catalyst contains a chiral component (*i.e.*, ligand).<sup>[22,29–36]</sup>

To date, and as summarized in the bibliographic chapter, only a handful of studies have focused on the stereocontrolled organocatalytic ROP of *rac*-LA using either achiral or chiral organic catalysts.<sup>[37–43]</sup> As with metal-based catalysis, stereoselective polymerization can be mediated by achiral species using steric hindrance. For example, when catalyzing the ROP of *rac*-LA by the *N*-heterocyclic carbene (Figure 2.2a) at  $-70\text{ }^{\circ}\text{C}$ , Lohmeijer *et al.* observed the formation of isotactic-enriched PLA, with a probability of forming meso dyads ( $P_m$ ) of 0.83.<sup>[44]</sup> Isotactic enchainment could be enhanced for the ROP of *rac*-LA at  $-70\text{ }^{\circ}\text{C}$  ( $P_m = 0.90$ ) in the presence of the more sterically hindered NHC (Figure 2.2a).<sup>[37]</sup> Zhang *et al.* employed the dimeric phosphazene organic base,  $P_2$ -*t*Bu (Figure 2.2b), to obtain a  $P_m$  value of 0.95 for the ROP of *rac*-LA at  $-75\text{ }^{\circ}\text{C}$ .<sup>[38]</sup> Very recently, Liu *et al.* reported that cyclic

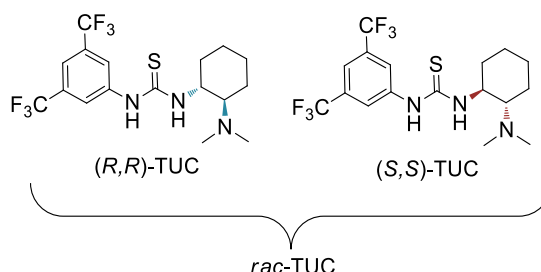
trimeric phosphazene (Figure 2.2c) enabled the synthesis of isotactic PLA with a  $P_m$  value up to 0.93 at  $-75\text{ }^{\circ}\text{C}$  (Figure 2.2d).<sup>[42]</sup> Chiral organocatalysts, including binaphthol-type phosphoric acids (Figure 2.2e),<sup>[40]</sup> a  $\beta$ -isocupreidine/thiourea/chiral binaphthylamine (Figure 2.2f),<sup>[27]</sup> and densely substituted proline-type amino acids (Figure 2.2g)<sup>[41]</sup> were also investigated for the mediation of stereospecific ROP of *rac*-LA and provided a  $P_m$  value of 0.86, 0.88, and 0.96 at 25, 45, and  $85\text{ }^{\circ}\text{C}$ , respectively. Although excellent stereocontrol can be achieved from both chiral and achiral organocatalysts, ROP reactions are generally conducted at low temperatures, and/or a detailed investigation into the underlying stereocontrol mechanism is lacking, the understanding of which could aid future organocatalyst design to address the challenge of controlling polymer stereochemistry at more easily accessible and even elevated temperatures.



**Figure 2.2.** Organic catalysts for the stereoregular ROP of lactide.

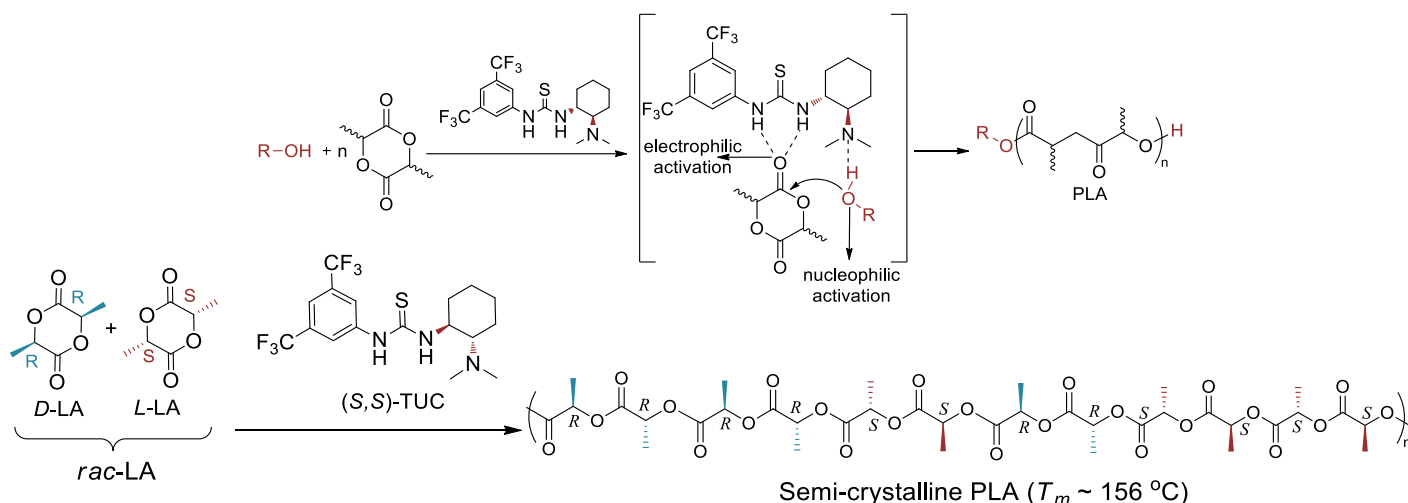
Organocatalysts based on thioureas<sup>[43,45,46]</sup> and amines have been extensively investigated in ROP of LA,<sup>[6]</sup> owing to their high selectivity, minimizing the occurrence of chain transesterification and providing excellent control over molar mass and dispersity of the resulting PLA.<sup>[46]</sup> In particular, the monocomponent thiourea-based catalyst (Figure 2.3), known as Takemoto's catalyst,<sup>[47]</sup> incorporating both a thiourea and a tertiary amino group, operates by a bifunctional cooperative mechanism; *i.e.*, the amino moiety activates the alcohol initiator, whereas the thiourea group activates the monomer.<sup>[44]</sup> Most studies have employed the racemic version, except in one report by Pratt *et al.* in 2006,<sup>[43]</sup> where the (*R,R*)-TUC (Figure 2.3) was applied and was observed to yield PLA with a  $P_m$  of 0.76,<sup>[48]</sup> roughly the

same as for the racemic catalyst, although the mechanism by which the catalyst was able to stereoselect was not determined. Knowing the broad applicability of PLA with a controlled tacticity, and given the interest in preparing PLA free of any metallic residues, both chiral (*R,R*) and (*S,S*) and commercially available versions of the Takemoto catalyst, were here (re)investigated for the stereoselective ROP of *rac*-LA.



**Figure 2.3.** The two enantiomeric structures of the thiourea-amino catalyst

Our motivation was to achieve metal-free and semi-crystalline PLAs at ambient temperature or above, rather than under more stringent conditions at very low temperature as previously reported.<sup>[38,42]</sup> Here, we report that both commercially available (*R,R*)- and (*S,S*)-enantiomers of chiral thiourea-amine Takemoto's organocatalysts promote efficient control and high isoselectivity at room temperature of the ring-opening polymerization (ROP) of racemic lactide by kinetic resolution, yielding highly isotactic, semi-crystalline and metal-free polylactide (PLA; Scheme 2.1). Kinetic investigations and combined analyses of the resulting PLAs have allowed the stereocontrol mechanism, which eventually involves both enantiomorphous site control and chain-end control, to be determined. Moreover, epimerization of *rac*-LA to *meso*-LA is identified as being responsible for the introduction of some stereoerrors during the ROP process.



**Scheme 2.1.** Stereoselective organocatalyzed ROP of *rac*-LA catalyzed by chiral (*S,S*)-TUC

This study reveals not only that unexpectedly this process yields semi-crystalline PLA at room temperature as well as at higher temperatures but also that both mechanisms of stereocontrol, *i.e.*, CEC and ESC mechanisms, operate during the ROP process.

## 2.2. Results and Discussion

### 2.2.1. Polymerization procedure

ROP experiments were carried out with both (*S,S*)- and (*R,R*)-TUCs in a temperature range of 25–85 °C. ROP reactions of *rac*-LA were performed in  $\text{CH}_2\text{Cl}_2$  or in toluene using benzyl alcohol (BnOH) as initiator, in the presence of either the (*S,S*)- or the (*R,R*)-TUC (Table 2.1). Table 2.1 summarizes the results of polymerizations conducted by (*S,S*)- and (*R,R*)-TUC catalyst.

The monocomponent thiourea-based catalyst (Figure 2.3) known as Takemoto's catalyst,<sup>[47]</sup> incorporating both a thiourea and a tertiary amino group, operates by a bifunctional cooperative mechanism. Namely, the amino moiety activates the alcohol initiator, whereas the thiourea group activates the monomer (Scheme 2.1).<sup>[44]</sup> Detailed information about bifunctional mechanism is provided in Chapter 1, section 1.4.2.3.

**Table 2.1.** Stereoselective ring-opening polymerizations of *rac*-LA catalyzed by (*S,S*)-TUC and (*R,R*)-TUC.<sup>a</sup>

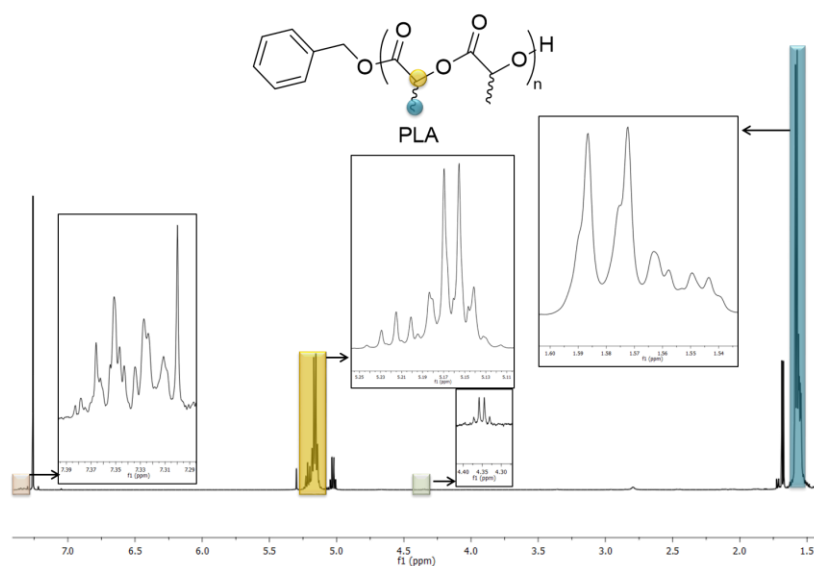
Entry	Catalyst	[M]/[C]/[I]	T [°C]	<i>t</i> [h]	Conv. [%] <sup>b</sup>	<i>M<sub>n</sub></i> [kg.mol <sup>-1</sup> ] <sup>c</sup>	<i>M<sup>calc</sup><sub>n</sub></i> [kg.mol <sup>-1</sup> ] <sup>d</sup>	<i>D<sub>M</sub></i> <sup>c</sup>	<i>T<sub>g</sub></i> [°C] <sup>e</sup>	<i>T<sub>m</sub></i> [°C] <sup>e</sup>	$\Delta H$ (j.cal <sup>-1</sup> ) <sup>e</sup>	<i>P<sub>m</sub></i> <sup>f</sup>
1	( <i>S,S</i> )-TUC	50:1:1	-40	168	69	6.8	5.0	1.06	45	145	15	0.85
2	( <i>S,S</i> )-TUC	200:5:1	25	238	85	24.8	24.6	1.16	59	152	16	0.87
3	( <i>S,S</i> )-TUC	200:10:1	25	215	93	27.6	27	1.15	56	156	24	0.87
4	( <i>S,S</i> )-TUC	200:5:1	45	161	87	15.7	25.2	1.25	52	131	8	0.80
5	( <i>S,S</i> )-TUC	200:10:1	45	91	95	18.8	27.5	1.24	54	143	17	0.82
6*	( <i>S,S</i> )-TUC	200:5:1	85	45	60	9.7	24.8	1.45	53	149	1.7	0.82
7*	( <i>S,S</i> )-TUC	200:10:1	85	90	54	10.0	15.7	1.83	58	141	7.6	0.85
8	( <i>S,S</i> )-TUC	200:10:1	25	72	90	9.7	26.0	1.12	39	-	-	0.61
9*	( <i>R,R</i> )-TUC	200:5:1	25	552	71	21.2	20.5	1.22	61	162	24.6	0.90
10	( <i>R,R</i> )-TUC	200:5:1	25	268	87	21.8	24.8	1.12	56	155	10	0.88
11	( <i>R,R</i> )-TUC	200:5:1	25	552	>95	29.4	27.4	1.13	57	166	11.7	0.87
12	( <i>R,R</i> )-TUC	200:5:1	85	18	52	8.4	15.0	1.16	54	-	-	0.83
13	( <i>R,R</i> )-TUC	200:5:1	85	56	88	13.3	25.4	1.21	44	-	-	0.83
14 <sup>§</sup>	( <i>R,S</i> )-TUC	200:5:1	150	24	95	5.9	27.4	1.53	49	-	-	0.67
15 <sup>§</sup>	( <i>R,S</i> )-TUC	200:10:1	150	24	>99	7.3	28.6	1.61	57	-	-	0.69

<sup>a</sup>Polymerizations were conducted in CH<sub>2</sub>Cl<sub>2</sub> unless otherwise stated. \*Reactions were performed in toluene. <sup>§</sup>ROP or *meso*-LA in the presence of (*S,S*)-TUC.

<sup>§</sup>Polymerizations were performed in bulk. <sup>b</sup> Conversion of polymerizations were determined by SEC in CHCl<sub>3</sub> and THF before polymer purification or by <sup>1</sup>H NMR spectroscopic analysis in CHCl<sub>3</sub>. <sup>c</sup> *M<sub>n</sub>* and *D<sub>M</sub>* are determined by SEC in THF or CHCl<sub>3</sub> (calibration using polystyrene standards). <sup>d</sup>Theoretical number-average molar mass  $M^{calc}_n = [LA]_0/[BnOH]_0 \times M_{LA} \times x_{LA} + M_{BnOH}$ . <sup>e</sup>*T<sub>g</sub>*, *T<sub>m</sub>* and  $\Delta H_m$  values are obtained by DSC measurements from 1<sup>st</sup> heating curve. <sup>f</sup>Probabilities of finding mesodyads are calculated from homonuclear decoupled <sup>1</sup>H by deconvolution technique. All calculations based on ESC statistics.<sup>[49]</sup>

### 2.2.2. Polymer Characterization

The chemical structures of the resulting polymers were assigned by  $^1\text{H}$  NMR measurement (Figure 2.4).  $^1\text{H}$  NMR,  $^{13}\text{C}$  NMR and homonuclear decoupled  $^1\text{H}$  NMR spectroscopic measurements were performed at room temperature on Bruker Advance instrument at 400 MHz.  $\text{CDCl}_3$  was used as an internal reference ( $\delta = 7.26$ ). The characteristic signals of PLA were observed in the range from 1.53 to 1.61 and from 5.11 to 5.23, which were attributable to the methyl and methine protons, respectively. Also the benzyl protons are determined in the range of 7.28-7.38, which confirmed the benzylate group as the  $\alpha$ -chain-end, *i.e.* BnOH acted as the initiating agent for the TUC catalyzed ROP system.



**Figure 2.4.**  $^1\text{H}$  NMR spectrum (400 MHz,  $\text{CDCl}_3$ ) of PLA prepared with (*S,S*)-TUC/ *rac*-LA at 25 °C Inset 1: Methine region of PLA, methyl region of PLA and end groups.

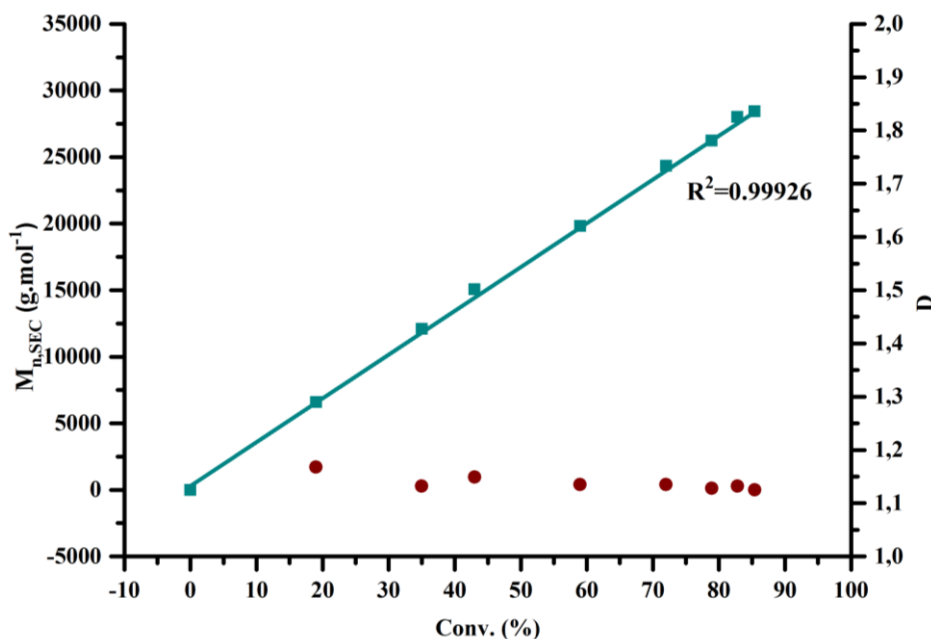
At room temperature, LA conversion reached 85% after 238 h for an initial  $[\text{LA}]_0/[(\text{S,S})\text{-TUC}]_0/[\text{BnOH}]_0$  ratio of 200/5/1, leading to a PLA with low dispersity and a number-average molar mass ( $M_n$ ) that was consistent with that expected based on the monomer-to-initiator ratio ( $M_n = 24,800 \text{ g}\cdot\text{mol}^{-1}$ ,  $\bar{D}_M = 1.16$ ; Table 2.1, entry 2).

The molar mass linearly increased with the increasing monomer conversion (Figure 2.5). Despite the process being slow, these conditions all enabled the formation of semi-crystalline PLAs with an excellent control over molar masses and narrow dispersities ( $\bar{D}_M \leq 1.25$ ). This was supported by combined analyses, including NMR spectroscopy (Figure 2.4), size exclusion chromatography, and MALDI-ToF mass spectrometry. In addition, apparent molar masses increased when increasing the initial monomer-to-initiator molar ratio. Similar



controlled polymerization process observed also in the presence of (*R,R*)-TUC. *Rac*-LA conversion was monitored 87% after 268 h for the initial ratio of 200/5/1. ( $M_n = 21,800 \text{ g.mol}^{-1}$ ,  $\bar{D}_M = 1.12$ ; Table 2.1, entry 10) While the initial catalytic loading was increased, the rate of the polymerization was increased, linearly.

Increasing the temperature from 25 to 45 °C did not alter the control of the ROP process, whereas 85 °C led to loss of polymerization control resulting in lower molar masses and broader distribution. *Rac*-LA conversion was monitored at 87% after 161 h for the initial ratio of 200/5/1 and 95% after 91 h for the 200/10/1 at 45 °C. ( $M_n = 15,700 \text{ g.mol}^{-1}$ ,  $\bar{D}_M = 1.25$  and  $M_n = 18,800 \text{ g.mol}^{-1}$ ,  $\bar{D}_M = 1.24$ , respectively; Table 2.1, entry 4-5). Regarding the reactions performed at 85 °C, 60% of LA conversion was obtained after 45 h within the  $M_n = 9,700 \text{ g.mol}^{-1}$ ,  $\bar{D}_M = 1.45$  for the initial ratio of 200/5/1, therefore proved the controlled polymerizations was no longer possible at high temperatures.



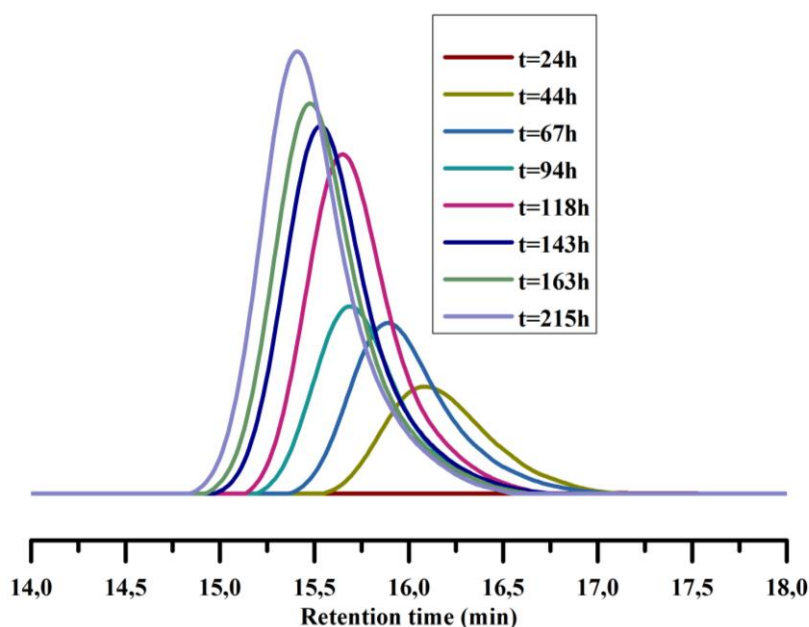
**Figure 2.5.**  $M_{n,SEC}$  and dispersity ( $\bar{D}_M$ ) vs. monomer conversion for PLA synthesized from (*S,S*)-TUC at RT (Table 2.1, entry 3).

The number average molar mass ( $M_n^{SEC}$ ) value agreed fairly well with the calculated one ( $M_n^{calc}$ ), which was determined by the  $^1\text{H}$  NMR measurement and calculated by the initial ratio of  $[\text{LA}]_0/[\text{BnOH}]_0$  and monomer conversions, respectively (see below)

$$M_n^{calc} = \frac{[\text{LA}]_t}{[\text{LA}]_0} \times \text{DP}_{poly} \times M_{w,LA} + M_{w,BnOH}$$

PLA samples were also prepared from the ROP of *rac*-LA in presence of the (*S,S*)-TUC in  $\text{CH}_2\text{Cl}_2$  at room temperature, with  $[\text{LA}]_0/[\text{TUC}]_0$  of 200. SEC traces of the resultants

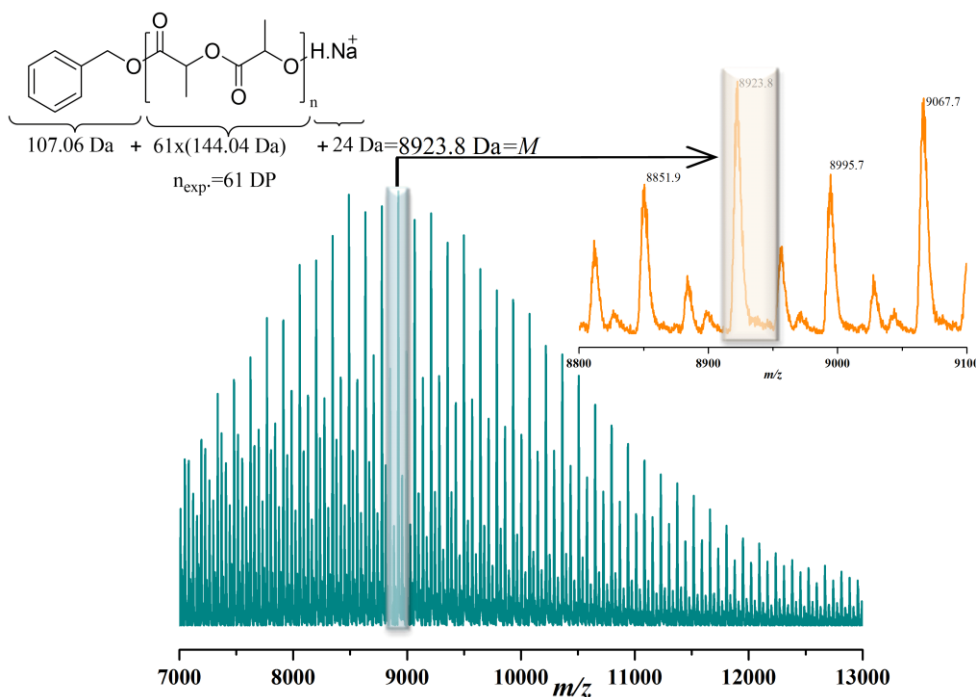
PLAs showed a monomodal distribution, as shown in Figure 2.6. The  $M_n$  value of 24,800 g.mol<sup>-1</sup> is in good agreement with the theoretical value of 24,600 g.mol<sup>-1</sup> (Table 2.1, entry 2). The same is true for the PLA obtained from the (*R,R*)-TUC organocatalysis : 21,800 g.mol<sup>-1</sup> vs. 24,800 g.mol<sup>-1</sup> for the experimental and theoretical molar mass, respectively (Table 2.1, entry 10). In contrast, apparent molar masses of PLAs synthesized at 45 and 85 °C slightly deviated from the expected values; for instance,  $M_n = 15,700$  g.mol<sup>-1</sup> as determined for the PLA obtained at 45 °C in CH<sub>2</sub>Cl<sub>2</sub>, for a theoretical value,  $M_n = 25,200$  g.mol<sup>-1</sup>. This discrepancy might be due to the occurrence of side transesterification reactions during the ROP process. The PLA sample obtained at 85 °C exhibited a molar mass,  $M_n = 9,700$  g.mol<sup>-1</sup> ( $M_n^{\text{calc}} = 24,800$  g.mol<sup>-1</sup>) with a dispersity  $D_M = 1.45$ , highlighting a loss of control to some extent.



**Figure 2.6.** Size exclusion chromatograms of PLA during ROP of *rac*-LA using (*S,S*)-TUC at 25°C (Table 2.1, entry 2)

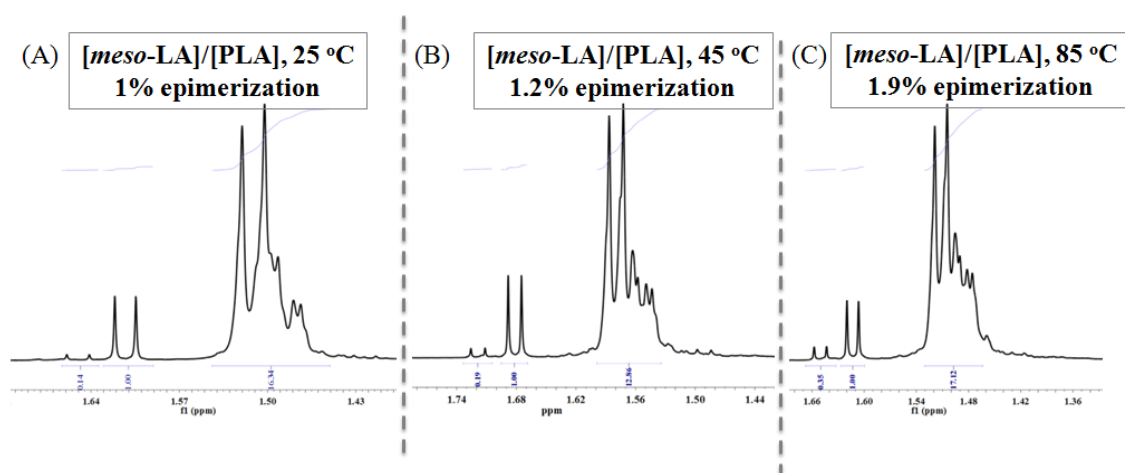
[illegible]

Side transesterifications were detected at 85 °C, especially when conversion was higher than 90%. Minor set of peaks corresponding to a repeating unit of 72 Da, indicative of the presence of intermolecular transesterification reactions, were indeed noticed (Figure 2.8). Any formation of macrocyclic polymer was not observed. Considering such system involving alcoholic initiator/catalyst, intramolecular transesterification reaction, known also as back-biting reaction, is unlikely to occur. Therefore, the probability of occurrence of intermolecular transesterification side reaction can assumed to be much higher than that of the intermolecular.

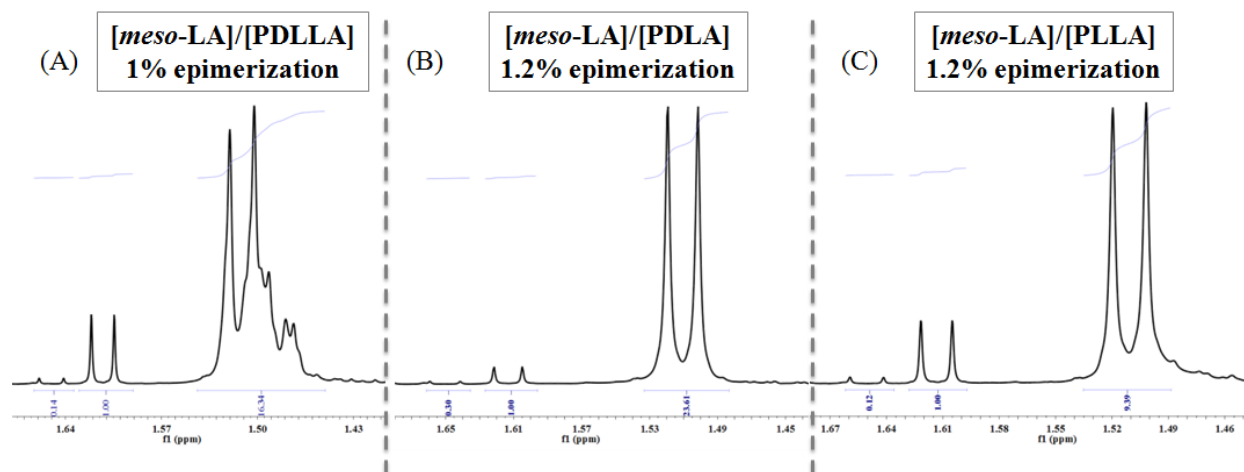


**Figure 2.8.** MALDI-ToF mass spectrum of PLA prepared with (*S,S*)-TUC/ *rac*-LA at 85 °C (Table 2.1, entry 6)

Epimerization of *rac*-LA to form *meso*-LA is a side event, which can bias the stereocontrol, creating additional stereoerrors. As a result of epimerization, the probability for forming *–RSR–* sequences increases, thus decreasing the *P<sub>m</sub>* value. Monitoring of the ROP of *rac*-LA in a conversion range of 74– 87% allowed us to calculate the [*meso*-LA]/[unreacted *rac*-LA] ratio by <sup>1</sup>H NMR spectra, which was found equal to 13, 17, and 26% at 25, 45, and 85 °C, respectively. Corresponding extent of epimerization, as determined through the [*meso*-LA]/[PLA] ratios, was as follows: 1, 1.2, and 1.9%, respectively (Figure 2.9). Thus, although these data show that epimerization did occur, the content in resulting *meso*-LA ratio remained very low during the whole ROP process and was considered as negligible. The higher epimerization at higher temperature, *i.e.* 2% at 85 °C, might explain the reduced crystallinity and hence *T<sub>m</sub>* observed by DSC under these conditions.



**Figure 2.9.** NMR spectra (400 MHz,  $\text{CDCl}_3$ ) of the methyl region of PLA (A) obtained at 25 °C (B) obtained at 45 °C (C) obtained at 85 °C indicates epimerization reaction from *rac*-LA and to *meso*-LA in the presence of (*S,S*)-TUC



**Figure 2.10.**  $^1\text{H}$  NMR spectra (400 MHz,  $\text{CDCl}_3$ ) of the methyl region of PLA indicates epimerization reaction from (A) *rac*-LA (B) *D*- and (C) *L*-LA and to *meso*-LA in the presence of (*S,S*)-TUC

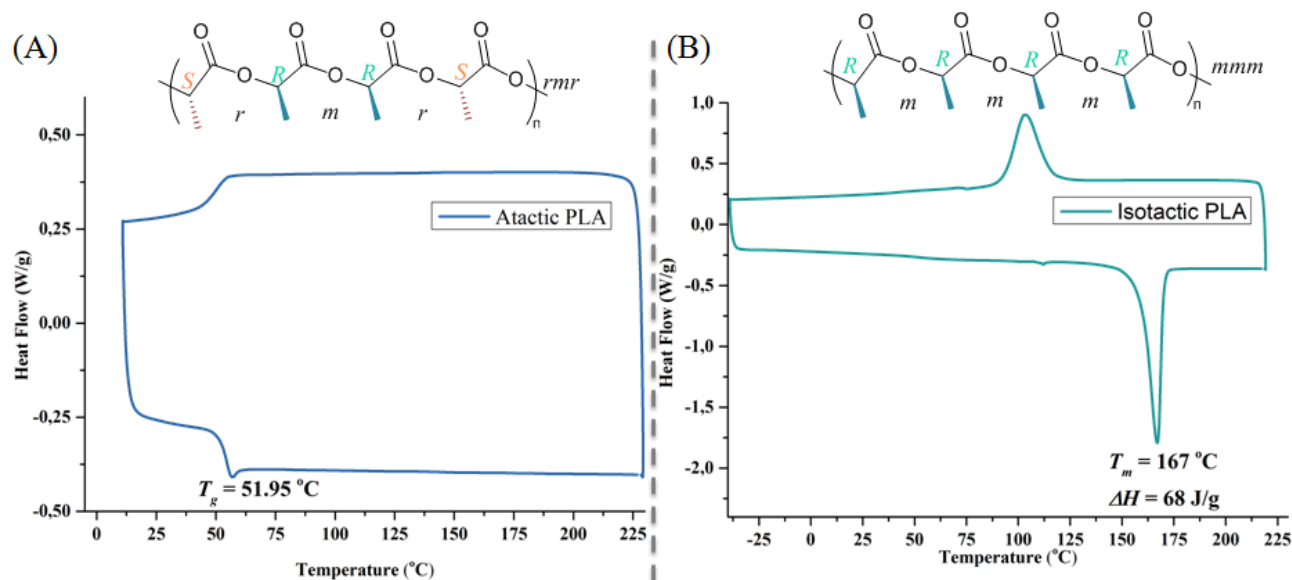
### 2.2.3. Analysis of the microstructure of PLA derived from chiral TUC's

#### 2.2.3.1. DSC Analysis

The thermal properties of the (*S,S*)- and (*R,R*)-TUC-derived PLAs were investigated by differential scanning calorimetry (DSC) using a DSC Q100 RCS TA Instrument. All samples were first heated up to 250 °C at a rate of 10 °C/min, left at this temperature for 10 min, then cooled to 0 °C at the same rate of 10 °C/min, and were left at 0 °C for 10 min. The same heating cycle was thus repeated. Thermal data provided hereafter were obtained from the first heating scan. The degree of crystallinity ( $x_c$ ) was calculated using  $\Delta H_m$  values, which were obtained by the integration of melting point surface areas. The equation is defined as

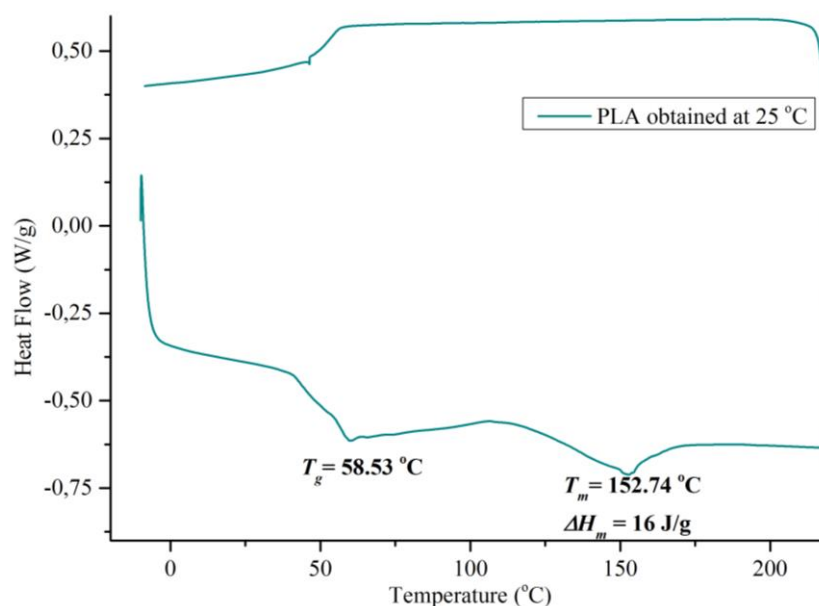
$$x_c = \frac{\Delta H_{m\text{exp}}}{\Delta H_{m\text{theo}}} \quad (\Delta H_{m\text{theo}} = 93.7 \text{ J/g}).^{[17,50]}$$

We initially synthesized purely atactic and crystalline PLAs and characterized their thermal properties to confirm the theoretical data mentioned above. Experimental data showed that while a totally atactic PLA gave a glass transition temperature ( $T_g$ ) at 52 °C, fully isotactic PLA exhibited a melting temperature ( $T_m$ ) at 167 °C with a corresponding  $\Delta H_{mtheo}$  = 68 J/g (Figure 2.11).



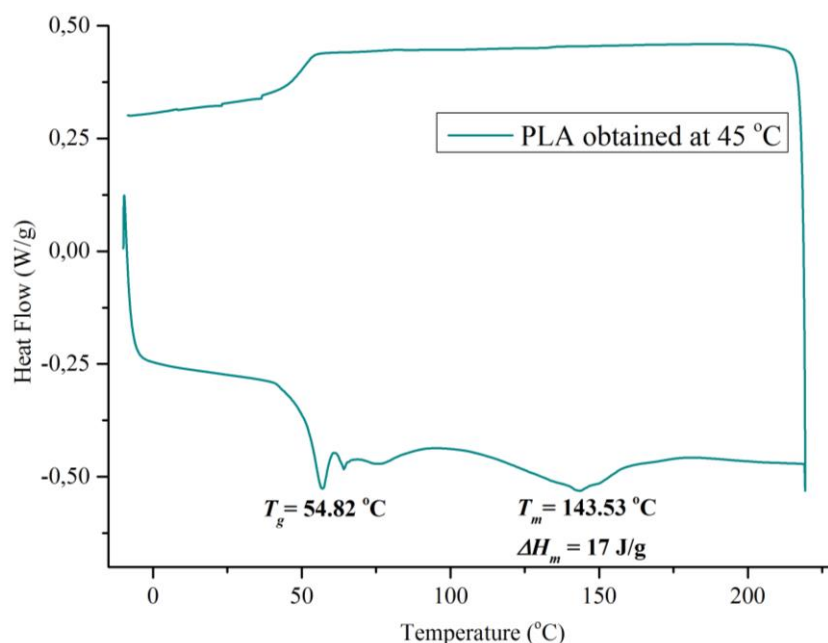
**Figure 2.11.** DSC thermograms (1<sup>st</sup> scan; 10 °C/min) of (A) atactic PLA (B) isotactic PLA obtained by (*S,S*)-TUC at 25 °C.

Intriguingly, DSC analysis of the (*S,S*)-TUC-derived PLA sample revealed a melting transition at  $T_m = 152\text{ }^{\circ}\text{C}$ , thus contrasting what was expected (no  $T_m$ ) from a polymer with an anticipated  $P_m = 0.76$  based on previous reports of its use (Figure 2.12).<sup>[43]</sup>



**Figure 2.12.** DSC thermogram (1<sup>st</sup> scan; 10 °C/min) of the PLA obtained by (*S,S*)-TUC at 25 °C (Table 2.1, entry 2).

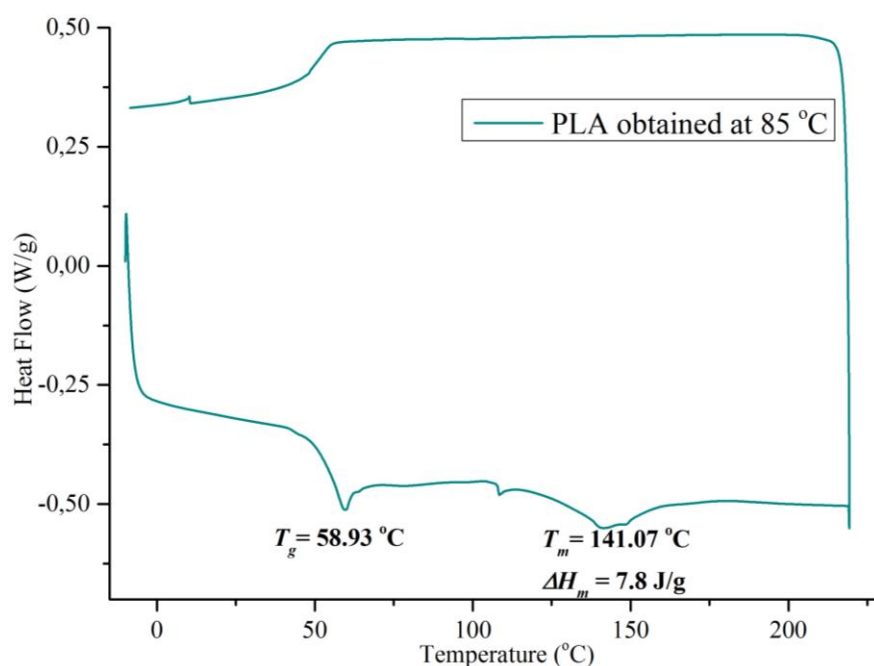
Analysis by DSC showed a defined  $T_g$  and  $T_m$  for PLAs obtained by (*S,S*)-TUC at 45 and 85 °C, respectively. The  $T_m$  for PLA obtained at 45 °C was slightly lower than that obtained at ambient temperature ( $T_m = 143\text{ °C}$ ; Figure 2.13)



**Figure 2.13.** DSC thermogram (1<sup>st</sup> scan; 10 °C/min) of the PLA obtained by (*S,S*)-TUC at 45 °C (Table 2.1, entry 5)

PLA samples synthesized at 85 °C in toluene were also examined by DSC. A  $T_m$  value around 141 °C was observed, a result consistent with the formation of a semi-crystalline

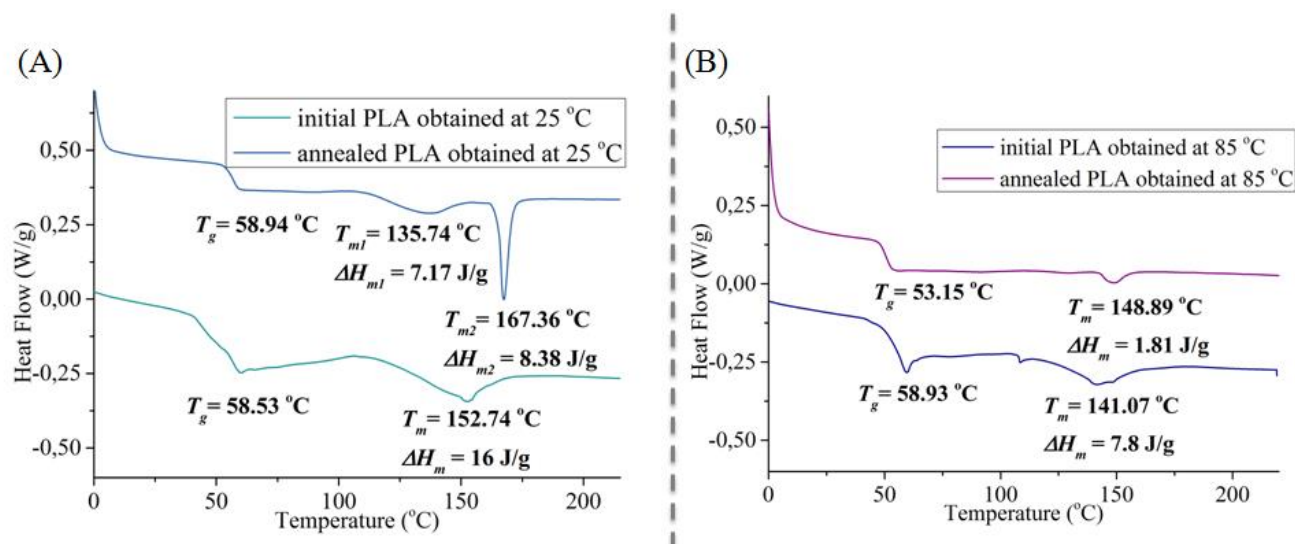
polymer (Figure 2.14). Thus, all PLAs prepared from chiral TUC's from 25 to 45 to 85 °C were shown to exhibit slightly semi-crystalline properties.



**Figure 2.14.** DSC thermogram (1<sup>st</sup> scan; 10 °C/min) of the PLA obtained by (*S,S*)-TUC at 85 °C (Table 2.1, entry 7)

Of particular interest, the extent of crystallinity could be significantly enhanced upon annealing the PLAs. For this purpose, a known amount of the polymer was stirred vigorously at 100 rpm with a magnetic stirrer for overnight close to the melting point of the polymer (~ 145-170 °C). The as-treated sample was then removed from the oil bath and allowed to cool down to room temperature, before re-analysis by DSC. Thus, the PLA prepared at 85 °C that was found slightly semi-crystalline, could be crystallized after annealing at 150 °C for 13 h (Figure 2.15,  $T_m = 149\text{ }^{\circ}\text{C}$ ).





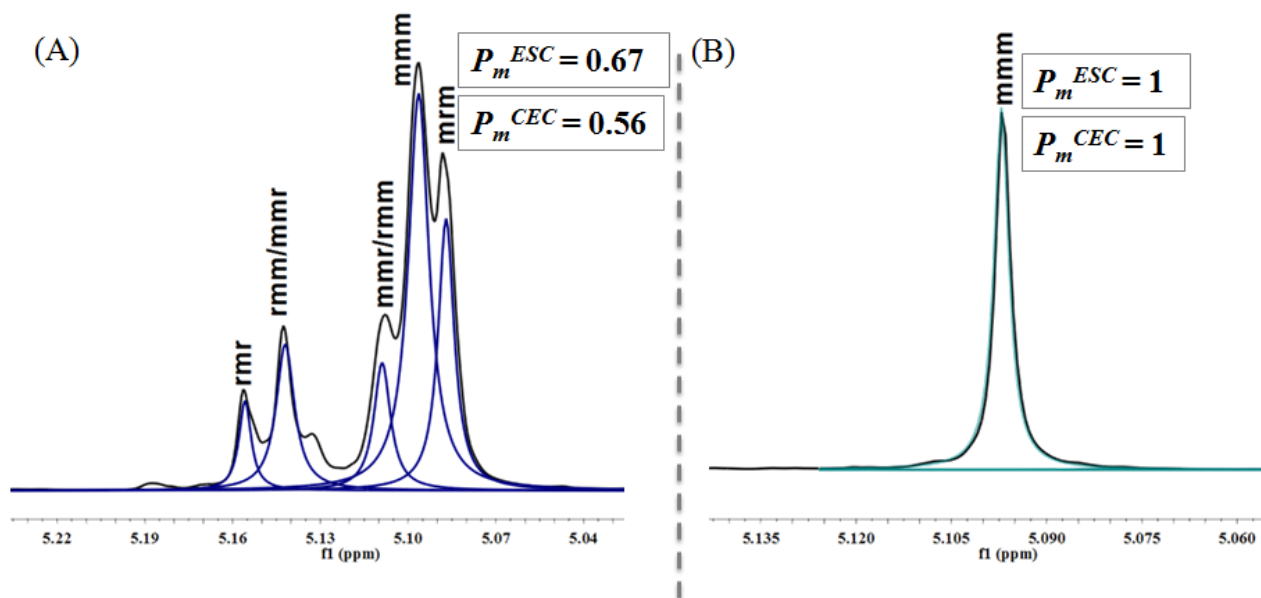
**Figure 2.15.** DSC thermogram (1<sup>st</sup> scan; 10 °C/min) of the (A) initial and annealed PLAs obtained at 25 °C (Table 2.1, entry 2) (B) initial and annealed PLAs obtained at 85 °C (Table 2.1, entry 7).

#### 2.2.3.2. Homonuclear decoupled <sup>1</sup>H NMR and quantitative <sup>13</sup>C NMR analysis

Investigations into stereoselectivity of the ROP process involving *rac*-LA is usually achieved by homonuclear decoupled <sup>1</sup>H NMR (<sup>1</sup>H {<sup>1</sup>H} NMR) and quantitative <sup>13</sup>C NMR spectroscopies.<sup>23</sup> These spectroscopic analyses were performed with Bruker Advance instrument at 400 MHz at room temperature, in CDCl<sub>3</sub> as solvent. The decoupling pulse was focused in the methyl region, at around 1.6 ppm for the separation of five tetrad signals<sup>54</sup> in methine region ( $\sim\delta = 5.00$ -5.20 ppm).<sup>[49,51-56]</sup>

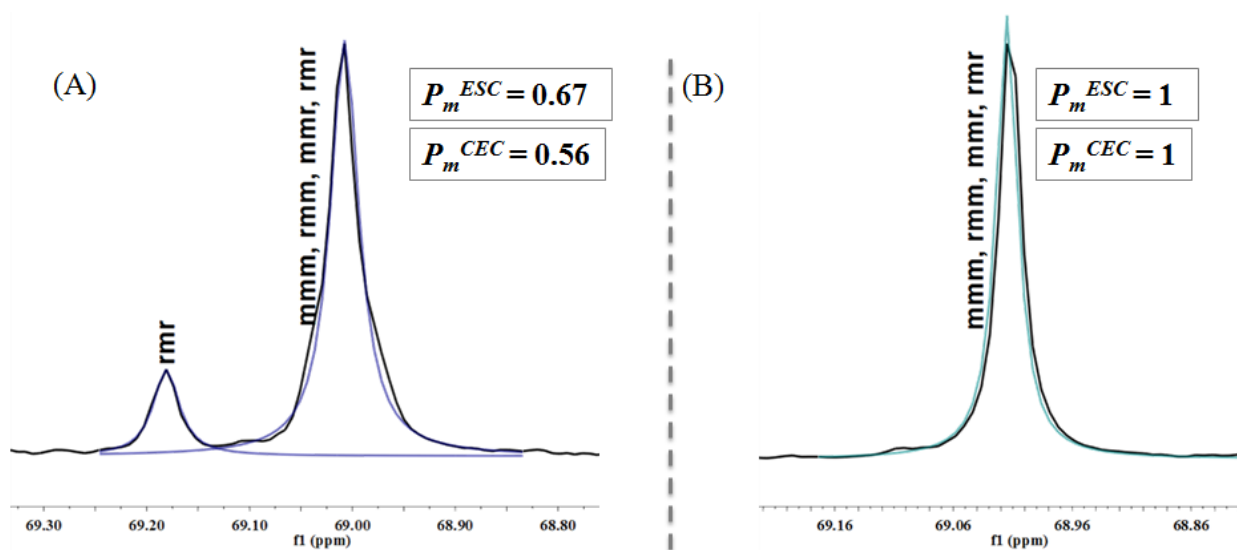
In the instances where five peaks are observed, the approximate integrations of these peaks correlate well with the probabilities for the possible tetrad sequences as predicted by Bernoullian or non-Bernoullian statistics.<sup>[57]</sup> Bernoullian and non-Bernoullian statistics are generally applied based on chain-end control mechanism (CEC) and enantiomorphic site control mechanism (ESC), respectively (Table 2.2). For a value of  $0 < P_m < 0.5$ , the polymerization proceeds preferentially through a heterotactic enchainment and for a value of  $0.5 < P_m < 1$ , the polymerization proceeds preferentially through an isotactic enchainment. As previously mentioned in chapter 1, section 1.5.2, these parameters can be directly calculated from the deconvoluted homonuclear decoupled <sup>1</sup>H NMR spectra<sup>[51,58]</sup> (see reference and section 1.5.3.2 for calculation). For both the ROP of *rac*- and *meso*-lactide,  $P_r$  or  $P_m = 0.50$  describes a completely atactic polymer. In the case of *rac*-lactide  $P_r = 1.00$  ( $P_m = 0.00$ ) and  $P_m = 1.00$  ( $P_r = 0.00$ ) describe perfect heterotactic and isotactic polymers, respectively, whereas

for the ROP of *meso*-lactide  $P_r = 1.00$  ( $P_m = 0.00$ ) and  $P_m = 1.00$  ( $P_r = 0.00$ ) describe perfect syndiotactic and heterotactic polymers, respectively.<sup>[22]</sup> Experimental  $^1\text{H}$   $\{^1\text{H}\}$  NMR spectra of atactic and isotactic PLA is demonstrated below in Figure 2.16.



**Figure 2.16.** Deconvoluted  $^1\text{H}$   $\{^1\text{H}\}$  NMR spectra (400 MHz,  $\text{CDCl}_3$ ) of the methine region of (A) atactic PLA (B) completely isotactic PLA.

Quantitative  $^{13}\text{C}$  NMR spectra also provide quantitative decoupling for the carbon atom bonded to the methine proton. Considering PLA tetrad assignment based on  $^{13}\text{C}$  NMR, the intensities of tetrad ratios are calculated from the considering two deconvoluted peak distributions ( $\sim\delta = 68.4 - 69.6$  ppm).<sup>[57]</sup> Experimental models of deconvoluted  $^{13}\text{C}$  NMR analysis related to atactic and isotactic PLAs are shown below (Figure 2.17).



**Figure 2.17.** Quantitative  $^{13}\text{C}$  NMR spectra (in  $\text{CDCl}_3$ ) of (A) an atactic (B) a completely isotactic PLA.

According to the stereocontrol mechanism of the catalyst (ESC or CEC), the tetrad intensities obtained from  $^{13}\text{C}$  and/or  $^1\text{H}$   $\{^1\text{H}\}$  NMR are applied in non-Bernoullan (used for ESC) or Bernoullan (used for CEC) statistics to calculate the meso ( $P_m$ ) or racemo ( $P_r$ ) chain distribution of the polymer (Table 2.2).

**Table 2.2.** Tetrad probabilities of ESC and CEC mechanisms based on non-Bernoullan and Bernoullan statistics.

tetrad	Probability of ESC (non-Bernoullan)	Probability of CEC (Bernoullan)
<i>mmm</i>	$[P_m^2 + (1 - P_m)^2 + P_m^3 + (1 - P_m)^3]/2$	$P_m^2 + 0.5 P_m P_r$
<i>mmr</i>	$[P_m^2(1 - P_m) + P_m(1 - P_m)^2]/2$	$0.5 P_m P_r$
<i>rmm</i>	$[P_m^2(1 - P_m) + P_m(1 - P_m)^2]/2$	$0.5 P_m P_r$
<i>rmr</i>	$[P_m^2(1 - P_m) + P_m(1 - P_m)^2]/2$	$0.5 P_r^2$
<i>mrmm</i>	$[P_m(1 - P_m)]$	$0.5 (P_m^2 + P_m P_r)$

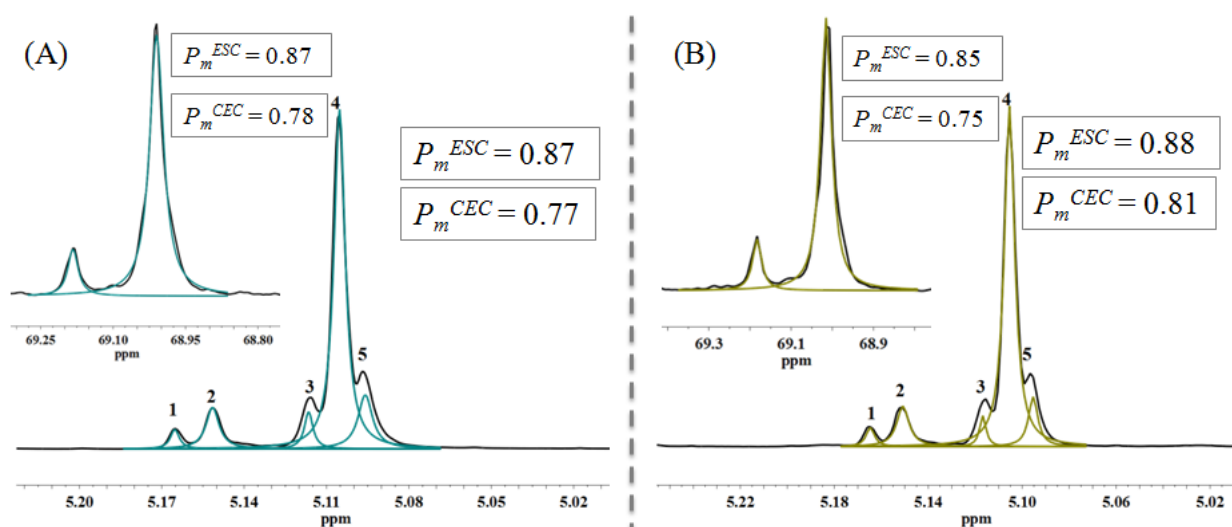
**Table 2.3.** Probabilities of tetrad mesodyads based on ESC and CEC statistics.<sup>a</sup>

Entry	Cat.	[M]/[C]/[I]	T [°C]	Conv. [%] <sup>b</sup>	$M_n$ [kg.mol <sup>-1</sup> ] <sup>c</sup>	$\bar{D}^c$	$P_m^d$ [Based on ESC mec.]		$P_m^d$ [Based on CEC mec.]	
							HD $^1\text{H}$ NMR	$^{13}\text{C}$ NMR	HD $^1\text{H}$ NMR	$^{13}\text{C}$ NMR
1	(S,S)-TUC	200:10:1	25	93	27.6	1.15	0.87	0.87	0.77	0.78
2	(S,S)-TUC	200:5:1	25	85	24.8	1.16	0.87	0.86	0.79	0.74
3	(S,S)-TUC	200:10:1	45	95	18.8	1.24	0.82	0.83	0.73	0.71
4	(S,S)-TUC	200:5:1	45	87	15.7	1.25	0.80	0.87	0.70	0.78
5*	(S,S)-TUC	200:10:1	85	54	10.0	1.83	0.85	0.85	0.77	0.74
6*	(S,S)-TUC	200:5:1	85	60	9.7	1.45	0.82	0.82	0.72	0.73
7*	(R,R)-TUC	200:5:1	25	71	21.2	1.22	0.90	0.87	0.82	0.77
8	(R,R)-TUC	200:5:1	25	87	21.8	1.12	0.88	0.85	0.81	0.75
9	(R,R)-TUC	200:5:1	25	>95	29.4	1.13	0.87	0.88	0.80	0.79
10*	(R,R)-TUC	200:5:1	85	52	8.4	1.16	0.83	0.85	0.74	0.75
11*	(R,R)-TUC	200:5:1	85	88	13.3	1.21	0.83	0.82	0.74	0.71

<sup>a</sup>Polymerizations were conducted in  $\text{CH}_2\text{Cl}_2$  unless otherwise stated. <sup>b</sup>Reactions were performed in toluene. <sup>c</sup>Conversion of polymerizations were determined by SEC in  $\text{CHCl}_3$  and THF before polymer purification or by  $^1\text{H}$  NMR spectroscopic analysis in  $\text{CHCl}_3$ . <sup>d</sup> $M_n$  and  $\bar{D}_M$  are determined by SEC in THF or  $\text{CHCl}_3$  (calibration using polystyrene standards). <sup>e</sup>Probabilities of finding mesodyads are calculated from homonuclear decoupled  $^1\text{H}$  and quantitative  $^{13}\text{C}$  NMR spectra by deconvolution technique. Calculations performed based on ESC and CEC statistics considering Bernoullan and non-Bernoullan statistics.<sup>[49]</sup>

Interestingly, calculation of the  $P_m$  value using CEC statistics after analysis by both  $^1\text{H}$  and quantitative  $^{13}\text{C}$  NMR spectroscopy was consistent with these findings and evidenced the formation of a moderately isotactic PLA with the presence of a large *mmm* tetrad peak. Notably, Pratt *et al.* applied the CEC statistical model to which our results provided a comparable  $P_m$ ; however, using an ESC statistical model,<sup>[59]</sup> a  $P_m = 0.87$  was calculated, much more in line with the observation of crystallinity in the resultant PLA. These preliminary results prompted us to investigate more in depth the mechanism of the ROP of *rac*-LA from chiral Takemoto's catalysts.

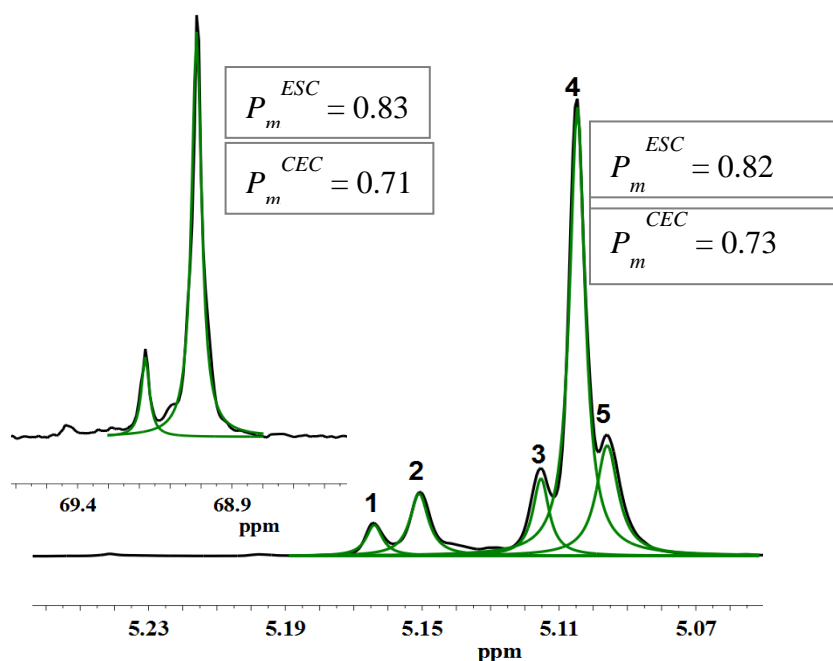
As mentioned previously, (*S,S*)-TUC produced a semicrystalline PLA ( $T_m = 152\text{ }^\circ\text{C}$ ) with a strong isotactic predominance (*it*-PLA) and a  $P_m$  value of 0.87, as determined by ESC statistical analysis (Table 2.3, entry 2) in  $\text{CH}_2\text{Cl}_2$  as solvent (Figure 2.18). In the case of (*R,R*)-TUC, a  $P_m$  value as high as 0.90 could be achieved in toluene (Table 2.3, entry 7) at room temperature, likely as a result of a solvent effect, toluene being less polar than DCM, increasing the probability for forming H-bonding. These  $P_m$  values, calculated by ESC statistical analysis, markedly contrasted with those reported earlier where chiral thiourea-amines showed a modest stereoselectivity ( $P_m$  in the range 0.64–0.77).<sup>[43]</sup>



**Figure 2.18.** Deconvoluted  $^1\text{H}$   $\{^1\text{H}\}$  NMR spectra (400 MHz,  $\text{CDCl}_3$ ) of the methine region of PLAs prepared by the catalysis of (A) (*S,S*)-TUC inset:  $^{13}\text{C}$  NMR spectrum (B) (*R,R*)-TUC inset:  $^{13}\text{C}$  NMR spectrum at  $25\text{ }^\circ\text{C}$  (Table 2.3, entry 1 and 8).

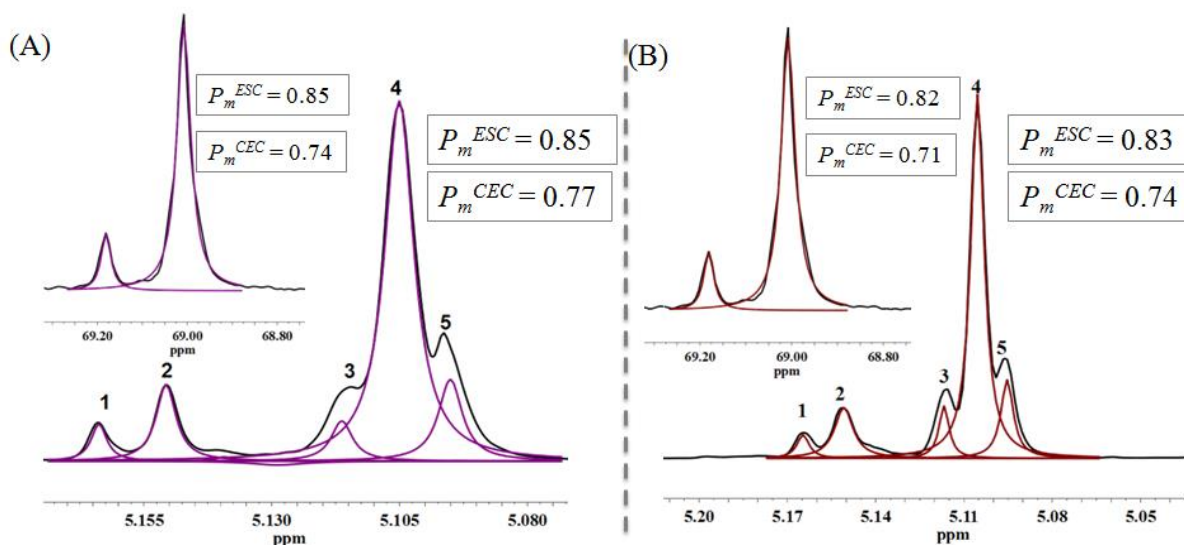
(*S,S*)-TUC also showed stereoselectivity at  $45\text{ }^\circ\text{C}$  in DCM. There was a linear correlation between the increase in temperature and decrease in stereocontrol. However, clearly, the  $P_m$  value obtained was still in an agreeable rate, *i.e.*,  $P_m^{\text{ESC}} = 0.82$  and  $P_m^{\text{CEC}} =$

0.73, which evidenced the stereocontrol of TUC catalyst at high temperatures. Here also,  $P_m$  values were also determined by  $^{13}\text{C}$  NMR ( $P_m^{\text{ESC}} = 0.83$  and  $P_m^{\text{CEC}} = 0.71$ ; Figure 2.19)



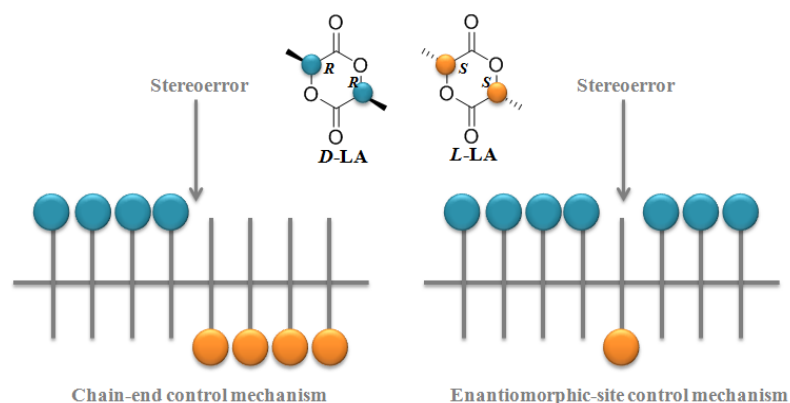
**Figure 2.19.** Deconvoluted  $^1\text{H}$  { $^1\text{H}$ } NMR spectra (400 MHz,  $\text{CDCl}_3$ ) of the methine region of PLA prepared by the catalysis of (*S,S*)-TUC at 45 °C inset:  $^{13}\text{C}$  NMR spectrum (Table 2.3, entry 3)

Interestingly, a  $P_m$  value as high as 0.82 could be obtained at 85 °C (Table 2.3, entry 6), further corroborating this stereoselective mechanism and potentially explaining the discrepancy in results between our study and that of Pratt *et al.* (Figure 2.20b).<sup>44</sup>



**Figure 2.20.** Deconvoluted  $^1\text{H}$  { $^1\text{H}$ } NMR spectra (400 MHz,  $\text{CDCl}_3$ ) of the methine region of PLAs prepared by the catalysis of (A) (*S,S*)-TUC inset:  $^{13}\text{C}$  NMR spectrum (B) (*R,R*)-TUC inset:  $^{13}\text{C}$  NMR spectrum at 85 °C (Table 2.3, entry 5 and 11).

Calculations of  $P_m$  values as a function of one or the other mechanism, *i.e.* CEC or ESC, lead to differing results and clearly, the mechanism of catalyst operation is critical in studies such as this because of the proved semi-crystalline polymer chain which was not the case of previous study by Pratt *et al.*<sup>[43]</sup> Assuming *it*-PLA would form by a CEC mechanism exclusively, relative tetrad intensities would be expected as follows:<sup>[53]</sup>  $[mmr] = [rmm] \neq [rmr]$ . In this case, stereoblocks could be generated when a growing PLA chain incidentally incorporated the LA enantiomer of opposite configuration to that of the last inserted enantiomer. This would create a stereoerror from which “normal” growth would form a new stereoblock of opposite configuration to the previous one (Figure 2.21). Conversely, the ESC mechanism should generate single insertion stereoerrors of the type  $-RRRRSSRRR/-SSSSRRSSSS-$ . In the latter case, the tetrad ratio should be  $[rmr] = [mmr] = [rmm] = 2/[mmr]$ .<sup>[49]</sup> The *rmr* signal is a clear indicator of mechanism.



**Figure 2. 21.** Mechanisms of stereocontrol forming stereoerrors.

Analysis of the NMR spectra of the PLAs produced here revealed the tetrad ratios to be  $[rmr] = 0.030$   $[mmr] = 0.055$   $[rmm] = 0.096$  and  $[mmr] = 0.13$ , which were consistent with neither the ESC nor the CEC mechanism, thus strongly suggesting that both mechanisms concomitantly occurred.

Chiral HPLC analysis and kinetic reactions also assumed that to contribute significantly to the clarification of the stereocontrol mechanism. The maximum catalyst selectivity supposed to be at 50% of monomer conversion. Thus, if the catalyst would exhibit pure stereoselectivity in the presence of ESC mechanism, one of the LA enantiomer would completely be consumed. For that purpose, aliquots were withdrawn on pre-determined time intervals and polymers were quenched and precipitated. Later on, the residual monomers were recovered from the hexane/isopropanol solvent and the enantiomeric excess (*ee*) of the

unreacted monomer was determined by a chiral HPLC measurement; this was carried out in Prof. A. Dove's laboratory at the University of Warwick.

**Table 2.4.** Chiral HPLC results of residual monomer which is recovered from hexane/isopropanol.<sup>a</sup>

Entry	Catalyst	[M]/[C]/[I]	<i>T</i> [°C]	<i>t</i> [h]	Conv. [%] <sup>b</sup>	<i>M<sub>n</sub></i> [kg.mol <sup>-1</sup> ] <sup>c</sup>	<i>M<sub>n</sub><sup>calc</sup></i> [kg.mol <sup>-1</sup> ] <sup>d</sup>	<i>D<sub>M</sub></i> <sup>c</sup>	<i>P<sub>m</sub></i> <sup>e</sup>	<i>s</i> ( <i>k<sub>fast</sub></i> / <i>k<sub>slow</sub></i> ) <sup>f</sup>	<i>ee</i> <sup>f</sup> (%)
1	( <i>S,S</i> )-TUC	200:5:1	25	32	42	9.3	12.2	1.07	0.88	3.6	32
2	( <i>S,S</i> )-TUC	200:10:1	25	25	47	13.3	13.5	1.05	0.84	3.0	34
3	( <i>R,R</i> )-TUC	200:5:1	25	96	55	20.0	16.0	1.12	0.86	3.4	41

<sup>a</sup>Polymerizations were conducted in CH<sub>2</sub>Cl<sub>2</sub> unless otherwise stated. <sup>b</sup> Conversion of polymerizations were determined by SEC in CHCl<sub>3</sub> and THF before polymer purification or by <sup>1</sup>H NMR spectroscopic analysis in CHCl<sub>3</sub>. <sup>c</sup> *M<sub>n</sub>* and *D<sub>M</sub>* are determined by SEC in THF or CHCl<sub>3</sub> (calibration using polystyrene standards). <sup>d</sup>Theoretical number-average molar mass  $M_n^{calc} = [LA]_0/[BnOH]_0 \times M_{LA} \times x_{LA} + M_{BnOH}$ . <sup>e</sup>*T<sub>g</sub>*, *T<sub>m</sub>* and  $\Delta H_m$  values are obtained by DSC measurements from 1<sup>st</sup> heating curve. <sup>f</sup>Probabilities of finding mesodyads are calculated from homonuclear decoupled <sup>1</sup>H by deconvolution technique. All calculations based on ESC statistics.<sup>51</sup> <sup>f</sup>Enantiomeric excess (e.e. %) of unreacted monomer was calculated by chiral HPLC.

Chiral HPLC analysis of unreacted monomer revealed an enantiomeric excess (ee) of 32%, corresponding to a stereoselectivity factor ( $s = k_D/k_L$ ) of 3.6 (Table 2.4, entry 1) at 42% monomer conversion in the presence of (*S,S*)-TUC, and  $s = 3.4$  at 55% of monomer conversion using (*R,R*)-TUC (Table 2.4, entry 3). Unexpectedly, increasing the catalyst loading from 5 to 10 equiv. led to a lower selectivity factor ( $s = 3.0$ ; Table 2.4, entry 2); hence, a loading of 5 mol % relative to the initiator was maintained for the rest of the study.

#### 2.2.4. Kinetics of the ring-opening polymerization's of *rac*-LA from chiral thiourea

Kinetic studies involving each enantiomeric form of the catalyst represents a powerful means to assess the stereocontrol of the ROP process. The determination of the propagation rate constant, denoted as  $k_p$ , indeed enables to estimate any preference of the catalyst for a given monomer (*D*-LA vs. *L*-LA).

First-order kinetics are applied on the ROP of LA and:

$$-\frac{d[LA]}{dt} = k_p[LA][I]_0^n$$

$[LA]$  = lactide concentration,  $[I]_0$  = initiator concentration,  $n$  = order of initiator.

And in case of propagation rate constant, the formula is described as below.

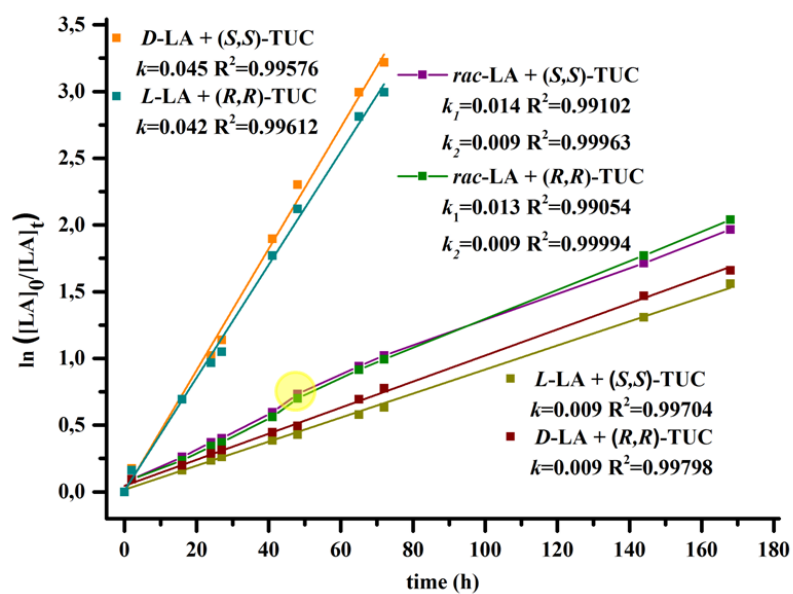
$$-\frac{d[LA]}{dt} = k_{obs}[LA]$$

$[LA]$  = lactide concentration,  $k_{obs}$  = observed rate constant

The observed rate constant,  $k_{obs}$ , is obtained by kinetic data points obtained during the polymerization. So each time, the value obtained is unique and special to that reaction conditions.

In further experiments, both *D*- and *L*-LA were thus polymerized using each chiral TUC in order to provide evidence for the stereoselective mechanism. The corresponding first-order kinetic plots (Figure 2.22) evidenced that (*S,S*)-TUC preferentially polymerized *D*-LA, whereas incorporation of *L*-LA was consistently favored using (*R,R*)-TUC. These kinetic studies enabled us to recalculate the selectivity factor:  $s = k_D/k_L = 5$  and  $s = k_D/k_L = 4.6$  for (*S,S*)-TUC and (*R,R*)-TUC, respectively. The latter values proved slightly higher than those determined above by chiral HPLC. Kinetic study of *rac*-LA ROP revealed first-order kinetic plots with two distinct slopes ( $k_1 = 0.014$ ,  $k_2 = 0.009$ ). A decrease in rate after roughly 65 h was observed with both the (*S,S*)- and the (*R,R*)-TUCs. Given the differing preference of each of the two chiral TUCs for the two monomers (*D*-LA and *L*-LA), this deceleration could be correlated to the preferential consumption of a given enantiomer by a given TUC, *i.e.*, to the selectivity factor. These results suggest that an ESC mechanism may be dominant.





**Figure 2.22.** Kinetic plots of the ROP of *rac*-LA, *D*-LA and *L*-LA catalyzed by (*S,S*)-TUC and (*R,R*)-TUC in CH<sub>2</sub>Cl<sub>2</sub> at RT in the presence of BnOH as a initiator: [LA]<sub>0</sub>: [TUC]: [BnOH] = 200:5:1, deceleration point is highlighted with yellow circle.

### 2.3. Conclusions and outlooks

In this chapter, both commercially available (*R,R*)- and (*S,S*)-enantiomers of chiral thiourea-amine Takemoto's organocatalysts have been shown to promote efficient control and high isoselectivity at room temperature of the ROP of *rac*-LA by kinetic resolution, yielding highly isotactic, semicrystalline and metal-free PLA. Kinetic investigations and combined analyses of the resulting PLAs have allowed to determine the stereocontrol mechanism, which eventually involves both enantiomeric site control and chain-end control, to be determined. Moreover, epimerization of *rac*-LA to *meso*-LA is identified as being responsible for the introduction of some stereoerrors during the ROP process.

The ROP of *rac*-LA using the two chiral version of Takemoto's thiourea-amine catalyst (TUC) enables the formation of semi-crystalline PLA free of any metallic residues, at room temperature, as a result of a highly isoselective ROP process. This study sheds light on the origin of the stereocontrol, evidencing the concomitant occurrence of both CEC and ESC mechanisms. Despite some epimerization, transforming *rac*- to *meso*-LA, isoselectivity remains high without the need to work at very low temperature, in the presence of the (*R,R*)- and the (*S,S*)-TUC. The former organocatalyst preferentially incorporates *L*-LA, whereas the (*S,S*)-catalyst preferentially polymerized *D*-LA. The selectivity for one or the other LA enantiomer can thus be switched by changing the configuration of the Takemoto's catalyst.

Future developments will undoubtedly look to further develop the range of stereospecific catalyst species to develop greater water tolerance, increased selectivity towards alcoholic initiators and propagating species over water, lower cost, recoverability and lowered toxicity. While metal-free catalysts demonstrate many of these attributes, the development of catalysts that display high levels of stereoselectivity at ambient temperature will also be important.

## 2.4. Experimental and supporting information

**Materials:** *D*-LA (Corbion-Purac), *L*-LA (Corbion-Purac) and *D,L*-LA (Sigma-Aldrich) were recrystallized three times from dry toluene. Afterwards, azeotropic distillation was performed for purification of the monomers. Lastly, they were dried under dynamic vacuum for overnight prior to use.<sup>[60]</sup> (*S,S*)- and (*R,R*)-TUC were received from Strem Chemicals, dried azeotropically under toluene 3 times. Benzyl alcohol (BnOH) was received from Alfa Aesar, distilled by cryo-distillation over calcium hydride (CaH<sub>2</sub>). Benzoic acid (≥99.5%, Sigma-Aldrich) was used as received. All dry solvents were collected from solvent drying machine. Afterwards, they stored over molecular sieves (3 Å) in a glovebox for no longer than 4 weeks.

**Instrumentation:** <sup>1</sup>H NMR, <sup>13</sup>C NMR and homonuclear decoupled <sup>1</sup>H NMR spectroscopic measurements were performed at room temperature on Bruker Advance instrument at 400 MHz. CDCl<sub>3</sub> was used as an internal reference ( $\delta = 7.26$ ) and the relaxation time was fixed to 2 s. For homonuclear decoupled <sup>1</sup>H NMR spectroscopic analysis, relaxation time was measured and fixed to 2.04 s. Samples were obtained in CDCl<sub>3</sub> solutions with the decoupling pulse based on the methyl region ( $\sim\delta = 1.5$  ppm). In case of the good separation of methine region ( $\sim\delta = 5.00$ - $5.20$  ppm), the global spectral deconvolution technique was implemented by attribution of five mesodyads based on both non-Bernoullan and Bernoullan statistics in case of the operated combination mechanism.<sup>[49,51–56]</sup>

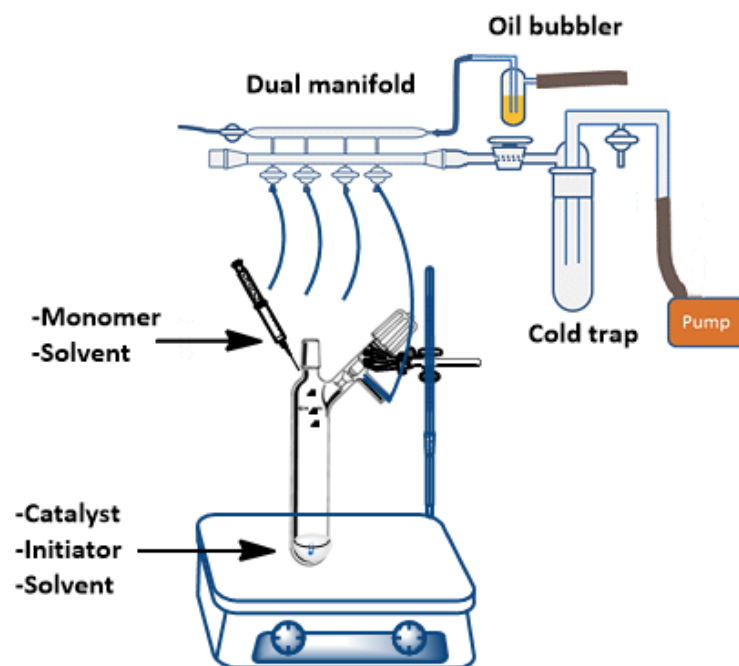
Polymer molar masses were determined by size exclusion chromatography (SEC) using tetrahydrofuran (THF) as the eluent. Measurements in THF were performed on an Ultimate 3000 system from Thermoscientific equipped with diode array detector DAD. The system also includes a multi-angles light scattering detector MALS and differential refractive index detector dRI from Wyatt technology. Polymers were separated on three G2000, G3000 and G4000 TOSOH HXL gel columns (300 x 7.8 mm) (exclusion limits from 1000 Da to 400 000 Da) at a flowrate of 1 mL/min. Columns temperature was held at 40°C. Polystyrene was used as the standard.

$T_g$ ,  $T_m$  and  $\Delta H_m$  values were analyzed by differential scanning calorimetry (DSC) using a DSC Q100 RCS TA Instrument. Polymer samples were first heated to 250 °C at 10 °C/min, equilibrated at this temperature for 10 min, then cooled to -10 °C at 10°C/min, held for 10 min, and reheated to 250 °C at 10 °C/min. All thermal data were obtained from the first scan. Degree of crystallinity ( $x_c$ ) was calculated using  $\Delta H_m$  values, which are obtained by the integration of melting point surface areas. The equation is defined as  $x_c = \frac{\Delta H_{mexp}}{\Delta H_{mtheo}}$ . ( $\Delta H_{mtheo} = 93.7$  J/g)<sup>[17,50]</sup>

**General polymerization methods:** In case of the polymerizations performed at R.T: dry 10 mL vials were first introduced into a Argon-filled glovebox. In a typical polymerization reaction catalyst (for 10 eq.; 28.68 mg, 0.069 mmol, for 5 eq; 14.34 mg, 0.034mmol) and external BnOH as an initiator (0.71  $\mu$ L, 0.0069 mmol) were dissolved in dichloromethane (0.42 mL). Shortly after, previously dissolved *rac*-LA (0.2 g, 1.38 mmol) in dichloromethane (1 mL) was added to the vigorously stirred solution. Polymerizations were performed in glovebox and monitored by  $^1\text{H}$  NMR spectroscopy and SEC before precipitation. Then they were quenched by addition of benzoic acid (4.15 mg, 0.034). The polymer was subsequently precipitated from cold methanol (MeOH), and after filtration, it was excessively washed with methanol to remove any impurities. All polymers were dried under dynamic vacuum for overnight. Monomer conversion was calculated by comparing the integration of the methyl signals of unreacted monomer to the methyl region of the polymer before precipitation. Theoretical molar masses ( $M_{\text{theo.}}$ ) were calculated from  $^1\text{H}$  NMR spectra from the monomer conversion factor ( $x_{\text{LA}}$ ).

Table 2.1, entry 9: A sealed ampoule equipped with a Teflon® valve was charged with *rac*-LA (0.2g, 1.38 mmol). A solution of TUC (14.4 mg), BnOH (70  $\mu$ L of a 0.1M solution of BnOH in toluene) in toluene (1.4 mL), was added to the *rac*-lactide and the heterogeneous solution was stirred at room temperature for the desired time.

Experiments carried out at higher temperature employed in a Schlenk system using dynamic vacuum and inert atmosphere. Binary Schlenk system refers dual manifold Schlenk line with several ports under it. Basically, one manifold is connected to a purified inert argon gas while the other is connected to a vacuum pump. The inert-gas line is gone through an oil bubbler, while solvent vapors and gaseous reaction products are hindered from contaminating the vacuum pump by a liquid-nitrogen trap (Figure 2.23).



**Figure S1.1.** Illustrated binary Schlenk system used in polymerizations.

Dry 10 mL Schlenk tubes were first introduced into an Argon-filled glovebox. In a typical polymerization reaction catalyst (for 10 eq.; 28.68 mg, 0.069 mmol, for 5 eq; 14.34 mg, 0.034mmol) and external BnOH as an initiator (0.71  $\mu$ L, 0.0069 mmol) were introduced to the Schlenk tube and dissolved in dichloromethane (0.42 mL). Shortly after, previously dissolved *rac*-LA (0.2 g, 1.38 mmol) in dichloromethane (1 mL) was added to the Schlenk tube. Then, the tightly closed Schlenk tube was removed from the glovebox and introduced inside the pre-heated oil bath at 45°C or 85 °C. Polymerization was performed under binary Schlenk system with dynamic vacuum and inert atmosphere in oil bath. Binary Schlenk system refers dual manifold Schlenk line with several ports under it. Basically, one manifold is connected to a purified inert argon gas while the other is connected to a vacuum pump. The inert-gas line is gone through an oil bubbler, while solvent vapors and gaseous reaction products are hindered from contaminating the vacuum pump by a liquid-nitrogen trap. Polymerizations monitored by  $^1\text{H}$  NMR spectroscopy and SEC before precipitation and were quenched by addition of benzoic acid (4.15 mg, 0.034). The polymer was subsequently precipitated from cold methanol (MeOH) and was collected by filtration before being washed with excess methanol to remove impurities. Afterwards, polymers obtained were dried under dynamic vacuum for overnight. Percent conversion was calculated by comparing the integration of the methyl signals of unreacted monomer to the methyl region of the polymer before precipitations from NMR spectra.

Bulk (solvent-free) conditions were also attempted on the ROP of *rac*-LA was carried out at 150 °C. Binary Schlenk system was used to perform the polymerizations. After reactants were prepared in schlenk tubes under glovebox, they were placed in pre-heated oil bath, immediately after. Polymerizations were monitored by  $^1\text{H}$  NMR spectroscopy and by SEC before purification by precipitation. The polymer was subsequently precipitated from cold methanol (MeOH) and was collected by filtration before being washed with excess methanol to remove impurities. Afterwards, polymers obtained were dried under dynamic vacuum for overnight. Percent conversion was calculated by comparing the integration of the methyl signals of unreacted monomer to the methyl region of the polymer before precipitations from NMR spectra.

All complementary studies were performed by (*R,R*)-TUC in the same conditions in chemistry laboratory in University of Warwick. Results were found in coherence with both (*S,S*) and (*R,R*) enantiomer of catalyst.

## 2.5. References

- [1] J. Kadota, D. Pavlović, J. P. Desvergne, B. Bibal, F. Peruch, A. Deffieux, *Macromolecules* **2010**, *43*, 8874.
- [2] M. Fèvre, J. Pinaud, Y. Gnanou, J. Vignolle, D. Taton, *Chem. Soc. Rev.* **2013**, *42*, 2142.
- [3] N. E. Kamber, W. Jeong, R. M. Waymouth, R. C. Pratt, B. G. G. Lohmeijer, J. L. Hedrick, *Chem. Rev.* **2007**, *107*, 5813.
- [4] X. Zhang, M. Fevre, G. O. Jones, R. M. Waymouth, *Chem. Rev.* **2018**, *118*, 839.
- [5] O. Coulembier, A. P. Dove, R. C. Pratt, A. C. Sentman, D. A. Culkin, L. Mespouille, P. Dubois, R. M. Waymouth, J. L. Hedrick, *Angew. Chemie - Int. Ed.* **2005**, *44*, 4964.
- [6] A. P. Dove, Organic catalysis for ring-opening polymerization. *ACS Macro Lett.* **2012**, 1409–1412.
- [7] M. K. Kiesewetter, E. J. Shin, J. L. Hedrick, R. M. Waymouth, *Macromolecules* **2010**, *43*, 2093.
- [8] S. Naumann, P. B. V Scholten, J. A. Wilson, A. P. Dove, *J. Am. Chem. Soc.* **2015**, *137*, 14439.
- [9] F. Nederberg, E. F. Connor, M. Möller, T. Glauser, J. L. Hedrick, *Angew. Chem. Int. Ed. Engl.* **2001**, *40*, 2712.
- [10] J. Raynaud, W. N. Ottou, Y. Gnanou, D. Taton, *Chem. Commun.* **2010**, *46*, 3203.
- [11] C. Thomas, F. Peruch, B. Bibal, *RSC Adv.* **2012**, *2*, 12851.
- [12] N. Zhang, H. Chen, Y. Fan, L. Zhou, S. Trépout, J. Guo, M. H. Li, *ACS Nano* **2018**, *12*, 4025.
- [13] J. Lou, F. Liu, C. D. Lindsay, O. Chaudhuri, S. C. Heilshorn, Y. Xia, *Adv. Mater.* **2018**, *30*, 1.
- [14] M. Li, S. Lv, Z. Tang, W. Song, H. Yu, H. Sun, H. Liu, X. Chen, *Macromol. Biosci.* **2013**, *13*, 1150.
- [15] H. Tsuji, *Macromol. Biosci.* **2005**, *5*, 569.
- [16] D. Garlotta, *J. Polym. Environ.* **2002**, *9*, 63.
- [17] D. Arbeiter, K. Schümann, O. Sahmel, T. Eickner, K.-P. Schmitz, N. Grabow, *Curr. Dir. Biomed. Eng.* **2016**, *2*, 27.
- [18] M. Wisniewski, A. Le Borgne, N. Spassky, *Macromol. Chem. Phys.* **1997**, *198*, 1227.
- [19] H. Tsuji, Y. Ikada, *Polymer (Guildf).* **1999**, *40*, 6699.
- [20] H. Tsuji, S. H. Hyon, Y. Ikada, *Macromolecules* **1991**, *24*, 5657.
- [21] H. Tsuji, Y. Ikada, F. Horii, M. Nakagawa, H. Odani, R. Kitamaru, *Macromolecules* **1992**, *25*, 4114.
- [22] M. J. Stanford, A. P. Dove, *Chem. Soc. Rev.* **2010**, *39*, 486.
- [23] C. Li, T. Jiang, J. Wang, H. Wu, S. Guo, X. Zhang, J. Li, J. Shen, R. Chen, Y. Xiong, *ACS Appl. Mater. Interfaces* **2017**, *9*, 25818.
- [24] J. Wang, Y. Liu, Y. Ma, C. Sun, W. Tao, Y. Wang, X. Yang, J. Wang, *Adv. Funct. Mater.* **2016**, *26*, 7516.
- [25] L. Tang, R. Tong, V. J. Coyle, Q. Yin, H. Pondenis, L. B. Borst, J. Cheng, T. M. Fan, *ACS Nano* **2015**, *9*, 5072.

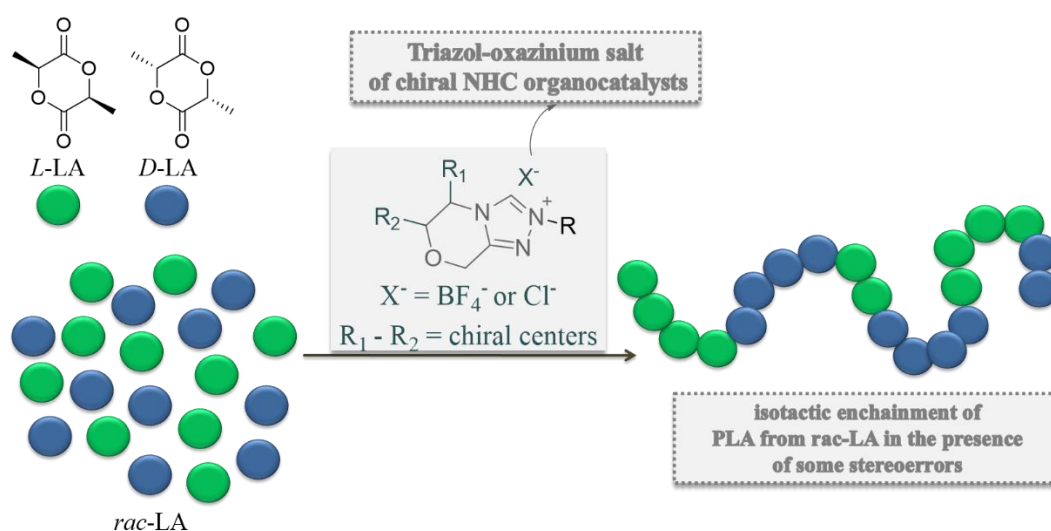
- [26] X. Wu, Y. Ma, G. Zhang, Y. Chu, J. Du, Y. Zhang, Z. Li, Y. Duan, Z. Fan, J. Huang, *Adv. Funct. Mater.* **2015**, 25, 2138.
- [27] J. B. Zhu, E. Y. X. Chen, *J. Am. Chem. Soc.* **2015**, 137, 12506.
- [28] M. H. Chisholm, *Pure Appl. Chem* **2010**, 82, 1647.
- [29] N. Spassky, M. Wisniewski, C. Pluta, A. Le, *Macromol. Chem. Phys.* **1996**, 2637, 2627.
- [30] N. Spassky, C. Pluta, V. Simic, M. Thiam, M. Wisniewski, *Macromol. Symp.* **1998**, 128, 39.
- [31] C. P. Radano, G. L. Baker, M. R. Smith, *J. Am. Chem. Soc.* **2000**, 122, 1552.
- [32] X. Pang, R. Duan, X. Li, C. Hu, X. Wang, X. Chen, *Macromolecules* **2018**, 51, 906.
- [33] Y. Chapurina, J. Klitzke, O. D. L. Casagrande, M. Awada, V. Dorcet, E. Kirillov, J. F. Carpentier, *Dalt. Trans.* **2014**, 43, 14322.
- [34] K. Majerska, A. Duda, *J. Am. Chem. Soc.* **2004**, 126, 1026.
- [35] C. M. Thomas, *Chem. Soc. Rev.* **2010**, 39, 165.
- [36] O. Dechy-Cabaret, B. Martin-Vaca, D. Bourissou, *Chem. Rev.* **2004**, 104, 6147.
- [37] A. P. Dove, H. Li, R. C. Pratt, B. G. G. Lohmeijer, D. A. Culkin, R. M. Waymouth, J. L. Hedrick, *Chem. Commun.* **2006**, 2881.
- [38] L. Zhang, F. Nederberg, J. M. Messman, R. C. Pratt, J. L. Hedrick, C. G. Wade, *J. Am. Chem. Soc.* **2007**, 129, 12610.
- [39] G. M. Miyake, E. Y. X. Chen, *Macromolecules* **2011**, 44, 4116.
- [40] K. Makiguchi, T. Yamanaka, T. Kakuchi, M. Terada, T. Satoh, *Chem. Commun.* **2014**, 50, 2883.
- [41] A. Sanchez-Sanchez, I. Rivilla, M. Agirre, A. Basterretxea, A. Etxeberria, A. Veloso, H. Sardon, D. Mecerreyes, F. P. Cossio, *J. Am. Chem. Soc.* **2017**, 139, 4805.
- [42] S. Liu, H. Li, N. Zhao, Z. Li, *ACS Macro Lett.* **2018**, 7, 624.
- [43] R. C. Pratt, B. G. G. Lohmeijer, D. A. Long, P. N. P. Lundberg, A. P. Dove, H. Li, C. G. Wade, R. M. Waymouth, J. L. Hedrick, *Macromolecules* **2006**, 39, 7863.
- [44] B. G. G. Lohmeijer, R. C. Pratt, F. Leibfarth, J. W. Logan, D. A. Long, A. P. Dove, F. Nederberg, J. Choi, C. Wade, R. M. Waymouth, J. L. Hedrick, *Macromolecules* **2006**, 39, 8574.
- [45] K. V. Fastnacht, S. S. Spink, N. U. Dharmaratne, J. U. Pothupitiya, P. P. Datta, E. T. Kiesewetter, M. K. Kiesewetter, *ACS Macro Lett.* **2016**, 5, 982.
- [46] A. P. Dove, R. C. Pratt, B. G. G. Lohmeijer, R. M. Waymouth, J. L. Hedrick, *J. Am. Chem. Soc.* **2005**, 127, 13798.
- [47] T. Okino, Y. Hoashi, Y. Takemoto, *J. Am. Chem. Soc.* **2003**, 125, 12672.
- [48] The value was calculated using CEC statistics.
- [49] T. M. Ovitt, G. W. Coates, **2002**, 284.
- [50] K. Jamshidi, S.-H. Hyon, Y. Ikada, *Polymer (Guildf)*. **1988**, 29, 2229.
- [51] J. Coudane, C. Ustariz-Peyret, G. Schwach, M. Vert, *J. Polym. Sci. Part A Polym. Chem.* **1997**, 35, 1651.
- [52] J. Kasperczyk, M. Bero, *Makromol. Chem.* **1993**, 194, 913.



- [53] B. M. Chamberlain, M. Cheng, D. R. Moore, T. M. Ovitt, E. B. Lobkovsky, G. W. Coates, *J. Am. Chem. Soc.* **2001**, *123*, 3229.
- [54] K. M. Thakur, R. T. Kean, E. S. Hall, J. J. Kolstad, T. A. Lindgren, M. A. Doscotch, J. I. Siepmann, E. J. Munson, *Macromolecules* **1997**, *30*, 2422.
- [55] K. A. M. Thakur, R. T. Kean, M. T. Zell, B. E. Padden, E. J. Munson, *Chem. Commun.* **1998**, 1913.
- [56] K. a. M. Thakur, R. T. Kean, E. S. Hall, J. J. Kolstad, E. J. Munson, *Macromolecules* **1998**, *31*, 1487.
- [57] M. H. Chisholm, S. S. Iyer, D. G. McCollum, M. Pagel, U. Werner-Zwanziger, *Macromolecules* **1999**, *32*, 963.
- [58] J. Belleney, M. Wisniewski, A. Le Borgne, *Eur. Polym. J.* **2004**, *40*, 523.
- [59] Y. Ikada, K. Jamshidi, H. Tsuji, S. H. Hyon, *Macromolecules* **1987**, *20*, 904.
- [60] O. Coulembier, P. Dubois, *J. Polym. Sci. Part A Polym. Chem.* **2012**, *50*, 1672.

### Chapter 3.

## Stereoselective Ring-Opening Polymerization of *rac*-Lactide Catalyzed by Chiral *N*-Heterocyclic Carbene Organocatalysts



**Keywords:** Stereoselective • Lactide • Carbene • Ring-Opening Polymerization • Organocatalyst

## Chapter 3

# Stereoselective Ring-Opening Polymerization of *rac*-Lactide Catalyzed by Chiral *N*-Heterocyclic Carbene Organocatalysts

### Contents

<b>Chapter 3. Stereoselective Ring-Opening Polymerization of <i>rac</i>-Lactide Catalyzed by Chiral <i>N</i>-Heterocyclic Carbene Organocatalysts .....</b>	<b>113</b>
3.1. Introduction.....	115
3.2. Generalities on <i>N</i> -heterocyclic carbenes (NHCs) and their use as organic catalysts in (macro)molecular chemistry .....	118
3.3. Stereoselective ROP of <i>rac</i> -LA using chiral NHCs as organocatalysts .....	127
3.3.1. Polymerization procedure .....	127
3.3.2. Characterization of chiral NHC-derived PLAs .....	131
3.3.3. Analysis of the stereoselectivity of NHC-derived PLAs .....	137
3.3.3.1. DSC Analysis .....	137
3.3.3.2. Homonuclear decoupled <sup>1</sup> H NMR and quantitative <sup>13</sup> C NMR analysis .....	137
3.3.4. Kinetic studies of the ROP of <i>rac</i> -LA .....	144
3.4. Conclusions and perspectives .....	148
3.5. Experimental and supporting informations .....	149
3.6. References.....	162

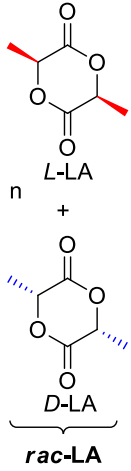
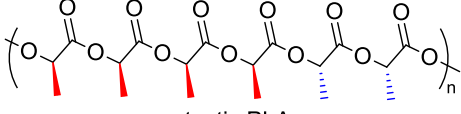
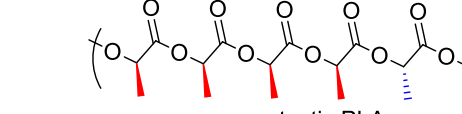
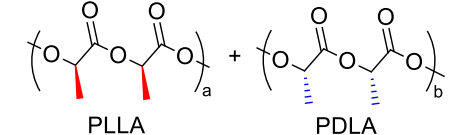
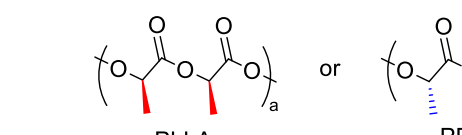

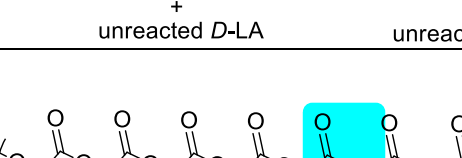
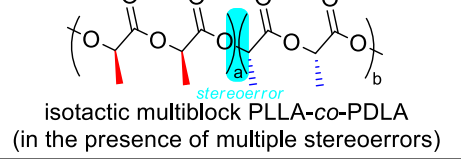
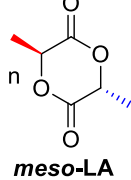
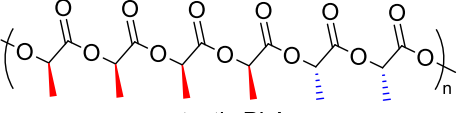
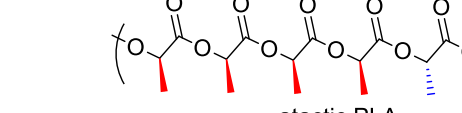
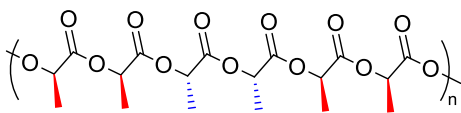
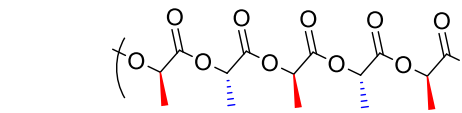
### 3.1. Introduction

Poly(lactide) (PLA) is a commercially available, bio-derived, fully biodegradable and recyclable thermoplastic.<sup>[1,2]</sup> PLA can be completely degraded into metabolites by hydrolysis after several months by exposure to moisture.<sup>[3,4]</sup> These features make PLA a very promising substitution of petroleum-based polymers in various applications, notably in the biomedical, pharmaceutical and packaging fields.<sup>[5–7]</sup> As emphasized in the previous chapters, the thermo-mechanical properties of PLA strongly depend on its microstructure, namely, on its tacticity.<sup>[8]</sup> While atactic PLA is amorphous showing only glass transition ( $T_g$ ) around 50 °C, both heterotactic and isotactic PLAs exhibit semi-crystalline properties, with a melting temperature ( $T_m$ ) around 130 - 180 °C, indicating an improved mechanical strength. Very interestingly, *L*-PLA and *D*-PLA enantiomers can co-crystallize when blended in a 1:1 molar ratio, forming a stereocomplex that has an even higher  $T_m$  up to 230 °C.<sup>[9,10]</sup> Thus, control over the stereochemistry of PLA plays a crucial role as it defines the physical properties, in particular their crystallinity and biodegradability, and the final usage of PLA-based materials.<sup>[11]</sup>

PLA is achieved by the stereoselective ring-opening polymerization (ROP) of lactide in presence of specific catalysts.<sup>[8,11,12]</sup> In this context, a challenging task relies on the preparation of stereoblocks or stereocomplexes based on PLA from a racemic lactide (*rac*-LA) feedstock by applying highly selective and active catalysts.<sup>[13–21]</sup>

Consistently, and as also emphasized in the previous chapters, two distinct mechanisms can take place during the stereoselective ROP of *rac*-LA, namely, the enantiomorphous site control (ESC) mechanism<sup>[17]</sup> and the chain-end control (CEC) mechanism<sup>[15]</sup> (Table 3.1). Isotactic polymer chains (PLLA or PDLA) and stereoblock PLA are produced by the ESC and the CEC mechanisms, respectively. It is worth noting that ROP of *rac*-LA operating by the ESC mechanism cannot combine both high rates and monomer conversions. Once the preferred enantiomer is indeed polymerized, the remaining enantiomer is consumed very slowly. The alternative CEC mechanism enables to overcome this limitation.

**Table 3.1.** Possible tacticities of PLA in the presence of chain-end and enantiomorph-site stereocontrol mechanisms during stereoselective ROP of *rac*- or *meso*-LA. (The reverse monomer sequencing is also possible considering to opposite enantioface of the catalyst used.)

	Chain-end Control Mechanism	Enantiomorph-site Control Mechanism
 <p><i>L</i>-LA <i>D</i>-LA <i>rac</i>-LA</p>	 <p>atactic PLA</p>	 <p>atactic PLA</p>
	 <p>PLLA PDLA</p>	 <p>PLLA + unreacted <i>D</i>-LA or PDLA + unreacted <i>L</i>-LA</p>
	 <p>isotactic diblock PLLA-<i>b</i>-PDLA (in the presence of a stereoerror)</p>	 <p>isotactic PDLA in the presence of a stereoerror</p>
	 <p>isotactic multiblock PLLA-co-PDLA (in the presence of multiple stereoerrors)</p>	
 <p><i>meso</i>-LA</p>	 <p>atactic PLA</p>	 <p>atactic PLA</p>
	 <p>heterotactic PLA</p>	 <p>syndiotactic PLA</p>

In the past decades, a wide range of catalysts and/or initiators, including enzymatic<sup>[22]</sup>, metal-based<sup>[21,23–28]</sup> and more recently, organic catalysts<sup>[29,30]</sup>, have proven efficient to control the ROP of LA. Though, only a few of them enable to access stereoregular PLAs from the stereoselective ROP of *rac*-LA.<sup>[8,11,31–35]</sup>

As highlighted in the bibliographic chapter (chapter 1), aluminum-based complexes featuring Salen-type ligands, as originally reported by Spassky *et al.*<sup>[13]</sup>, and further by many other research groups,<sup>[14–19,21]</sup> are representative metal-based catalysts that have attracted a lot of attention. Many of the metal-based catalysts have been shown to trigger the ROP of *rac*-LA by the CEC mechanism.<sup>[15]</sup> While excellent stereocontrol can be achieved from

organometallic catalytic systems, they often suffer from low activities, low stabilities and elevated costs of production. This has opened the way to the development of metal-free catalysis.

Organocatalysts have emerged as alternative and attractive components in ROP reactions, due to the high polymerization control they provide, some of them, such as thioureas,<sup>[36,37]</sup> amidines,<sup>[38]</sup> phosphazenes<sup>[39]</sup> or *N*-heterocyclic carbenes (NHCs)<sup>[40,41]</sup> exhibiting high polymerization rates.<sup>[30,42–44]</sup> Only a handful of organocatalysts have been evaluated for the stereoselective ROP of *rac*-LA. For example, binaphthol-derived phosphoric acid,<sup>[32]</sup> chiral synthetic prolines ( $P_m = 0.87\text{--}0.96$ )<sup>[34]</sup> and a chiral thiourea ( $P_m = 0.82$ )<sup>[35]</sup> have been shown to operate through the kinetic resolution following the ESC mechanism, thus produce isotactic enriched PLLA. For some other non-chiral organocatalysts, including phosphazene derivatives,<sup>[45,46]</sup> and cinchona alkaloids,<sup>[33]</sup> there are some evidences or clues that they would operate by the CEC mechanism.

In this context, our group has recently reported that the commercially available (*R,R*)- and (*S,S*) enantiomers of chiral thiourea-amine Takemoto's organocatalysts can promote efficient control and high isoselectivity at room temperature during the *rac*-LA ROP, yielding isotactic enriched, semi-crystalline and metal-free PLA.<sup>[35]</sup> The origin of the stereocontrol has been examined through kinetic investigations and combined analyses of the resulting PLAs, evidencing the concomitant occurrence of both CEC and ESC mechanisms.

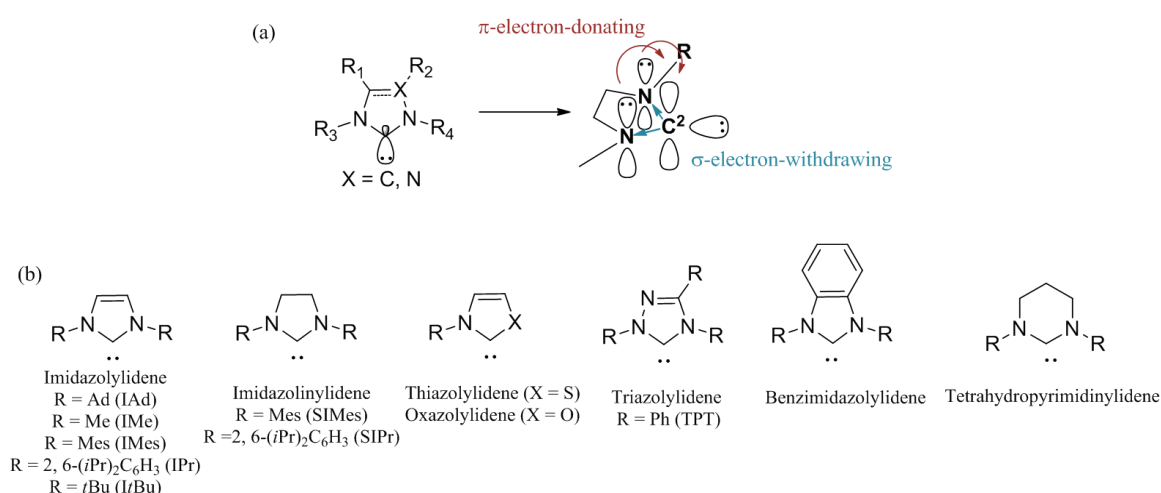
In a general manner, although good stereocontrol can be achieved by organocatalyzed and metallic catalyzed ROP of *rac*-LA, there are still some limitations to overcome. In particular, catalysts that could combine both a high stereoselectivity and catalytic activity are scarce. In addition, catalyst synthesis and/or storage is often tedious and complicated adding to the cost of the final PLA material. The catalytic structure, thereby the catalytic activity, can also be hardly tuned. Finally, ROP reactions usually require stringent conditions (low or high temperature, pressure). Consequently, there is still a need to develop catalytic systems that could simultaneously exhibit high activity, selectivity at room temperature and above, easy synthesis and facile handling.

This chapter shows the use of different chiral *N*-heterocyclic carbenes (NHCs) as organocatalysts to trigger the stereoselective ROP of *rac*-LA. These NHCs have been *in situ* generated by simple basic treatment of their corresponding salts, namely, chiral imidazolium-type ionic liquids that are commercially available. The effect of the NHC structure on the

polymerization outcomes, in particular on the control over the stereoselectivity of the ROP process, is discussed. As a preamble, a short introduction about NHCs and their interest as organic catalysts both in molecular and macromolecular synthesis is presented.

### 3.2. Generalities on *N*-heterocyclic carbenes (NHCs) and their use as organic catalysts in (macro)molecular chemistry

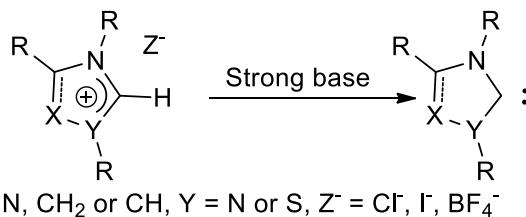
Carbenes are highly reactive species containing a neutral divalent carbon atom with six valence electrons (four electrons are included in  $\sigma$ -bonds and other two at the central carbon; Figure 3.1a).<sup>[47]</sup> NHCs show a singlet ground-state electronic configuration with the highest occupied molecular orbital (HOMO) and the lowest unoccupied molecular orbital (LUMO) best described as a formally  $sp^2$  – hybridized lone pair and an unoccupied  $p$  – orbital at the  $C^2$  carbon, respectively. The adjacent  $\sigma$ -electron withdrawing and  $\pi$ -electron-donating nitrogen atoms stabilize the structure of NHC both inductively by lowering the energy of the occupied  $\sigma$ -orbital and mesomerically by donating electron density into the empty  $p$  – orbital.<sup>[48,49]</sup> Reactivity of NHCs is directly associated with their ground-state electronic structure. The lone pair situated in the  $C^2$  atom renders NHCs nucleophilic. Consequently, NHCs behave as a  $\sigma$ -donors and bind to a wide range of metallic or non-metallic species<sup>[50]</sup> (Figure 3.1). The  $\sigma$ -donor properties enable both Brønsted base ( $pK_a \sim 15$ -30 in  $H_2O$ )<sup>[51,52]</sup> and active nucleophilic type catalytic characters to the NHCs. Due to these properties, NHCs have received a considerable attention in molecular synthesis<sup>[42,53,54]</sup> and in macromolecular chemistry.<sup>[55–57]</sup>



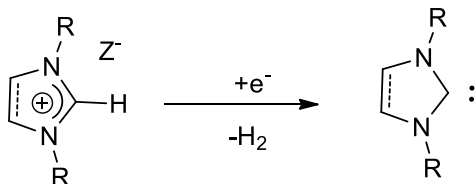
**Figure 3.1.** (a) Ground-state electronic structure of imidazol-2-ylidenes (NHCs) (Adapted from reference 30) (b) The most common types of NHCs

In general, NHCs are obtained either by deprotonation of imidazol(in)ium salts or generation from “masked” NHCs (Scheme 3.1). However, chemical reduction of imidazolthiones or electrochemical reduction of azolium precursors can also be used to obtain NHCs. The most frequent method to prepare a free NHC is to deprotonate NHC salts using a strong base (NaH, *t*-BuOK, DBU, etc.).<sup>[58]</sup> So, most of the imidazole- and imidazoline-type NHCs can be achievable using their commercially available corresponding imidazol(in)ium salts.

(a) deprotonation of an imidazol(in)ium salt with a strong base



(b) electrochemical reduction of an azolium salt



**Scheme 3.1.** Possible generation routes to NHCs.

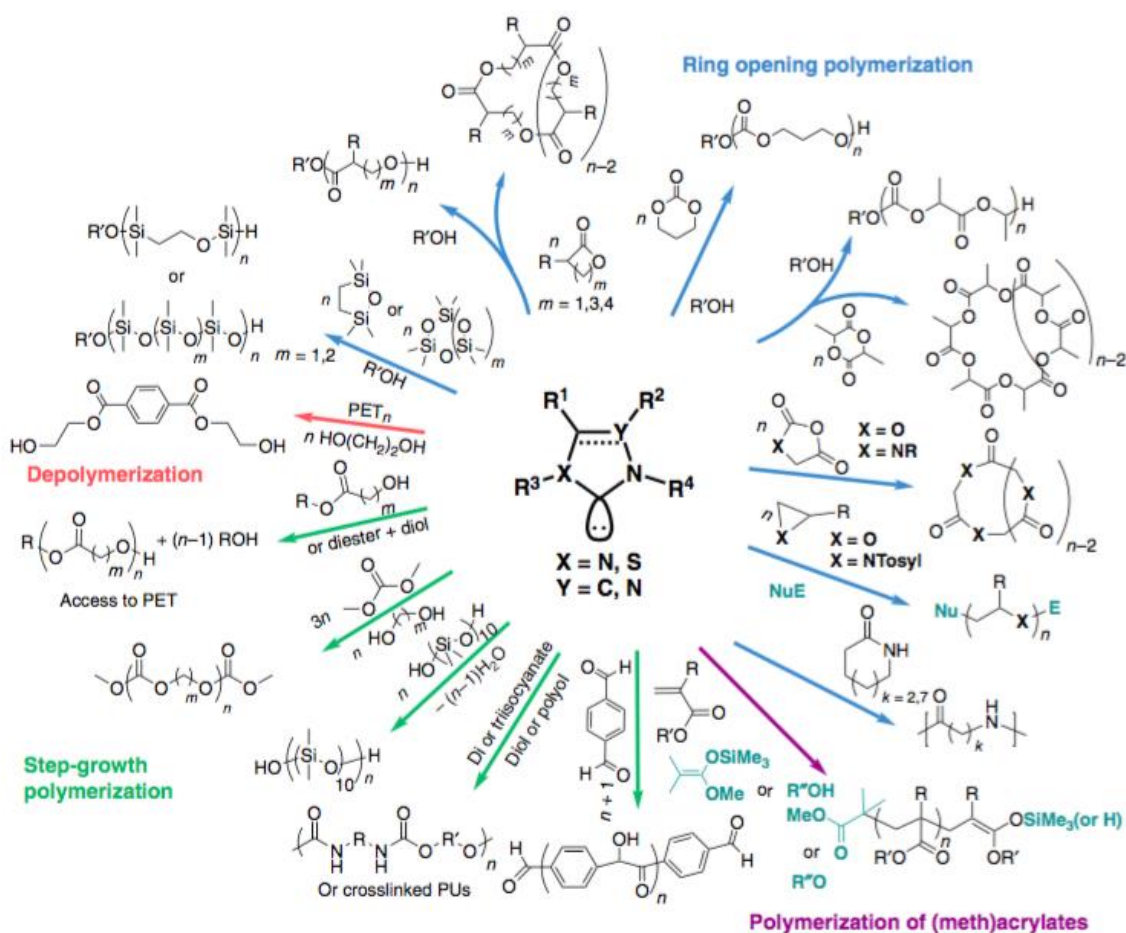
Besides many advantages, most of the free NHCs are known as air and moisture sensitive, which restricts their storability and their use in some molecular and macromolecular chemistry. Thus, masked, *i.e.* protected NHCs have been developed in time and used as latent catalysts in polymer synthesis. Imidazol(in)ium carboxylates (NHC-CO<sub>2</sub>), NHC-hydrogen carbonates, NHC-alcohol adducts, NHC-haloalkane adducts and NHC-metal complexes can be classified under typical masked- or protected-NHCs. These carbene precursors can form free NHCs in the presence of an appropriate solvent or temperature.<sup>[59]</sup> It has to be considered, however, that protected NHCs can exhibit low catalytic activity, if the generation of free NHCs is incomplete.

NHCs provide metal-free, versatile and straightforward route for the construction of C-C and C-X (X=O, N) bonds, under relatively mild reaction conditions.<sup>[60–62]</sup> Transformations catalyzed by NHCs include condensation, 1,2-, 1,4-additions, transesterification, ring-opening reactions, etc.<sup>[53]</sup> Due to their nucleophilic character, NHCs can react with aldehyde or ester substrates (benzoin condensation, Stetter reactions<sup>[63,64]</sup>). Besides, the high Lewis basicity of NHCs also led them activate the silylated substrates

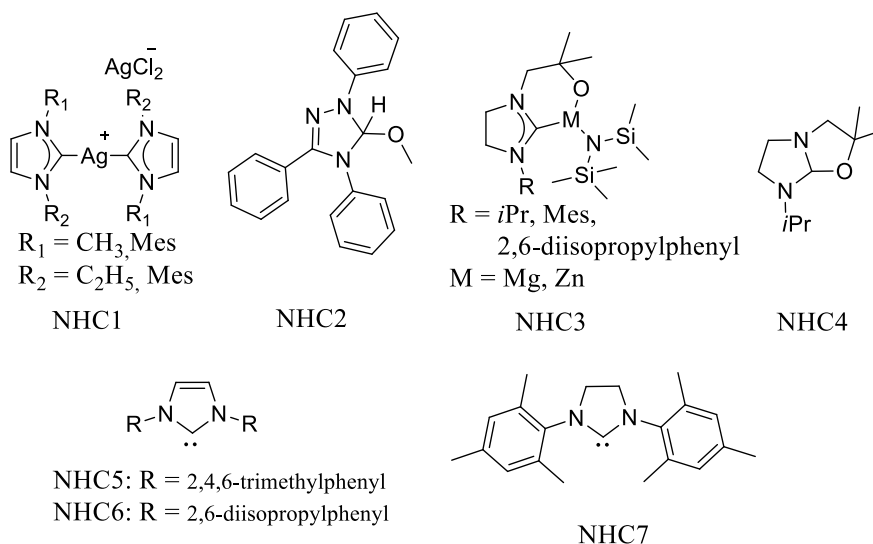


(Mukaiyama-aldol reaction<sup>[65]</sup>). Finally, the Brønsted basicity character allows NHCs to activate alcohol and amines *via* H-bonding (transesterification reaction<sup>[66]</sup>).

In macromolecular chemistry, their facile preparation<sup>[67]</sup>, nucleophilic properties<sup>[42,68,69]</sup> and their almost unlimited structural diversity have made them among the most powerful organocatalysts.<sup>[53,62,70–72]</sup> NHCs can indeed catalyze various polymerization reactions, including step-growth and chain-growth polymerizations. NHCs exhibits catalytic property for the polymerization of large number of monomers, such as lactones, lactide, cyclic carbonates, cyclic siloxanes and carbosiloxanes, epoxides, *N*-carboxyanhydrides, (meth)acrylic monomers, bis-aldehydes, diols with multiisocyanates, bis-silanol, etc (Figure 3.2).<sup>[43,55,56,72]</sup>



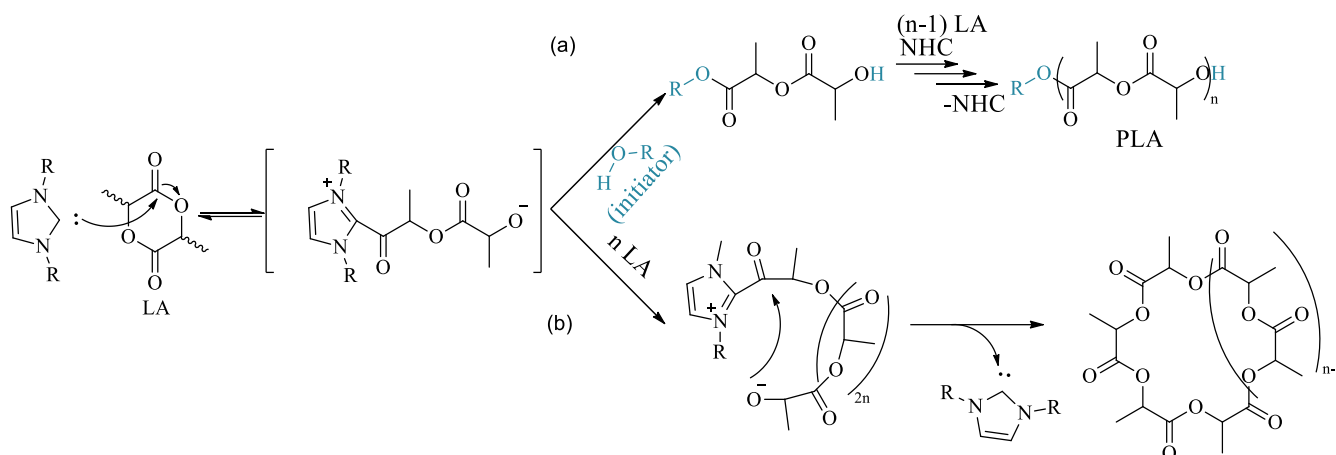
**Figure 3.2.** Scope of NHC-mediated polymerization reactions; adapted from ref. 30, 62 and



**Figure 3.3.** Some examples of masked NHCs used for ROP of cyclic esters.

Regarding the masked carbenes, adducts of NHCs with silver<sup>[73]</sup> (Figure 3.3, **NHC1**) and alcohols<sup>[40]</sup> (Figure 3.3, **NHC2**) can induce the generation of free NHCs upon thermal activation, and found to activate the lactide polymerization in a control polymerization manner. Furthermore, NHC-silver complexes allow for relatively effective catalysis for the ROP of LA under bulk conditions to produce PLA with  $M_n \sim 3,000 - 10,000 \text{ g mol}^{-1}$  and  $\bar{D} = 1.1 - 1.5$ .<sup>[74]</sup> Similarly, Arnold *et al.* investigated that NHCs with tethered nucleophilic chelating ligands<sup>[75]</sup> could catalyze the ROP of LA as a bifunctional catalyst (Figure 3.3, **NHC3**). Controlled ROP of LA was performed using **NHC3**, and PLAs with  $M_n \sim 1,800 - 77,000 \text{ g mol}^{-1}$  ( $\bar{D} = 1.1 - 1.2$ ) were prepared. Lastly, in the presence of **NHC4** (Figure 3.3), ROP of LA was completed in 15 min which was faster than the polymerization with **NHC3**, and  $M_n = 45,000 \text{ g mol}^{-1}$  was obtained within  $\bar{D} < 1.5$ . However, Taton and co-workers reported that the free imidazolium catalysts with the least-bulky functional groups present a higher catalytic activity than the masked NHCs.<sup>[76]</sup>

Owing to their  $\sigma$ -donor properties, NHCs can behave either as Brønsted bases ( $\text{p}K_a \sim 15\text{-}30$  in  $\text{H}_2\text{O}$ )<sup>[51,52]</sup> or as nucleophilic-type catalysts, depending on the monomer and/or the initiator –if present- to activate. There is still an argument about a real conducting mechanism of NHCs for some polymerizations, which is highly dependent on various parameters including the nature of both the NHC and the initiator, and the overall experimental conditions as well (solvent polarity, temperature).



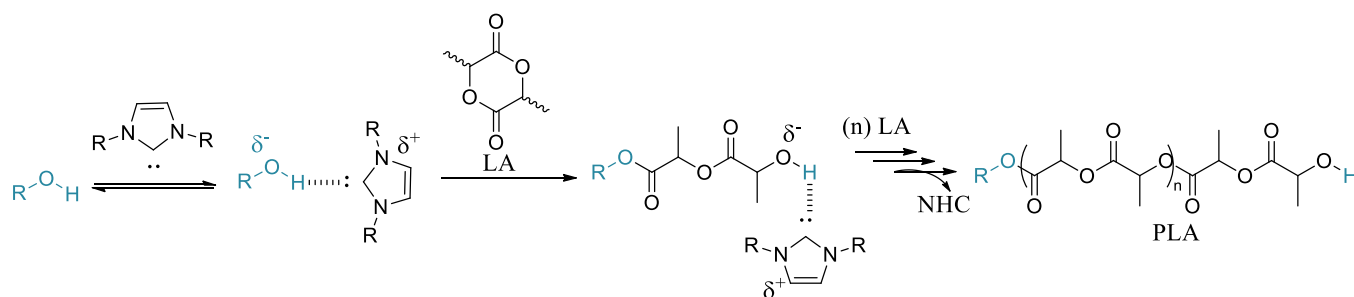
**Scheme 3.2.** (a) Nucleophilic monomer activated mechanism for the ROP of LA in the presence of alcoholic initiator (b) Nucleophilic mechanism for the zwitterionic ROP of LA in the absence of initiator (Adapted from reference 52).

NHCs eventually behave as nucleophiles in direct reaction with the neutral monomer. This mode of action has been proposed, not only in NHC-mediated of heterocycles (e.g. lactide,<sup>[57,77,78]</sup> epoxides,<sup>[76,79,80]</sup> phosphoesters,<sup>[81]</sup>), but also for methacrylate monomers involving selective 1,4-conjugate addition reactions (Scheme 3.2a).<sup>[82–85]</sup> In these cases, the nucleophilic attack of the monomer by the NHC yields a zwitterionic intermediate that is sometimes regarded as an “activated monomer”, hence the related mechanisms also refers to as the activated monomer mechanism. Subsequent protonation of this zwitterionic species, for instance, by an exogenous alcohol initiator (ROH), and concomitant release of the NHC catalyst, gives rise to a mono-adduct (= extended alcohol). A similar catalytic cycle utilizing the latter mono-adduct will form the bis-adduct, and so on and so forth, so that the polymerization can proceed in a controlled manner.

In absence of any (ROH) initiator, the nucleophilic NHC is no more a catalyst and instead plays the role of a true initiator. Thus, it will be incorporated in  $\alpha$ -position of the polymer, chain-growth occurring by a zwitterionic mechanism. In this way, macrocyclic polymers can be achieved, providing a new synthetic route to these architectures under relatively mild conditions (Scheme 3.2b). In 2015, Chang *et al.* investigated the influence of added LiCl to the NHC-mediated ZROP of  $\delta$ -valerolactone (VL) in THF. Firstly, they observed that the molar masses of the resultant PVL are higher than the expected from the initial ratio of  $[\text{VL}]_0/[\text{NHC}]_0$  and the molar mass distributions are bimodal and broad ( $M_w/M_n = 1.35$ ) in the absence of LiCl. Afterwards, they reported the matching molar masses with the expected ones from  $[\text{VL}]_0/[\text{NHC}]_0$ , and the molar mass distributions are monomodal and

narrow ( $M_w/M_n = 1.08 - 1.26$ ) in the presence of LiCl. Using LiCl, the polymerization rate successfully accelerated.<sup>[86]</sup>

Polymerization reactions involving selective activation of the initiator by the NHC - and later on activation of the polymer chain-end- refers to as the basic mechanism, also sometimes called the activated chain-end mechanism. In such a case, the NHC plays the role of a Brønsted base interacting with –or even deprotonating- the initiator, then with the polymer chain-ends, favoring the addition of the latter to the neutral monomer substrate (Scheme 3.3). The ensuing mono-adduct can then propagate an anionic-type polymerization by the same catalytic cycle, with the protonated NHC, *i.e.* a soft and generally bulky azolium-type counter ion. Such a mechanism has been postulated in many situations, where alcoholic initiators are employed, not only for OROP,<sup>[72,87–89]</sup> but also for the NHC-catalyzed polymerization of MMA.<sup>[85]</sup> The interactions developed between the selected NHC and the protic component are obviously correlated to the  $pK_a$  values of both reaction partners.



**Scheme 3.3.** Basic mechanism for ROP of LA conducted by NHC

Another situation where NHCs would operate as Brønsted bases, is encountered when the monomer itself contains an acidic proton that can be readily abstracted. This has been proposed in step-growth polymerizations involving OH-containing monomers, for instance, to achieve polyurethanes<sup>[90,91]</sup> and polysiloxanes,<sup>[92]</sup> from a diol and a diisocyanate and from a disilanol, respectively. In these cases, indeed, the NHC catalyst is thought to selectively interact with the hydroxyl function, before the attack of the as-activated alcohol.

Owing to NHC's unique properties, they become by far the most studied members of the family of organocatalysts, especially for the ROP of lactones.<sup>[43,93]</sup> In 2002, Connor *et al.* reported the first example of NHCs as catalysts for the ROP of cyclic esters.<sup>[57]</sup> In this study, **NHC5** (Figure 3.3, IMes) was applied as a catalyst for the ROP of LA,  $\epsilon$ -CL and  $\beta$ -BL, and in each case polymerization was proceeded efficiently, producing polymers of predictable molar mass (based on initial [LA]:[I] ratio) and narrow polymer distribution with high end-group fidelity. Monomer conversion of LA was achieved to 92% after 2 h with a dispersity value of

1.15. Less reactive  $\epsilon$ -CL was almost quantitatively converted in 24 h. The linear increase in molar mass with monomer conversion was demonstrated with PLAs.<sup>[57]</sup> A monomer-activated mechanism was proposed in the presence of an alcohol. Besides, in the absence of protic initiators, Waymouth and coworkers exhibited that the synthesis of cyclic polymers is possible.<sup>[94,95]</sup> The ROP of LA was reported to produce cyclic PLA with  $M_n$  up to 30,000 g mol<sup>-1</sup> and  $\bar{D} < 1.35$  (< 90% of conv.) with a linear increase of molar mass with monomer conversion, however, it is a non-living polymerization.<sup>[94]</sup> The cyclic structure was then proved by MALDI-ToF mass spectroscopy in the presence of some transesterification reaction. IMes was reported non-active for the ROP of  $\epsilon$ -CL, however, less sterically hindered  $\beta$ -BL and  $\beta$ -PL were polymerized efficiently to form cyclic polyesters using **NHC7** (Figure 3.3).<sup>[95]</sup>

As emphasized in the bibliographic chapter, examples of stereocontrolled organocatalytic ROP reactions involving *rac*-LA, using either achiral or chiral organic catalysts, are scarce.<sup>[31–34,39,41,46]</sup> Regarding the possibility to trigger the stereoselective ROP of either the racemic or the meso version of LA from NHCs, only a handful of studies have been reported. In 2004, Tolman *et al.* reported a new Zn alkoxide catalyst supported by an NHC that rapidly polymerized *rac*-LA to heterotactic enriched PLA, while the free carbene and analogs instead yield highly isotactic enriched PLA. They used **NHC5** and **6** (Figure 3.3) and BnOH as initiator. The highest level of PLA isotacticity obtained was with the IMes (**NHC5**, Figure 3.3) and 0.67 equiv. BnOH at -20 °C in CH<sub>2</sub>Cl<sub>2</sub> ( $P_m \sim 0.75$ ). That material, produced in 71% yield from *rac*-LA, showed a  $T_m$ , measured by differential scanning calorimetry, of 153 °C ( $\Delta H_m = 0.8 \text{ J g}^{-1}$ ) consistent with the presence of a small amount of semicrystalline material.<sup>[24]</sup> Later on, Dove *et al.* synthesized and used new sterically encumbered NHC catalysts to polymerize *rac*-LA to give isotactic PLA or *meso*-LA to give heterotactic PLA. They have postulated that the ROP of *rac*-LA was under the chain-end control (CEC) mechanism.<sup>[96]</sup> Afterwards, they have employed another achiral but sterically encumbered NHC derivative organic catalyst to conduct the ROP of both the *meso*- and the *rac*-LA, which has led to PLAs showing  $P_m = 0.90$  and  $P_r = 0.83$  at -70 and -40 °C, respectively. Catalysis by this catalyst thus resulted in the formation of an isotactic-enriched PLA from *rac*-LA, and in a heterotactic PLA from *meso*-LA.

Besides their use as organic catalysts, NHCs have also been employed as ligands of metal-based catalysts to control the stereoselectivity during the ROP of LA. For instance, a readily accessible and robust zirconium–NHC complex was found to polymerize *rac*-LA in a

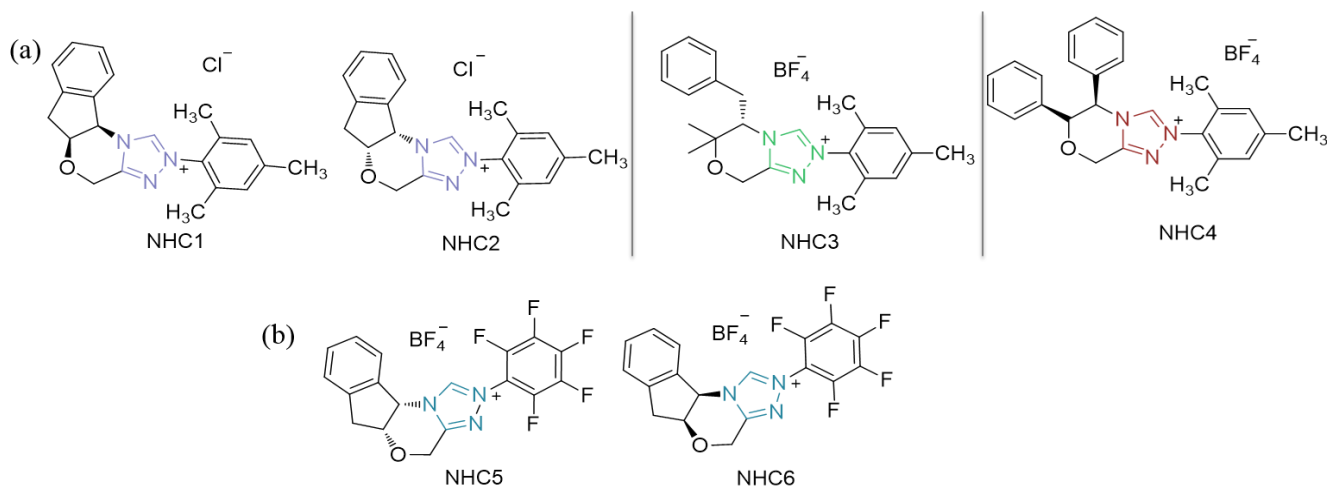
controlled, living and stereoselective manner to afford heterotactic PLA. Followingly, a controlled ROP of trimethylene carbonate (TMC) initiated by Zr-NHC catalyst (60 equiv. TMC, r.t), subsequent addition of *rac*-LA (40 equiv.) yielded the formation of well-defined, molar mass controlled and highly stereoregular (heterotactic) PLA-*b*-PTMC (40/60), as deduced from NMR and SEC data ( $P_r \geq 0.95$ ,  $D = 1.24$ ,  $M_n = 19,700 \text{ g mol}^{-1}$ ). DSC data showed an amorphous material with one single glass transition [ $T_g = 15 \text{ }^\circ\text{C}$ , thus lying between that for PTMC ( $\sim -15 \text{ }^\circ\text{C}$ ) and for heterotactic PLA ( $\sim 45 \text{ }^\circ\text{C}$ )], which was consistent with no phase separation between the PLA and the PTMC blocks.<sup>[97]</sup> In another study, the reaction of NHC with dimeric dialkylgallium alkoxides, acting as nonselective or heteroselective catalysts in the polymerization of *rac*-LA, led to highly active and isoselective monomeric  $\text{Me}_2\text{Ga}(\text{NHC})\text{OR}$  catalysts, resulting for the first time in the facile switch of stereoselectivity. For the polymerization of *rac*-LA with this catalyst at r.t. the formation of isotactically enriched PLA ( $P_m = 0.65$ ) was found by homonuclear decoupled  $^1\text{H}$  NMR. Notably, the decrease of temperature to  $20 \text{ }^\circ\text{C}$  resulted in the substantial increase in isoselectivity ( $P_m = 0.78$ ), which makes the catalyst a rare example of an isoselective catalyst operating at low temperatures.<sup>[98]</sup>

The diverse reactivity of NHCs found in organocatalyzed reactions of molecular chemistry has been successfully applied to polymer synthesis.<sup>[57,99,100]</sup> NHCs have thus grown significantly in organopolymerization in the past 15 years, through the activation of a wide range of monomer substrates and involving various reaction mechanisms, including chain-growth processes and step-growth reactions as well. They can behave as Brønsted and/or Lewis bases. Subtle changes in their chemical structure sometimes cause dramatic differences in reaction outcomes with specific substrates. This diversity of mechanistic pathways can not only provide opportunities for enhancing the rate of the polymerization and influencing the selectivity but also to generate original polymeric structures.<sup>[41,57,77,101]</sup> By far, cyclic esters, such as lactones and lactides, have been the most investigated as monomer substrates via chain-growth ROP.

Of particular interest, many chiral versions of NHCs –or of NHC precursors- are easily available or readily accessible.<sup>[42]</sup> Chiral NHCs have been extensively exploited as organocatalysts in many asymmetric reactions (e.g. Diels-Alder,<sup>[102]</sup> Stetter reaction,<sup>[64]</sup> [3+2] Annulation reaction,<sup>[103]</sup> etc.), enabling the synthesis of various optically active molecular compounds. In contrast, the use of chiral NHCs for stereoselective ROP of *rac*-LA has been overlooked.<sup>[41]</sup> Up to date, it has been achieved at very low temperature ( $\sim -75 \text{ }^\circ\text{C}$ )

by employing sterically encumbered NHCs ( $P_m = 0.90$ ,  $-70\text{ }^\circ\text{C}$ ), as the catalysts that are postulated by a chain-end control with stereoerror mechanism.<sup>[41]</sup> Very recently, Li *et al.* reported organocatalytic stereoselective ROP of *rac*-LA utilizing bulky chiral and achiral NHCs by introducing naphthyl groups on the nitrogen side to enhance the steric hindrance of the carbene center, which triggered the formation of isotactic-rich stereoblock PLA ( $P_m = 0.81$ ,  $-78\text{ }^\circ\text{C}$ ) in the presence of benzyl alcohol as initiator.<sup>[42]</sup>

In the continuity of efforts to derive metal-free and semi-crystalline PLAs under mild conditions (see chapter 2), typically at room temperature, we report in this chapter that some commercially available chiral NHC precursors can serve to promote efficient control and appreciable isoselectivity of the ROP of racemic lactide. Analyses of the resulting PLAs by decoupled NMR and by DSC allowed us to establish that the stereocontrol involves a chain-end control mechanism with some NHCs.



**Figure 3.4.** Triazolo-oxazinium derivative chiral *N*-heterocyclic carbenes studied (a) saturated with tetrafluoroborate salts (b) saturated with chloride salts.

For this purpose, chiral triazole-oxazinium derivatives were used as NHC precursors for the ROP of *rac*-LA. We selected saturated and sterically encumbered NHCs bearing different substituents on the nitrogen atoms, in the form on their different ionic salt precursors. One important goal of this study was to understand the effect of these steric and electronic effects of the carbene catalyst on the stereoselectivity of the ROP process. Four different chiral NHC organic catalysts were thus tested for the ROP of *rac*-LA, at two different reaction temperatures, i.e.  $-50$  and  $25\text{ }^\circ\text{C}$ . The chiral NHCs were *in situ* generated under basic conditions using 3 different bases, namely,  $\text{K}_2\text{CO}_3$ , *t*-BuOK and DBU. In order to elucidate the stereocontrol mechanism, kinetic studies were conducted by homonuclear decoupled  $^1\text{H}$  and quantitative  $^{13}\text{C}$  NMR spectroscopy.

These investigations revealed that some chiral NHCs can produce semi-crystalline PLAs under the aforementioned conditions from *rac*-LA, following an exclusive chain-end control mechanism (CEC) during the ROP process.

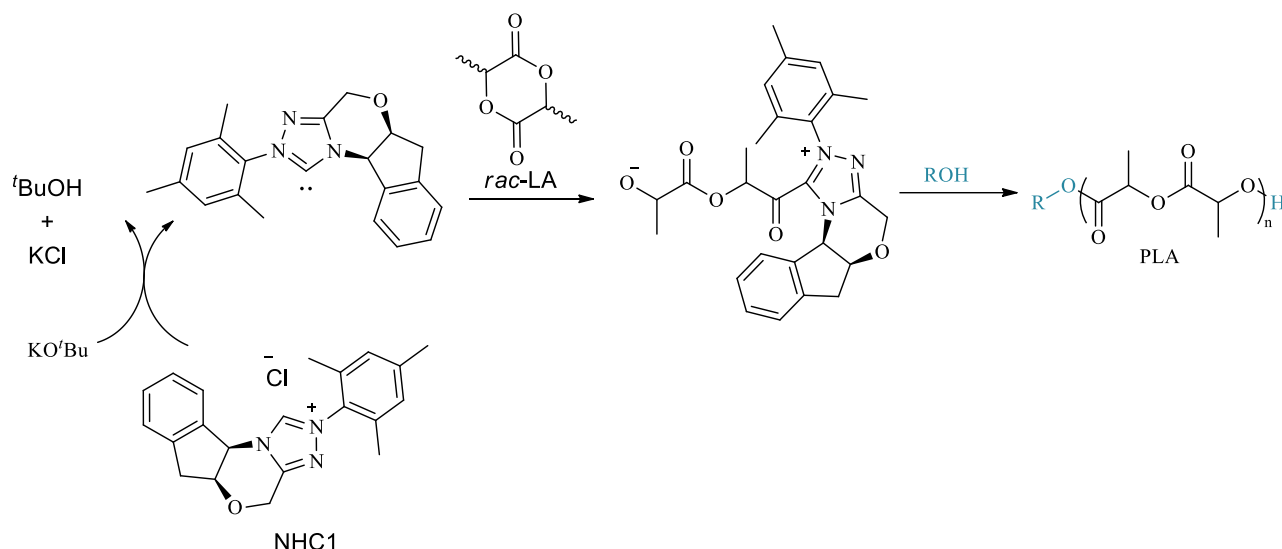
### 3.3. Stereoselective ROP of *rac*-LA using chiral NHCs as organocatalysts

#### 3.3.1. Polymerization procedure

The NHC precursors used for this study are shown in Figure 3.4. As mentioned, we aimed at unraveling the effect of the structural parameters on both the organocatalytic activity and the stereoselectivity of the NHC organic catalysts. ROP of *rac*-, *D*- and *L*-LA were thus performed using benzyl alcohol as alcohol initiator, in presence of chiral triazol-oxazinium derivative and a deprotonating base.

Polymerization reactions were performed in CH<sub>2</sub>Cl<sub>2</sub> using initial ratios of [LA]<sub>0</sub>/[Cat.]<sub>0</sub>/[base]<sub>0</sub>/[I]<sub>0</sub> = 50:0.5:0.5:1. Carbene salt precursors were generated via an *in situ* method using K<sub>2</sub>CO<sub>3</sub>, *t*-BuOK or DBU to avoid the difficulty of isolating sensitive carbene complexes and to facilitate polymerization studies. Herein, it would be worth clarifying that *t*-BuOK as tertiary alcohol is going to be unable to initiate the polymerization, since the *in situ* generation of NHC salts, and thus the active species of NHC precursors have already been done before the monomer adding.<sup>[104]</sup> In the glovebox, a previously flamed and dried schlenk vessel equipped with a stirbar was charged with corresponding NHC salt (0.5 eq., the same molarity of catalysts were applied in each case), and an equimolar amount of corresponding base (0.5 eq., the same molarity of generation base were applied in each case), then stirred 1 hour for the NHC activation in CH<sub>2</sub>Cl<sub>2</sub> (Scheme 3.4). When the solution turned from a light-yellow color to a dark yellow/orange color, the external initiator BnOH, and immediately after previously dissolved lactide monomer were added into the catalyst solution, as explained in experimental part. Corresponding results are summarized in Table 3.2.





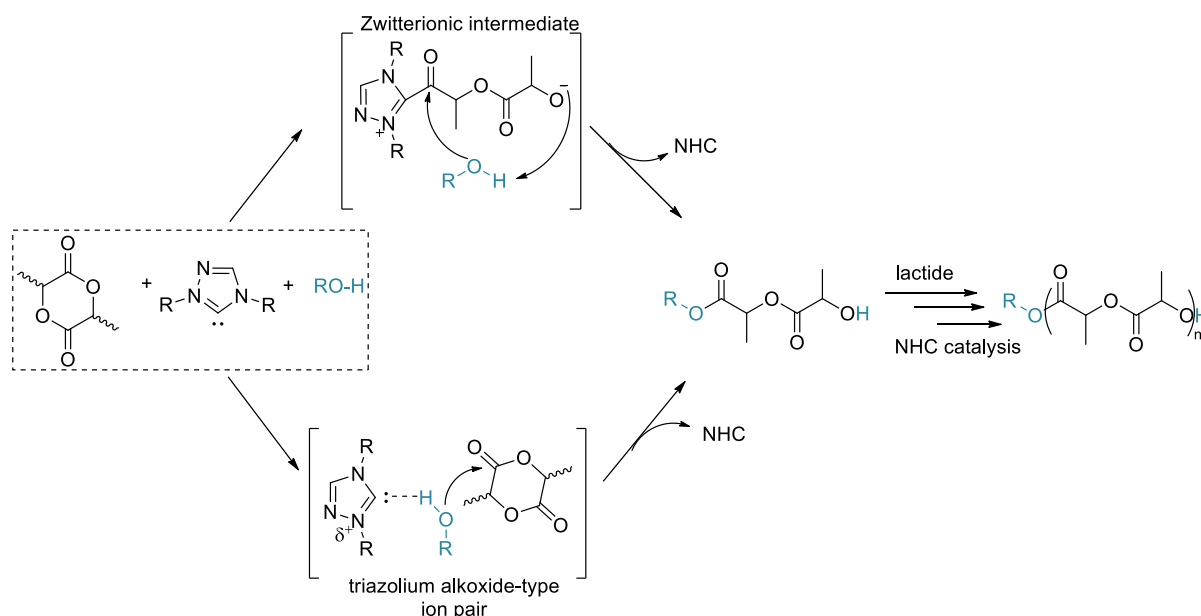
**Scheme 3.4.** *In situ* generation of **NHC1** salt with an appropriate base and nucleophilic ROP mechanism of *rac*-LA using generated **NHC1**

From a structural point of view, the commercially available and chiral NHC precursors were selected with different sterically hindered groups. **NHC1** and **2** can be found as enantiomeric pairs, the active triazole-type group being connected to a mesityl group. Chiral carbon atoms are envired by bulky dihydroindene group, which provides stability to the chiral moiety of the catalyst. While other NHCs are protected as tetrafluoroborate salts, **NHC1** and **2** are saturated chlorinated salts. In the case of the **NHC3**, a methyl-benzyl group is attached to the chiral carbon atom. As illustrated in Figure 3.4, there is no bulky group near the chiral moiety in the latter case. Also, a mesityl group, the bulkiest, is attached to the active triazole part for **NHC3**, as well. As for **NHC4**, due to the benzene groups, more steric hindrance is brought on the catalyst relatively to **NHC3**. Such benzene rings, when bound to the chiral carbon atom, are expected to affect the stereocontrol of the catalysis. A similar effect can be anticipated with the bulky mesityl moiety in vicinity of the active triazole group for **NHC4**, **NHC5** and **6**, as enantiomeric pairs, are structurally similar to **NHC1** and **2**, expect being  $-\text{BF}_4$  salt precursors and having the largest bulky group, namely pentafluorobenzyl, attached to the active triazole part. These catalysts are not expected to show a major difference in terms of stereocontrol compared to others but are expected to be more difficult to activate due to their larger sterically hindered groups.

Both the catalytic activity and the stereoselectivity were assessed upon carrying out the ROP reactions of *rac*-LA at two different temperatures, *i.e.* at  $-50\text{ }^\circ\text{C}$  and  $25\text{ }^\circ\text{C}$ . As a

means to deprotonate the C-2 position and thus generate the corresponding chiral NHC *in situ*, three different bases were employed.

As previously mentioned in introduction part, the two different mechanisms, namely nucleophilic or basic mechanism, could be operated by these NHC catalysts for the ROP of LA are depicted in Scheme 3.5. The possible mechanisms are summarized in Scheme 3.5.



**Scheme 3.5.** Nucleophilic *versus* basic mechanism in competition, here for the NHC-ROP of *rac*-LA

**Table 3.2.** Stereoselective ring-opening polymerizations of *D*-, *L*- and *rac*-LA catalyzed by chiral NHC precursors.<sup>a</sup>

Entry	Catalyst	Base	T [°C]	<i>t</i> [h]	Conv. [%] <sup>b</sup>	$M_n^{calc}$ [kg.mol <sup>-1</sup> ] <sup>c</sup>	$M_n$ [kg.mol <sup>-1</sup> ] <sup>c</sup>	$\bar{D}_M$ <sup>c</sup>	$T_g$ [°C] <sup>d</sup>	$T_m$ [°C] <sup>d</sup>	$P_m^{ESC}$		$P_m^{CEC}$	
											<i>H.D</i> <sup>e</sup>	<i>Q</i> . <sup>13</sup> C <sup>f</sup>	<i>H.D</i> <sup>e</sup>	<i>Q</i> . <sup>13</sup> C <sup>f</sup>
1	NHC1	K <sub>2</sub> CO <sub>3</sub>	-50	70	90	6.6	6.3	1.06	-	157	0.89	0.84	0.82	0.78
2	NHC1	K <sub>2</sub> CO <sub>3</sub>	25	64	99	7.2	4.6	1.05	54	145	0.86	0.87	0.78	0.77
3	NHC1	<i>t</i> -BuOK	25	2	95	6.9	2.7	1.18	-	166	0.86	0.89	0.75	0.78
4	NHC1	DBU	25	2	85	6.2	5.6	1.20	52	-	0.79	0.84	0.70	0.73
5	NHC2	K <sub>2</sub> CO <sub>3</sub>	-50	70	91	6.6	3.5	1.06	-	154	0.88	0.86	0.81	0.79
6	NHC2	K <sub>2</sub> CO <sub>3</sub>	25	64	>99	7.2	5.2	1.06	55	147	0.86	0.87	0.79	0.78
7	NHC2	<i>t</i> -BuOK	25	2	92	6.7	5.1	1.13	50	143	0.86	0.85	0.77	0.75
8	NHC2	DBU	25	2	>99	7.2	6.0	1.28	52	-	0.78	0.79	0.69	0.67
9	NHC3	K <sub>2</sub> CO <sub>3</sub>	-50	18	>99	7.2	6.2	1.08	54	149	0.87	0.85	0.80	0.77
10	NHC3	K <sub>2</sub> CO <sub>3</sub>	25	2	99	7.1	6.0	1.05	49	131	0.84	0.86	0.75	0.76
11	NHC3	<i>t</i> -BuOK	25	2	98	7.1	8.0	1.10	53	-	0.80	0.83	0.70	0.72
12	NHC3	DBU	25	2	99	7.2	6.7	1.6	23	-	0.72	0.78	0.61	0.66
13	NHC4	K <sub>2</sub> CO <sub>3</sub>	-50	81	>99	7.2	4.1	1.05	43	-	0.77	0.80	0.67	0.70
14	NHC4	K <sub>2</sub> CO <sub>3</sub>	25	64	96	7.0	6.0	1.07	38	-	0.72	0.74	0.61	0.62
15	NHC4	<i>t</i> -BuOK	25	2	98	7.1	6.2	1.14	24	-	0.72	0.78	0.61	0.65
16	NHC4	DBU	25	2	99	7.2	7.3	1.6	28	-	0.72	0.75	0.62	0.67

<sup>a</sup>Polymerizations were conducted in CH<sub>2</sub>Cl<sub>2</sub> with the initial ratio of [LA]<sub>0</sub>/[NHC1]<sub>0</sub>/[Base]<sub>0</sub>/[BnOH]<sub>0</sub> = 50:0.5:0.5:1 unless otherwise stated. <sup>b</sup>Conversion of polymerizations were determined by <sup>1</sup>H NMR spectroscopic analysis in CDCl<sub>3</sub>. <sup>c</sup> $M_n$  and  $\bar{D}_M$  values are determined by SEC in THF (calibration using polystyrene standards).  $M_{n,SEC}$  values are corrected by Mark-Houwink correction factor (0.58). <sup>d</sup> $T_g$  and  $T_m$  values are obtained by DSC measurements from 1<sup>st</sup> heating curve. <sup>e</sup>Probabilities of finding mesodyads are calculated from homonuclear decoupled <sup>1</sup>H NMR by deconvolution technique. <sup>f</sup>Probabilities of finding mesodyads are calculated from <sup>13</sup>C NMR by deconvolution technique.

Most of the NHC precursors tested were found to be active in presence of  $K_2CO_3$ , *t*-BuOK and DBU bases, with the noticeable exception of salts **5** and **6**. Moreover, all polymerizations performed with *t*-BuOK and DBU as bases went to completion in 2 h at 25 °C, achieving PLAs with a dispersity in the range of 1.10-1.60 for a molar mass,  $M_n = 6.2 - 7.2 \text{ kg mol}^{-1}$ . Comparatively, ROP reactions induced by  $K_2CO_3$  as a base required much longer polymerization times (64 h), providing both a better controlled molar mass distribution (1.05 - 1.07) and a higher isoselectivity (see further). Therefore, further ROP experiments were performed using  $K_2CO_3$  to generate the NHCs *in situ*.

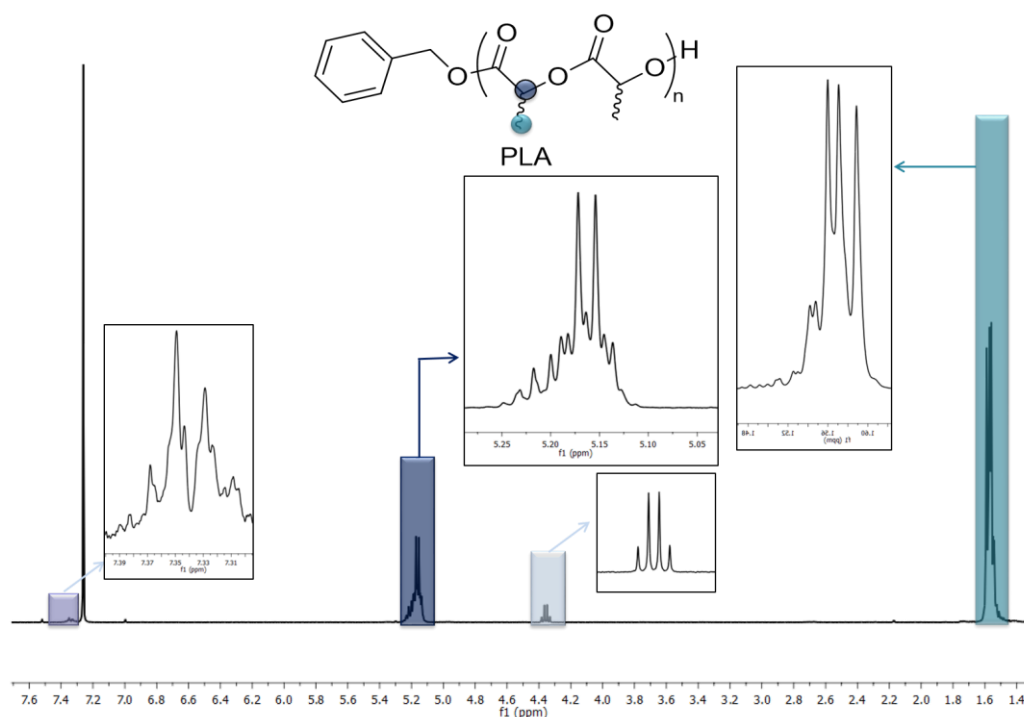
$K_2CO_3$ -activated **NHC1**, **2** and **4** were found to be active under such polymerization conditions, yielding almost similar monomer conversion (>96%) in 64 h at 25 °C, with an excellent controlled molar mass distribution (1.05-1.07; entries 2,6,10 and 14, Table 3.2). In comparison, **NHC3** was found to be more active than the other *in situ* generated NHCs, showing >99% of monomer conversion in 2 h at R.T. The fact that **NHCs 5** and **6** were inactive for the ROP of LA may be explained by the pentafluorobenzyl group, which creates more sterically encumbered space relatively to the mesityl group attached to the active triazole part in **NHC5** and **6**.

As expected, polymerizations performed at -50 °C required extended reaction times to reach completion. For example, monomer conversion reached 90% after 70 h in presence of **NHC1** and **NHC2** in  $CH_2Cl_2$  (entries 1 and 5, Table 3.2). While the polymerization was completed after 18 h using **NHC3** (entry 9, Table 3.2), **NHC4** required longer polymerization time (81 h) for an almost completion of the reaction (>99%, entry 13, Table 3.2). No significant changes in polymer dispersity were observed. In contrast, and as also expected, decreasing the temperature allowed increasing the stereoselectivity (see discussion further).

### 3.3.2. Characterization of chiral NHC-derived PLAs

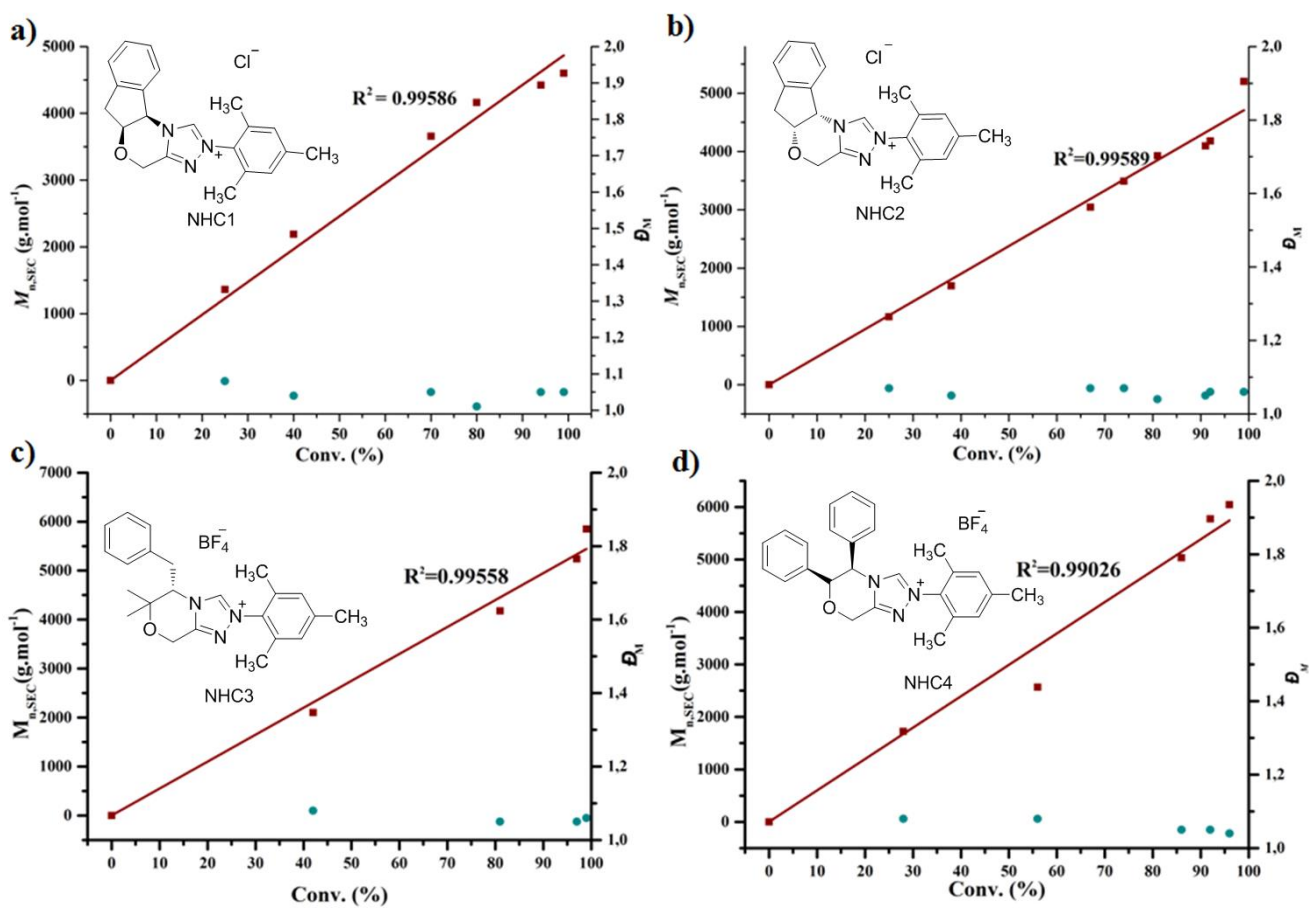
Analysis of the resultant PLAs was achieved by  $^1H$  NMR spectroscopy. A typical  $^1H$  NMR spectrum is displayed in Figure 3.5. The diagnostic signals of the benzyloxy group arising from the initiator (BnOH) were observed at 7.33–7.34 ppm, due to the resonance of the phenyl protons adjacent to the ester linkage. In addition, the signal to the terminal methine proton adjacent to the  $\omega$ -hydroxyl chain end was observed at 4.34 ppm, while signals at around 5.11 – 5.23 ppm and 1.53 – 1.61 ppm could be assigned to the main chain methine and methyl protons, respectively. One benzyloxy initiator fragment per polymer chain was thus determined, attesting to the relatively good agreement between the theoretical and

experimental degrees of polymerization in general,  $DP_{th}$  and  $DP_{exp}$ , up to high conversion, and to the high end-group fidelity.



**Figure 3.5.** Representative  $^1H$  NMR spectrum (400 MHz,  $CDCl_3$ ) of PLA prepared with **NHC1**/ $K_2CO_3$  *rac*-LA at 25 °C: inset 1 (navy colored): Methine region of PLA, inset 2 (dark blue colored): methyl region of PLA and inset 3 (light blue colored):  $\omega$ -hydroxy proton of terminal methine group.

Polymer number average molar masses, as determined by SEC ( $M_{n,SEC}$ ), showed a relatively good agreement with  $M_n$  values calculated from the initial  $[rac-LA]_0/[BnOH]_0$  ratio. Moreover,  $M_{n,SEC}$  values increased linearly with monomer conversion (Fig. 3.6) and dispersities remained low consistently with a “controlled/living” ROP for all  $K_2CO_3$ -activated NHCs (entries 2,6,10 and 14, Table 3.2). The results also attest the absence of transfer reactions.

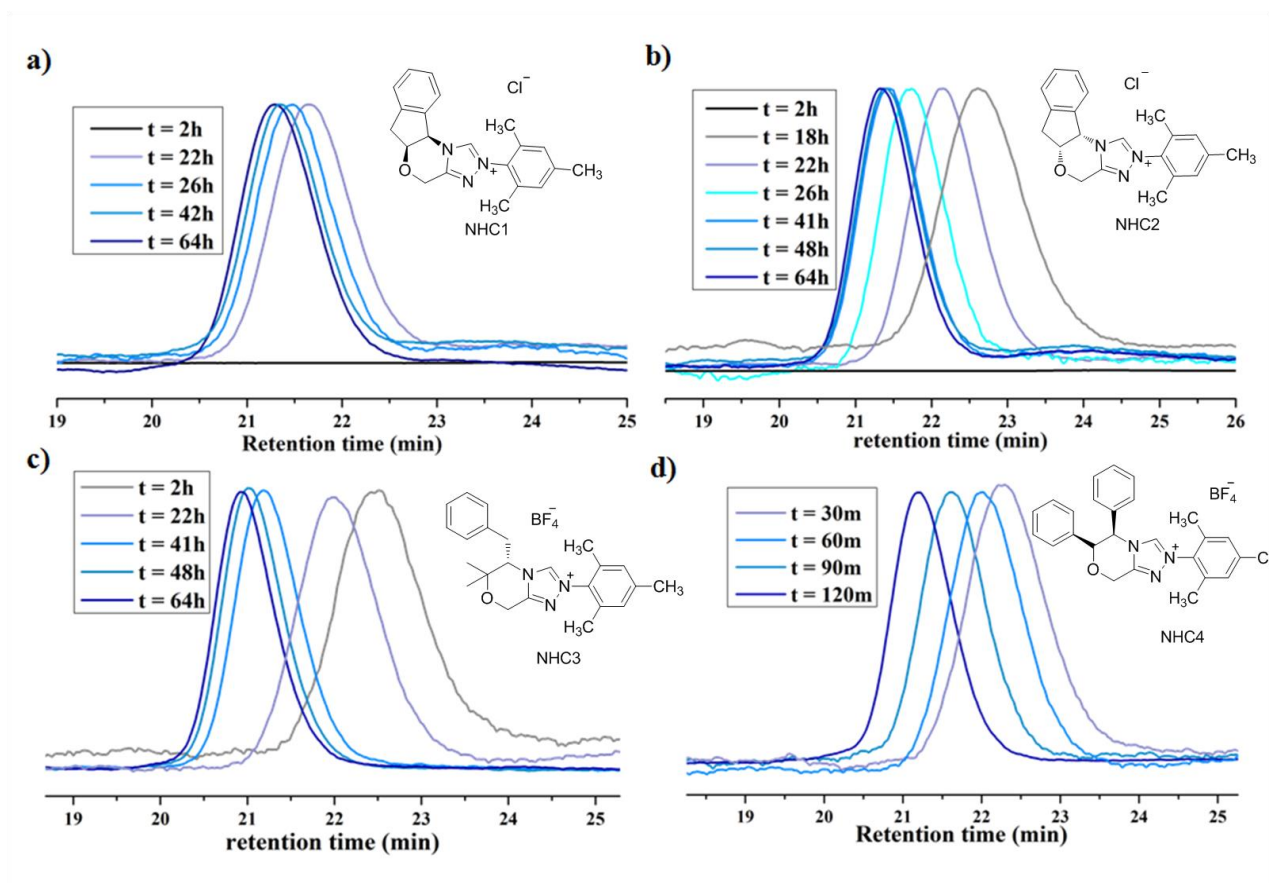


**Figure 3.6.** Evolution of corrected  $M_{n,SEC}$  (■) and dispersity  $D_M$  (●) vs. monomer conversion for PLA synthesized from (a) **NHC1** (b) **NHC2** (c) **NHC3** and (4) **NHC4** at RT.;  $[LA]_0/[BnOH]_0 = 50 : 1$  (entries 2,6,10 and 14, Table 3.2).

However, experimental  $M_{n,SEC}$  values were reconsidered by using the Mark-Houwink correcting factor equal to 0.58.<sup>[105]</sup> PLAs with a theoretical molar mass of 4.6 kg mol<sup>-1</sup> and an experimental molar mass of 7.2 kg mol<sup>-1</sup> were thus obtained using **NHC1** (entry 2, Table 3.2).

More consistent values were determined for PLAs resulting from **NHC2**:  $M_{n,theo} = 7.2$  kg mol<sup>-1</sup> and  $M_{n,SEC} = 5.2$  kg mol<sup>-1</sup> (entry 6, Table 3.2). As for polymers deriving from **NHC3** and **NHC4**, the following values were calculated:  $M_{n,theo} = 7.1$  kg mol<sup>-1</sup> and  $M_{n,SEC} = 6.0$  kg mol<sup>-1</sup> (entry 10, Table 3.2), and  $M_{n,theo} = 7.0$  kg mol<sup>-1</sup> and  $M_{n,SEC} = 6.0$  kg mol<sup>-1</sup> (entry 14, Table 3.2). Regarding these results, experimental molar masses were found to be correlated with the theoretical values.

Most importantly, the corresponding SEC traces exhibited monomodal peaks with narrow distributions (Figure 3.7), with a dispersity ( $D$ ) found as low as 1.05 – 1.08, using K<sub>2</sub>CO<sub>3</sub>-activated NHCs at R.T. All these findings attested to a controlled / living ROP of *rac*-LA in presence of K<sub>2</sub>CO<sub>3</sub>.



**Figure 3.7.** Normalized monomodal SEC traces of PLAs obtained by (a) **NHC1** (entry 2, Table 3.2), (b) **NHC2** (entry 6, Table 3.2), (c) **NHC3** (entry 10, Table 3.2) and (d) **NHC4** (entry 14, Table 3.2) catalysis at in CH<sub>2</sub>Cl<sub>2</sub> at R.T; [LA]<sub>0</sub> / [BnOH]<sub>0</sub> = 50 : 1.

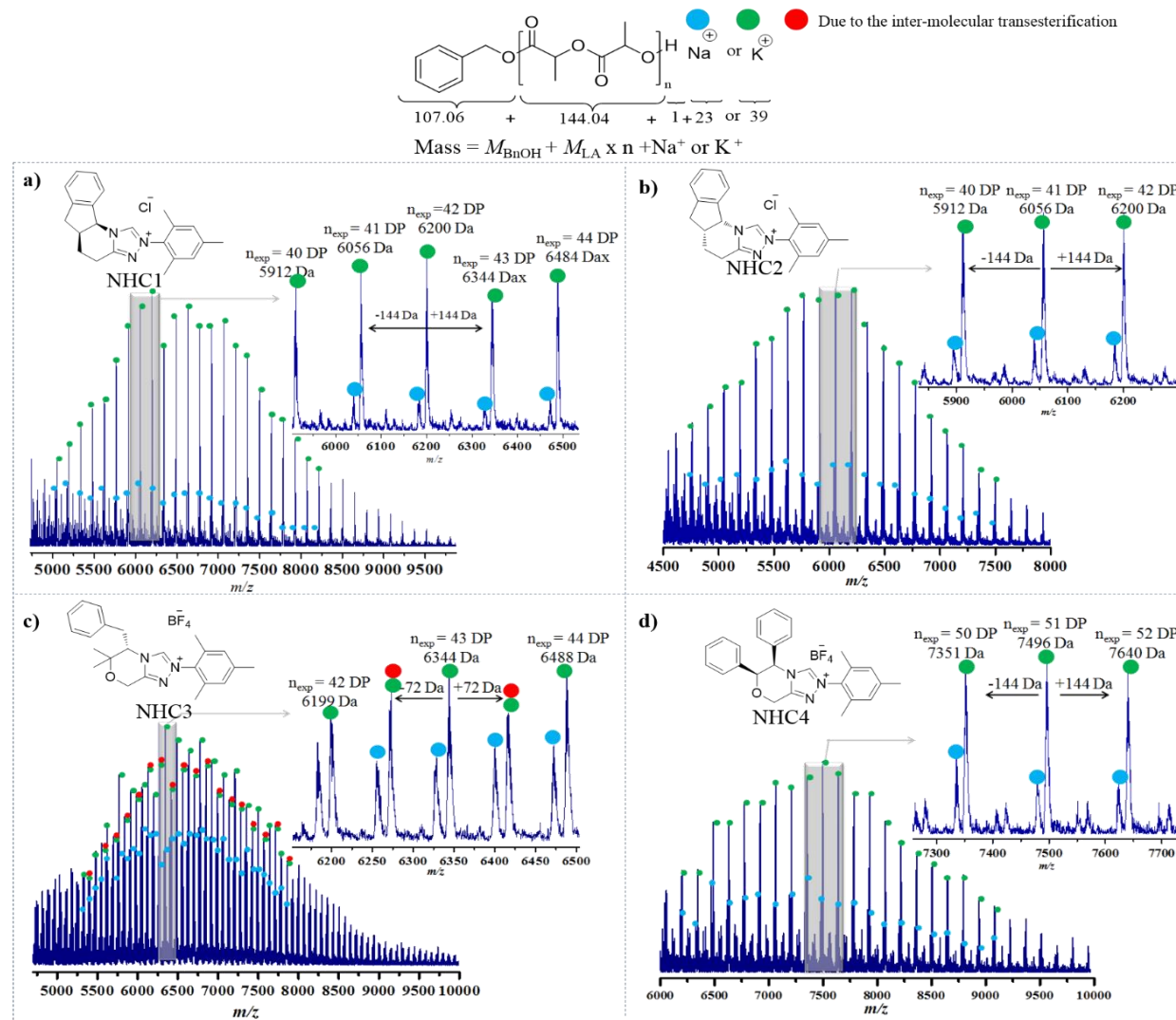
As a general trend, the change of activation bases caused an increase in polymer dispersions (entry 2 vs. entry 3 and 4, entry 6 vs. entry 7 and 8, entry 10 vs. entry 11 and 12, entry 14 vs. entry 15 and 16, Table 3.2). Except using with **NHC3**, when *t*-BuOK was used instead of K<sub>2</sub>CO<sub>3</sub>, it was observed that the polymerization time was considerably decreased, but desperately, polymer distributions increased assuming that the side reactions may have occurred. The use of DBU increased these polymer distributions more, thus supporting the argument of undesirable reactions, such as transesterifications.

All PLAs produced from **NHC1**, **NHC2**, **NHC3** and **NHC4** organocatalysts were also analyzed by MALDI-ToF mass spectrometry. A representative mass spectrum is shown in Figure 3.7. In general, a series of main peaks corresponds to PLA chains cationized with potassium appeared at regular intervals of 144 *m/z* (Figure 3.7, ●), that were, in accordance with the molar mass of LA units (entries 2, 6, 10 and 14, Table 3.2). A minor series of peaks corresponds to PLA chains was also observed at certain intervals of 144 *m/z* (Figure 3.7, ●). The (DP)<sub>n</sub> of PLAs, evaluated from the main signals, was found equal to 42, 41, 43 and 51 in

the case of  $K_2CO_3$ -activated **NHCs** **1**, **2**, **3** and **4**, respectively. Importantly,  $M_{n,MALDI}$  values proved consistent with  $M_{n,theo}$  values. For instance, the  $K_2CO_3$ -activated **NHC1**-derived PLA gave a  $M_{n,MALDI}$  equal to 6.6 kDa, in good agreement with the  $M_{n,theo}$  value of 7.2 kDa. Likewise, the observation of  $M_{n,MALDI}$  values of 6.0, 6.5 and 7.4 kDa which were obtained using  $K_2CO_3$ -activated **NHC2**, **3** and **4**, remarkably matched theoretical ones ( $M_{n,theo}$ = 7.2, 7.1 and 7.0 Da, respectively).

Another set of peaks corresponding to a repeating unit of 72 Da (Figure 3.7, ●) could be observed in the case of the PLA synthesized from the by  $K_2CO_3$ -activated **NHC3**. Such peaks are clearly indicative of the occurrence of transesterification reactions, *i.e.* intermolecular chain transfer occurring during the ROP process. Similar peaks due to ester exchange side reactions were also observed for PLAs prepared at -50 °C from this  $K_2CO_3$ -activated **NHC3** catalysis (Figure S3.10), so that **NHC3** did not appear suitable as organic catalyst to achieve well defined PLAs under such conditions. Similarly, PLA samples resulting from the DBU *in situ* forming NHCs also revealed the presence of side peaks due to transesterification reactions, as can be seen in Figures S3.6, S3.9, S3.12 and S3.15). The same was true for polymers obtained by the *t*-BuOK activated-**NHC4** (Figure S3.13).





**Figure 3.8.** MALDI-ToF mass spectrum of PLA prepared using (a) **NHC1** (b) **NHC2** (c) **NHC3** and (d) **NHC4** in  $\text{CH}_2\text{Cl}_2$  at 25 °C (entry 2, 8, 14 and 20, Table 3.2) respectively.

### 3.3.3. Analysis of the stereoselectivity of NHC-derived PLA materials

#### 3.3.3.1. DSC Analysis

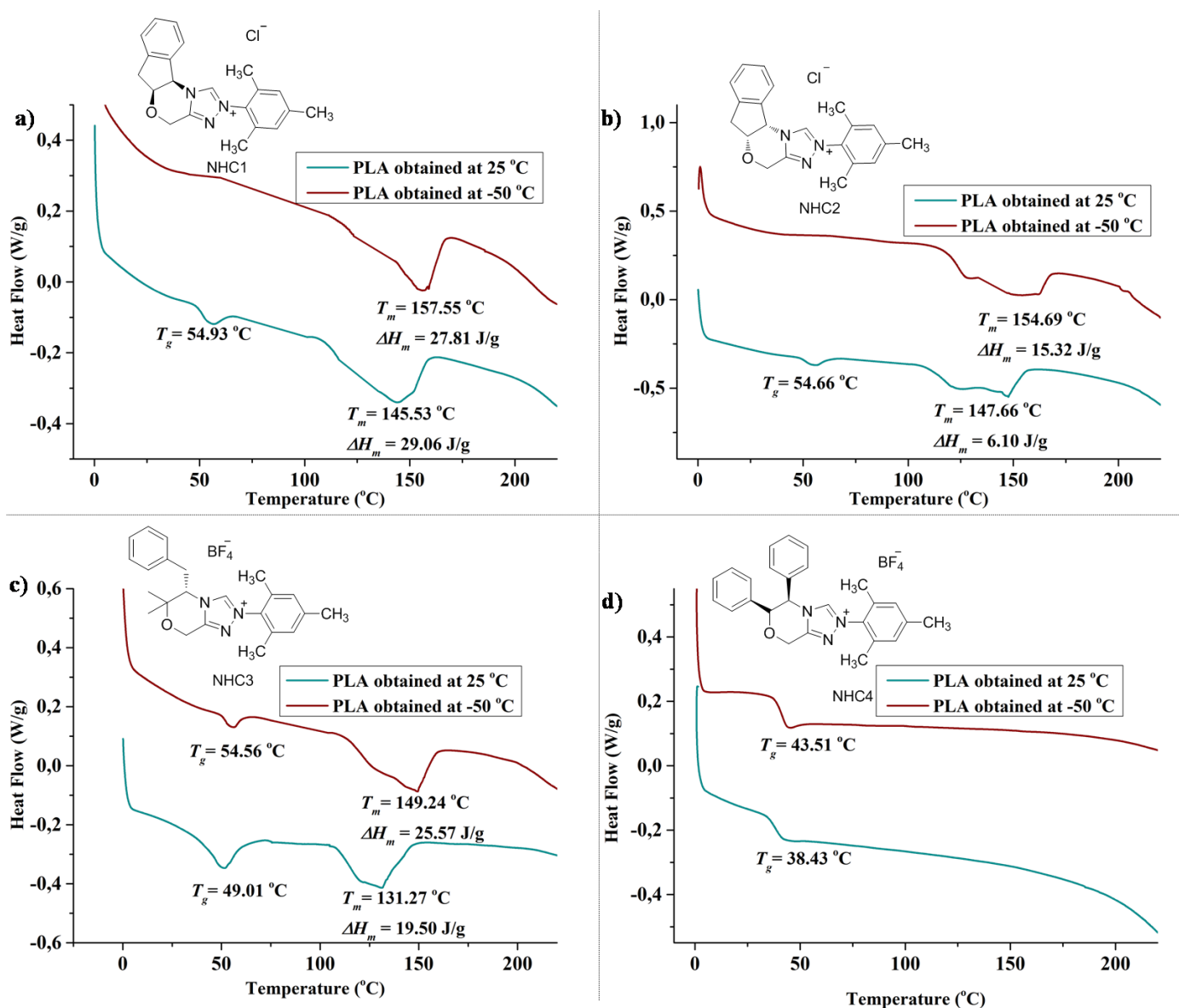
To gain an insight into the physical properties of the NHC-derived PLA materials, DSC analyses were performed. Thermal data were obtained from the 1<sup>st</sup> and 2<sup>nd</sup> scans. The degree of crystallinity ( $x_c$ ) was calculated using equation of  $x_c = \frac{\Delta H_{m,exp}}{\Delta H_{m,theo}}$  and melting enthalpies ( $\Delta H_m$ ) of polymers were determined by the integration of melting transition area (theoretical melting enthalpy of PLA homocrystallite ( $\Delta H_{m,theo}$ ) is 93.7 J/g).<sup>[106,107]</sup>

DSC analyses revealed both a defined glass transition temperature ( $T_g$ ) and a melting temperature ( $T_m$ ) for all PLA polymers synthesized from the K<sub>2</sub>CO<sub>3</sub>-activated **NHCs 1, 2** and **3** catalysis in CH<sub>2</sub>Cl<sub>2</sub> at 25 °C. Corresponding results are shown in Figure 3.9.

In case of PLAs obtained from the K<sub>2</sub>CO<sub>3</sub>-activated **NHC1** and **NHC2** organocatalysis, a  $T_g$  value of 54-55 °C and a  $T_m$  around 145 to 147 °C were detected (entries 2 and 6, Table 3.2). Slightly distinct  $T_m$  value, and correspondingly a different  $\Delta H_m$  value were observed for PLAs achieved with the K<sub>2</sub>CO<sub>3</sub>-activated **NHC3** catalysis:  $T_g$  = 49 and  $T_m$  = 131 °C (entry 10, Table 3.2). All these data are consistent with the formation of optically active and semi-crystalline PLAs.

Interestingly, the ROP of *rac*-LA in CH<sub>2</sub>Cl<sub>2</sub> at -50 °C using **NHCs 1** and **2** yielded PLAs exhibiting a melting point at 157 and 154 °C ( $\Delta H_m$  = 27.81 and 15.84 J/g), respectively, suggesting the production of a polymer material with an even higher degree of isotacticity and crystallinity (Figure 3.9a and 3.9b). Similarly, the lower reaction temperature also enabled the formation of a more crystalline PLA, using the K<sub>2</sub>CO<sub>3</sub>-activated **NHC3**, as the  $T_g$  value could be increased from 49 to 54 °C, while  $T_m$  value was increased from 131 to 149 °C. In contrast, PLAs synthesized from the *in situ* generated **NHC4** by K<sub>2</sub>CO<sub>3</sub> did not show any  $T_m$  value, neither at 25 °C nor at -50 °C (entries 13 and 14, Table 3.2). The presence of only a  $T_g$  at 43 and 38 °C, respectively, was consistent with the formation of an amorphous and atactic PLA.

Generation of **NHCs 1** and **2** by *t*-BuOK for the ROP of *rac*-LA also led to a semi-crystalline PLA at 25 °C (entries 3 and 7, Table 3.2). In contrast, activation of the triazolium salt precursor by DBU provided an atactic PLA under otherwise identical reaction conditions (entries 4 and 8, Table 3.2).

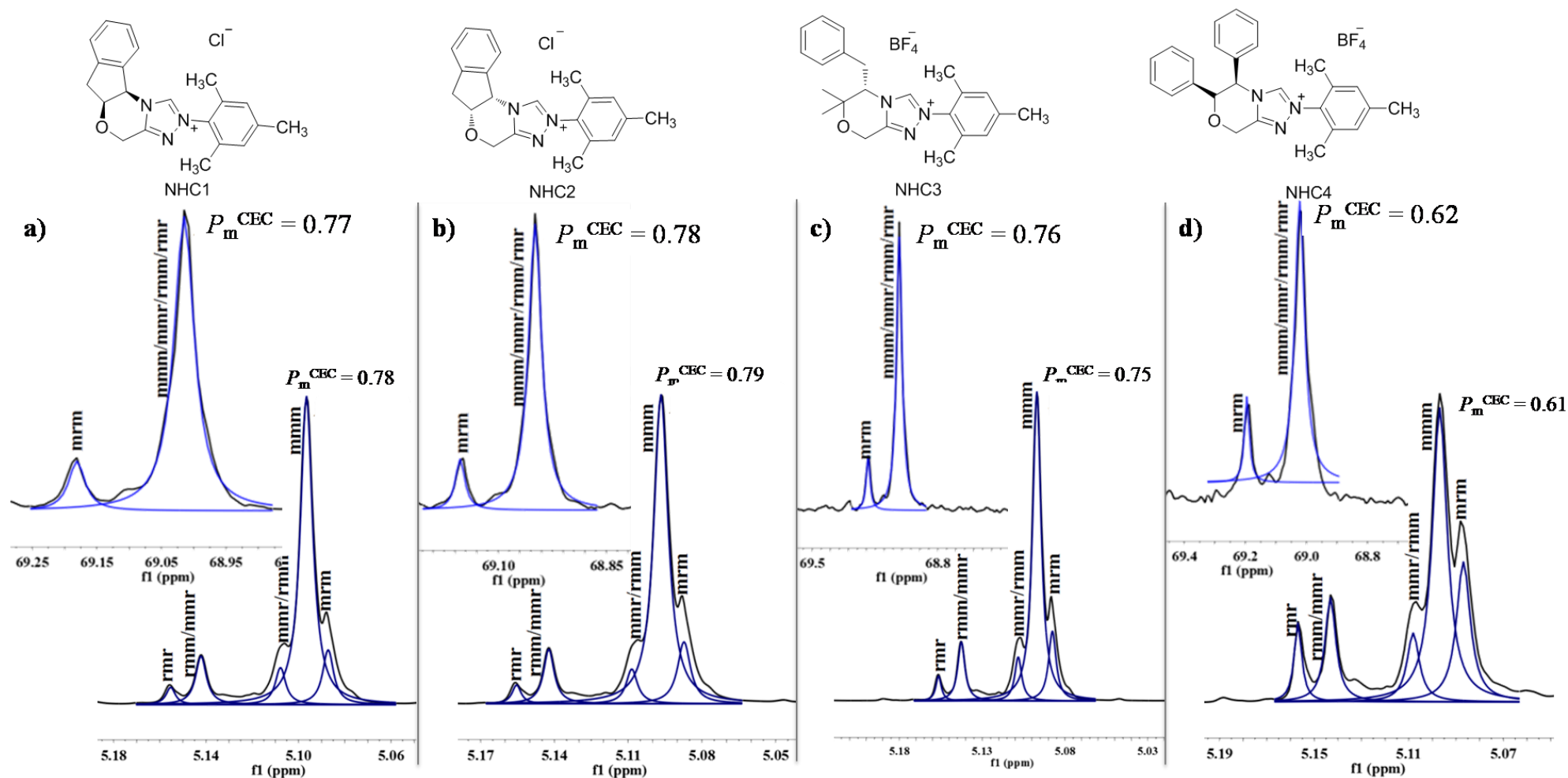


**Figure 3.9.** DSC thermograms (1<sup>st</sup> scan; 10 °C/min) of PLA prepared with (a) **NHC1**, (b) **NHC2**, (c) **NHC3** and (d) **NHC4** at both 25 and -50 °C.

Attempts to increase the melting temperature further by annealing was not successful. To this end, a predetermined amount of each NHC-derived PLA was weighted into a small vial and stirred homogeneously at 100 rpm with a magnetic stirrer for overnight, at a temperature close to their melting point (~ 145-157 °C). No significant difference of the  $T_m$  values was however noted.

### 3.3.3.2. Homonuclear decoupled $^1\text{H}$ NMR and quantitative $^{13}\text{C}$ NMR analysis

The microstructure of the different PLAs resulting from the NHC-mediated ROP of *rac*-LA was next investigated by homonuclear decoupled  $^1\text{H}$  NMR ( $^1\text{H}$  { $^1\text{H}$ } NMR) and quantitative  $^{13}\text{C}$  NMR (Q.  $^{13}\text{C}$  NMR) spectroscopies. From the integrals of the methine signals in  $^1\text{H}$  { $^1\text{H}$ } NMR ( $\delta = 5.03\text{--}5.18$  ppm), and in Q.  $^{13}\text{C}$  NMR ( $\delta = 68.8\text{--}69.5$  ppm) the probability of isotactic enchainment ( $P_m$ ) could thus be calculated, giving a quantitative measure of stereoselectivity.<sup>[17,108]</sup> Figure 3.10 summarizes the different results of such analyses.



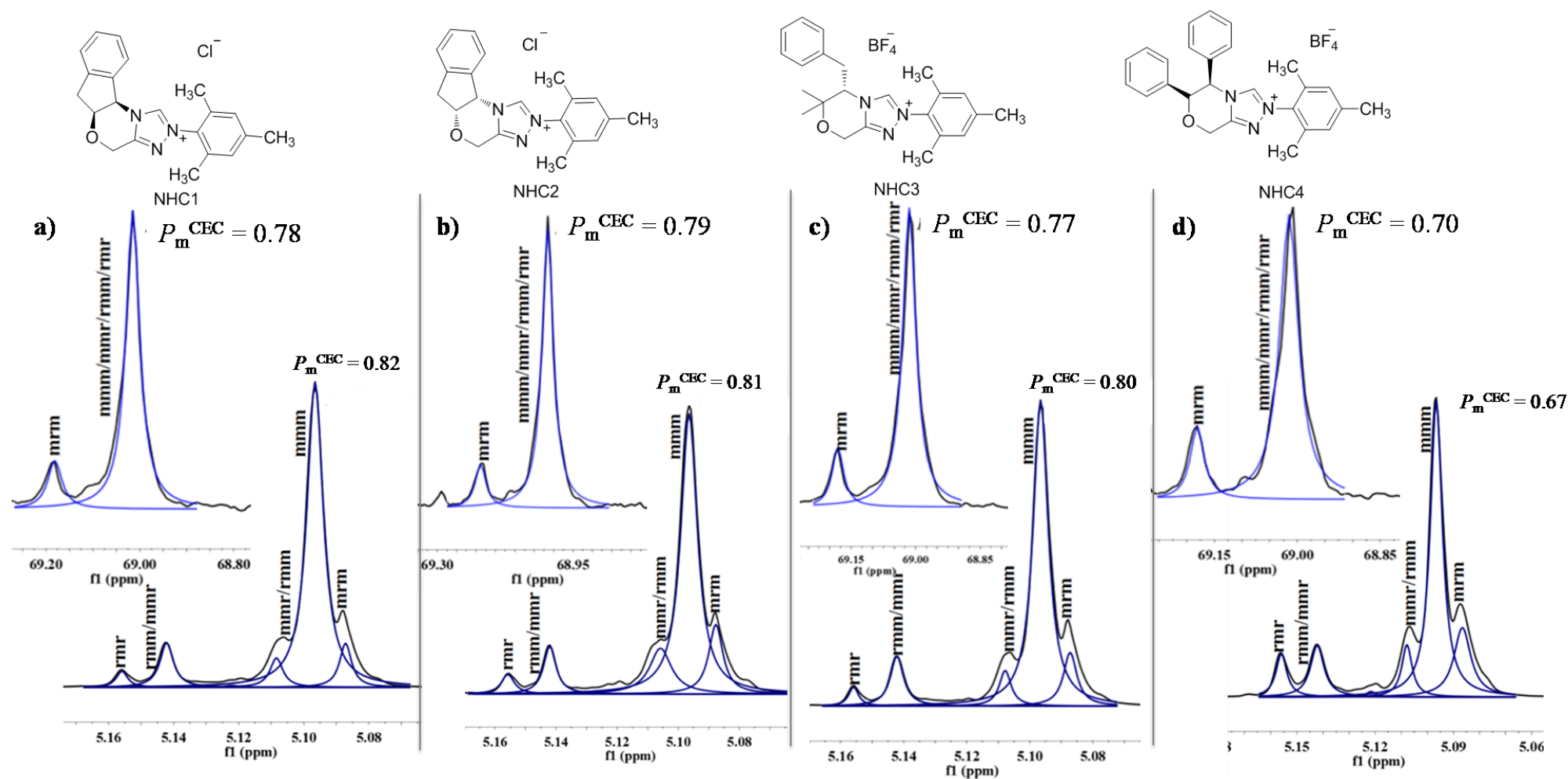
**Figure 3.10.**  $^1\text{H}$  { $^1\text{H}$ } NMR spectra (400 MHz,  $\text{CDCl}_3$ ) of the methine region of PLA obtained from: (a)  $\text{K}_2\text{CO}_3$ -activated **NHC1** at 25 °C (entry 2, Table 3.2); (b)  $\text{K}_2\text{CO}_3$ -activated **NHC2** at 25 °C (entry 6, Table 3.2); (c)  $\text{K}_2\text{CO}_3$ -activated **NHC3** at 25 °C (entry 10, Table 3.2); (d)  $\text{K}_2\text{CO}_3$ -activated **NHC4** at 25 °C (entry 14, Table 3.2); Inset: quantitative  $^{13}\text{C}$  NMR spectra.

The probability of finding mesodyads, referred to as  $P_m$ , was determined from  $^1\text{H}$   $\{^1\text{H}\}$  NMR and quantitative  $^{13}\text{C}$  NMR spectroscopy, decoupled from the polymer doublet at  $\sim 1.62$  ppm and calculated using Bernoullian statistics.<sup>[109]</sup>

The polymer tacticity, assessed by  $^1\text{H}$   $\{^1\text{H}\}$  NMR spectroscopy, showed that both **NHC1** and **NHC2**, as generated *in situ* by  $\text{K}_2\text{CO}_3$ , produced a PLA with an appreciable isotacticity ( $P_m = 0.78$  and  $0.79$ , respectively; see Table 3.2, entries 2 and 6). The two other bases, DBU and *t*BuOK, led to a reduced stereoregularity: for **NHC1**,  $P_{m,t\text{-BuOK}} = 0.75$  and  $P_{m,\text{DBU}} = 0.70$ , while for **NHC2**,  $P_{m,t\text{-BuOK}} = 0.77$  and  $P_{m,\text{DBU}} = 0.69$  (see Figure S3.15 & 3.16). Since **NHC1** and **2** are the two different enantiomers of the same catalyst, they were expected to show similar stereocontrol results. Thus, it can be concluded that, while catalytic activity increases, stereoselectivity of the catalysts becomes moderate.

In addition, results obtained by  $^1\text{H}$   $\{^1\text{H}\}$  NMR analysis proved consistent with those determined by quantitative  $^{13}\text{C}$  NMR spectroscopy. Thus, PLA showing a  $P_m$  value of  $0.79$  as calculated by  $^1\text{H}$   $\{^1\text{H}\}$  NMR spectroscopy, gave  $P_m = 0.78$  by quantitative  $^{13}\text{C}$  NMR spectroscopy (entry 6, Table 3.2). The  $P_m$  values could be slightly further increased, from  $0.79$  to  $0.81$  (Figure 3.11b), by decreasing the reaction temperature, from  $25\text{ }^\circ\text{C}$  to  $-50\text{ }^\circ\text{C}$  (entries 7 and 8, Table 3.2). On the other hand, the *in situ* generated **NHC3** provided a lower stereoselectivity relatively to **NHCs 1** and **2**.

However, despite the significant amount of transesterification reactions, the ROP of *rac*-LA performed in  $\text{CH}_2\text{Cl}_2$  afforded PLAs with a rather high stereoselectivity in the presence of  $\text{K}_2\text{CO}_3$ -activated **NHC3** (Figure 3.10c; see also Table 3.2, entry 10:  $P_{m,\text{CEC}} = 0.75$ ). In contrast, PLA samples prepared from either *t*-BuOK or DBU-activated **NHC3** revealed an almost random incorporation of both *D*- and *L*-LA isomers during the ROP process, since values were found as follows:  $P_{m,t\text{-BuOK}} = 0.70$  and  $P_{m,\text{DBU}} = 0.61$  (entries 15,16, Table 3.2). Yet, a significant isotactic enrichment could be reached upon using **NHC3** at a polymerization temperature of  $-50\text{ }^\circ\text{C}$ , with  $P_m = 0.80$ , as illustrated in Figure 3.11c (see also entry 9, Table 3.2).



**Figure 3.11.**  $^1\text{H}$  { $^1\text{H}$ } NMR spectra (400 MHz,  $\text{CDCl}_3$ ) of the methine region of PLA obtained from: (a)  $\text{K}_2\text{CO}_3$ -activated **NHC1** at  $-50^\circ\text{C}$  (entry 1, Table 3.2); (b)  $\text{K}_2\text{CO}_3$ -activated **NHC2** at  $-50^\circ\text{C}$  (entry 5, Table 3.2); (c)  $\text{K}_2\text{CO}_3$ -activated **NHC3** at  $-50^\circ\text{C}$  (entry 9, Table 3.2); (d)  $\text{K}_2\text{CO}_3$ -activated **NHC4** at  $-50^\circ\text{C}$  (entry 13, Table 3.2); Inset: quantitative  $^{13}\text{C}$  NMR spectra

In case of  $K_2CO_3$ -activated **NHC4** organocatalysis, PLA samples that were amorphous as evidenced by DSC analysis,  $P_m$  values of 0.61 and 0.62 were calculated by  $^1H$  { $^1H$ } NMR and quantitative  $^{13}C$  NMR spectroscopy for the polymer obtained at 25 °C (Figure 3.10d; see also entry 14, Table 3.2). A slight change was observed in  $P_m$  to 0.67 for the PLA obtained at -50 °C (Figure 3.11d; entry 13, Table 3.2). In addition, the change of activation base didn't alter the tacticity. While *t*-BuOK-activated **NHC4** showed  $P_m$  at 0.61 (entry 15, Table 3.2, Figure S3.18), DBU-activated **NHC4** showed  $P_m$  at 0.62 (entry 16, Table 3.2, Figure S3.16).

The stereocontrol mechanism was then investigated with the help of the aforementioned analyses by  $^1H$  { $^1H$ } NMR and quantitative  $^{13}C$  NMR spectroscopies combined with kinetic studies. Specifically, and as already discussed in the previous chapters, a close look at the intensity of the different tetrad ratio allowed us to elucidate the stereocontrol mechanism employing chiral NHCs. As already discussed also, the *rmr* signal is a clear indicator of the mechanism. Assuming that the non-Bernoullian enantiomorphous site control (ESC) mechanism would operate, relative tetrad intensities would be expected as follows:<sup>[17]</sup>  $[rmr] = [mmr] = [rmm] = 2/[mrm]$ . In the case of the Bernoullian chain end control (CEC) mechanism, the relationship between the tetrad ratios should be as follows:  $[rmm] = [mmr] \neq [rmr]$ .<sup>[110]</sup> Analysis of NMR spectra for the PLA sample obtained by  $K_2CO_3$ -activated **NHC1** organocatalysis (entry 2, Table 3.2) revealed the tetrad ratios to be:  $[rmr] = 0.028$ ,  $[mmr] = 0.071$ ,  $[rmm] = 0.099$  and  $[mrm] = 0.109$ . In the case of the PLA prepared from  $K_2CO_3$ -activated **NHC2** (entry 6, Table 3.2), the tetrad ratios were found as follows:  $[rmr] = 0.026$ ,  $[mmr] = 0.059$ ,  $[rmm] = 0.095$  and  $[mrm] = 0.126$ . Therefore, comparison of these experimental findings with the two predictive models clearly support that both **NHCs 1** and **2** trigger the ROP of *rac*-LA following the chain-end control mechanism. Likewise, analysis of the PLA prepared by  $K_2CO_3$ -activated **NHC3** catalysis (entry 10, Table 3.2) led to a tetrad ratio as follows:  $[rmr] = 0.033$ ,  $[mmr] = 0.076$ ,  $[rmm] = 0.10$  and  $[mrm] = 0.13$ . These ratios are indeed also consistent with the occurrence of the CEC mechanism from that particular carbene.

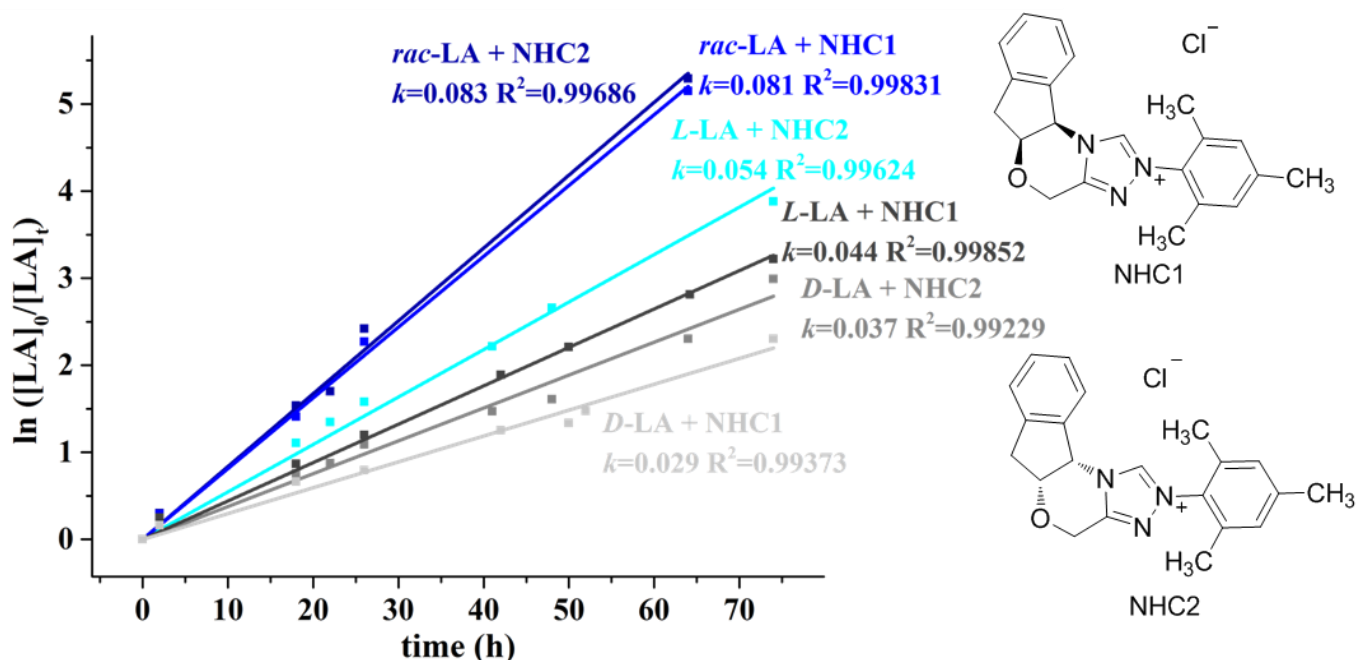
Finally, analysis by NMR of the  $K_2CO_3$ -activated **NHC4**-derived PLA, which also proved a semi-crystalline polymer formation, led to tetrad ratios of  $[mrm] = 0.220$ ,  $[mmr] = 0.095$ ,  $[rmm] = 0.126$  and  $[rmr] = 0.067$ . However, these values were consistent with neither the ESC nor the CEC mechanism. Such features have already been discussed in the previous chapter regarding the use of chiral versions of the Takemoto catalysts. In the latter case, we postulated that both mechanisms could concomitantly operate during the ROP of *rac*-LA. As



discussed in the next section, further investigations through kinetic studies were carried out to gain more insight into the ROP reaction employing chiral NHCs.

### 3.3.4. Kinetic studies of the ROP of *rac*-LA

Kinetic studies were performed in order to further account for the mechanism of stereocontrol taking place during the ROP of *rac*-LA from chiral NHCs. Corresponding kinetic studies revealed first order kinetic plots for the ROP of *rac*-LA in presence of all NHC precursors, using an initial ratio of  $[LA]/[Cat.]/[K_2CO_3]/[BnOH] = 50:0.5:0.5:1$  in  $CH_2Cl_2$  at 25 °C. The pseudo first-order rate constants,  $k_{obs}$ , could be determined from the slope of the linear evolution of  $\ln([LA]_0/[LA]_t)$  versus time, as illustrated in Figure 3.12.



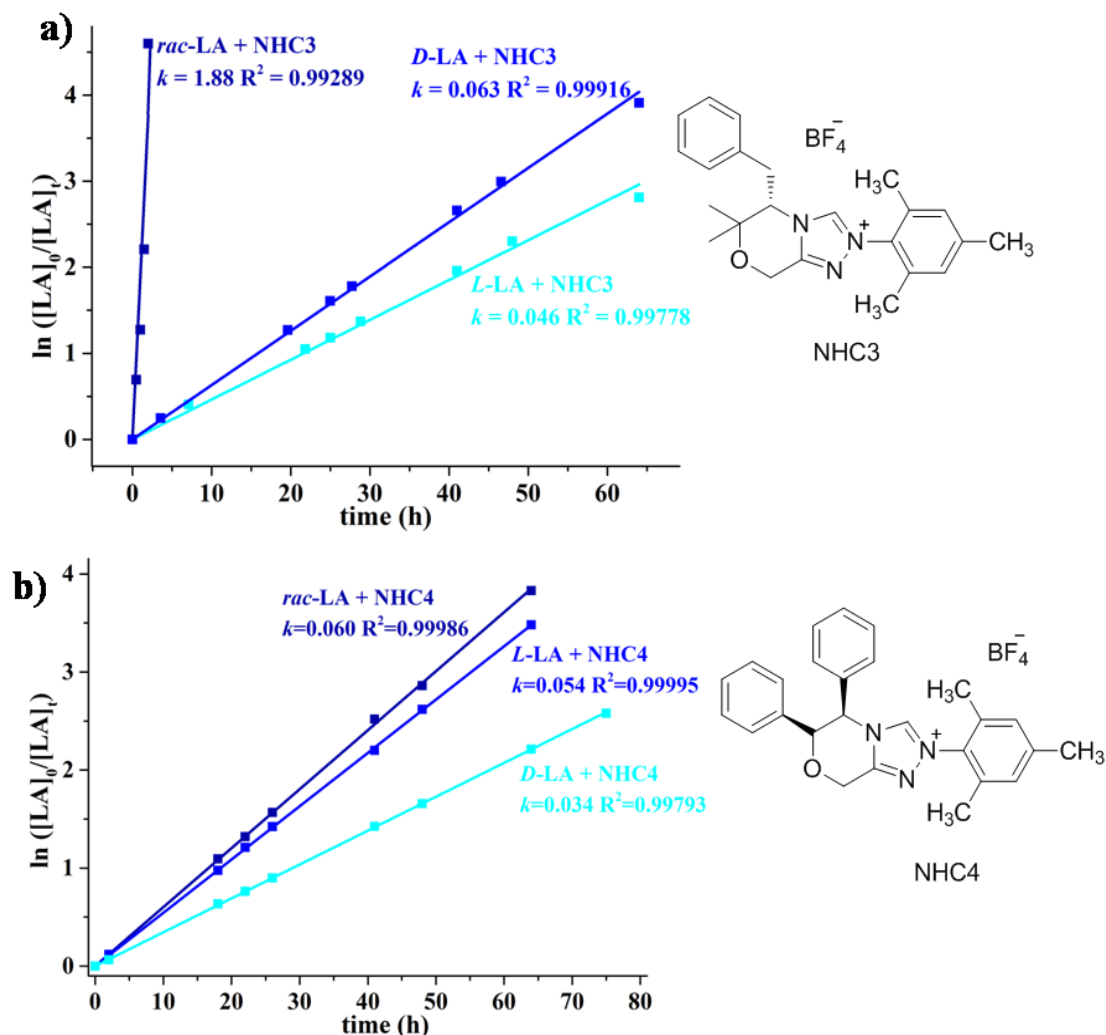
**Figure 3.12.** Semi-logarithmic plots of the ROP of *rac*-LA, *D*-LA and *L*-LA catalyzed by **NHC1** and **NHC2** (entries 2 and 6, Table 3.2; entries 1, 2, 3 and 4, Table 3.3) in  $CH_2Cl_2$  at RT in the presence of BnOH as a  $[LA]/[Cat.]/[K_2CO_3]/[BnOH] = 50:0.5:0.5:1$

In accordance with the results above, **NHC1** and **2** showed faster activation with the racemic mixture of LA ( $k_{obs} = 0.081$  for **NHC1**,  $k_{obs} = 0.083$  for **NHC2**) supporting these catalysts has no preferential selectivity of one of the enantiopure monomer. (Figure 3.12). Considering these results, the chain-end activation mechanism has thus been supported in the case of **NHC1** and **2** catalysis.

**Table 3.3.** Stereoselective ring-opening polymerizations of *D*-, and *L*- catalyzed by chiral NHC precursors.<sup>a</sup>

Entry	Monomer	Catalyst	Base	T [°C]	<i>t</i> [h]	Conv. [%] <sub>b</sub>	$M_n^{calc}$ [kg.mol <sup>-1</sup> ] <sub>d</sub>	$M_n$ [kg.mo l <sup>-1</sup> ] <sub>c</sub>	$\bar{D}_M$ <sup>c</sup>	$T_m$ [°C] <sup>e</sup>	$P_m$
1	<i>L</i> -LA	<b>NHC1</b>	K <sub>2</sub> CO <sub>3</sub>	25	74	96	6.5	9.6	1.05	157	1
2	<i>D</i> -LA	<b>NHC1</b>	K <sub>2</sub> CO <sub>3</sub>	25	74	90	5.8	8.7	1.04	155	1
3	<i>L</i> -LA	<b>NHC2</b>	K <sub>2</sub> CO <sub>3</sub>	25	74	99	7.2	3.4	1.08	151	1
4	<i>D</i> -LA	<b>NHC2</b>	K <sub>2</sub> CO <sub>3</sub>	25	74	95	6.9	3.0	1.07	148	1
5	<i>L</i> -LA	<b>NHC3</b>	K <sub>2</sub> CO <sub>3</sub>	25	64	94	6.8	5.4	1.07	154	1
6	<i>D</i> -LA	<b>NHC3</b>	K <sub>2</sub> CO <sub>3</sub>	25	64	98	7.1	6.0	1.08	155	1
7	<i>L</i> -LA	<b>NHC4</b>	K <sub>2</sub> CO <sub>3</sub>	25	64	95	6.9	5.8	1.07	153	1
8	<i>D</i> -LA	<b>NHC4</b>	K <sub>2</sub> CO <sub>3</sub>	25	75	96	7.0	6.0	1.08	151	1

<sup>a</sup>Polymerizations were conducted in CH<sub>2</sub>Cl<sub>2</sub> with the initial ratio of [LA]<sub>0</sub>/[NHC]<sub>0</sub>/[Base]<sub>0</sub>/[BnOH]<sub>0</sub> = 50:0.5:0.5:1 unless otherwise stated. <sup>b</sup> Conversion of polymerizations were determined by <sup>1</sup>H NMR spectroscopic analysis in CDCl<sub>3</sub>. <sup>c</sup> $M_n$  and  $\bar{D}_M$  values are determined by SEC in THF (calibration using polystyrene standards).  $M_{n,SEC}$  values are corrected by Mark-Houwink correction factor (0.58). <sup>d</sup> $T_m$  values are obtained by DSC measurements from 1<sup>st</sup> heating curve. <sup>e</sup>Probabilities of finding mesodyads are calculated from homonuclear decoupled <sup>1</sup>H NMR by deconvolution technique.



**Figure 3.13.** Semi-logarithmic kinetic plots of the ROP of *rac*-LA, *D*-LA and *L*-LA catalyzed by (a) **NHC3** (entries 10, 14, Table 3.2; and entries 5, 6, 7 and 8, Table 3.3) and (b) **NHC4** (entries 20, 23 and 24, Table 3.2,) in  $\text{CH}_2\text{Cl}_2$  at R.T in the presence of BnOH as a initiator:  $[\text{LA}]_0 : [\text{BnOH}]_0 = 50 : 1$ .

Organocatalysis by **NHC3** proved to be significantly faster with *rac*-LA ( $k_{\text{obs}} = 1.88$ ), with a full conversion being achieved within 2 h. However, *L*- and *D*-LA exhibited slower activation with a 64 h of monomer consumption. ( $k_{\text{obs,L}} = 0.046$ ,  $k_{\text{obs,D}} = 0.063$ , Figure 3.13). Thus, showing no enantiomeric selectivity for homoenantiomers of LA. Lastly, since none of the stereocontrol approach (ESC or CEC) was fitting for **NHC4** catalyzed ROP of *rac*-LA, kinetic studies have led guiding to investigate it. As also observed for other NHCs, **NHC4** showed rapid activation with the *rac*-LA ( $k_{\text{obs}} = 0.060$ ) and did not show any enantioselectivity. In summary, the chiral organic NHC precursors have no preferential enantioselectivity for enantiopure LA, but only for the *rac*-LA. As previously discussed in chapters above, in a chain end controlled mechanism, the chirality of the propagating chain end bound to the catalyst determines the chirality of the next monomer to be inserted, which is

generally associated with hindered but achiral catalyst systems, while the chirality of the catalyst, dictates the chirality of the next insertion for the enantiomorphic site control mechanism. Clearly, these findings are definitely in line with the chain-end control mechanism approach.

### 3.4. Conclusions and perspectives

Highly efficient chiral organic *in situ* generated NHC catalysts were investigated for the first time for the stereoselective ROP of *rac*-LA. At room temperature, the ROP of *rac*-LA with fast rate (99% conversion within 2 h) has been achieved using *in situ* generated (*S*)-Benzyl-mesityl-6,6-dimethyl-triazolooxazinium tetrafluoroborate (**NHC3**) by K<sub>2</sub>CO<sub>3</sub>, while 64 h are required for the complete monomer conversion in the case of **NHC1** [(5a*S*,10b*R*)-dihydro-(2,4,6-trimethylphenyl)-indeno-triazolooxazinium chloride], **NHC2** [(5a*R*,10b*S*)-dihydro-(2,4,6-trimethylphenyl)-indeno-triazolooxazinium chloride] and **NHC3**. Narrow polymer distributions (*M<sub>w</sub>* ~ 1.05-1.07) with expected molar mass can be achieved attesting to a living/controlled polymerization process have been demonstrated by combined methods, including SEC and <sup>1</sup>H NMR analysis. The use of other bases for *in situ* generation, such as *t*-BuOK and DBU enables to considerably shorten these periods from 64 h to 2 h. However, enhanced catalytic activations caused undesirable transesterification reactions, which was proved by MALDI-ToF analysis, had adverse effects on both control of the polymerization and stereo-control. Above all, the structural differences of the NHCs raise the most important effect on their catalytic activity. Comparatively, since **NHC3** is structurally less rigid and stable than the other NHCs, the catalytic triazole moiety can be easily activated and realize the polymerization. In contrast, **NHC5** and **6** showed no catalytic activity, because of their bulky and the most sterically encumbered moiety of pentafluorophenyl attached to the active triazole part.

The microstructures and thermal properties of the produced PLAs have been carefully analyzed and characterized by <sup>1</sup>H {<sup>1</sup>H} NMR, quantitative <sup>13</sup>C NMR, and DSC. Additionally, the stereoselectivities of the catalysts have been evaluated by kinetic studies performing polymerizations of different enantiomers of lactide monomers. Relatively high stereoselectivities can be achieved using **NHC1**, **NHC2** and **NHC3** (*P<sub>m</sub>* = 0.78, 0.79 and 0.75, respectively). However, almost random insertion of lactide enantiomers into the polymer sequence using **NHC4** was observed (*P<sub>m</sub>* = 0.61). Other bases for *in situ* generation, such as *t*-BuOK and DBU do not alter stereoselectivity significantly. Formation of semi-crystalline formations of PLAs using **NHC1**, **NHC2** and **NHC3** has been supported by DSC (*T<sub>m</sub>* = 145, 147 and 131 °C, respectively). In the case of K<sub>2</sub>CO<sub>3</sub>-activated **NHC1** and **NHC2**, only *T<sub>m</sub>* values have been observed at low temperatures, indicating a quite high semi-crystalline PLA.

At low temperature, a  $P_m$  value up to 0.82 using **NHC1** has been obtained and the polymerization rates remain fast (over 90% conversion within 70 h).

The structural differences of the NHCs have considerable effects on their stereoselectivities as much as their catalytic activities. For instance, it could be expected that the stereoselectivity of **NHC1** and **NHC2** would be higher than the other NHCs due to its structurally more stable chiral moiety. In the case of **NHC4**, two separate branches which involves the chiral carbon increase the possibility of unstable conformations, thus decrease the stereocontrol. Comparatively, **NHC3** has only one branch attached to the chiral carbon, which enables more stability on the chiral moiety than the **NHC4**. Moreover, although significant amount of transesterification reactions, high stereoselectivity is achieved using  $K_2CO_3$ -activated **NHC3** for the the ROP of *rac*-LA.

Kinetic studies and  $^1H$  { $^1H$ } NMR spectra have revealed that the ROP process operates via a chain-end control mechanism in the case of **NHC1**, **NHC2**, **NHC3** and **NHC4**. In light of kinetic investigations, it has been observed that no catalyst selectively consumes an enantiopure lactide monomer, and the fastest activation was achieved with the racemic mixture. As previously discussed, in a chain end-controlled mechanism, the chirality of the propagating chain end bound to the catalyst determines the chirality of the next monomer to be inserted; this is generally associated with hindered but achiral catalyst systems. However, enantiomorphic site control is demonstrated when the chirality of the catalyst, and not the chain end, dictates the chirality of the next insertion. In this study, the stereocontrol of NHCs operates with chain-end activation mechanism similar as steric hindered catalysts.

These high performances on catalysis together with the easy *in situ* preparation and stable structures make this protected NHC salt precursors of great potential in practical application.

### 3.5. Experimental and supporting information

**Materials:** *D*-LA (Corbion-Purac), *L*-LA (Corbion-Purac) and *rac*-LA (Sigma-Aldrich) were recrystallized three times from dry toluene. Afterwards, lactide was purified by azeotropic distillation. Lastly, they were dried under dynamic vacuum for overnight prior to use.<sup>[111]</sup> All NHC catalysts were received from Sigma-Aldrich under argon, and directly stored in glovebox. K<sub>2</sub>CO<sub>3</sub> was received from Sigma-Aldrich and used as received. Benzyl alcohol (BnOH), *t*-BuOK and 1,8-diazabicyclo[5,4,0]undec-7-ene (DBU) were received from Alfa Aesar. DBU and BnOH were distilled by cryo-distillation over calcium hydride (CaH<sub>2</sub>). Benzoic acid (≥99.5%, Sigma-Aldrich) was used as received. All dry solvents were collected from solvent drying machine. Afterwards, they stored over molecular sieves (3 Å) in a glovebox for no longer than 4 weeks.

**Instrumentation:** <sup>1</sup>H NMR and <sup>13</sup>C NMR spectra were recorded in CDCl<sub>3</sub> on Bruker Advance instrument at 400 MHz at room temperature. Homonuclear decoupled <sup>1</sup>H NMR spectroscopic measurements and quantitative <sup>13</sup>C NMR spectra were recorded at room temperature on Bruker Advance instrument at 400 MHz and CDCl<sub>3</sub> was used as an internal reference ( $\delta = 7.26$ ). The relaxation time was fixed to 2 s. For homonuclear decoupled <sup>1</sup>H NMR spectroscopic analysis, relaxation time was measured and fixed to 2.04 s. Samples were obtained in CDCl<sub>3</sub> solutions with the decoupling pulse based on the methyl region ( $\sim\delta = 1.5$  ppm). In case of the good separation of methine region ( $\sim\delta = 5.00$ - $5.20$  ppm), the global spectral deconvolution technique was implemented by attribution of five mesodyads based on both non-Bernouillan and Bernouillan statistics in case of the operated combination mechanism.<sup>[17,110,112–116]</sup>

Polymer molar masses were determined by size exclusion chromatography (SEC) using tetrahydrofuran (THF) as the eluent. Measurements in THF were performed on an Ultimate 3000 system from ThermoScientific equipped with diode array detector DAD. The system also includes a multi-angles light scattering detector MALS and differential refractive index detector dRI from Wyatt technology. Polymers were separated on three G2000, G3000 and G4000 TOSOH HXL gel columns (300 x 7.8 mm) (exclusion limits from 1000 Da to 400 000 Da) at a flowrate of 1 mL/min. Columns temperature was held at 40°C. Polystyrene was used as the standard.

Positive-ion MALDI-MS experiments were conducted using a Waters QTOF Premier mass spectrometer equipped with a Nd:YAG laser (third harmonic) operating at 355 nm with

a maximum output of 65  $\mu\text{J}$  delivered to the sample in 2.2 ns pulses at 50 Hz repeating rate. Time-of-flight mass analysis was performed in the refraction mode at a resolution of about 10K. All samples were analyzed using trans-2-[3-(4-tert-butylphenyl)-2-methylprop-2-enylidene]malononitrile (DCTB) as a matrix. Polymer samples were dissolved in THF to obtain mg/ mL solution. Additionally, 50  $\mu\text{L}$  of 2 mg/mL NaI solution in acetonitrile was added to the polymer solution.

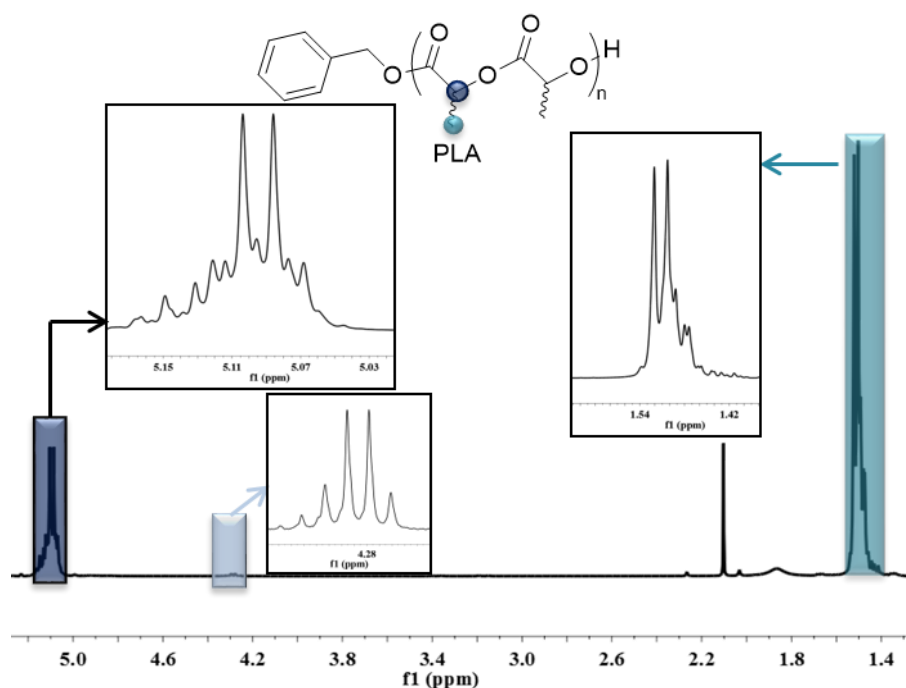
$T_g$ ,  $T_m$  and  $\Delta H_m$  values were analyzed by differential scanning calorimetry (DSC) using a DSC Q100 RCS TA Instrument. Polymer samples were first heated to 250  $^{\circ}\text{C}$  at 10  $^{\circ}\text{C}/\text{min}$ , equilibrated at this temperature for 10 min, then cooled down to 0  $^{\circ}\text{C}$  at 10  $^{\circ}\text{C}/\text{min}$ , held for 10 min, and lastly re-heated to 250  $^{\circ}\text{C}$  at the same rate. All thermal data were obtained from the first scan. Degree of crystallinity ( $x_c$ ) was calculated using  $\Delta H_m$  values, which are obtained by the integration of melting point surface areas. The equation is defined as  $x_c = \frac{\Delta H_{m\text{exp}}}{\Delta H_{m\text{theo}}}$ . ( $\Delta H_{m\text{theo}} = 93.7 \text{ J/g}$ ) [106,107]

**General polymerization methods:** In case of the polymerizations performed at -50  $^{\circ}\text{C}$ : Pre-dried 10 mL Schlenk tubes equipped with magnetic stirrer were first introduced into an Argon-filled glovebox. In a typical polymerization, catalyst (for 0.5 eq., 0.0138 mmol) and activation reagent ( $\text{K}_2\text{CO}_3$ , *t*-BuOK or DBU) was introduced into the Schlenk tube and treated for 1 hour in dichloromethane. Afterwards, external BnOH as an initiator (2,78  $\mu\text{L}$ , 0.0027 mmol) were added into the catalyst solution and stirred for 1 hour. Immediately after, previously dissolved *rac*-LA (0.2 g, 1.38 mmol) in dichloromethane (1 mL) was added to the vigorously stirred solution. Then the Schlenk tube was tightly closed, removed from glovebox and put into the Dewar including cold ethanol + liquid nitrogen solution at -50  $^{\circ}\text{C}$ . Polymerizations were monitored by  $^1\text{H}$  NMR spectroscopy and SEC before precipitation. Then they were quenched by addition of benzoic acid (4.15 mg, 0.034). The polymer was subsequently precipitated from cold methanol (MeOH), and after filtration it was excessively washed with methanol to remove any impurities. All polymers were dried under dynamic vacuum for overnight. Monomer conversion was calculated by comparing the integration of the methyl signals of unreacted monomer to the methyl region of the polymer before precipitation. Theoretical molar masses ( $M_{\text{theo}}$ ) were calculated from  $^1\text{H}$  NMR spectra from the monomer conversion factor ( $x_{\text{LA}}$ ).

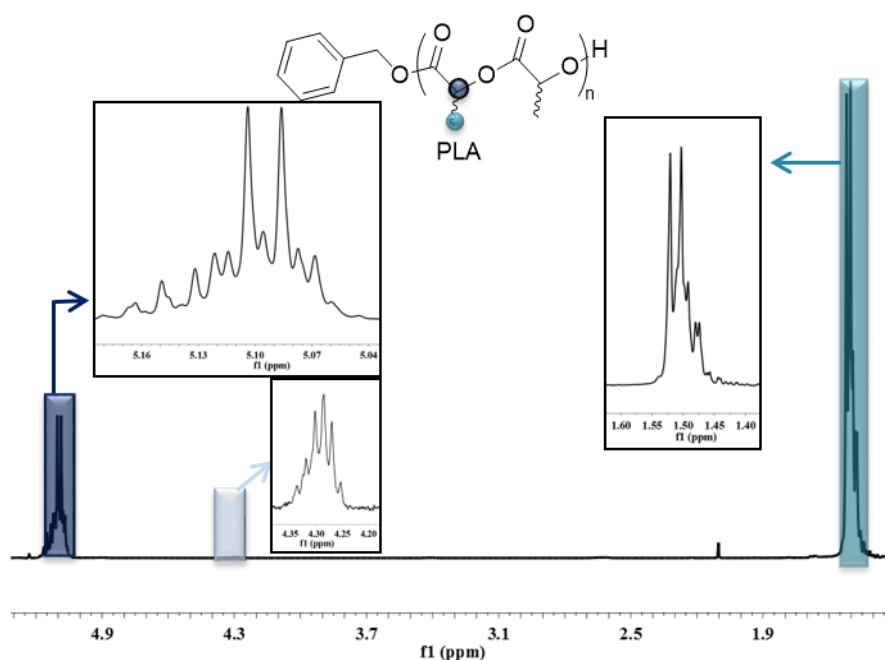
For the polymerizations performed at 25  $^{\circ}\text{C}$ : All experiments were carried out under argon using Schlenk flasks. In a typical polymerization, LA (*L*-, *D*- or *rac*-LA) (0.2 g, 1,38



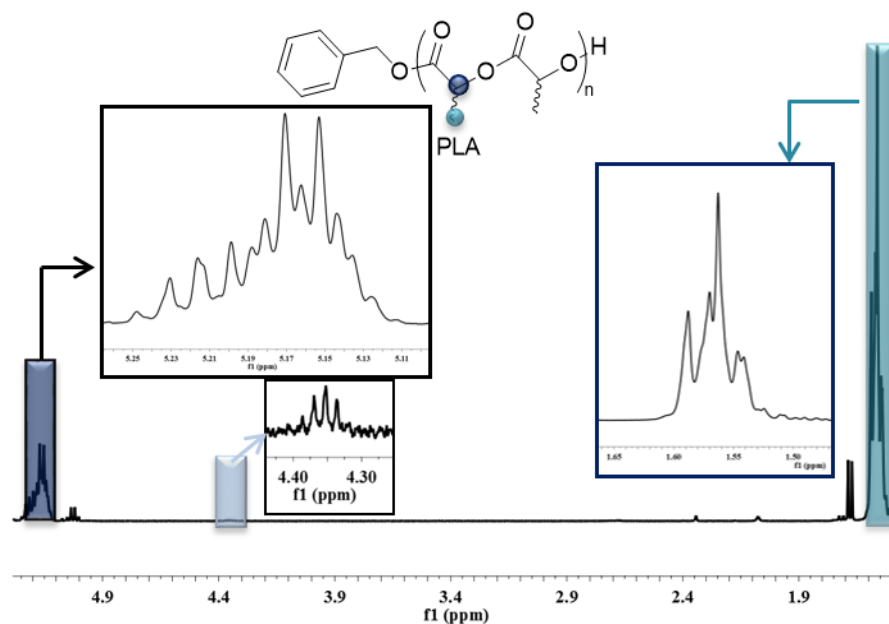
mmol) was introduced into a previously flamed and dried Schlenk vessel equipped with a magnetic stirring bar and dissolved in  $\text{CH}_2\text{Cl}_2$ . Meanwhile, NHC precursors (0.0138 mmol, 0.5 eq.) was introduced in another dried Schlenk vessel with an equimolar amount of base (0.0138 mmol, 0.5 eq.) and stirred 1 hour for the NHC activation in  $\text{CH}_2\text{Cl}_2$ . Afterwards, BnOH (2.78  $\mu\text{l}$ , 0.0277 mmol, 1 eq.) was added into the catalyst solution and stirred for 1 hour. Immediately after the filtration, the catalyst mixture was transferred into the monomer solution. The Schlenks were carefully sealed before being introduced on a magnetic stirrer. Pre-determined time intervals, aliquots were withdrawn for follow the kinetic of polymerization by  $^1\text{H}$  NMR and the average molar mass ( $M_n$ ) and dispersity ( $\mathcal{D}$ ) by SEC. To quench the polymerization excess amount of benzoic acid was introduced into the Schlenk and stirred for 1 h. Polymers were precipitated in cold methanol and excessively washed with methanol to remove any impurities. Thereafter, polymers were dried under reduced pressure by vacuum pump overnight. Monomer conversion was calculated by comparing the integration of the methyl signals of unreacted monomer to the methyl region of the polymer before precipitation. Theoretical molar masses ( $M_{\text{ntheo.}}$ ) were calculated from  $^1\text{H}$  NMR spectra from the monomer conversion factor ( $x_{\text{LA}}$ ).



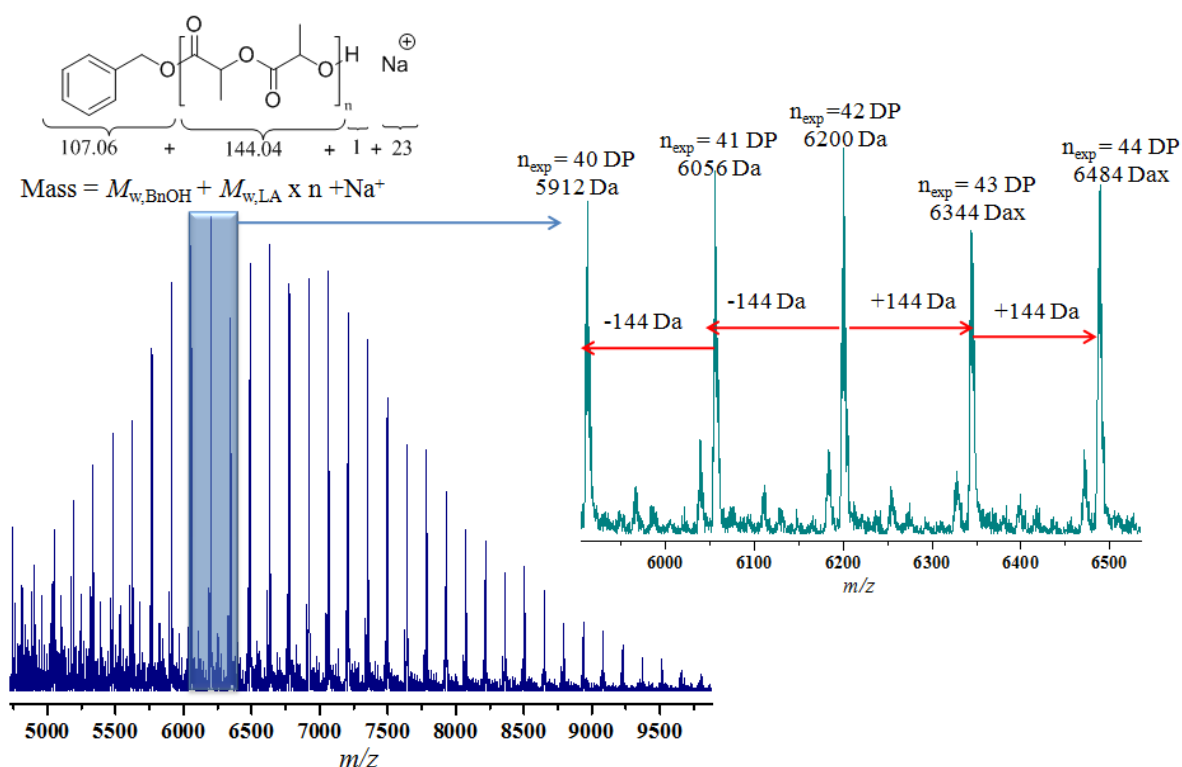
**Figure S3.1.**  $^1\text{H}$  NMR spectrum (400 MHz,  $\text{CDCl}_3$ ) of PLA prepared with **NHC2**/*rac*-LA at 25 °C Inset 1 (navy colored): Methine region of PLA, inset 2 (dark blue colored): methyl region of PLA and inset 3 (light blue colored):  $\omega$ -hydroxy proton of terminal methine group (Table 3.1, entry 6)



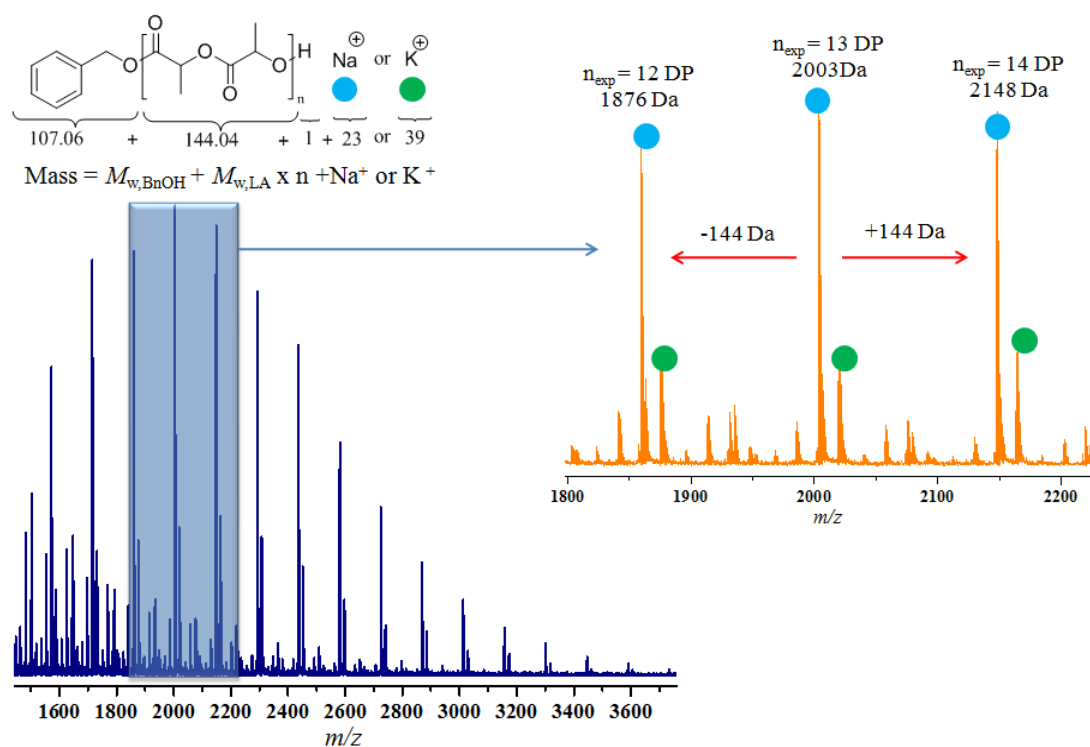
**Figure S3.2.**  $^1\text{H}$  NMR spectrum (400 MHz,  $\text{CDCl}_3$ ) of PLA prepared with **NHC3**/*rac*-LA at 25 °C Inset 1 (navy colored): Methine region of PLA, inset 2 (dark blue colored): methyl region of PLA and inset 3 (light blue colored):  $\omega$ -hydroxy proton of terminal methine group (Table 3.1, entry 10)



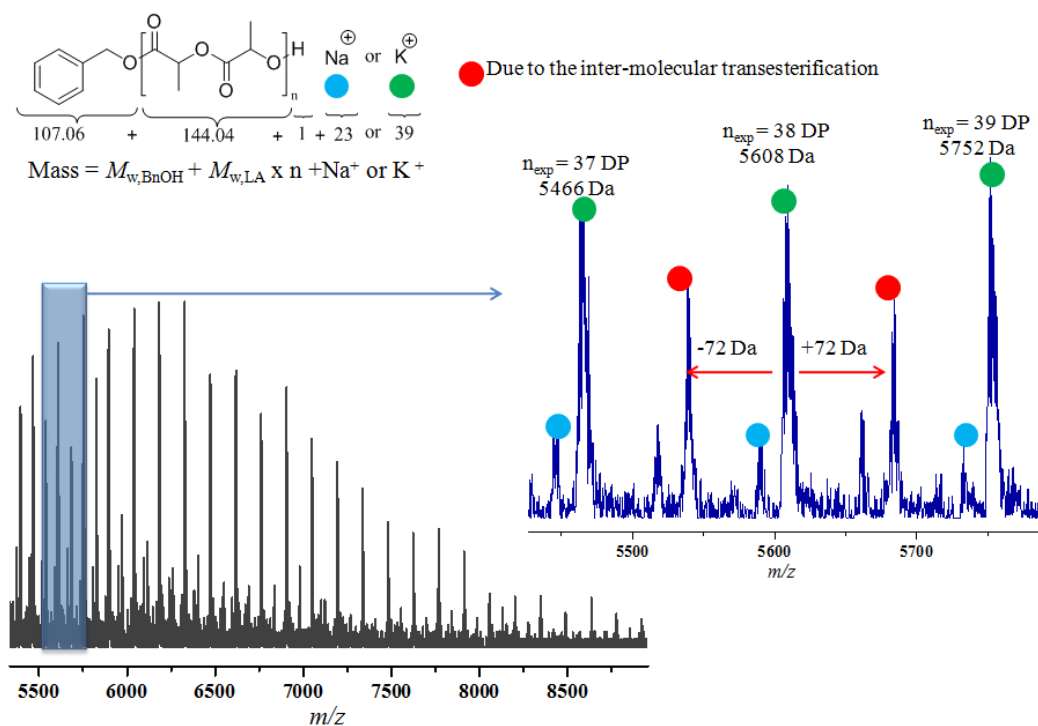
**Figure S3.3.**  $^1\text{H}$  NMR spectrum (400 MHz,  $\text{CDCl}_3$ ) of PLA prepared with **NHC4**/*rac*-LA at 25 °C Inset 1 (navy colored): Methine region of PLA, inset 2 (dark blue colored): methyl region of PLA and inset 3 (light blue colored):  $\omega$ -hydroxy proton of terminal methine group (Table 3.1, entry 14)



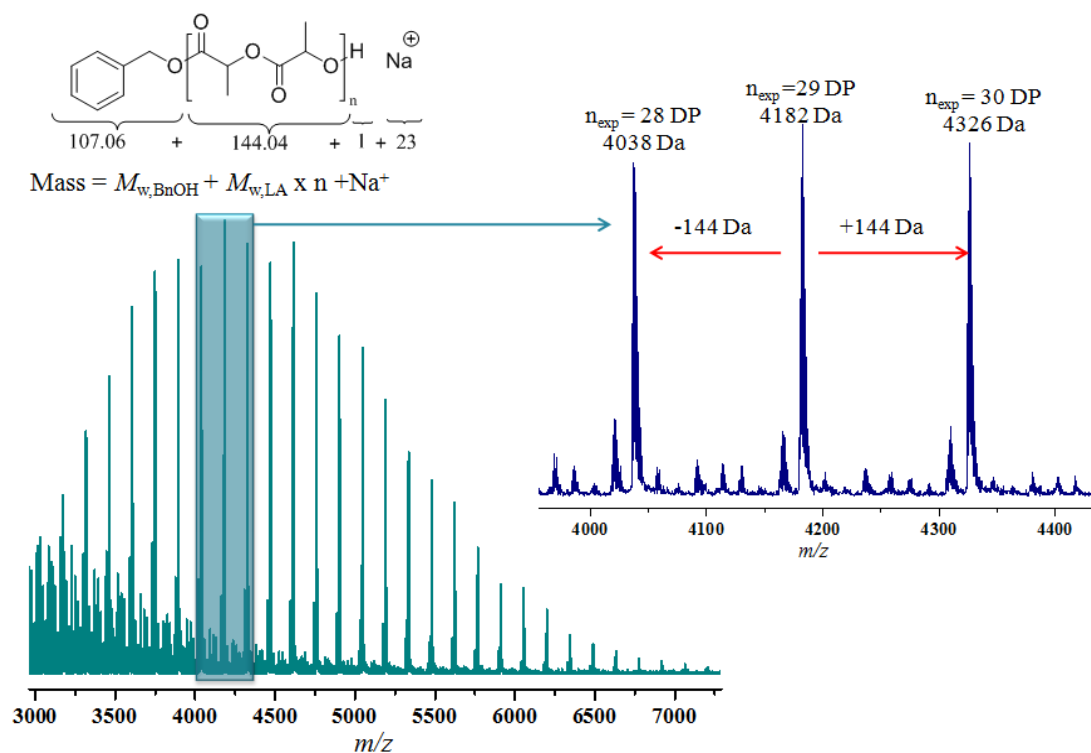
**Figure S3.4.** MALDI-ToF mass spectrum of PLA obtained  $\text{K}_2\text{CO}_3$ -activated **NHC1** at -50 °C (entry 1, Table 3.2)



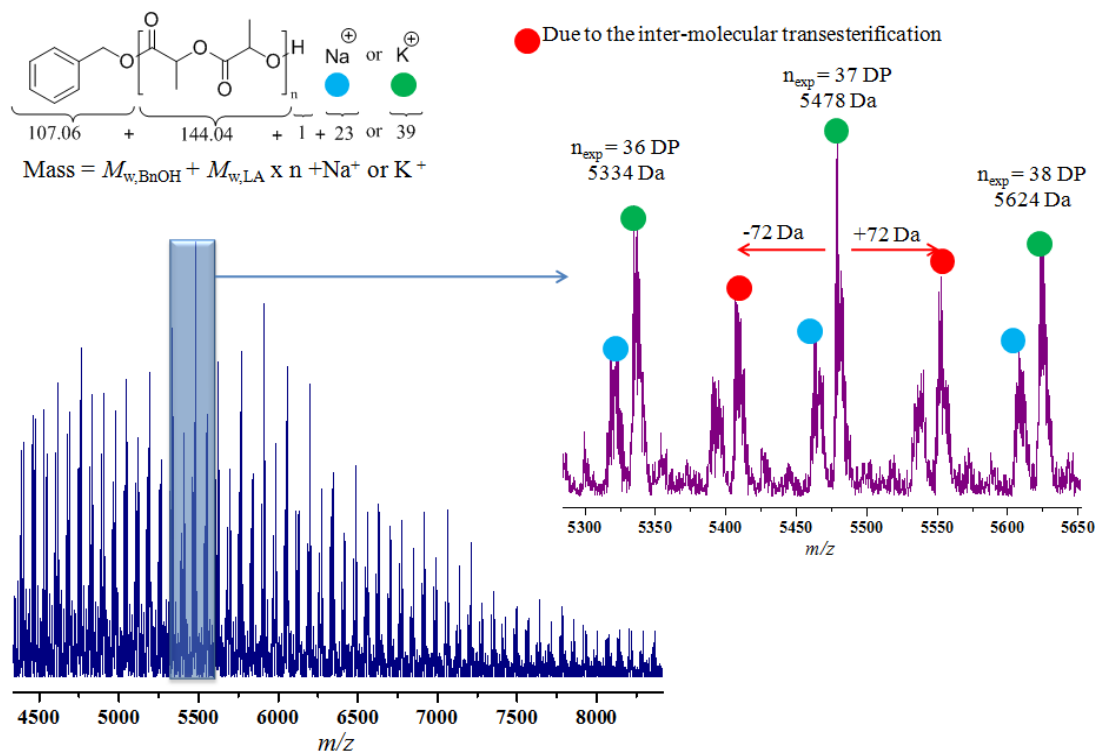
**Figure S3.5.** MALDI-ToF mass spectrum of PLA obtained by **NHC1**/*t*-BuOK (entry 3, Table 3.2)



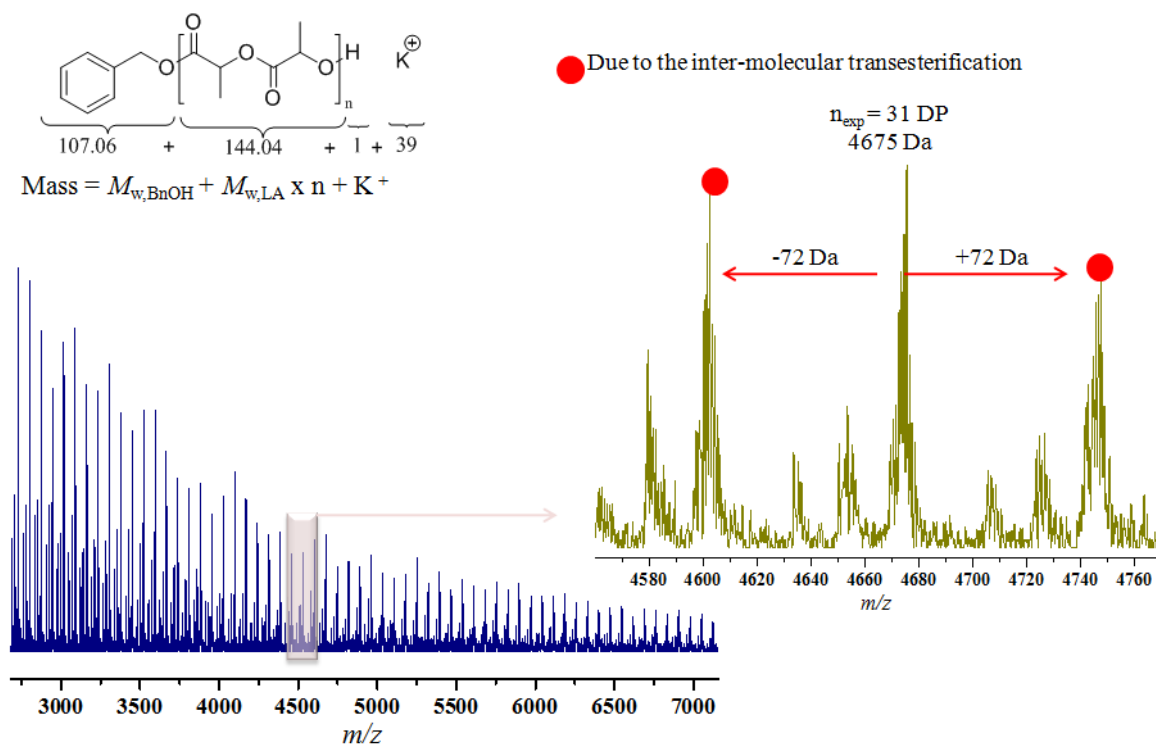
**Figure S3.6.** MALDI-ToF mass spectrum of PLA obtained by **NHC1**/DBU (entry 4, Table 3.2)



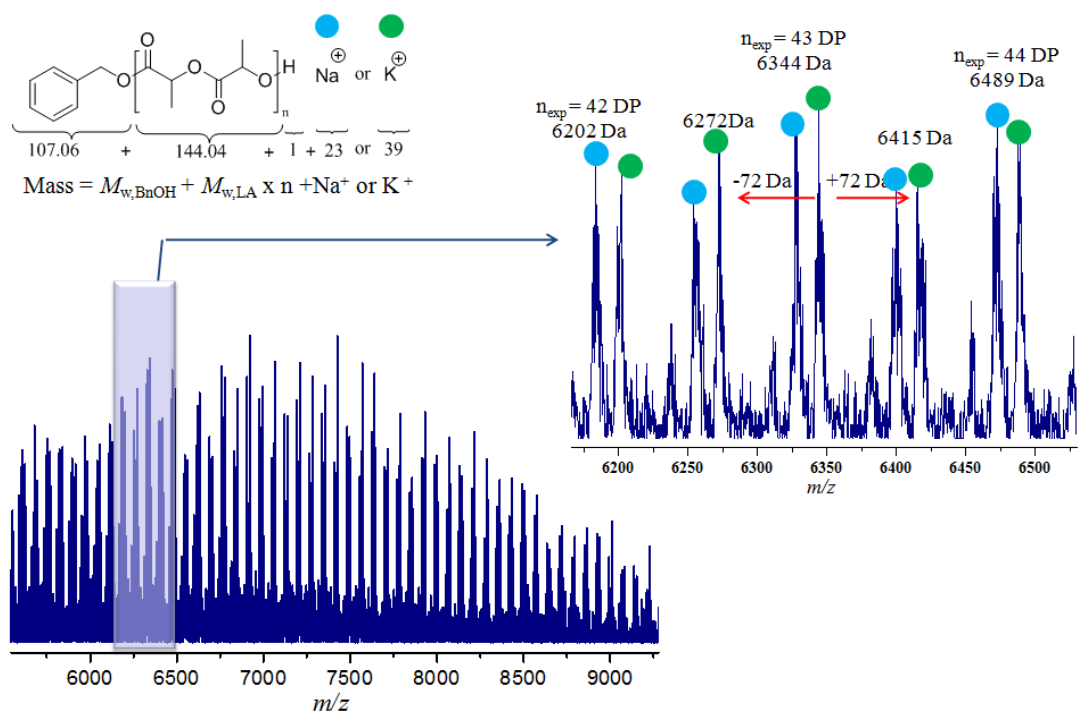
**Figure S3.7.** MALDI-ToF mass spectrum of PLA obtained by  $\text{K}_2\text{CO}_3$ -activated **NHC2** at  $-50^\circ\text{C}$  (entry 5, Table 3.2)



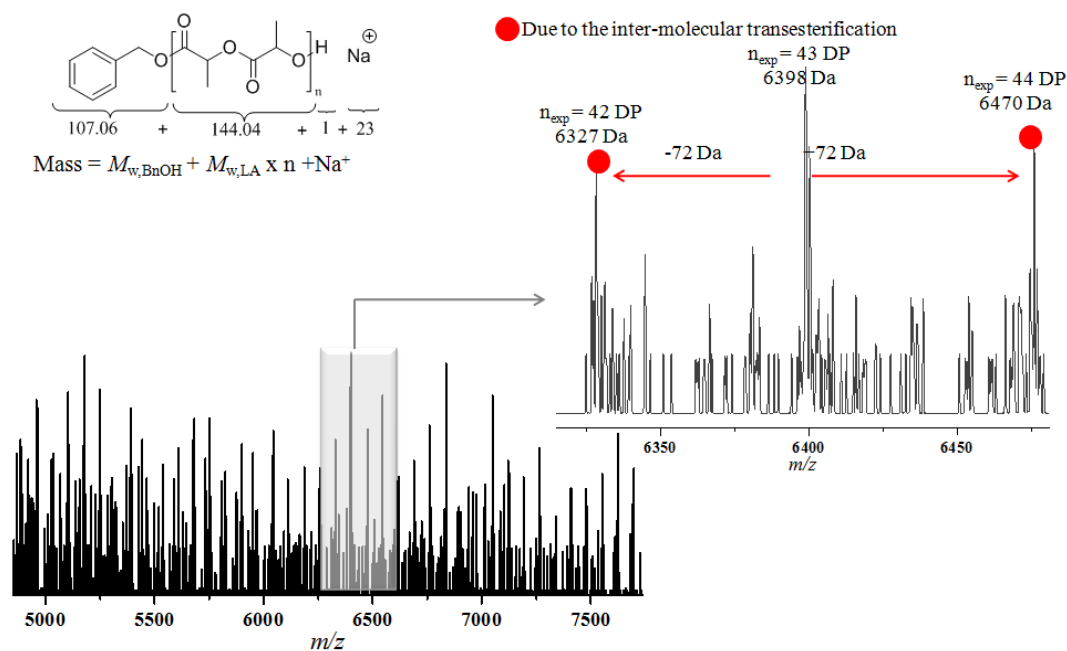
**Figure S3.8.** -ToF mass spectrum of PLA obtained by **NHC2**/*t*-BuOK (entry 7, Table 3.2)



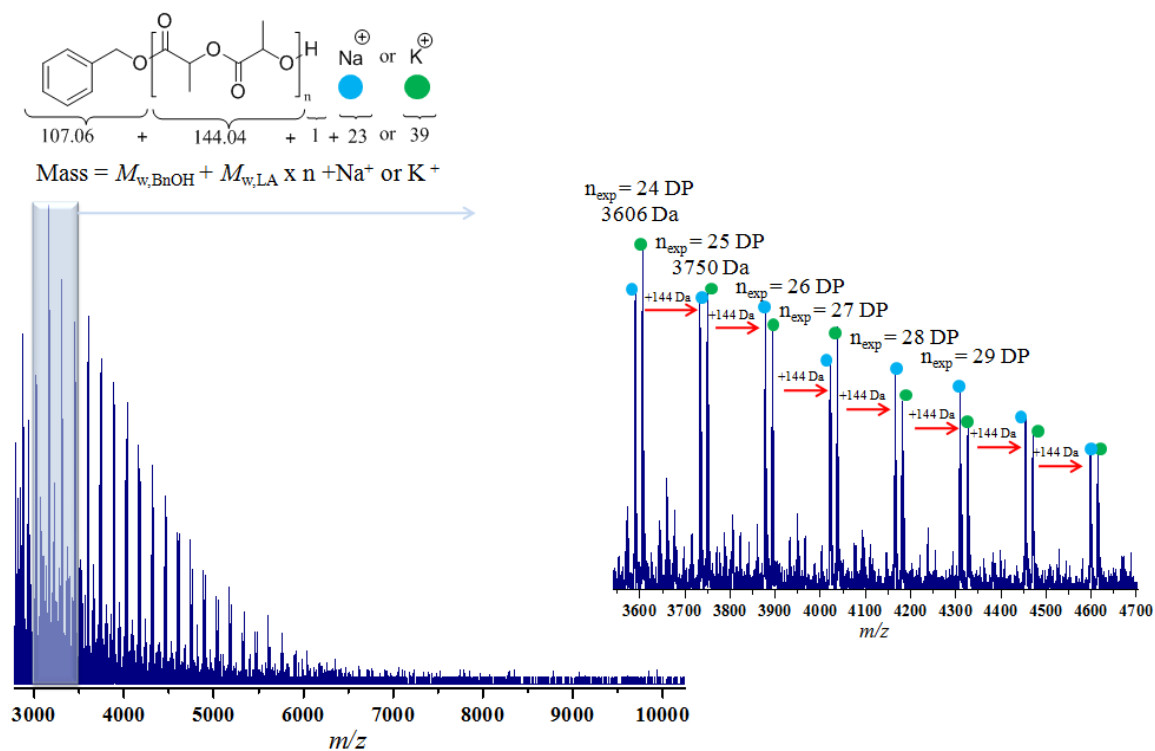
**Figure S3.9.** MALDI-ToF mass spectrum of PLA obtained by **NHC2**/DBU (entry 8, Table 3.2)



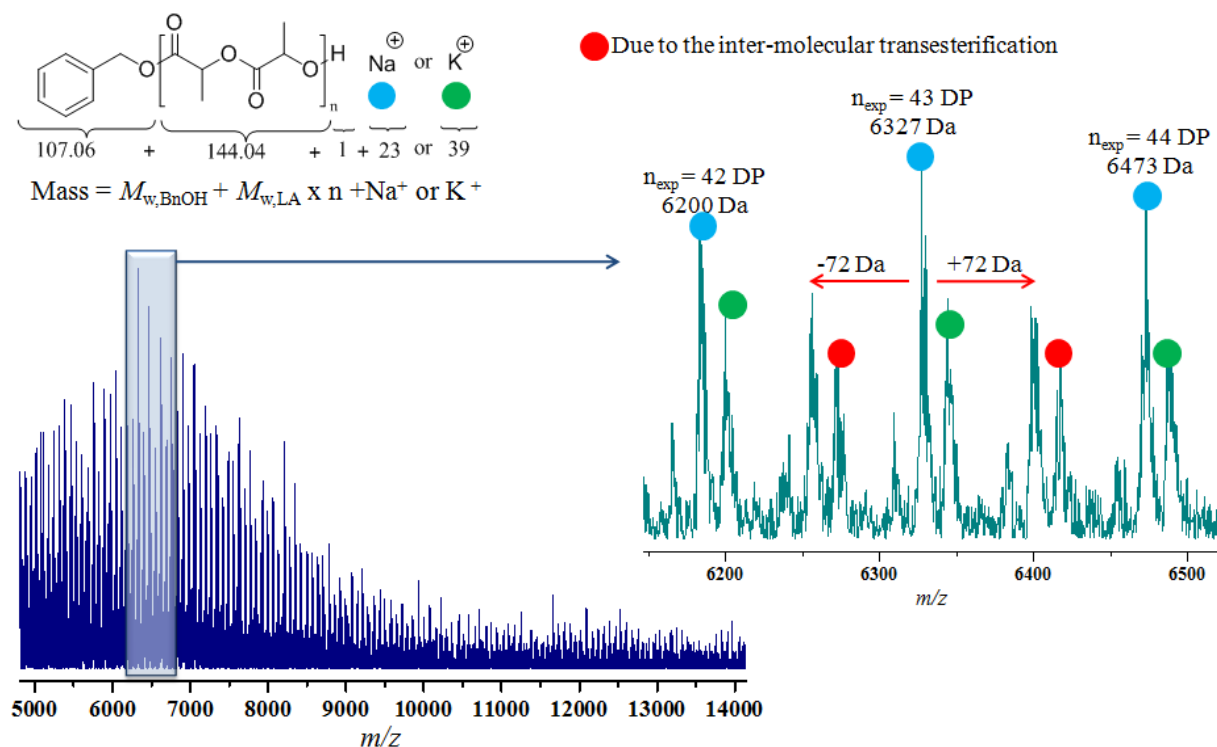
**Figure S3.10.** MALDI-ToF mass spectrum of PLA obtained by  $K_2CO_3$ -activated **NHC3** at -50 °C (entry 9, Table 3.2)



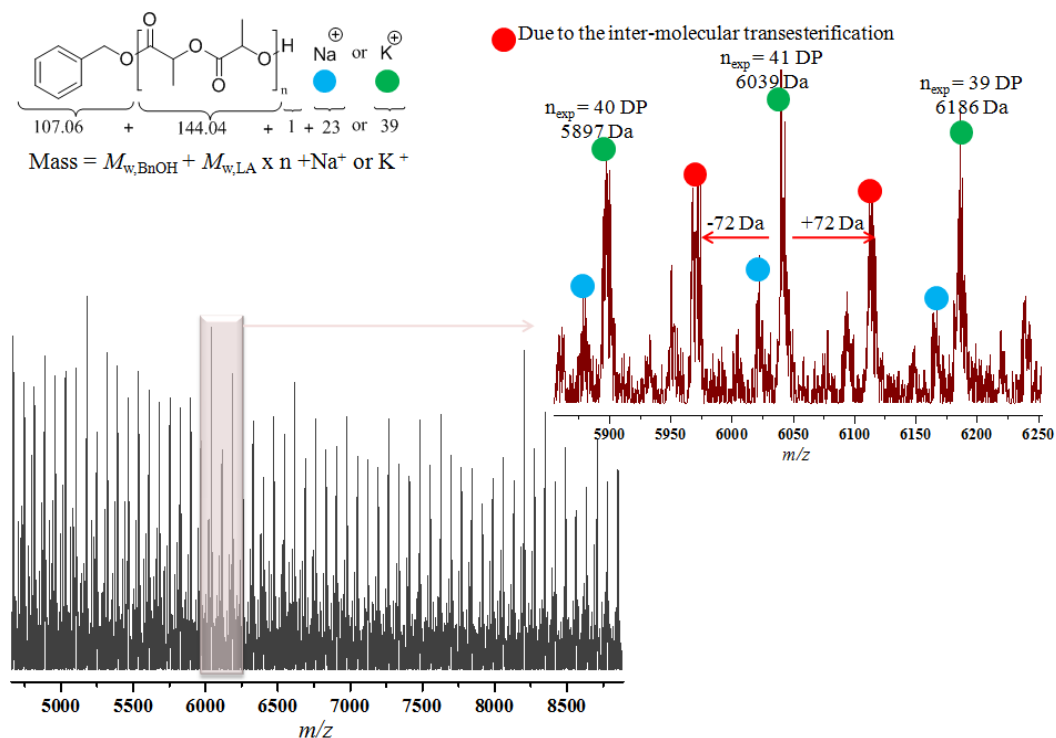
**Figure S3.11.** MALDI-ToF mass spectrum of PLA obtained by **NHC3**/DBU catalysis (entry 12, Table 3.2)



**Figure S3.12.** MALDI-ToF mass spectrum of PLA obtained by  $\text{K}_2\text{CO}_3$ -activated **NHC4** catalysis at  $-50^\circ\text{C}$  (entry 13, Table 3.2)

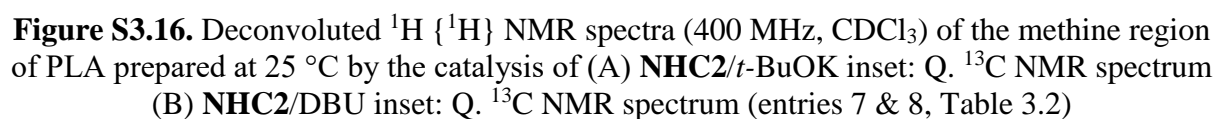
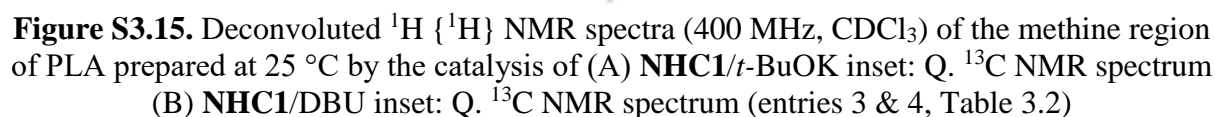


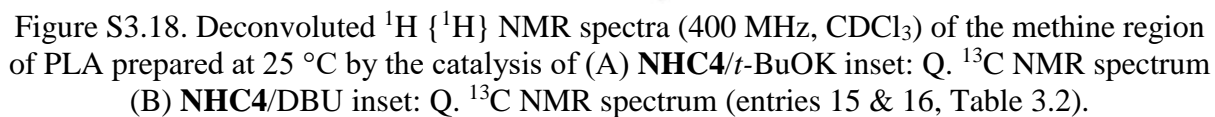
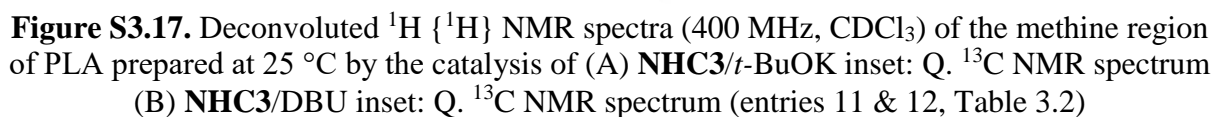
**Figure S3.13.** MALDI-ToF mass spectrum of PLA obtained by **NHC4**/*t*-BuOK catalysis (entry 15, Table 3.2)



**Figure S3.14.** MALDI-ToF mass spectrum of PLA obtained by **NHC4**/DBU catalysis (entry 16, Table 3.2)







### 3.6. References

- [1] O. Dechy-Cabaret, B. Martin-Vaca, D. Bourissou, *Chem. Rev.* **2004**, *104*, 6147.
- [2] J. M. Raquez, Y. Habibi, M. Murariu, P. Dubois, *Prog. Polym. Sci.* **2013**, *38*, 1504.
- [3] E. Castro-Aguirre, F. Iñiguez-Franco, H. Samsudin, X. Fang, R. Auras, *Adv. Drug Deliv. Rev.* **2016**, *107*, 333.
- [4] S. Farah, D. G. Anderson, R. Langer, *Adv. Drug Deliv. Rev.* **2016**, *107*, 367.
- [5] M. Cheng, A. B. Attygalle, E. B. Lobkovsky, G. W. Coates, *J. Am. Chem. Soc.* **1999**, *121*, 11583.
- [6] I. Vroman, L. Tighzert, *Materials* **2009**, *2*, 307.
- [7] Y. Ikada, H. Tsuji, *Macromol. Rapid Commun.* **2000**, *21*, 117.
- [8] M. J. Stanford, A. P. Dove, *Chem. Soc. Rev.* **2010**, *39*, 486.
- [9] H. Tsuji, Y. Ikada, F. Horii, M. Nakagawa, H. Odani, R. Kitamaru, *Macromolecules* **1992**, *25*, 4114.
- [10] H. Tsuji, Y. Ikada, *Polymer (Guildf)*. **1999**, *40*, 6699.
- [11] C. M. Thomas, *Chem. Soc. Rev.* **2010**, *39*, 165.
- [12] P. J. Dijkstra, H. Du, J. Feijen, *Polym. Chem.* **2011**, *2*, 520.
- [13] N. Spassky, M. Wisniewski, C. Pluta, A. Le, *Macromol. Chem. Phys.* **1996**, *2637*, 2627.
- [14] C. P. Radano, G. L. Baker, M. R. Smith, *J. Am. Chem. Soc.* **2000**, *122*, 1552.
- [15] N. Nomura, R. Ishii, M. Akakura, K. Aoi, *J. Am. Chem. Soc.* **2002**, *124*, 5938.
- [16] N. Nomura, R. Ishii, Y. Yamamoto, T. Kondo, *Chem. - A Eur. J.* **2007**, *13*, 4433.
- [17] T. M. Ovitt, G. W. Coates, *J. Am. Chem. Soc.* **2002**, *124*, 1316.
- [18] Z. Zhong, P. J. Dijkstra, J. Feijen, *Angew. Chem. Int. Ed.* **2002**, *41*, 4510.
- [19] K. Majerska, A. Duda, *J. Am. Chem. Soc.* **2004**, *126*, 1026.
- [20] P. Hornmair, E. L. Marshall, V. C. Gibson, R. I. Pugh, A. J. P. White, *Proc. Natl. Acad. Sci.* **2006**, *103*, 15343.
- [21] W. Luo, T. Shi, S. Liu, W. Zuo, Z. Li, *Organometallics* **2017**, *36*, 1736.
- [22] H. Ö. Düşkünkörür, A. Bégué, E. Pollet, V. Phalip, Y. Güvenilir, L. Avérous, *J. Mol. Catal. B Enzym.* **2015**, *115*, 20.
- [23] B. J. O. Keefe, M. A. Hillmyer, W. B. Tolman, *Dalt. Perspect.* **2001**, 2215.
- [24] T. R. Jensen, L. E. Breyfogle, M. A. Hillmyer, W. B. Tolman, *Chem. Commun. (Camb)*. **2004**, 0135, 2504.
- [25] A. Arbaoui, C. Redshaw, D. L. Hughes, *Chem. Commun.* **2008**, 0, 4717.
- [26] J.-F. Carpentier, *Macromol. Rapid Commun.* **2010**, *31*, 1696.
- [27] A. Sauer, A. Kapelski, C. Fliedel, S. Dagorne, M. Kol, J. Okuda, *Dalt. Trans.* **2013**, *42*, 9007.
- [28] A. C. Redshaw, X. Wang, K. Zhao, Y. Al-khafaji, *Eur. J. Inorg. Chem.* **2017**, 1951.
- [29] N. E. Kamber, W. Jeong, R. M. Waymouth, R. C. Pratt, B. G. G. Lohmeijer, J. L. Hedrick, *Chem. Rev.* **2007**, *107*, 5813.
- [30] W. N. Ottou, H. Sardon, D. Mecerreyes, J. Vignolle, D. Taton, *Prog. Polym. Sci.* **2016**, *56*, 64.
- [31] R. C. Pratt, B. G. G. Lohmeijer, D. A. Long, P. N. P. Lundberg, A. P. Dove, H. Li, C. G. Wade, R. M. Waymouth, J. L. Hedrick, *Macromolecules* **2006**, *39*, 7863.
- [32] K. Makiguchi, T. Yamanaka, T. Kakuchi, M. Terada, T. Satoh, *Chem. Commun.* **2014**, *50*, 2883.
- [33] G. M. Miyake, E. Y. X. Chen, *Macromolecules* **2011**, *44*, 4116.
- [34] A. Sanchez-Sanchez, I. Rivilla, M. Agirre, A. Basterretxea, A. Etxeberria, A. Veloso, H. Sardon, D. Mecerreyes, F. P. Cossío, *J. Am. Chem. Soc.* **2017**, *139*, 4805.

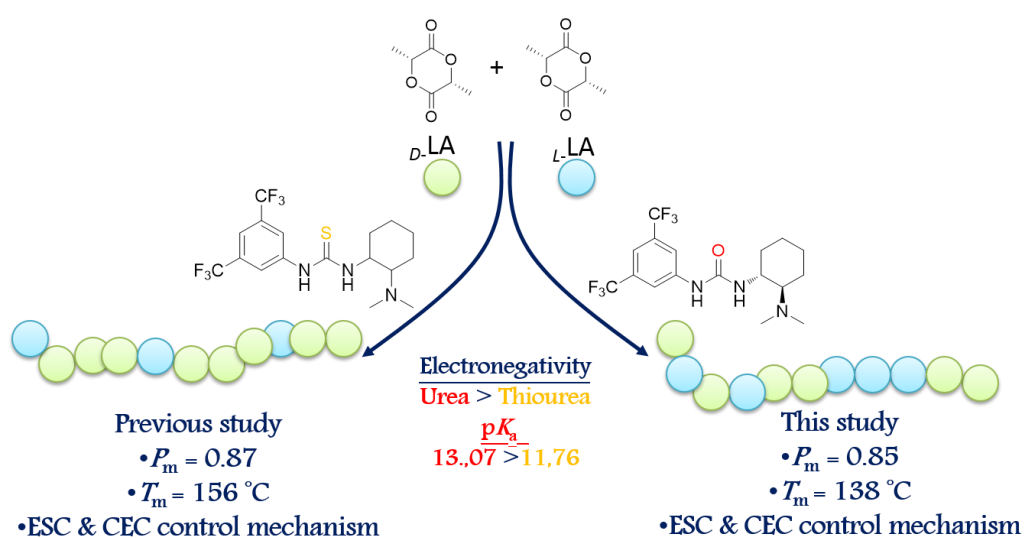
- [35] B. Orhan, M. J.-L. Tschan, A.-L. Wirotius, A. P. Dove, O. Coulembier, D. Taton, *ACS Macro Lett.* **2018**, 1413.
- [36] J. U. Pothupitiya, R. S. Hewawasam, M. K. Kiesewetter, *Macromolecules* **2018**, *51*, 3203.
- [37] B. Lin, R. M. Waymouth, *J. Am. Chem. Soc.* **2017**, *139*, 1645.
- [38] B. G. G. Lohmeijer, R. C. Pratt, F. Leibfarth, J. W. Logan, D. A. Long, A. P. Dove, F. Nederberg, J. Choi, C. Wade, R. M. Waymouth, J. L. Hedrick, *Macromolecules* **2006**, *39*, 8574.
- [39] L. Zhang, F. Nederberg, R. C. Pratt, R. M. Waymouth, J. L. Hedrick, C. G. Wade, *Macromolecules* **2007**, *40*, 4154.
- [40] O. Coulembier, B. G. G. Lohmeijer, A. P. Dove, R. C. Pratt, L. Mespouille, D. A. Culkin, S. J. Benight, P. Dubois, R. M. Waymouth, J. L. Hedrick, *Macromolecules* **2006**, *39*, 5617.
- [41] A. P. Dove, H. Li, R. C. Pratt, B. G. G. Lohmeijer, D. A. Culkin, R. M. Waymouth, J. L. Hedrick, *Chem. Commun.* **2006**, 2881.
- [42] N. Marion, D.-G. Silvia, S. P. Nolan, *Angew. Chemie - Int. Ed.* **2007**, *46*, 2988.
- [43] M. Fèvre, J. Vignolle, Y. Gnanou, D. Taton, *Organocatalyzed Ring-Opening Polymerizations*; Elsevier B.V., 2012; Vol. 4.
- [44] X. Zhang, M. Fevre, G. O. Jones, R. M. Waymouth, *Chem. Rev.* **2017**, 839.
- [45] L. Zhang, F. Nederberg, J. M. Messman, R. C. Pratt, J. L. Hedrick, C. G. Wade, *J. Am. Chem. Soc.* **2007**, *129*, 12610.
- [46] S. Liu, H. Li, N. Zhao, Z. Li, *ACS Macro Lett.* **2018**, *7*, 624.
- [47] K. Williams, B. Neilson, C. Bielawski, In *Synthesis of Polymers*; 2012; pp. 973–1010.
- [48] M. N. Hopkinson, C. Richter, M. Schedler, F. Glorius, *Nature* **2014**, *510*, 485.
- [49] M. Fèvre, Phosphines, Carbènes N-Hétérocycliques (Nhcs) Et Nouveaux Précurseurs De Nhcs Pour La Catalyse Organique De Réactions (Macro)Moléculaires, University Of Bordeaux, 2012.
- [50] P. de Frémont, N. Marion, S. P. Nolan, *Coord. Chem. Rev.* **2009**, *253*, 862.
- [51] E. M. Higgins, J. A. Sherwood, A. G. Lindsay, J. Armstrong, R. S. Massey, R. W. Alder, A. C. O'Donoghue, *Chem. Commun.* **2011**, *47*, 1559.
- [52] A. M. Magill, K. J. Cavell, B. F. Yates, *J. Am. Chem. Soc.* **2004**, *126*, 8717.
- [53] D. Enders, O. Niemeier, A. Henseler, *Chem. Rev.* **2007**, *107*, 5606.
- [54] A. J. Arduengo, R. L. Harlow, M. Kline, *J. Am. Chem. Soc.* **1991**, 361.
- [55] N. E. Kamber, W. Jeong, R. M. Waymouth, R. C. Pratt, B. G. G. Lohmeijer, J. L. Hedrick, *Chem. Rev.* **2007**, *107*, 5813.
- [56] M. K. Kiesewetter, E. J. Shin, J. L. Hedrick, R. M. Waymouth, *Macromolecules* **2010**, *43*, 2093.
- [57] E. F. Connor, G. W. Nyce, M. Myers, A. Möck, J. L. Hedrick, *J. Am. Chem. Soc.* **2002**, *124*, 914.
- [58] A. J. Arduengo, H. V. R. Dias, R. L. Harlow, M. Kline, *J. Am. Chem. Soc.* **1992**, *114*, 5530.
- [59] S. Naumann, M. R. Buchmeiser, *Catal. Sci. Technol.* **2014**, *4*, 2466.
- [60] P. Dubois, O. Coulembier, J. Raquez, *Handbook of Ring-Opening Polymerization*; 2009.
- [61] M. C. Jahnke, F. E. Hahn, *N-Heterocyclic Carbenes: From Laboratory Curiosities to Efficient Synthetic Tools*; 2016.
- [62] R. Lambert, J. Vignolle, D. Taton, In *N-Heterocyclic Carbenes in Organocatalysis*; Royal Society of Chemistry, 2019; pp. 309–344.
- [63] D. Enders, T. Balensiefer, Nucleophilic carbenes in asymmetric organocatalysis. *Acc.*

- Chem. Res.* **2004**, *37*, 534–541.
- [64] J. R. De Alaniz, M. S. Kerr, J. L. Moore, T. Rovis, *J. Org. Chem.* **2008**, *73*, 2033.
- [65] B. Maji, M. Breugst, H. Mayr, *Angew. Chemie - Int. Ed.* **2011**, *50*, 6915.
- [66] J. Pinaud, J. Vignolle, Y. Gnanou, D. Taton, *Macromolecules* **2011**, *44*, 1900.
- [67] G. R. J. Herrmann, W. a; Goossen, L. J.; Kocher, C.; Artus, *Chem. Rev.* **2011**, *111*, 2705.
- [68] A. P. Dove, R. C. Pratt, B. G. G. Lohmeijer, D. A. Culkin, E. C. Hagberg, G. W. Nyce, R. M. Waymouth, J. L. Hedrick, *Polymer (Guildf)*. **2006**, *47*, 4018.
- [69] M. Fèvre, J. Pinaud, Y. Gnanou, J. Vignolle, D. Taton, *Chem. Soc. Rev.* **2013**, *42*, 2142.
- [70] A. P. Dove, Organic catalysis for ring-opening polymerization. *ACS Macro Lett.* **2012**, 1409–1412.
- [71] L. Candish, C. M. Forsyth, D. W. Lupton, *Angew. Chemie - Int. Ed.* **2013**, *52*, 9149.
- [72] M. Fèvre, J. Pinaud, Y. Gnanou, J. Vignolle, D. Taton, *Chem. Soc. Rev.* **2013**, *42*, 2142.
- [73] A. C. Sentman, S. Csihony, R. M. Waymouth, J. L. Hedrick, *J. Org. Chem* **2005**, *70*, 2391.
- [74] M. K. Samantaray, V. Katiyar, K. Pang, H. Nanavati, P. Ghosh, *J. Organomet. Chem.* **2007**, *692*, 1672.
- [75] P. Arnold, I. J. Casely, Z. R. Turner, R. Bellabarba, R. B. Tooze, *Dalt. Trans.* **2009**, 7236.
- [76] J. Raynaud, W. N. Ottou, Y. Gnanou, D. Taton, *Chem. Commun.* **2010**, *46*, 3203.
- [77] H. A. Brown, R. M. Waymouth, *Acc. Chem. Res.* **2013**, *46*, 2585.
- [78] N. E. Kamber, W. Jeong, S. Gonzalez, J. L. Hedrick, R. M. Waymouth, *Macromolecules* **2009**, *42*, 1634.
- [79] J. Raynaud, C. Absalon, Y. Gnanou, D. Taton, *J. Am. Chem. Soc.* **2009**, *131*, 3201.
- [80] J. Raynaud, C. Absalon, Y. Gnanou, D. Taton, *Macromolecules* **2010**, *43*, 2814.
- [81] T. S. Stukenbroeker, D. Solis-Ibarra, R. M. Waymouth, *Macromolecules* **2014**, *47*, 8224.
- [82] Y. Zhang, E. Y. X. Chen, *Angew. Chemie - Int. Ed.* **2012**, *51*, 2465.
- [83] S. Naumann, F. G. Schmidt, W. Frey, M. R. Buchmeiser, *Polym. Chem.* **2013**, *4*, 4172.
- [84] G. Nyce, T. Glauser, E. F. Connor, A. Möck, R. M. Waymouth, J. L. Hedrick, *J. Am. Chem. Soc.* **2003**, *125*, 3046.
- [85] W. Nzahou Ottou, D. Bourichon, J. Vignolle, A.-L. Wirotius, F. Robert, Y. Landais, J.-M. Sotiropoulos, K. Miqueu, D. Taton, *Chem. - A Eur. J.* **2014**, *20*, 3989.
- [86] Y. A. Chang, R. M. Waymouth, *Polym. Chem.* **2015**, *6*, 5212.
- [87] S. Naumann, A. P. Dove, *Polym. Int.* **2016**, *65*, 16.
- [88] S. Naumann, A. P. Dove, *Polym. Chem.* **2015**, *6*, 3185.
- [89] B. G. G. Lohmeijer, G. Dubois, F. Leibfart, R. C. Pratt, F. Nederberg, A. Nelson, R. M. Waymouth, C. Wade, J. L. Hedrick, *Org. Lett.* **2006**, *8*, 4683.
- [90] B. Bantu, G. M. Pawar, U. Decker, K. Wurst, A. M. Schmidt, M. R. Buchmeiser, *Chem. - A Eur. J.* **2009**, *15*, 3103.
- [91] O. Coutelier, M. El Ezzi, M. Destarac, F. Bonnette, T. Kato, A. Baceiredo, G. Sivasankarapillai, Y. Gnanou, D. Taton, *Polym. Chem.* **2012**, *3*, 605.
- [92] S. Marrot, F. Bonnette, T. Kato, L. Saint-Jalmes, E. Fleury, A. Baceiredo, *J. Organomet. Chem.* **2008**, *693*, 1729.
- [93] W. N. Ottou, H. Sardon, D. Mecerreyes, J. Vignolle, D. Taton, *Prog. Polym. Sci.* **2016**, *56*, 64.
- [94] D. A. Culkin, W. Jeong, S. Csihony, E. D. Gomez, N. P. Balsara, J. L. Hedrick, R. M.

- Waymouth, *Angew. Chemie - Int. Ed.* **2007**, *46*, 2627.
- [95] W. Jeong, E. J. Shin, D. A. Culkin, J. L. Hedrick, R. M. Waymouth, *J. Am. Chem. Soc.* **2009**, *131*, 4884.
- [96] A. P. Dove, H. Li, R. C. Pratt, B. G. G. Lohmeijer, D. A. Culkin, R. M. Waymouth, J. L. Hedrick, *Chem. Commun.* **2006**, 2881.
- [97] C. Romain, B. Heinrich, S. B. Laponnaz, S. Dagorne, *Chem. Commun.* **2012**, *48*, 2213.
- [98] P. Horeglad, G. Szczepaniak, M. Dranka, J. Zachara, *Chem. Commun.* **2012**, *48*, 1171.
- [99] A. J. Arduengo, *Acc. Chem. Res.* **1999**, *32*, 913.
- [100] Didier Bourissou, O. Guerret, F. P. Gabbaï, G. Bertrand, *Chem. Rev.* **2000**, *100*, 39.
- [101] O. Coulembier, A. P. Dove, R. C. Pratt, A. C. Sentman, D. A. Culkin, L. Mespouille, P. Dubois, R. M. Waymouth, J. L. Hedrick, *Angew. Chemie - Int. Ed.* **2005**, *44*, 4964.
- [102] E. N. Jacobsen, A. Pfaltz, H. Yamamoto, *Comprehensive Asymmetric Catalysis*; Springer-Verlag Berlin Heidelberg, 1999; Vol. Chapter 36.
- [103] C. Wang, S. Zhu, G. Wang, Z. Li, X. P. Hui, *European J. Org. Chem.* **2016**, 5653.
- [104] O. Coulembier, S. Moins, J. De Winter, P. Gerbaux, P. Lecle, R. Lazzaroni, P. Dubois, *Macromolecules* **2010**, *43*, 575.
- [105] A. Duda, A. Kowalski, S. Penczek, *Macromolecules* **1998**, 9297, 2114.
- [106] D. Arbeiter, K. Schümann, O. Sahmel, T. Eickner, K.-P. Schmitz, N. Grabow, *Curr. Dir. Biomed. Eng.* **2016**, *2*, 27.
- [107] K. Jamshidi, S.-H. Hyon, Y. Ikada, *Polymer (Guildf)*. **1988**, *29*, 2229.
- [108] Z. Zhong, P. J. Dijkstra, J. Feijen, *J. Am. Chem. Soc.* **2003**, *125*, 11291.
- [109] M. H. Chisholm, S. S. Iyer, D. G. McCollum, M. Pagel, U. Werner-Zwanziger, *Macromolecules* **1999**, *32*, 963.
- [110] B. M. Chamberlain, M. Cheng, D. R. Moore, T. M. Ovitt, E. B. Lobkovsky, G. W. Coates, *J. Am. Chem. Soc.* **2001**, *123*, 3229.
- [111] O. Coulembier, P. Dubois, *J. Polym. Sci. Part A Polym. Chem.* **2012**, *50*, 1672.
- [112] J. Coudane, C. Ustariz-Peyret, G. Schwach, M. Vert, *J. Polym. Sci. Part A Polym. Chem.* **1997**, *35*, 1651.
- [113] J. Kasperczyk, M. Bero, *Makromol. Chem.* **1993**, *194*, 913.
- [114] K. M. Thakur, R. T. Kean, E. S. Hall, J. J. Kolstad, T. A. Lindgren, M. A. Doscotch, J. I. Siepmann, E. J. Munson, *Macromolecules* **1997**, *30*, 2422.
- [115] K. A. M. Thakur, R. T. Kean, M. T. Zell, B. E. Padden, E. J. Munson, *Chem. Commun.* **1998**, 1913.
- [116] K. a. M. Thakur, R. T. Kean, E. S. Hall, J. J. Kolstad, E. J. Munson, *Macromolecules* **1998**, *31*, 1487.

## Chapter 4.

# Chiral Unimolecular Bifunctional Urea Organocatalyst for the Stereoselective Ring-Opening Polymerization of *rac*-Lactide



**Keywords:** Stereoselective • Lactide • Urea • Ring-Opening Polymerization

## Chapter 4

# Chiral Unimolecular Bifunctional Urea Organocatalyst for the Stereoselective Ring-Opening Polymerization of *rac*-Lactide

### Contents

<b>Chapter 4. Chiral Unimolecular Bifunctional Urea Organocatalyst for the Stereoselective Ring-Opening Polymerization of <i>rac</i>-Lactide.....</b>	<b>164</b>
4.1. Introduction.....	169
4.2. Results and Discussion .....	177
4.2.1. Polymerization procedure .....	177
4.2.2. Polymer Characterization.....	176
4.2.3. Microstructure analysis of PLA derived from chiral ( <i>S,S</i> )-UC.....	184
4.2.3.1. DSC Analysis .....	181
4.2.3.1. Homonuclear decoupled <sup>1</sup> H NMR and quantitative <sup>13</sup> C NMR analysis . .....	184
4.2.4. Polymerization Kinetics .....	190
4.3. Conclusions and perspectives .....	192
4.4. Experimental and supporting informations .....	193
4.5. References.....	196



## 4.1. Introduction

In recent years, considerable research effort has been devoted to the use of polymeric biodegradable materials in plastic applications, such as packaging, microelectronics, and biomedical fields.<sup>[1–4]</sup> Poly(lactide) (PLA) is currently the gold standard in the field of biodegradable and biorenewable polyesters.

Lactide, the cyclic diester of lactic acid, possesses two stereocentres and three distinct diastereoisomers: (*S,S*)-lactide or *L*-lactide (*L*-LA); (*R,R*)-lactide or *D*-lactide (*D*-LA); and the optically inactive *meso*-lactide, which contains one of each stereocentre. All isomers are commercially available as enantioenriched samples or as a racemic mixture of *L*-LA and *D*-LA (*rac*-lactide). In turn, a variety of microstructures (for example, atactic, isotactic, heterotactic and syndiotactic) can be constructed from this basic set of monomers, with each one possessing unique physicochemical and thermomechanical properties, as well as different degradation profiles.<sup>[1,5,6]</sup> For instance, heterotactic PLA exhibits a  $T_g$  of 49 °C and no noticeable  $T_m$  (thus an amorphous material)<sup>[7]</sup> while isotactic PLA shows a  $T_m$  of up to 180 °C and a  $T_g$  of about 50 °C.<sup>[1–4]</sup> It has been well documented that the ring-opening polymerization (ROP) of the enantiopure LA monomer, in the absence of any epimerization, leads to PLA with quantitative isotacticity, and if isotactic PLLA and PDLA are mixed in a 1:1 equimolar ratio, a crystalline stereocomplex exhibiting a  $T_m$  above 230 °C can be formed.<sup>[8,9]</sup>

Metal alkoxides and some achiral organometallic catalysts have shown to be efficient to promote the synthesis of stereoregular PLA.<sup>[10,11]</sup> Given the excellent performance and almost limitless opportunities of ligand/metal combinations, it is not surprising that transition metals and organometallic catalysts have dominated the field of stereocontrolled ROP of LA.<sup>[12–14]</sup> Undoubtedly, the most important breakthrough was Spassky's discovery of stereoselective lactide polymerization, applying aluminum complexes of a chiral binaphthyl Schiff's base (IV).<sup>[15]</sup> At low conversion, the aluminum methoxide complex of (*R*)-catalysts demonstrated a preference for *D*-LA over *L*-LA to yield an optically active essentially isotactic *D*-LA polymer from *rac*-LA in toluene at 70 °C. However, the toxicity of conventional organometallic catalysts is accelerating the development of organic catalysts.<sup>[1,16,17]</sup>

Organocatalysts do not contain any metals, and are therefore advantageous from environmental and resource perspectives. These catalysts hold considerable promise as cheap,

stable, moisture-insensitive, reproducible, and easy-to-construct alternatives to well-studied metal-based catalysts. Hence, organic catalysts such as *N*-heterocyclic carbenes,<sup>[18,19]</sup> phosphazenes<sup>[20]</sup> or (*R*)-binaphthol derived phosphoric acids<sup>[21]</sup> have shown the ability to promote the stereocontrolled polymerization of *rac*-LA.

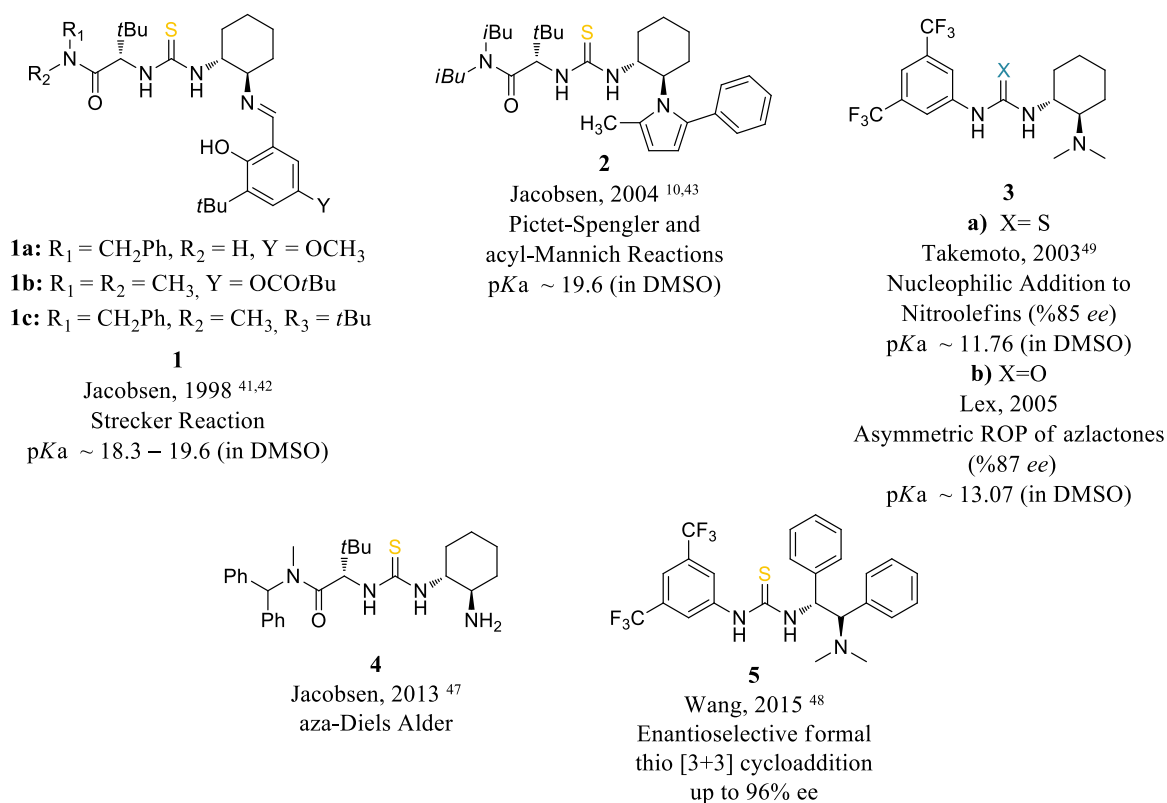
The Chen group has prepared some new bifunctional chiral catalysts based on  $\beta$ -isocupreidine core, thiourea and chiral binaphthyl-amine as hydrogen bonding (H-bonding) catalysts.<sup>[22]</sup>

Thereafter, and as discussed in chapter 2, our group reported that both commercially available (*R,R*)- and (*S,S*)-enantiomers of chiral unimolecular thiourea-amine Takemoto's organocatalysts promote efficient control and high isoselectivity at room temperature of the ROP of *rac*-LA by kinetic resolution, yielding highly isotactic ( $P_m = 0.87$ , 25 °C), semicrystalline ( $T_g = 56$  °C,  $T_m = 156$  °C) and metal-free polylactide (PLA). Kinetic investigations and combined analyses of the resulting PLAs have allowed the stereocontrol mechanism, which eventually involves both enantiomorphous site control and chain-end control, to be determined.<sup>[23]</sup> Even recently, Kan *et al.* reported a binary urea/alkoxide catalytic system that could catalyze ROP of *rac*-LA in a fast (over 90% conversion within 1–2min), stereoselective ( $P_m$  up to 0.93) and controlled manner, indicated by narrow  $M_w$  distributions, linear relationship between the monomer conversions and  $M_n$  values, end-group fidelity, and chain extension experiments.<sup>[24]</sup> As one can see, catalysis employing H-bonding for initiator or monomer activation is an effective and versatile strategy in ROP, but stereoselective ROP of a chiral monomer using this methodology is still in the infancy.

Over the past decade, the process of asymmetric catalysis on the basis of H-bonding has made continuous progress in the field of synthetic chemistry<sup>[25–30]</sup>, and the use of bifunctional organocatalysts has made a significant contribution.<sup>[31–36]</sup> In this context, chiral (thio)ureas and derivatives have emerged as powerful catalysts for a range of asymmetric transformations.<sup>[37,38]</sup> The most remarkable advances in the field of (thio)urea catalysts were achieved by Jacobsen's group.<sup>[10,11,39–44]</sup> The focus of these works was the activation of alkyl- or acyl-substituted imines and identified and optimized a series of urea- and thiourea-containing Schiff-base catalysts for various types of asymmetric reactions, such as Strecker<sup>[40]</sup> (Figure 4.1, catalyst **1a**), Mannich<sup>[11,43]</sup> (catalyst **1b**, **1c**), hydrophosphonylation<sup>[11]</sup>, and acyl Pictet–Spengler reactions<sup>[10]</sup> (catalyst **2**).

In 2011, De *et al.* reported a dual-catalysis strategy for the enantioselective Steglich rearrangement with the assistance of Jacobsen's thiourea catalyst and DMAP (up to 91% ee).<sup>[45,46]</sup> Lalonde *et al.* reported a new primary amino-thiourea catalyst (catalyst **4**), which enabling the formal aza-Diels Alder reaction of enones and cyclic imines for the enantioselective synthesis of chiral indolo- and benzoquinolizidine compounds.<sup>[47]</sup> The hydrogen-bond donor and primary amine are essential functional components of the catalyst for simultaneous activation of both the enone and imine reaction components.

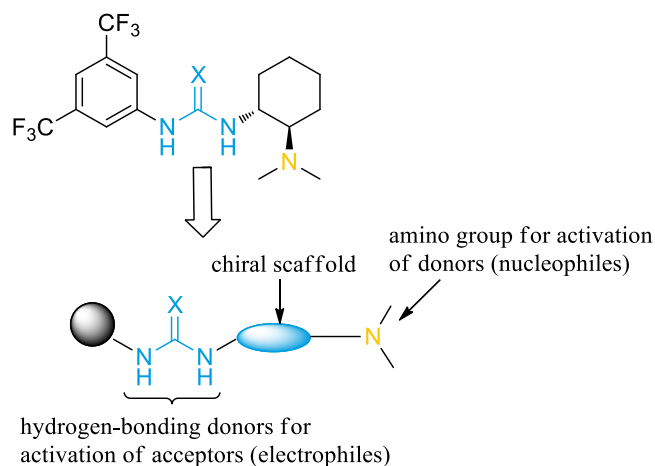
More recently, Wang *et al.* presented the first asymmetric formal thio [3+3] cycloaddition for the construction of optically active thiopyrano-indole annulated heterocyclic compounds in high yields with up to 96% ee, using a novel bifunctional tertiary amine-thiourea catalyst (catalyst **5**) derived from 1,2-diphenylethane-1,2-diamine (DPEN).<sup>[48]</sup>



**Figure 4.1.** Some representative H-bond donor (thio)ureas for organocatalytic transformations.

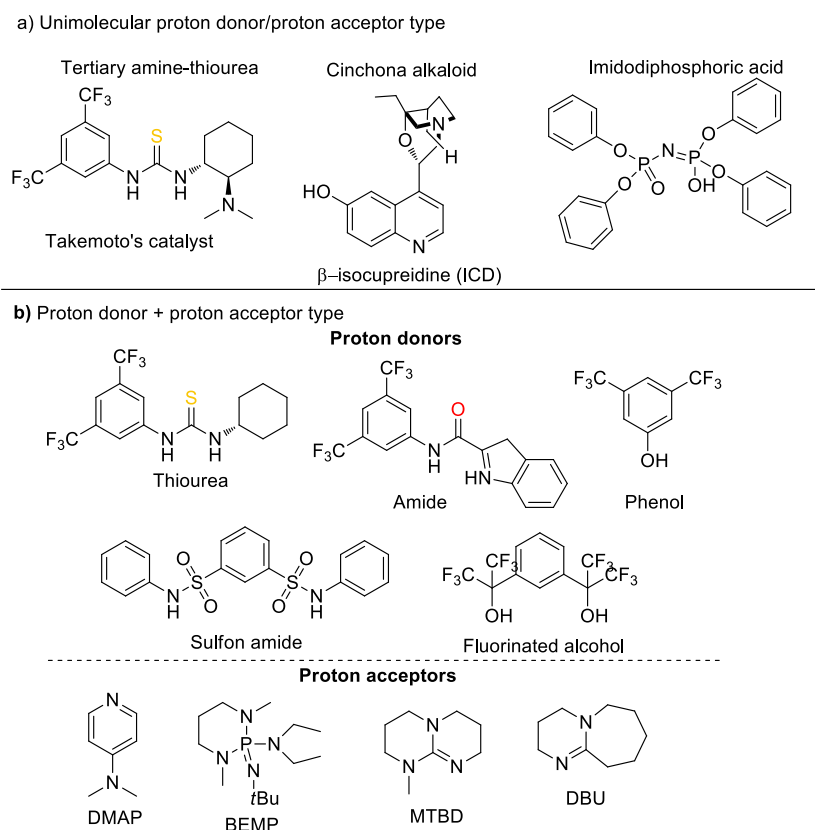
Based on the structure of bifunctional Schiff base-thiourea (catalyst **1a**) by Jacobsen<sup>[39]</sup> and tertiary amine-thiourea (catalyst **3a**) by Takemoto,<sup>[49]</sup> the development of unimolecular bifunctional amine-based (thio)urea derivatives has created new impulses to the field of organocatalysis (Figure 4.2). This type of catalysts possesses a thiourea or a urea

moiety (hydrogen-donor site) and a basic group such as tertiary amine, which not only activate both nucleophilic and electrophilic reactions simultaneously, but also can control the approach of the substrates stereoselectivity.<sup>[50]</sup>



**Figure 4.2.** Pioneering bifunctional amine-thiourea organocatalyst and its general structure (adapted from reference [50]).

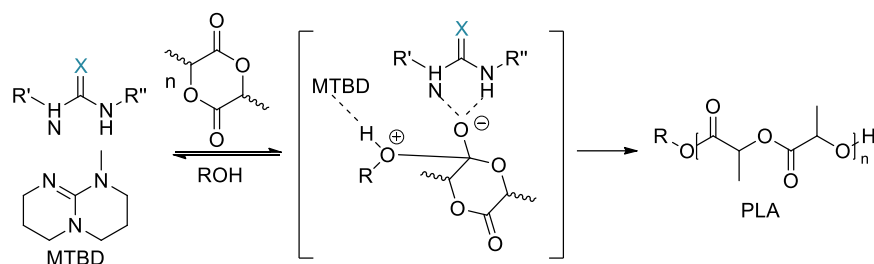
As previously declared, this type of catalysts generate effective and versatile strategy in ROP, and also exhibits great success in asymmetric transformations but stereoselective ROP of a chiral monomer using this methodology is still in the infancy. Moreover, they have been widely adopted due to their high functional group tolerance and their extraordinary selectivity to lead ring-opening monomer reactions rather than chain transesterifications, allowing then for a precise control of the molar mass and the distribution of the resultant polymers. Catalyst **3a**, as unimolecular bifunctional organocatalyst, was the first reported catalyst to introduce the concept of monomer activation and chain-end activation combination for the ROP of LA.<sup>[51,52]</sup> Although the use of unimolecular bifunctional (thio)urea catalysts is advantageous in terms of reaction conditions, alternative bifunctional H-bonding systems are of interest to enhance their general catalytic activity (Figure 4.3a). H-bond donor and acceptor did not necessarily need to be covalently tethered (Figure 4.3b).<sup>[53]</sup> In 2006, promising results have been obtained by combining the Takemoto's catalyst and (-)-sparteine, with 95% monomer conversions being achievable in only 2 hours at room temperature (25-fold faster compared to the unimolecular bifunctional system).<sup>[54]</sup>



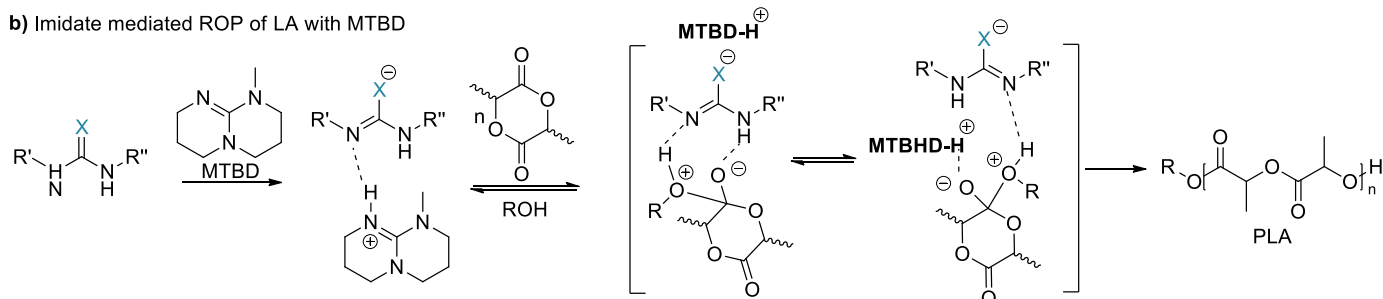
**Figure 4.3.** Representative bifunctional organocatalysts for ROP; (a) unimolecular proton donor/proton acceptor type and (b) proton donor + external proton acceptor type.

In 2017, a class of (thio)urea anions catalysts were disclosed, such catalytic systems exhibit both high activity and selectivity for the ROP of a variety of cyclic esters and carbonates.<sup>[17,55]</sup> These ionic catalysts are prepared by simple deprotonation of the neutral ureas or thioureas (Scheme 4.1). The rate of the polymerization can be tuned over several orders of magnitude by modifying the urea or thiourea substituents. ROP of *L*-LA,  $\epsilon$ -CL,  $\delta$ -valerolactone ( $\delta$ -VL) and trimethylene carbonate (TMC) polymerizations were completed in just seconds (<12 s) with excellent control on distributions ( $\bar{D} = 1.06$ –1.14).<sup>[56]</sup> DFT calculations suggested a bifunctional mechanism analogous to that of TBD,<sup>[55]</sup> where the (thio)imidiates behave as a proton shuttle to pick up the proton from the initiator/chain end, stabilize the tetrahedral intermediate via double H-bonds, and to deliver the proton back to the chain end after ring-opening.

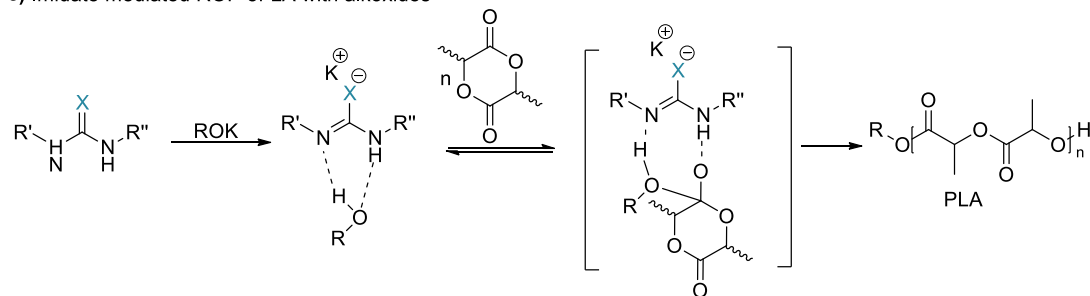
## a) Neutral H-bonding mediated ROP of LA



## b) Imidate mediated ROP of LA with MTBD



## c) Imidate mediated ROP of LA with alkoxides

**Scheme 4.1.** Neutral versus imidate mediated ROP of LA (adapted from reference 53).

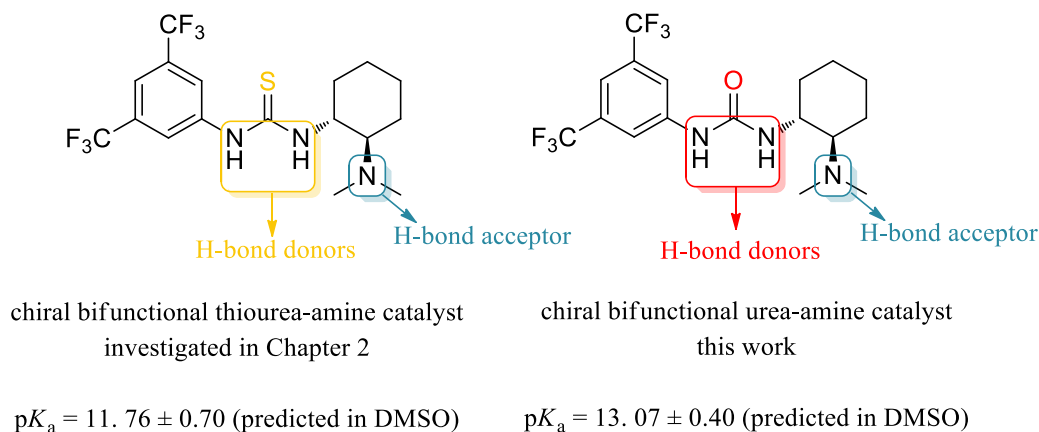
Fastnacht *et al.* reported a series of bis- and tris(thio)urea based H-bond donors, which exhibited dramatic rate acceleration compared to the mono-thiourea/amine systems, yet retaining the high selectivity for propagation over transesterification.<sup>[57,58]</sup> The most active one, a tris-urea/MTBD, was approximately 100 times faster than mono-TU/MTBD for the ROP of CL, with equally good control on molar masses and distributions ( $\bar{D} < 1.05$ ).<sup>[59]</sup> The polarity of the solvents also plays a crucial role for the activation of H-bonding catalysts during polymerization.<sup>[53]</sup> Pothupitiya *et al.* revealed that while polar solvents favor a (thio)imidate mechanism, nonpolar solvents favor a classic H-bond mediated ROP.<sup>[60]</sup> Very recently, Coderre *et al.* investigated different (thio)imidates using various (thio)ureas and MTBD for the ROP of LA and  $\epsilon$ -caprolactone (CL) at elevated temperatures (60, 80 and 110 °C).<sup>[61]</sup> They proved a monourea and bis-urea H-bond donor plus MTBD co-catalyst, are stable up to 110 °C. Lately, Kan *et al.* reported a binary urea/alkoxide catalytic system that could catalyze the ROP of *rac*-LA in a fast (over 90% conversion within 1–2min), stereoselective ( $P_m$  up to 0.93) and controlled manner, indicated by narrow molar mass

distributions.<sup>[24]</sup> Although potent nucleophiles<sup>[19,62–64]</sup> or strongly basic catalysts<sup>[52,65,66]</sup> lead to exceptionally fast rates, these catalysts exhibit a compromise between selectivity and reactivity: increasing the nucleophilicity or basicity of the catalysts enhances the rates but also promotes transesterification and competitive nucleophilic pathways<sup>[64,67,68]</sup>, resulting in broader distributions.<sup>[17]</sup>

Although catalysis employing H-bonding for initiator or monomer activation is an effective and versatile strategy in ROP, stereoselective ROP of a *rac*-LA using this methodology is still in the infancy. For now,  $\beta$ -isocupreidine reported by Chen<sup>[69]</sup> and benzyl bispidine/thiourea reported by Dove<sup>[54]</sup>, containing chiral centers, are efficient unimolecular bifunctional catalysts for stereocontrolled ROP of *rac*-LA through the kinetic resolution, and thus produce isotactic-enriched PLLA<sup>[69,70]</sup>. So far, the examples of bifunctional catalysis employing H-bonding strategy that could prepare stereoblock PLA from *rac*-LA are rare and limited. As mentioned above, recently, Waymouth reported a binary catalytic system containing alkali metal alkoxides and organic ureas<sup>[56]</sup>, which was hyperactive for ROP of different classes of cyclic monomers at room temperature.

Studying urea and thiourea catalysts can be difficult because of the complicated and sensitive interplay of interactions that give rise to catalysis. Even though, thiourea and urea catalysts exhibit superior similarities in many properties, indeed, the urea class of H-bond donors has been shown to be more active than their corresponding thioureas.<sup>[53]</sup> In order to clarify, since oxygen is more electronegative than sulphur, urea based catalysts show higher basicity than thiourea counterparts. Thus, urea based catalysts can be used as efficient bifunctional catalysts for ROP of LA. Moreover, Jakab *et al.* has pointed out the effect of substituent on (thio)ureas  $pK_a$ .<sup>[71]</sup> They observed a linear decrease in  $pK_a$  with the number of  $CF_3$  substituents attached to the aromatic rings of diaryl ureas and thioureas in DMSO.<sup>[71,72]</sup> Supportively, Lin *et al.* reported that there is a clear negative linear correlation between  $\ln(k_p)$  and the number of  $CF_3$  substituents on the diaryl ureas.<sup>[56]</sup> This argument indicates a correlation between the rate of polymerization and the  $pK_a$  of the neutral ureas; that is, less acidic ureas (more basic urea anions) correlate to faster rates for the ROP. This basis triggered us to investigate urea counterpart of Takemoto's catalyst which has higher basicity ( $pK_{a, \text{urea}} = 13.07$ ,  $pK_{a, \text{thiourea}} = 11.76$ ) for the stereoselective ROP of *rac*-LA. In addition, to the best of our knowledge, no studies have been conducted so far studying the effects because of the difference in basicity between thiourea and urea derivative H-bonding catalysts in stereoselective ROP of LA.

In summary, H-bonding (thio)ureas exhibit unique behavior as polymerization catalysts in that they exhibit high selectivities for the ROP of LA relative to transesterification and epimerization. They enable the synthesis of narrow distributed polymers, but also can control the approach of the substrates by stereoselectivity.<sup>[52,73,74]</sup> Although these catalysts typically suffer from modest activities and slow kinetics, the selectivity can be tuned by the structure and acidity of the hydrogen-bond donors.<sup>[75–80]</sup> As mentioned above, effective catalytic systems are developed to this end, such as combination of (thio)urea H-bond donors and strong bases, (thio)imidates (deprotonated (thio)ureas by strong bases, sodium or potassium alkoxides). But, catalysts with a high activity tend to promote side reactions which are undesired especially in stereoselective ROP, such as chain transfer and epimerization especially at high conversions. Moreover, unfortunately, these (thio)imidates can no longer be described as metal-free catalysts. In this chapter, corresponding urea counterpart ((*S,S*)-UC) of the chiral unimolecular bifunctional thiourea catalyst (Figure 4.4) which was investigated in Chapter 2, was studied for the stereoselective ROP of *rac*-LA at room temperature or higher. Thus, we assumed that the stereoselective ROP of *rac*-LA can be achieved with the urea catalyst in which activation is enhanced by increasing basicity, in metal-free conditions and lack of any side reaction risk.



**Figure 4.4.** Chemical structures of catalysts employed in this thesis and their  $pK_a$  values (adapted from ref. [71]).

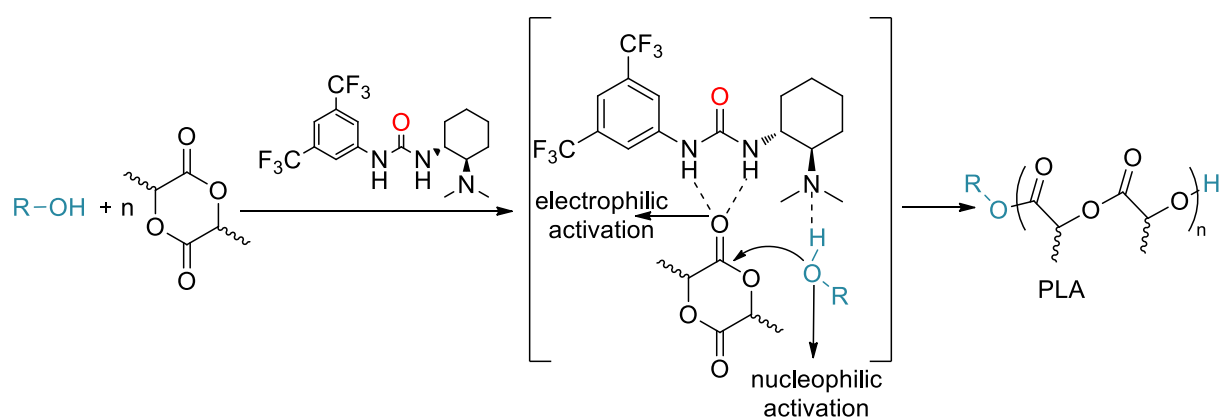


## 4.2. Results and Discussion

### 4.2.1. Polymerization procedure

ROP of LA was performed with (*S,S*)-UC in a temperature range of 25-85 °C in CH<sub>2</sub>Cl<sub>2</sub>, using benzyl alcohol (BnOH) as initiator. Table 4.1 summarizes the polymerization conditions and the results of polymerizations performed with (*S,S*)-UC catalyst.

The unimolecular bifunctional tertiary amine-urea catalyst (Scheme 4.2) operates by a bifunctional cooperative mechanism. As shown in scheme 4.2, while the amino moiety activates the alcohol initiator, the urea group activates the monomer.



**Scheme 4.2.** Proposed bifunctional activation mechanism for ROP of LA using (*S,S*)-UC.

**Table 4.1.** Stereoselective ring-opening polymerizations of *rac*-LA catalyzed by (*S,S*)-UC.<sup>a</sup>

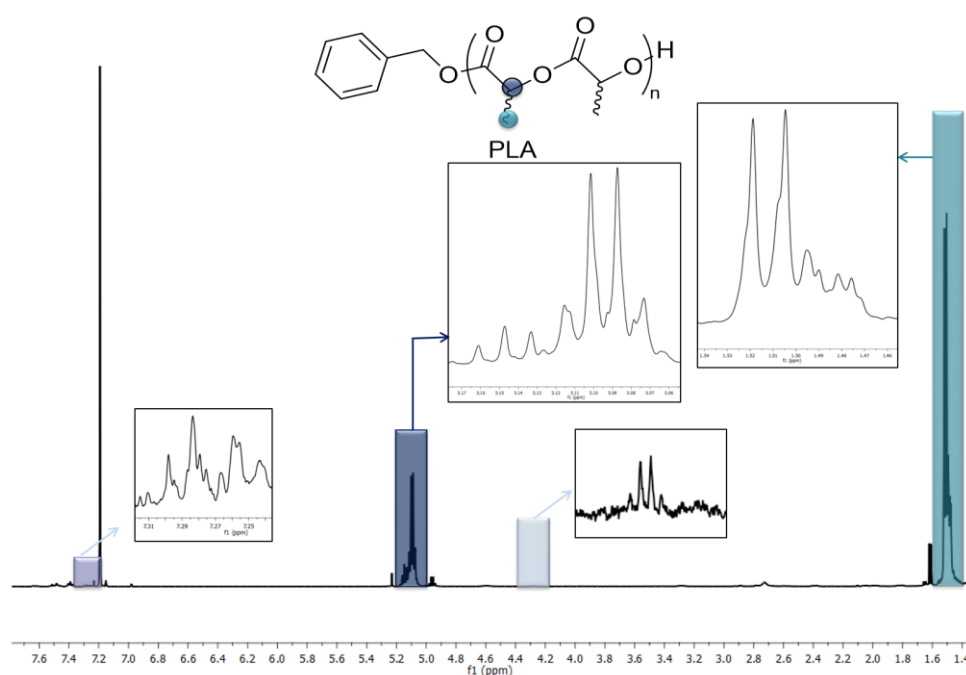
Entry	[M]0/[C]0/[I] 0	T [°C]	<i>t</i> [h]	Conv. [%] <sup>b</sup>	<i>M<sub>n</sub></i> ,SEC [kg.mol <sup>-1</sup> ] <sup>c</sup>	<i>M<sub>n</sub></i> ,calc. [kg.mol <sup>-1</sup> ] <sup>c</sup>	<i>M<sub>n</sub></i> ,MALDI [kgDa]	<i>Đ<sub>M</sub></i> <sup>c</sup>	<i>T<sub>g</sub></i> [°C] <sup>d</sup>	<i>T<sub>m</sub></i> [°C] <sup>d</sup>	<i>ΔH</i> (J.cal <sup>-1</sup> ) <sup>d</sup>	<i>P<sub>m</sub></i> <sup>e</sup>
1	200:5:1	25	214	93	13.3	26.9	13.1	1.06	44	138	15	0.85
2	200:10:1	25	198	94	14.3	27.2	n.d	1.05	48	133	12.4	0.87
3	200:5:1	45	208	95	14.9	27.4	16.2	1.05	55	-	-	0.82
4	200:10:1	45	137	95	13.2	27.4	16.2	1.09	55	-	-	0.81
5*	200:5:1	85	64	87	6.4	25.1	11.9	1.08	52	-	-	0.81
6*	200:10:1	85	69	97	8.4	28.0	n.d	1.19	51	-	-	0.77

<sup>a</sup>Polymerizations were conducted in CH<sub>2</sub>Cl<sub>2</sub> unless otherwise stated. <sup>\*</sup>Reactions were performed in toluene. <sup>b</sup> Conversion of polymerizations were determined by <sup>1</sup>H NMR spectroscopic analysis in CDCl<sub>3</sub>. <sup>c</sup> Corrected *M<sub>n</sub>* values and *Đ<sub>M</sub>* are determined by SEC in THF (calibration using polystyrene standards), Mark-Houwink correction factor is 0.585.

<sup>d</sup>*T<sub>g</sub>*, *T<sub>m</sub>* and *ΔH<sub>m</sub>* values are obtained by DSC measurements from 1<sup>st</sup> heating curve. <sup>e</sup> Probabilities of finding mesodyads are calculated from homonuclear decoupled <sup>1</sup>H by deconvolution technique. All calculations based on ESC statistics.<sup>[81]</sup> n.d.: not determined.

### 4.2.2. Polymer Characterization

Polymeric structures were confirmed by  $^1\text{H}$  NMR spectroscopy (Figure 4.5).  $^1\text{H}$  NMR,  $^{13}\text{C}$  NMR and homonuclear decoupled  $^1\text{H}$  NMR spectroscopic measurements were performed at room temperature on Bruker Advance instrument at 400 MHz.  $\text{CHCl}_3$  was used as an internal reference ( $\delta = 7.26$ ). The characteristic signals of PLA were monitored in the range from 1.53 to 1.61 ppm for methyl (Figure 4.5, green region) and from 5.11 to 5.23 ppm for methine (blue region) protons. Benzyl protons was determined at  $\sim 7.28$  ppm, indicates the  $\alpha$ -chain end was efficiently occurred and the methine hydroxyl terminated proton was assigned at  $\sim 4.34$  ppm, was also indicating  $\omega$ -chain end resulted successively.

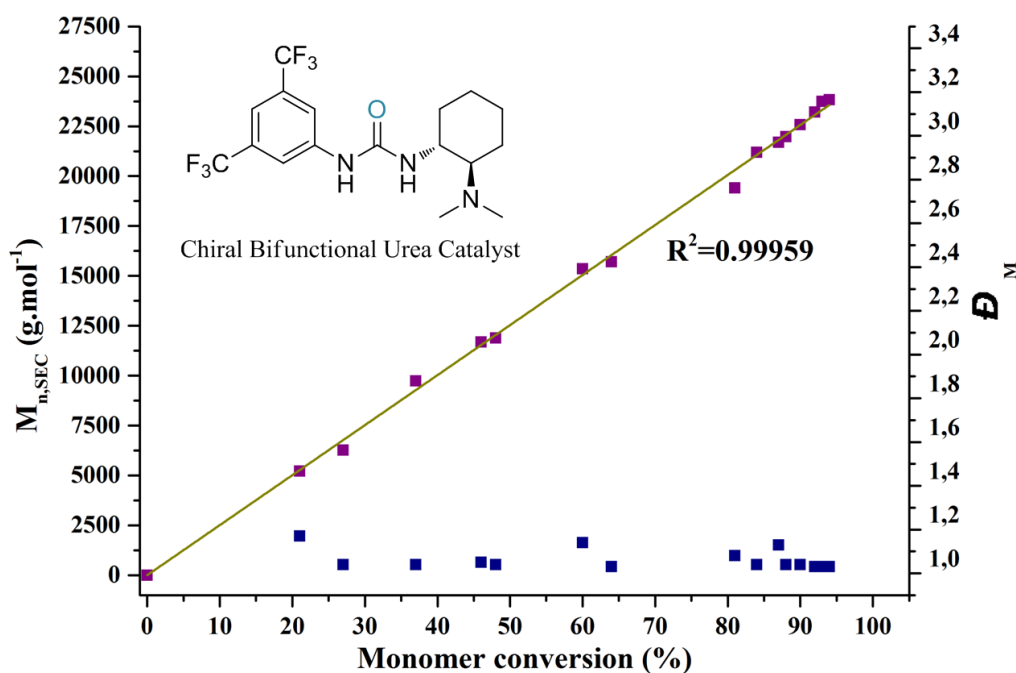


**Figure 4.5.**  $^1\text{H}$  NMR spectrum (400 MHz,  $\text{CDCl}_3$ ) of PLA prepared with (*S,S*)-UC/ *rac*-LA at 25 °C Inset 1: Methine region of PLA (dark blue), methyl region of PLA (turquoise) and  $\omega$ -methine hydroxyl proton of terminated group (light blue).

Monomer conversion reached 93% after 214 h for an initial ratio of  $[\text{LA}]_0/[(\text{S,S})\text{-UC}]_0/[\text{BnOH}]_0 = 200/5/1$  (Table 4.1, entry 1), and the high degree of control was demonstrated by linear relationship between recorded conversions and experimental molar masses (Figure 4.6). It was observed that (*S,S*)-UC showed more catalytic activity than the one that of the corresponding thiourea (Table 4.1). While 93% of monomer conversion was achieved in 214 h using (*S,S*)-UC, 85% of monomer conversion could be obtained in 238 h using the corresponding thiourea, as expected. Polymerization rate increased with the increasing catalytic loading.

Combined analyses, including NMR spectroscopy, size exclusion chromatography, and MALDI-ToF mass spectroscopy confirmed that these conditions enabled excellent control over molar mass, narrow dispersities ( $D_M = 1.19$ ) and high chain-end fidelity.

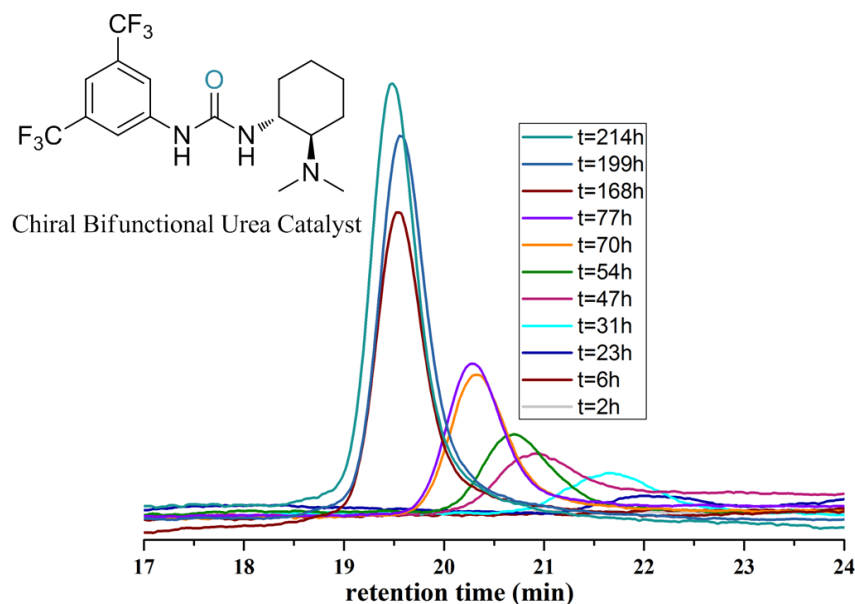
Elevating the polymerization temperature from 25 to 45 and 85 °C didn't cause any considerable loss of polymerization control, and polymer distributions were only increasing from 1.05 to 1.19. In the case of reaction performed at 85 °C, 97% of monomer conversion was achieved in 69 h, and the PLA obtained showed  $M_n = 8,400 \text{ g.mol}^{-1}$ ,  $D_M = 1.19$  for the initial ratio of 200/10/1, therefore proved the (*S,S*)-UC catalyst is more able to work in elevated temperatures than corresponding thiourea, which only enabled 54% of LA conversion in 90 h under the same reaction conditions. Thus, more controlled polymerizations were observed in the presence of (*S,S*)-UC catalyst.



**Figure 4.6.**  $M_{n,SEC}$  and dispersity ( $D_M$ ) vs. monomer conversion for PLA synthesized from (*S,S*)-UC at RT.

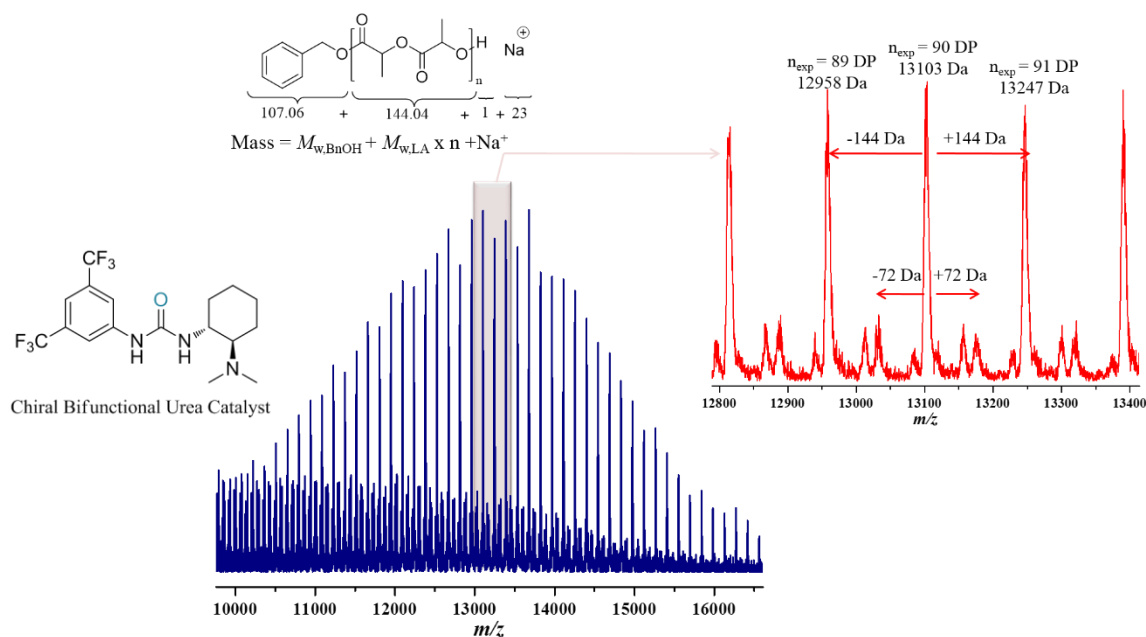
The number-average molar mass of the polymers ( $M_n$ ) was determined by SEC in THF (Figure 4.7). SEC traces of the resultants PLAs showed a monomodal distribution, as shown in Figure 4.7. The corrected  $M_n$  value of  $13,300 \text{ g.mol}^{-1}$  is in good agreement with the one that obtained by MALDI-ToF analysis is of  $13,100 \text{ g.mol}^{-1}$  (Table 4.1, entry 1). In contrast, apparent molar masses of PLAs synthesized at 85 °C slightly deviated from the expected values; for instance,  $M_n = 6,400 \text{ g.mol}^{-1}$  as determined for the PLA obtained at 85 °C in

toluene, for a value obtained by MALDI-ToF,  $M_n = 11,900$  Da. This discrepancy might be due to the occurrence of side transesterification reactions during the ROP process.



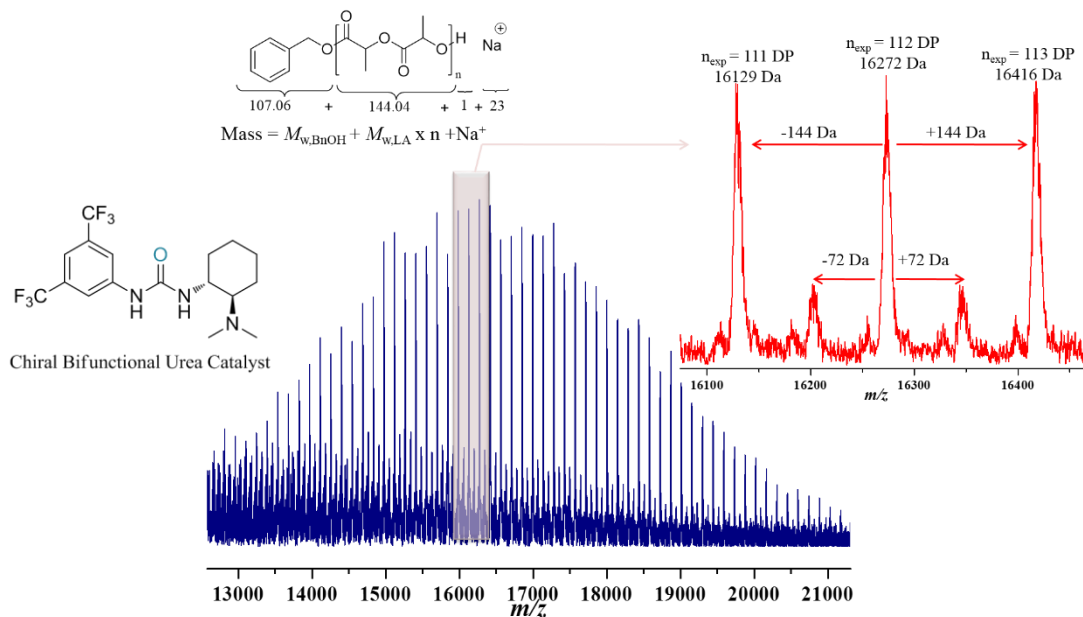
**Figure 4.7.** Size exclusion chromatograms of PLA during ROP of *rac*-LA using (*S,S*)-UC at 25°C

Polymers obtained with (*S,S*)-UC with a monomer to initiator ratio of 200 at room temperature, was analyzed by MALDI-ToF mass spectrometry to certify on the end-group fidelity and also fate of the back-bite reactions. The major series of signals with a mass difference 144 Da was consistent with the exact mass of LA unit (Figure 4.8). And also the  $\alpha$ -benzylate and  $\omega$ -hydroxyl end groups were confirmed. However, the minor but regular series of signals with a mass difference 72 Da were also observed. Considering this results, we might mention that inter-molecular transesterification reactions occurred to some extent in this system.



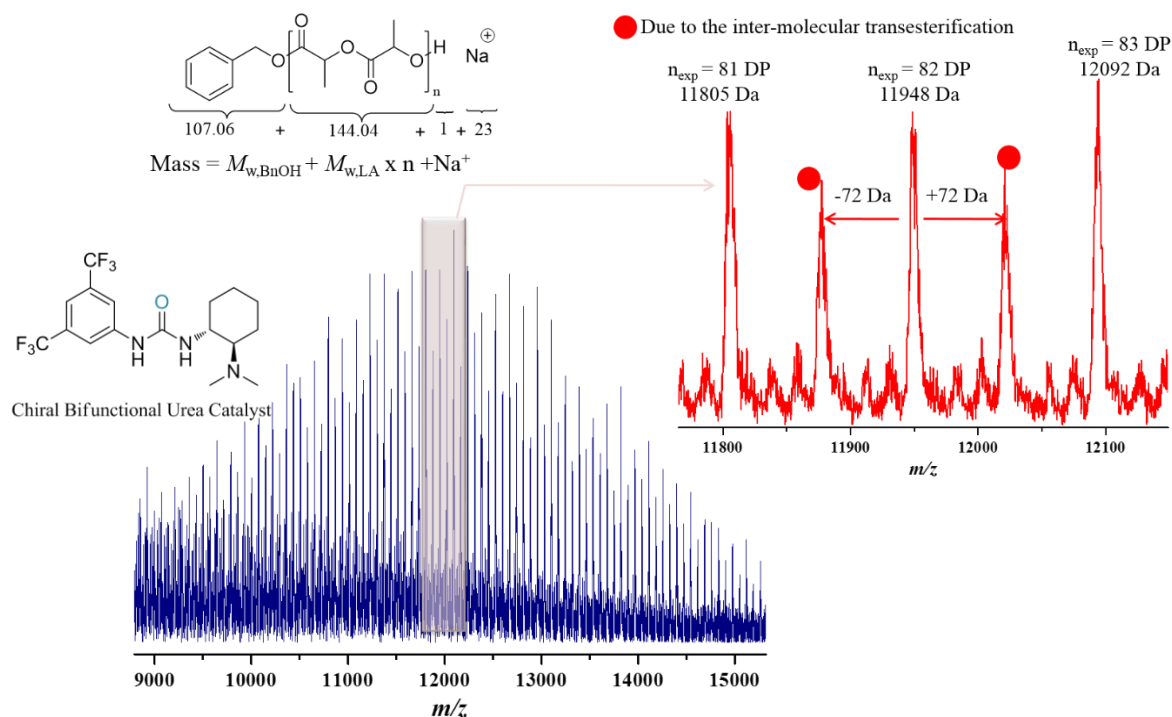
**Figure 4.8.** MALDI-ToF mass spectrum of PLA obtained at 25 °C using (*S,S*)-UC (Table 4.1, entry 1)

Consistently, PLA which is prepared at 45 °C, also showed the minor but regular series of signals with a mass difference 72 Da by MALDI-ToF (Figure 4.9) indicative of the occurrence of inter-molecular transesterification reactions. Thus, (*S,S*)-UC catalyst leads to some side reactions to a larger extent than its corresponding thiourea counterpart. This output can be attributed to higher catalytic activation of the urea catalyst than thiourea counterpart.



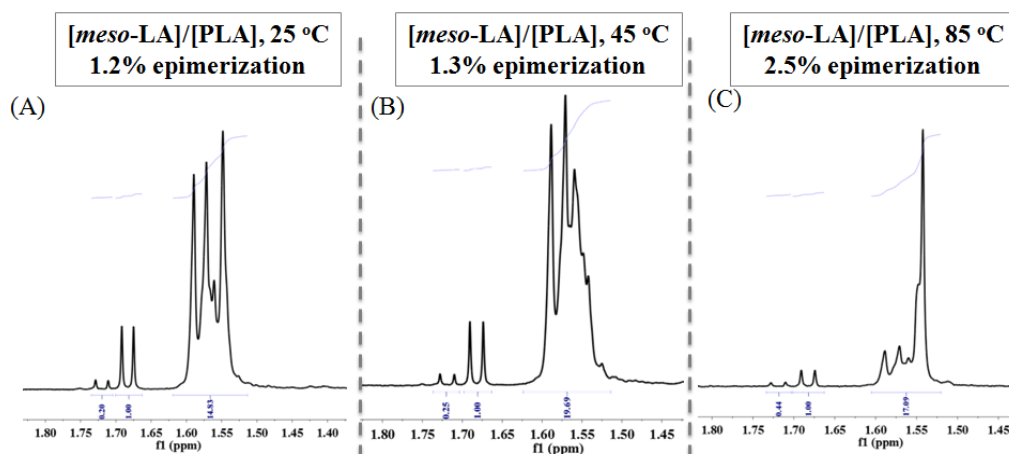
**Figure 4.9.** MALDI-ToF mass spectrum of PLA obtained at 45 °C using (*S,S*)-UC (Table 4.1, entry 3)

The series of peaks also evidenced as repeating unit of 72 Da with well higher intensities attesting more pronounced side reactions. Any formation of macrocyclic polymer was not observed. Apparently, the increment of reaction temperature triggers the inter-molecular transesterification formation, as also observed with corresponding thiourea catalysis at 85 °C.



**Figure 4.10.** MALDI-ToF mass spectrum of PLA obtained at 85 °C (Table 4.1, entry 5)

As also observed when the (*S,S*)-TUC catalyst was used (Chapter 2), epimerization side reactions were observed when ROPs of *rac*-LA are conducted with (*S,S*)-UC catalyst whatever the temperature used (Figure 4.11). As clearly indicated before, epimerization of *rac*-LA to *meso*-LA can bias the stereocontrol, creating considerable stereoerrors, if the polymerization rate is significantly high. Epimerization rates can be calculated by  $^1\text{H}$  NMR from the *meso*-LA formation signal at  $\delta \sim 1.72$  ppm. Due to the fact that the ROP was faster with (*S,S*)-UC than the corresponding (*S,S*)-TUC catalyzed polymerizations, there was an expected increment in epimerization rates. The extent of epimerization was 1.2, 1.3 and 2.5% using (*S,S*)-UC, while the corresponding thiourea led 1, 1.2 and 1.9% of epimerization at 25, 45 and 85 °C, respectively. Clearly, the epimerization side reaction is more triggered with the urea catalyst than the thiourea counterpart. However, there is no clue about which catalyst is more prompt to incorporate *meso*-LA into the polymer chain.

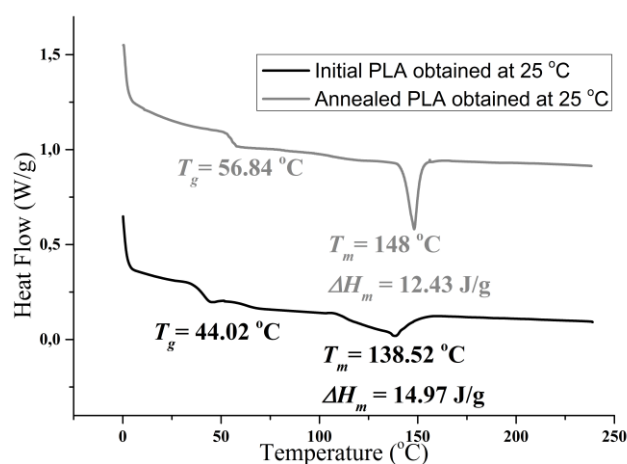


**Figure 4.11.** NMR spectra (400 MHz,  $\text{CDCl}_3$ ) zoomed in the methyl region of PLA obtained at (A) 25 °C, (B) 45 °C and (C) 85 °C. Those indicate epimerization reactions from *rac*-LA and to *meso*-LA in the presence of (*S,S*)-UC

### 4.2.3. Microstructure analysis of PLA derived from chiral (*S,S*)-UC

#### 4.2.3.1. DSC Analysis

The thermal properties of the (*S,S*)- and (*R,R*)-TUC-derived PLAs were investigated by DSC using a DSC Q100 RCS TA Instrument. All samples were first heated up to 250 °C at a rate of 10 °C/min, left at this temperature for 10 min, then cooled to 0 °C at the same rate of 10 °C/min, and were left at 0 °C for 10 min. The same heating cycle was thus repeated. Thermal data provided hereafter were obtained from the first heating scan. The degree of crystallinity ( $x_c$ ) was calculated using  $\Delta H_m$  values, which were obtained by the integration of melting point surface areas. The equation is defined as  $x_c = \frac{\Delta H_{m\text{exp}}}{\Delta H_{m\text{theo}}} (\Delta H_{m\text{theo}} = 93.7 \text{ J/g})$ .<sup>[82,83]</sup>

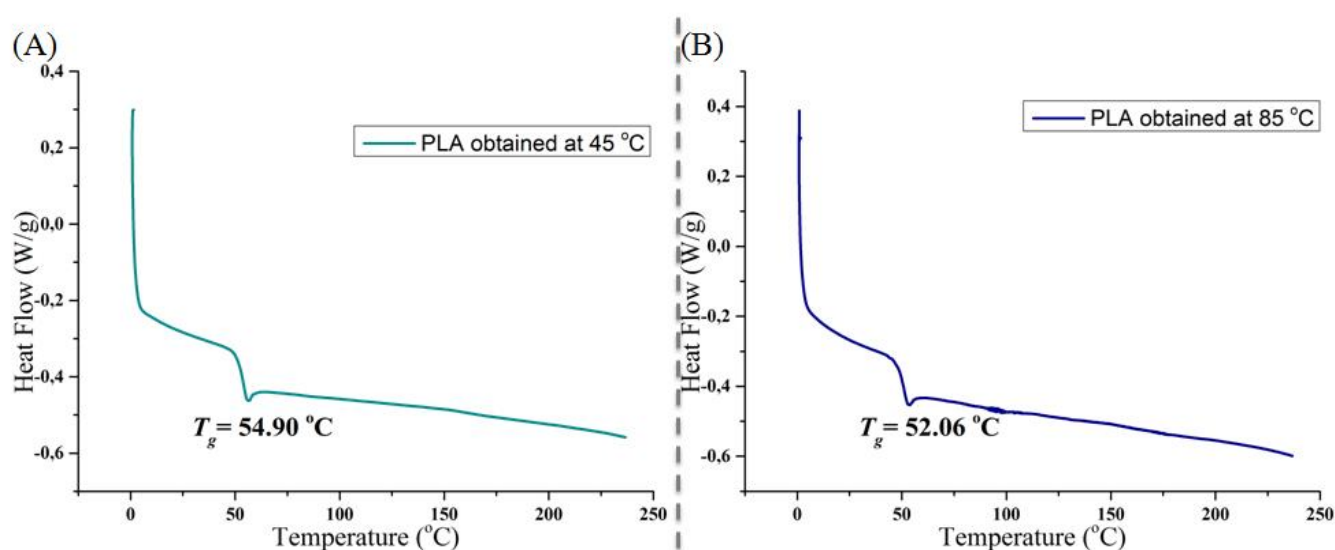


**Figure 4.12.** DSC thermogram (1<sup>st</sup> scan; 10 °C/min) of the initial and annealed PLAs obtained at 25 °C (Table 4.1, entry 1)



Analysis by DSC showed a defined melting transition at  $T_m = 138\text{ }^{\circ}\text{C}$  (Figure 4.12) with a  $\Delta H_m = 14.8\text{ J/g}$  for (*S,S*)-UC-derived PLA at  $25\text{ }^{\circ}\text{C}$ . Since,  $T_m = 152\text{ }^{\circ}\text{C}$  was detected using corresponding thiourea under the same reaction conditions (Figure 2.12, Chapter 2), it is observed that the rate of the crystallinity was reduced. Afterwards,  $T_m$  of polymer prepared at room temperature showed significant enhancement from  $138\text{ }^{\circ}\text{C}$  to  $148\text{ }^{\circ}\text{C}$  after annealing process and  $\Delta H_m = 12.4\text{ J/g}$  was calculated.

PLAs prepared at  $45$  and  $85\text{ }^{\circ}\text{C}$  did not show any  $T_m$ , even after annealing (Figure 4.13). Therefore, it was assumed that the stereocontrol of the catalyst was restricted under high reaction temperatures. However, corresponding thiourea was provided clear  $T_m$  of PLA under high reaction temperatures. This can be either attributed that (*S,S*)-TUC can show higher thermal stability, or it would less prompt to incorporate the *meso*-LA formed during the ROP process than (*S,S*)-UC. Thus, (*S,S*)-TUC provided higher stereocontrol than (*S,S*)-UC during the ROP of *rac*-LA.



**Figure 4.13.** DSC thermograms (1<sup>st</sup> scan;  $10\text{ }^{\circ}\text{C/min}$ ) of PLAs obtained by (*S,S*)-UC at (A)  $45\text{ }^{\circ}\text{C}$ , and (B)  $85\text{ }^{\circ}\text{C}$  (Table 4.1, entries 3 & 5)

#### 4.2.3.2. Homonuclear decoupled $^1\text{H}$ NMR and quantitative $^{13}\text{C}$ NMR analysis

In order to analyze the stereoselectivity of the ROP process, homonuclear decoupled  $^1\text{H}$  NMR ( $^1\text{H}\{^1\text{H}\}$  NMR) and quantitative  $^{13}\text{C}$  NMR (Q.  $^{13}\text{C}$  NMR) spectroscopies were performed. For those analyses, Bruker Advance instrument at  $400\text{ MHz}$  was used at room temperature in  $\text{CDCl}_3$  as solvent. The decoupling pulse was focused in the methyl region, at

around 1.6 ppm for the separation of five tetrad signals<sup>54</sup> in methine region ( $\sim\delta = 5.00$ -5.20 ppm). All calculated  $P_m$  values using the equations in Table 4.2 attributed to ESC and CEC mechanisms using five tetrad signals ratios from the corresponding  $^1\text{H}$   $\{^1\text{H}\}$  NMR and Q.  $^{13}\text{C}$  NMR (see explanations in 2.2.3 in Chapter 2). All results are summarized in Table 4.3.

**Table 4.2.** Tetrad probabilities of ESC and CEC mechanisms based on non-Bernoullan and Bernoullan statistics.

tetrad	Probability of ESC (non-Bernoullan)	Probability of CEC (Bernoullan)
<i>mmm</i>	$[P_m^2 + (1 - P_m)^2 + P_m^3 + (1 - P_m)^3]/2$	$P_m^2 + 0.5 P_m P_r$
<i>mmr</i>	$[P_m^2(1 - P_m) + P_m(1 - P_m)^2]/2$	$0.5 P_m P_r$
<i>rmm</i>	$[P_m^2(1 - P_m) + P_m(1 - P_m)^2]/2$	$0.5 P_m P_r$
<i>rmr</i>	$[P_m^2(1 - P_m) + P_m(1 - P_m)^2]/2$	$0.5 P_r^2$
<i>rrm</i>	$[P_m(1 - P_m)]$	$0.5 (P_m^2 + P_m P_r)$

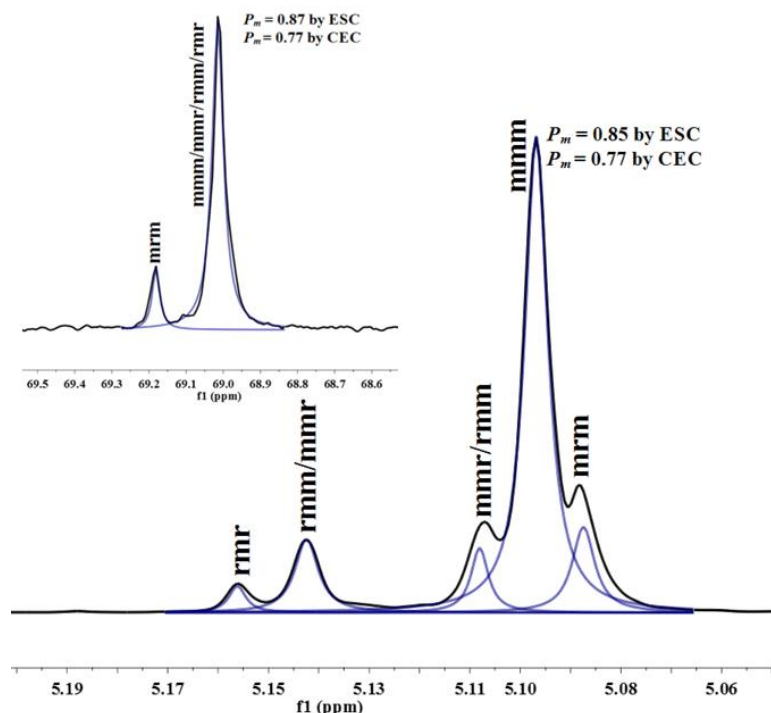
**Table 4.3.** Probabilities of tetrad mesodyads based on ESC and CEC statistics.<sup>a</sup>

Entry	[M]/[C]/[I]	T [°C]	Conv. [%] <sup>b</sup>	$M_n$ [kg.mol <sup>-1</sup> ] <sup>c</sup>	$\bar{D}$ <sup>c</sup>	$P_m^d$ [Based on ESC mec.]		$P_m^d$ [Based on CEC mec.]	
						HD $^1\text{H}$ NMR	Q. $^{13}\text{C}$ NMR	HD $^1\text{H}$ NMR	Q. $^{13}\text{C}$ NMR
1	200:5:1	25	93	22.8	1.06	0.85	0.87	0.77	0.77
2	200:10:1	25	94	24.6	1.05	0.87	0.86	0.79	0.74
3	200:5:1	45	95	25.6	1.05	0.82	0.85	0.73	0.75
4	200:10:1	45	95	22.6	1.09	0.82	0.89	0.73	0.81
5*	200:5:1	85	87	11.0	1.08	0.81	0.84	0.77	0.74
6*	200:10:1	85	97	14.4	1.19	0.77	0.83	0.67	0.72

<sup>a</sup>Polymerizations were conducted in  $\text{CH}_2\text{Cl}_2$  unless otherwise stated. <sup>\*</sup>Reactions were performed in toluene. <sup>b</sup>Conversion of polymerizations were determined by  $^1\text{H}$  NMR spectroscopic analysis in  $\text{CHCl}_3$ . <sup>c</sup> $M_n$  and  $\bar{D}_M$  are determined by SEC in THF (calibration using polystyrene standards). <sup>d</sup>Probabilities of finding mesodyads are calculated from homonuclear decoupled  $^1\text{H}$  and quantitative  $^{13}\text{C}$  NMR spectra by deconvolution technique. Calculations performed based on ESC and CEC statistics considering Bernoullan and non-Bernoullan statistics.<sup>[81]</sup>

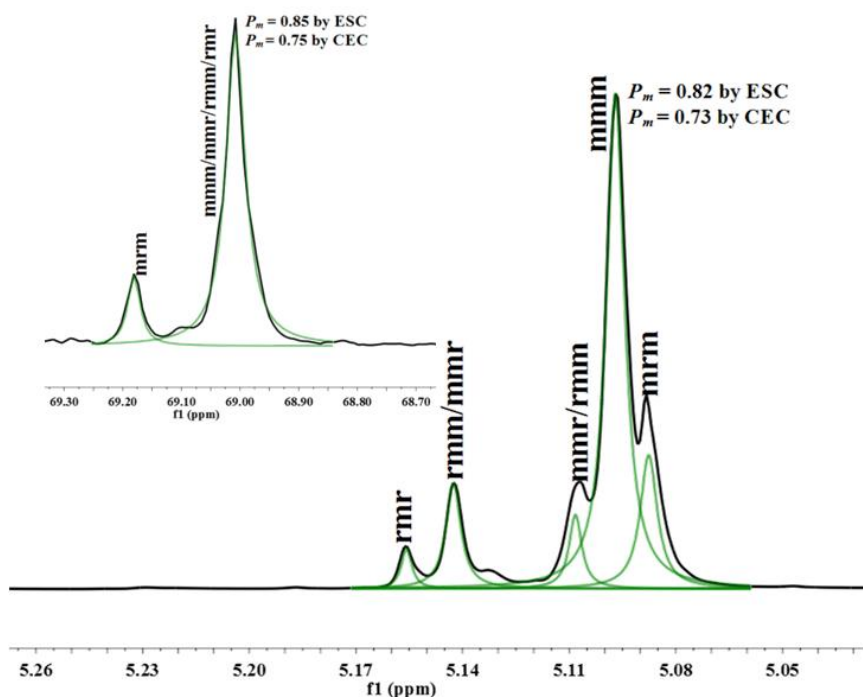
Isotactic PLA enchainment at room temperature was confirmed by  $^1\text{H}$   $\{^1\text{H}\}$  NMR and Q.  $^{13}\text{C}$  NMR analysis.  $P_m^{\text{ESC}} = 0.85$  and  $P_m^{\text{CEC}} = 0.77$  were calculated from  $^1\text{H}$   $\{^1\text{H}\}$  NMR considering ESC and CEC mechanisms, respectively (Table 4.3, entry 1). The results obtained

from Q.  $^{13}\text{C}$  NMR, found to be consistent with the one obtained using  $^1\text{H} \{^1\text{H}\}$  NMR ( $P_m^{\text{ESC}} = 0.87$  and  $P_m^{\text{CEC}} = 0.77$ ). Mesotacticity ratios of the polymer obtained with (*S,S*)-UC was observed slightly lower than that obtained with corresponding thiourea ( $P_m^{\text{ESC}} = 0.87$  and  $P_m^{\text{CEC}} = 0.79$ , Table 2.3, Chapter 2). This result was in line with the polymer thermal properties. Predominantly isotactic PLA was, however, confirmed with the sharp and dense *mmm* tetrad signal (Figure 4.14). Little differences between the calculated results of Q.  $^{13}\text{C}$  NMR and  $^1\text{H} \{^1\text{H}\}$  NMR corresponds to the experimental and software errors.



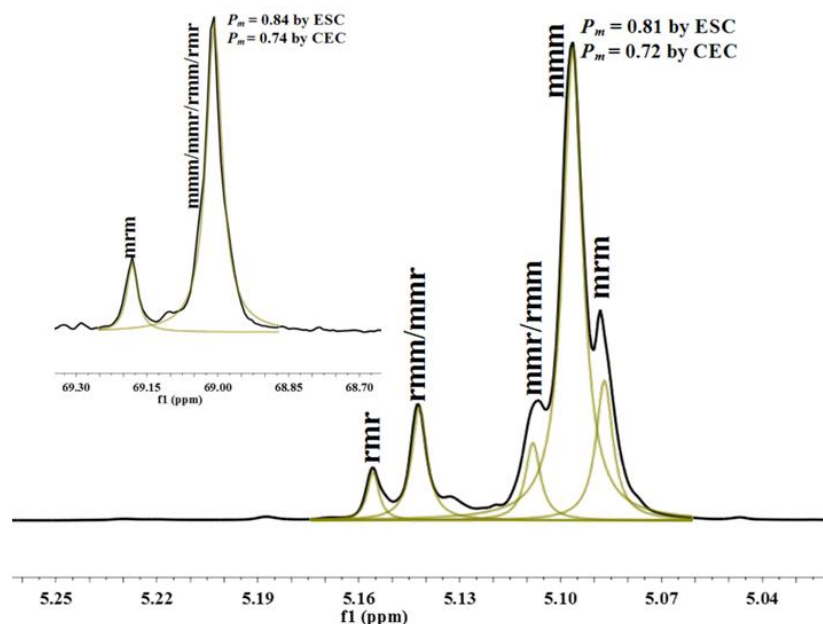
**Figure 4.14.** Deconvoluted  $^1\text{H} \{^1\text{H}\}$  NMR spectra (400 MHz,  $\text{CDCl}_3$ ) of the methine region of PLAs prepared by the catalysis of (*S,S*)-UC. Inset: Q.  $^{13}\text{C}$  NMR spectrum at 25 °C (Table 4.3, entry 1).

Relatively isotactic polymer formation was still confirmed at elevated temperatures. According to  $^1\text{H} \{^1\text{H}\}$  NMR spectra (Figure 4.15),  $P_m$  values are obtained as 0.82 and 0.73 using ESC and CEC equations, respectively (Table 4.3, entry 3). On the other hand, using Q.  $^{13}\text{C}$  NMR technique  $P_m^{\text{ESC}} = 0.85$  and  $P_m^{\text{CEC}} = 0.75$  values were calculated which was a bit overestimated due to the experimental errors. Compared to the  $P_m$  values of PLA obtained by (*S,S*)-TUC-catalysis ( $P_m^{\text{ESC}} = 0.82$  and  $P_m^{\text{CEC}} = 0.73$ ), (*S,S*)-UC revealed the same  $P_m$  values for the PLA obtained at 45 °C.



**Figure 4.15.** Deconvoluted  $^1\text{H}$  { $^1\text{H}$ } NMR spectra (400 MHz,  $\text{CDCl}_3$ ) of the methine region of PLA prepared by the catalysis of (*S,S*)-UC at 45 °C inset: Q.  $^{13}\text{C}$  NMR spectrum (Table 4.3, entry 3)

When PLAs are prepared at 85 °C,  $P_m$  values are slightly lower but still impressive. Interestingly, a  $P_m$  value as high as 0.81 is determined by ESC statistics (Table 4.3, entry 5; Figure 4.16). As expected, (*S,S*)-UC catalyst has provided predominantly isotactic PLA, which confirms that almost the same microstructure of (*S,S*)-TUC- derived PLA is obtained.



**Figure 4.16.** Deconvoluted  $^1\text{H}$  { $^1\text{H}$ } NMR spectra (400 MHz,  $\text{CDCl}_3$ ) of the methine region of PLAs prepared by the catalysis of (*S,S*)-UC. Inset: Q.  $^{13}\text{C}$  NMR spectrum at 85 °C (Table 4.3, entry 5).

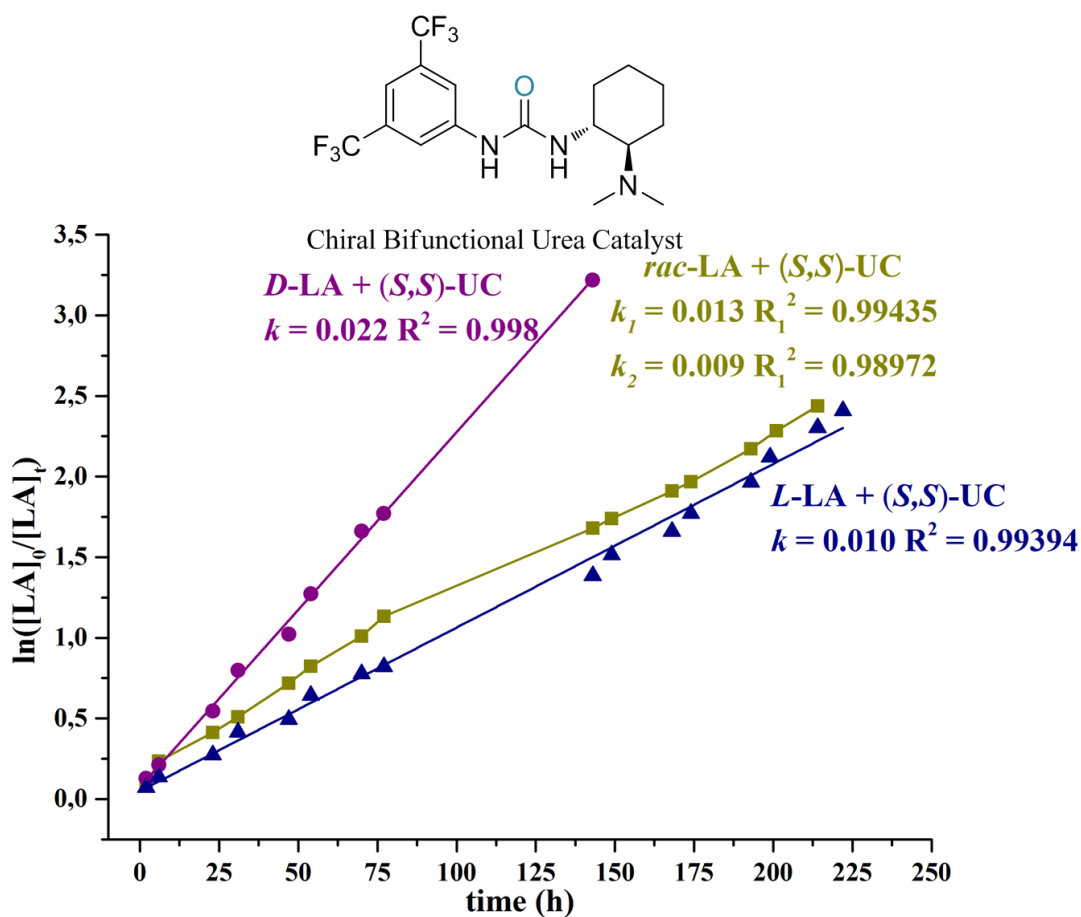
Calculations of  $P_m$  values as a function of one or the other mechanism, *i.e.* CEC or ESC, lead to differing results and clearly, the mechanism of catalyst operation is critical in studies such as those because of the proved semi-crystalline polymer chain which was not the case of previous study by Pratt *et al.*<sup>[54]</sup> Assuming *it*-PLA would be formed by a CEC mechanism exclusively, relative tetrad intensities would be expected as follows:<sup>[84]</sup>  $[\text{mmr}] = [\text{rmm}] \neq [\text{rmr}]$ . In this case, stereoblocks could be generated when a growing PLA chain incidentally incorporated the LA enantiomer of opposite configuration to that of the last inserted enantiomer. This would create a stereoerror from which “normal” growth would form a new stereoblock of opposite configuration to the previous one. Conversely, the ESC mechanism should generate single insertion stereoerrors of the type  $-\text{RRRRSSRRR}-/-\text{SSSSRRSSSS}-$ . In the latter case, the tetrad ratio should be  $[\text{rmr}] = [\text{mmr}] = [\text{rmm}] = 2/[\text{mmr}]$ .<sup>[81]</sup> The *rmr* signal is a clear indicator of mechanism.

The intensities of five corresponding tetrad peaks obtained by  $^1\text{H}$  { $^1\text{H}$ } NMR spectroscopy was  $[\text{rmr}] = 0.027$ ,  $[\text{mmr}] = 0.105$ ,  $[\text{rmm}] = 0.069$  and  $[\text{mmm}] = 0.119$ . As also previously observed for corresponding thiourea, tetrad ratios were not consistent neither with ESC nor CEC statistics in the case of (*S,S*)-UC catalysis. Additionally, the stereocontrol mechanism of (*S,S*)-TUC was demonstrated to be an occasional concomitant mechanism of

ESC & CEC mechanism. Due to the similarities in tacticity analysis, concomitant mechanism of ESC & CEC would most likely be conducted by the (*S,S*)-UC, as well.

#### 4.2.4. Polymerization Kinetics

To receive further information about stereocontrol mechanism, kinetic studies of ROP of LA stereoisomers were performed. Both *D*- and *L*-LA were thus polymerized using (*S,S*)-UC. More information about reaction kinetics and the equations can be found in Chapter 2, section 2.2.4. The polymerization kinetics were monitored using monomer conversion obtained by  $^1\text{H}$  NMR analysis. Results showed first-order dependence on LA concentration in each case; the pseudo first-order rate constants,  $k_{\text{obs}}$ , were obtained as the gradient of the linear fits to plots of  $\ln([\text{LA}]_0/[\text{LA}]_t)$  versus time (Figure 4.18).



**Figure 4.17.** Kinetic plots of the ROP of *rac*-LA, *D*-LA and *L*-LA catalyzed by (*S,S*)-UC and in  $\text{CH}_2\text{Cl}_2$  at RT in the presence of BnOH as a initiator:  $[\text{LA}]_0:[\text{UC}]:[\text{BnOH}]=200:5:1$ .

Kinetic studies revealed that (*S,S*)-UC selectively polymerized *D*-LA ~2 times faster than the *L*-LA. The kinetic studies enabled us to calculate the selectivity factor:  $s = k_D/k_L = 2.2$

for (*S,S*)-UC, whereas the  $s = k_D/k_L$  was calculated as 5 for the (*S,S*)-TUC. The stereoselective ROP of *rac*-LA showed 2 distinct slopes ( $k_{obs-I} = 0.013$ ,  $k_{obs-II} = 0.009$ ) indicating preferential selectivity of the (*S,S*)-UC during the stereoselective ROP. The selectivity factor of (*S,S*)-UC catalyst was found to be quite low in comparison with the one of corresponding thiourea. Reduction in selectivity can be attributed to a faster catalytic activation.

### 4.3. Conclusions and perspectives

In this chapter, a chiral unimolecular bifunctional tertiary amine-urea catalyst was investigated for the stereoselective ROP of *rac*-LA for the first time. To the best of our knowledge, the difference in stereoselectivity resulting from the difference in electronegativity between urea and corresponding thiourea had not been studied before. Compared with corresponding thiourea, the polymerization time can be reduced by almost 24 hours, without significant reduction in stereoselectivity ( $P_m = 0.85$ , 25 °C). The rather well controlled character of the polymerization was confirmed by the observation of a narrow polymer molar mass distribution. In the case of the (*S,S*)-UC-conducted ROP at 25 and 45 °C, however, low-extent of inter-molecular transesterification reactions were induced more compared to the corresponding thiourea, monitored by MALDI-ToF analysis. Moreover, as a result of the higher epimerization ratios obtained by (*S,S*)-UC, the urea organocatalyst appears to be more prompt to form *meso*-LA during the ROP process. As a matter of fact, more stereoerrors are introduced, achieving less stereocontrol. This is reflected by the absence of any  $T_m$  values in DSC analysis of the resultant PLAs obtained at 45 and 85 °C.

The formation of semi-crystalline PLAs at 25 °C was confirmed by thermal analysis, with a  $T_m$  value detected at 138 °C, which can even improved to 148 °C by further annealing. The isoselective ROP of *rac*-LA was attested by  $^1\text{H} \{^1\text{H}\}$ NMR analysis, showing a  $P_m$  value of 0.85. Although elevated temperatures did not alter the mesotacticity, in comparison to PLAs synthesized from the thiourea homologue, semi-crystalline materials could not be evidenced by thermal analysis. Kinetic investigations have established that the organocatalyst selectively polymerized the *D*-LA, with selectivity factor  $x_s = k_D / k_L$  of 2.2 during the ROP of *rac*-LA. The lower selectivity than the corresponding thiourea catalyst can be attributed to the increased catalyst activation.

However, considering these results and the ratios of the five tetrad peaks calculated by corresponding  $^1\text{H} \{^1\text{H}\}$ NMR spectra, concomitant ESC & CEC mechanism was demonstrated as a conducted stereocontrol mechanism. Due to its relatively high basicity, thus its higher polymerization rate, a faster polymerization is achieved using (*S,S*)-UC, while stereocontrol properties remains similar than the corresponding thiourea. Thus, it is demonstrated that the urea catalyst may bring new catalytic approach for well controlled, selective ROP of LA in a metal-free medium with an increased catalytic activation comparing to that of thiourea catalyst.



#### 4.4. Experimental and supporting informations

**Materials:** *D*-LA (Corbion-Purac), *L*-LA (Corbion-Purac) and *rac*-LA (Sigma-Aldrich) were recrystallized three times from dry toluene. Afterwards, lactide was purified by azeotropic distillation. Lastly, they were dried under dynamic vacuum for overnight prior to use.<sup>[85]</sup> (*S,S*)-UC was received from Strem Chemicals, dried azeotropically under toluene 3 times. Benzyl alcohol (BnOH) was received from Alfa Aesar, distilled by cryo-distillation over calcium hydride (CaH<sub>2</sub>). Benzoic acid (≥99.5%, Sigma-Aldrich) was used as received. All dry solvents were collected from solvent drying machine. Afterwards, they stored over molecular sieves (3 Å) in a glovebox for no longer than 4 weeks.

**Instrumentation:** <sup>1</sup>H NMR and <sup>13</sup>C NMR spectra were recorded in CDCl<sub>3</sub> on Bruker Advance instrument at 400 MHz at room temperature. Homonuclear decoupled <sup>1</sup>H NMR spectroscopic measurements and quantitative <sup>13</sup>C NMR spectra were recorded at room temperature on Bruker Advance instrument at 400 MHz and CDCl<sub>3</sub> was used as an internal reference ( $\delta = 7.26$ ). The relaxation time was fixed to 2 s. For homonuclear decoupled <sup>1</sup>H NMR spectroscopic analysis, relaxation time was measured and fixed to 2.04 s. Samples were obtained in CDCl<sub>3</sub> solutions with the decoupling pulse based on the methyl region ( $\sim\delta = 1.5$  ppm). In case of the good separation of methine region ( $\sim\delta = 5.00$ - $5.20$  ppm), the global spectral deconvolution technique was implemented by attribution of five mesodyads based on both non-Bernouillan and Bernouillan statistics in case of the operated combination mechanism.<sup>[14,81,84,86–89]</sup>

Polymer molar masses were determined by size exclusion chromatography (SEC) using tetrahydrofuran (THF) as the eluent. Measurements in THF were performed on an Ultimate 3000 system from Thermoscientific equipped with diode array detector DAD. The system also includes a multi-angles light scattering detector MALS and differential refractive index detector dRI from Wyatt technology. Polymers were separated on three G2000, G3000 and G4000 TOSOH HXL gel columns (300 x 7.8 mm) (exclusion limits from 1000 Da to 400 000 Da) at a flowrate of 1 mL/min. Columns temperature was held at 40°C. Polystyrene was used as the standard.

Positive-ion MALDI-MS experiments were conducted using a Waters QTOF Premier mass spectrometer equipped with a Nd:YAG laser (third harmonic) operating at 355 nm with a maximum output of 65  $\mu$ J delivered to the sample in 2.2 ns pulses at 50 Hz repeating rate. Time-of-flight mass analysis was performed in the refraction mode at a resolution of about

10K. All samples were analyzed using trans-2-[3-(4-tert-butylphenyl)-2-methylprop-2-enylidene]malononitrile (DCTB) as a matrix. Polymer samples were dissolved in THF to obtain mg/ mL solution. Additionally, 50  $\mu$ L of 2 mg/mL NaI solution in acetonitrile was added to the polymer solution

$T_g$ ,  $T_m$  and  $\Delta H_m$  values were analyzed by differential scanning calorimetry (DSC) using a DSC Q100 RCS TA Instrument. Polymer samples were first heated to 250  $^{\circ}$ C at 10  $^{\circ}$ C/min, equilibrated at this temperature for 10 min, then cooled to -10  $^{\circ}$ C at 10 $^{\circ}$ C/min, held for 10 min, and reheated to 250  $^{\circ}$ C at 10  $^{\circ}$ C/min. All thermal data were obtained from the first scan. Degree of crystallinity ( $x_c$ ) was calculated using  $\Delta H_m$  values, which are obtained by the integration of melting point surface areas. The equation is defined as  $x_c = \frac{\Delta H_{mexp}}{\Delta H_{mtheo}}$ . ( $\Delta H_{mtheo} = 93.7$  J/g) [82,83]

**General polymerization methods:** In case of the polymerizations performed at R.T: Pre-dried 10 mL vials were first introduced into an Argon-filled glovebox. In a typical polymerization reaction catalyst (for 10 eq.; 28.68 mg, 0.069 mmol, for 5 eq; 14.34 mg, 0.034mmol) and external BnOH as an initiator (0.71  $\mu$ L, 0.0069 mmol) were dissolved in dichloromethane (0.42 mL). Shortly after, previously dissolved *rac*-LA (0.2 g, 1.38 mmol) in dichloromethane (1 mL) was added to the vigorously stirred solution. Polymerizations were performed in glovebox and monitored by  $^1$ H NMR spectroscopy and SEC before precipitation. Then they were quenched by addition of benzoic acid (4.15 mg, 0.034). The polymer was subsequently precipitated from cold methanol (MeOH), and after filtration it was excessively washed with methanol to remove any impurities. All polymers were dried under dynamic vacuum for overnight. Monomer conversion was calculated by comparing the integration of the methyl signals of unreacted monomer to the methyl region of the polymer before precipitation. Theoretical molar masses ( $M_{ntheo.}$ ) were calculated from  $^1$ H NMR spectra from the monomer conversion factor ( $x_{LA}$ ).

Considering polymerization performed at 45 and 85  $^{\circ}$ C: Dry 10 mL Schlenk tubes were first introduced into an Argon-filled glovebox. In a typical polymerization reaction catalyst (for 10 eq.; 28.68 mg, 0.069 mmol, for 5 eq; 14.34 mg, 0.034mmol) and external BnOH as an initiator (0.71  $\mu$ L, 0.0069 mmol) were introduced to the Schlenk tube and dissolved in dichloromethane (0.42 mL). Shortly after, previously dissolved *rac*-LA (0.2 g, 1.38 mmol) in dichloromethane (1 mL) was added to the Schlenk tube. Then, the tightly closed Schlenk tube was removed from the glovebox and introduced inside the pre-heated oil bath at 45 $^{\circ}$ C or 85

°C. Polymerization was performed under binary Schlenk system with dynamic vacuum and inert atmosphere in oil bath. Binary Schlenk system refers dual manifold Schlenk line with several ports under it. Basically, one manifold is connected to a purified inert argon gas while the other is connected to a vacuum pump. The inert-gas line is gone through an oil bubbler, while solvent vapors and gaseous reaction products are hindered from contaminating the vacuum pump by a liquid-nitrogen trap. Polymerizations monitored by  $^1\text{H}$  NMR spectroscopy and SEC before precipitation and were quenched by addition of benzoic acid (4.15 mg, 0.034). The polymer was subsequently precipitated from cold methanol (MeOH) and was collected by filtration before being washed with excess methanol to remove impurities. Afterwards, polymers obtained were dried under dynamic vacuum for overnight. Percent conversion was calculated by comparing the integration of the methyl signals of unreacted monomer to the methyl region of the polymer before precipitations from NMR spectra.

#### 4.5. References

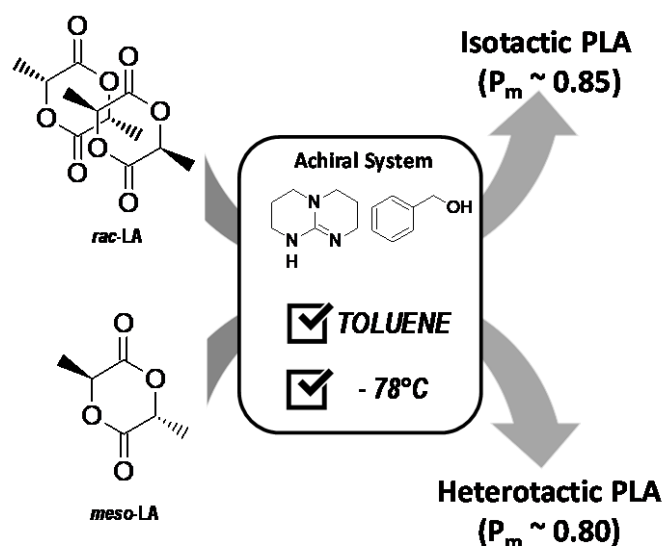
- [1] M. J. Stanford, A. P. Dove, *Chem. Soc. Rev.* **2010**, 39, 486.
- [2] C. M. Thomas, *Chem. Soc. Rev.* **2010**, 39, 165.
- [3] L. M. Hodgson, R. H. Platel, A. J. P. White, C. K. Williams, *Macromolecules* **2008**, 41, 8603.
- [4] O. Dechy-Cabaret, B. Martin-Vaca, D. Bourissou, *Chem. Rev.* **2004**, 104, 6147.
- [5] M. Hong, E. Y.-X. Chen, *Nat. Chem.* **2016**, 8.
- [6] L. E. Chile, P. Mehrkhodavandi, S. G. Hatzikiriakos, *Macromolecules* **2016**, 49, 909.
- [7] M. Cheng, A. B. Attygalle, E. B. Lobkovsky, G. W. Coates, *J. Am. Chem. Soc.* **1999**, 121, 11583.
- [8] J.-C. Buffet, A. N. Martin, M. Kol, J. Okuda, *Polym. Chem.* **2011**, 2, 2378.
- [9] T. M. Ovitt, G. W. Coates, *J. Am. Chem. Soc.* **1999**, 121, 4072.
- [10] M. S. Taylor, E. N. Jacobsen, *J. Am. Chem. Soc.* **2004**, 126, 10558.
- [11] G. D. Joly, E. N. Jacobsen, *J. Am. Chem. Soc.* **2004**, 126, 4102.
- [12] B. J. O. Keefe, M. A. Hillmyer, W. B. Tolman, *Dalt. Perspect.* **2001**, 2215.
- [13] H. R. Kricheldorf, I. Kreiser-Saunders, A. Stricker, *Macromolecules* **2000**, 33, 702.
- [14] J. Coudane, C. Ustariz-Peyret, G. Schwach, M. Vert, *J. Polym. Sci. Part A Polym. Chem.* **1997**, 35, 1651.
- [15] N. Spassky, M. Wisniewski, C. Pluta, A. Le Borgne, *Macromol. Chem. Phys.* **1996**, 197, 2627.
- [16] W. N. Ottou, H. Sardon, D. Mecerreyes, J. Vignolle, D. Taton, *Prog. Polym. Sci.* **2016**, 56, 64.
- [17] M. K. Kiesewetter, E. J. Shin, J. L. Hedrick, R. M. Waymouth, *Macromolecules* **2010**, 43, 2093.
- [18] A. P. Dove, H. Li, R. C. Pratt, B. G. G. Lohmeijer, D. A. Culkin, R. M. Waymouth, J. L. Hedrick, *Chem. Commun.* **2006**, 2881.
- [19] M. Fèvre, J. Pinaud, Y. Gnanou, J. Vignolle, D. Taton, *Chem. Soc. Rev.* **2013**, 42, 2142.
- [20] L. Zhang, F. Nederberg, J. M. Messman, R. C. Pratt, J. L. Hedrick, C. G. Wade, *J. Am. Chem. Soc.* **2007**, 129, 12610.
- [21] K. Makiguchi, T. Yamanaka, T. Kakuchi, M. Terada, T. Satoh, *Chem. Commun.* **2014**, 50, 2883.
- [22] A. Sanchez-Sanchez, I. Rivilla, M. Agirre, A. Basterretxea, A. Etxeberria, A. Veloso, H. Sardon, D. Mecerreyes, F. P. Cossío, *J. Am. Chem. Soc.* **2017**, 139, 4805.
- [23] B. Orhan, M. J.-L. Tschan, A.-L. Wirotius, A. P. Dove, O. Coulembier, D. Taton, *ACS Macro Lett.* **2018**, 1413.
- [24] Z. Kan, W. Luo, T. Shi, C. Wei, B. Han, D. Zheng, S. Liu, *Front. Chem.* **2018**, 6, 1.
- [25] B. List, R. A. Lerner, C. F. Barbas III, *J. Am. Chem. Soc.* **2000**, 122, 2395.
- [26] A. G. Doyle, E. N. Jacobsen, *Chem. Rev.* **2007**, 107, 5713.
- [27] M. S. Taylor, E. N. Jacobsen, *Angew. Chemie* **2006**, 45, 1520.
- [28] T. Akiyama, J. Itoh, K. Yokota, K. Fuchibe, *Angew. Chemie - Int. Ed.* **2004**, 43, 1566.
- [29] S. Hoffmann, A. M. Seayad, B. List, *Angew. Chemie - Int. Ed.* **2005**, 44, 7424.
- [30] R. I. Storer, D. E. Carrera, Y. Ni, D. W. C. MacMillan, *J. Am. Chem. Soc.* **2006**, 128, 84.
- [31] Z. Zhang, P. R. Schreiner, *Chem. Soc. Rev.* **2009**, 38, 1187.
- [32] J. F. Brière, S. Oudeyer, V. Dalla, V. Levacher, *Chem. Soc. Rev.* **2012**, 41, 1696.
- [33] Y. Takemoto, *Chem. Pharm. Bull.* **2010**, 58, 593.
- [34] K. Asano, S. Matsubara, *Org. Lett.* **2012**, 14, 1620.
- [35] J. Bai, L. Wang, L. Peng, Y. Guo, L. Jia, F. Tian, G. He, X. Xu, L. Wang, **2012**.

- [36] F. Zhong, J. Luo, G. Y. Chen, X. Dou, Y. Lu, *J. Am. Chem. Soc.* **2012**, *134*, 10222.
- [37] E. M. O. Yeboah, S. O. Yeboah, G. S. Singh, *Tetrahedron* **2011**, *67*, 1725.
- [38] T. Marcelli, H. Hiemstra, *Synth.* **2012**, *44*, 2114.
- [39] M. S. Sigman, E. N. Jacobsen, *J. Am. Chem. Soc.* **1998**, *120*, 4901.
- [40] S. Reaction, M. S. Sigman, P. Vachal, E. N. Jacobsen, *Angew. Chem. Int. Ed.* **2000**, 1336.
- [41] P. Vachal, E. N. Jacobsen, *Org. Lett.* **2000**, *2*, 867.
- [42] P. Vachal, E. N. Jacobsen, *J. Am. Chem. Soc.* **2002**, *124*, 10012.
- [43] A. G. Wenzel, E. N. Jacobsen, *J. Am. Chem. Soc.* **2002**, *124*, 12964.
- [44] T. P. Yoon, E. N. Jacobsen, *Angew. Chemie - Int. Ed.* **2005**, *44*, 466.
- [45] D. Seidel, *Synlett* **2014**, *25*, 783.
- [46] C. K. De, N. Mittal, D. Seidel, *J. Am. Chem. Soc.* **2011**, 16802.
- [47] M. P. Lalonde, M. A. McGowan, N. S. Rajapaksa, E. N. Jacobsen, *J. Am. Chem. Soc.* **2013**, *135*, 1891.
- [48] X. Chen, Z. H. Qi, S. Y. Zhang, L. P. Kong, Y. Wang, X. W. Wang, *Org. Lett.* **2015**, *17*, 42.
- [49] T. Okino, Y. Hoashi, Y. Takemoto, *J. Am. Chem. Soc.* **2003**, *125*, 12672.
- [50] F. E. Held, S. B. Tsogoeva, *Catal. Sci. Technol.* **2016**, *6*, 645.
- [51] A. P. Dove, R. C. Pratt, B. G. G. Lohmeijer, R. M. Waymouth, J. L. Hedrick, *J. Am. Chem. Soc.* **2005**, *127*, 13798.
- [52] B. G. G. Lohmeijer, R. C. Pratt, F. Leibfarth, J. W. Logan, D. A. Long, A. P. Dove, F. Nederberg, J. Choi, C. Wade, R. M. Waymouth, J. L. Hedrick, *Macromolecules* **2006**, *39*, 8574.
- [53] N. U. Dharmaratne, J. U. Pothupitiya, M. K. Kiesewetter, *Org. Biomol. Chem.* **2019**, *17*, 3305.
- [54] R. C. Pratt, B. G. G. Lohmeijer, D. A. Long, P. N. P. Lundberg, A. P. Dove, H. Li, C. G. Wade, R. M. Waymouth, J. L. Hedrick, *Macromolecules* **2006**, *39*, 7863.
- [55] S. M. Quan, X. Wang, R. Zhang, P. L. Diaconescu, *Macromolecules* **2016**, *49*, 6768.
- [56] B. Lin, R. M. Waymouth, *J. Am. Chem. Soc.* **2017**, *139*, 1645.
- [57] S. S. Spink, O. I. Kazakov, E. T. Kiesewetter, M. K. Kiesewetter, *Macromolecules* **2015**, *48*, 6127.
- [58] K. V. Fastnacht, S. S. Spink, N. U. Dharmaratne, J. U. Pothupitiya, P. P. Datta, E. T. Kiesewetter, M. K. Kiesewetter, *ACS Macro Lett.* **2016**, *5*, 982.
- [59] X. Zhang, M. Fevre, G. O. Jones, R. M. Waymouth, *Chem. Rev.* **2017**, 839.
- [60] J. U. Pothupitiya, N. U. Dharmaratne, T. M. M. Jouaneh, K. V. Fastnacht, D. N. Coderre, M. K. Kiesewetter, *Macromolecules* **2017**, *50*, 8948.
- [61] D. N. Coderre, K. V. Fastnacht, T. J. Wright, N. U. Dharmaratne, M. K. Kiesewetter, *Macromolecules* **2018**, acs.macromol.8b02219.
- [62] D. A. Culkin, W. Jeong, S. Csihony, E. D. Gomez, N. P. Balsara, J. L. Hedrick, R. M. Waymouth, *Angew. Chemie - Int. Ed.* **2007**, *46*, 2627.
- [63] G. Nyce, T. Glauser, E. F. Connor, A. Möck, R. M. Waymouth, J. L. Hedrick, *J. Am. Chem. Soc.* **2003**, *125*, 3046.
- [64] H. A. Brown, R. M. Waymouth, *Acc. Chem. Res.* **2013**, *46*, 2585.
- [65] R. C. Pratt, B. G. G. Lohmeijer, D. A. Long, R. M. Waymouth, J. L. Hedrick, *J. Am. Chem. Soc.* **2006**, *128*, 4556.
- [66] L. Zhang, F. Nederberg, R. C. Pratt, R. M. Waymouth, J. L. Hedrick, C. G. Wade, *Macromolecules* **2007**, *40*, 4154.
- [67] H. A. Brown, A. G. De Crisci, J. L. Hedrick, R. M. Waymouth, *ACS Macro Lett.* **2012**, *1*, 1113.
- [68] X. Zhang, R. M. Waymouth, *ACS Macro Lett.* **2014**, *3*, 1024.

- [69] G. M. Miyake, E. Y. Chen, **2011**, 4116.
- [70] R. Todd, G. Rubio, D. Hall, S. Tempelaar, A. P. Dove, *Chem. Sci.* **2013**.
- [71] G. Jakab, C. Tancon, Z. Zhang, K. M. Lippert, P. R. Schreiner, *Org. Lett.* **2012**, *14*, 1724.
- [72] M. Blain, H. Yau, L. Jean-Gérard, R. Auvergne, D. Benazet, P. R. Schreiner, S. Caillol, B. Andrioletti, *ChemSusChem* **2016**, *9*, 2269.
- [73] O. Coulembier, T. Josse, B. Guillermin, P. Gerbaux, P. Dubois, *Chem. Commun. (Camb)*. **2012**, *48*, 11695.
- [74] C. Pérez-Casas, A. K. Yatsimirsky, *J. Org. Chem.* **2008**, *73*, 2275.
- [75] O. Coulembier, D. P. Sanders, A. Nelson, A. N. Hollenbeck, H. W. Horn, J. E. Rice, M. Fujiwara, P. Dubois, J. L. Hedrick, *Angew. Chem. Int. Ed.* **2009**, *48*, 5170.
- [76] S. Gazeau-Bureau, D. Delcroix, B. Martín-Vaca, D. Bourissou, C. Navarro, S. Magnet, *Macromolecules* **2008**, *41*, 3782.
- [77] D. Delcroix, A. Couffin, N. Susperregui, C. Navarro, L. Maron, B. Martin-Vaca, D. Bourissou, *Polym. Chem.* **2011**, *2*, 2249.
- [78] K. Makiguchi, T. Satoh, T. Kakuchi, *Macromolecules* **2011**, *44*, 1999.
- [79] D. J. Coady, K. Fukushima, H. W. Horn, J. E. Rice, J. L. Hedrick, *Chem. Commun.* **2011**, *47*, 3105.
- [80] O. Coulembier, T. Josse, B. Guillermin, P. Gerbaux, P. Dubois, *Chem. Commun.* **2012**, *48*, 11695.
- [81] T. M. Ovitt, G. W. Coates, *J. Am. Chem. Soc.* **2002**, *124*, 1316.
- [82] D. Arbeiter, K. Schumann, O. Sahmel, T. Eickner, K.-P. Schmitz, N. Grabow, *Curr. Dir. Biomed. Eng.* **2016**, *2*, 27.
- [83] K. Jamshidi, S.-H. Hyon, Y. Ikada, *Polymer (Guildf)*. **1988**, *29*, 2229.
- [84] B. M. Chamberlain, M. Cheng, D. R. Moore, T. M. Ovitt, E. B. Lobkovsky, G. W. Coates, *J. Am. Chem. Soc.* **2001**, *123*, 3229.
- [85] O. Coulembier, P. Dubois, *J. Polym. Sci. Part A Polym. Chem.* **2012**, *50*, 1672.
- [86] J. Kasperczyk, M. Bero, *Makromol. Chem.* **1993**, *194*, 913.
- [87] K. M. Thakur, R. T. Kean, E. S. Hall, J. J. Kolstad, T. A. Lindgren, M. A. Doscotch, J. I. Siepmann, E. J. Munson, *Macromolecules* **1997**, *30*, 2422.
- [88] K. A. M. Thakur, R. T. Kean, M. T. Zell, B. E. Padden, E. J. Munson, *Chem. Commun.* **1998**, 1913.
- [89] K. a. M. Thakur, R. T. Kean, E. S. Hall, J. J. Kolstad, E. J. Munson, *Macromolecules* **1998**, *31*, 1487.

## Chapter 5.

### Selective ROP of *rac*- and *meso*-Lactides from TBD under Cryogenic Conditions: A Tripartite Tetris Interaction Explanation



**Keywords:** Stereoselective • Lactide • TBD • Ring-Opening Polymerization

## Chapter 5

# Selective ROP of *rac*- and *meso*-Lactides from TBD under Cryogenic Conditions: A Tripartite Tetris Interaction Explanation

### Contents

<b>Chapter 5. Selective ROP of <i>rac</i>- and <i>meso</i>-Lactides from TBD under Cryogenic Conditions: A Tripartite Tetris Interaction Explanation.....</b>	<b>199</b>
5.1. Introduction.....	201
5.2. Results and Discussion .....	203
5.2.1. Polymerization procedure .....	203
5.2.2. Polymer Characterization.....	205
5.2.3. Analysis of the microstructure of PLA derived from achiral TBD....	205
5.2.4. Theoretical Investigations .....	207
5.3. Conclusions and perspectives .....	212
5.4. Experimental and supporting informations .....	213
5.5. References.....	220

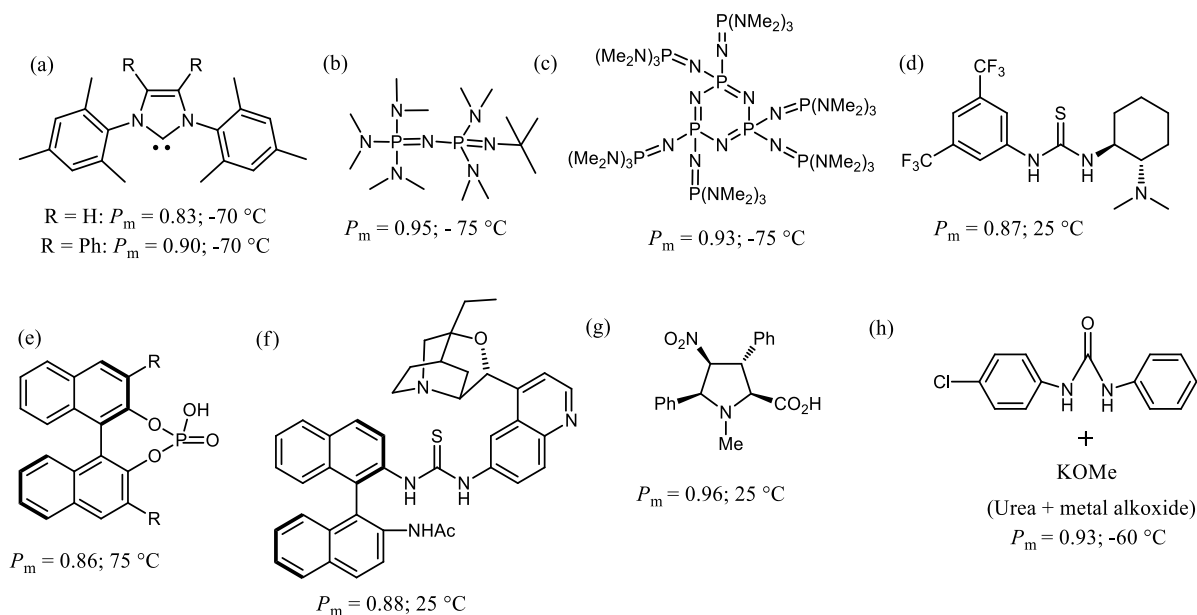


## 5.1. Introduction

Poly(lactide) (PLA) is a versatile, bioplastic, raw material made from renewable resources. PLA can be synthesized *via* polycondensation of lactic acid however, ring-opening polymerization (ROP) of lactide (LA) is by far preferred on account of the more facile access to higher molar mass polymers with control over the molecular parameters and end groups.<sup>[1]</sup> LA possesses two stereocenters conferring it three distinct isomers: *R,R*-LA (*D*-LA), *S,S*-LA (*L*-LA) and *R,S*-LA (*meso*-LA). In addition to the three diastereomers, a commercially available racemate of *D*- and *L*-LA also exists as *rac*-LA. Because the chemical and physical properties of PLA are drastically affected by its tacticity,<sup>[2]</sup> the nature of the enantiopure monomer involved in the ROP process or the application of stereocontrolled polymerizations in which stereoregular polymers result from diastereomeric mixtures of LA, are of high importance.

During the past decades, there has been significant emphasis placed on the preparation of catalysts that are able to produce isotactic PLA directly from *rac*-LA.<sup>[3,4]</sup> The isoselective ROP of *rac*-LA is by far dominated by metal-salts and coordination complexes that operate by a coordination-insertion mechanism. Generally, the significant difference in the rates of insertion of both *D*- and *L*-LA is created by the association of the ligand system and the growing polymer chain end. While excellent stereocontrol is achieved by those catalysts, they are commonly complex and costly to prepare which, in part, motivated the development of simple, metal-free organocatalytic systems.<sup>[5]</sup>

To date, only a handful of studies of stereocontrolled ROPs of *rac*-LA using either chiral or achiral organo-based catalysts have been reported.<sup>[6–15]</sup> Chiral organo-based catalysts, including binaphthol-type phosphoric acids (Figure 5.1, **e**),  $\beta$ -isocupreidine/thiourea/chiral binaphthylamines (Figure 5.1, **f**), Takemoto's catalyst (Figure 5.1, **d**) and densely substituted proline-type amino acids (Figure 5.1, **g**) are known to produce isotactic PLA, presenting a probability of isotactic dyad ( $P_m$ ) of 0.82 – 0.96, for ROP reactions performed at 25 to 85°C (Figure 5.1).<sup>[10–15]</sup> Comparatively, achiral catalysts, including *N*-heterocyclic carbenes (Figure 5.1, **a**)<sup>[6,7]</sup> and phosphazenes (Figure 5.1, **b** and **c**)<sup>[8,9]</sup> necessitate cryogenic conditions to increase the stereoselectivity for ROP of *rac*-LA. In these systems, ROP at low temperatures (-75 °C) resulted in a marked increase in isotacticity with  $P_m$  values between 0.83 and 0.95 (Figure 5.1).



**Figure 5.1.** Structures of chiral and achiral catalysts employed for the stereoselective ROP of *rac*-LA.

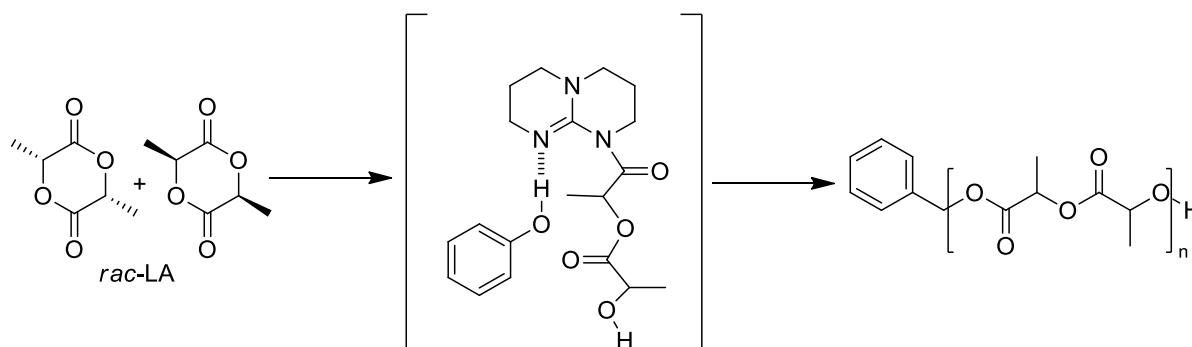
In all cases, the authors postulated that stereocontrol is the result of a sterically hindrance at the propagating chain end involving a chain-end control (CEC) mechanism - although no mechanistic investigations were performed to confirm that hypothesis. While several of these catalysts prove very sterically-demanding or chiral bases, the high level of stereocontrol at cryogenic temperatures observed with 1-*tert*-butyl-2,2,4,4,4-pentakis(dimethylamino)-2 $\Lambda^5$ ,4 $\Lambda^5$ -catenadi(phosphazene), **b**, raised question about the primary reason for such high levels of stereocontrol. Polylactide (PLA) is a commercially available biodegradable and bio-sourced polymer for which properties depend on its stereochemistry. In this chapter, a new means to stereoselectively control both *rac*- and *meso*-LA ROPs with achiral triazabicyclo[4.4.0]dec-5-ene (TBD) under cryogenic (at  $-75\text{ }^{\circ}\text{C}$ ) conditions is described. TBD polymerizes *rac*-LA to form highly isotactic PLA, while *meso*-LA yields heterotactic PLA. Considering the size and geometry of the TBD molecule, along with its mode of action, we demonstrate that the stereocontrol of the cryogenic-based ROP comes from a perfect imbrication of both chiral LA and the propagating chiral end-group both in interaction with the TBD catalyst.<sup>[9,16]</sup>

## 5.2. Results and Discussion

### 5.2.1. Polymerization procedure

Extending these concepts, we postulated that other non-sterically encumbered and achiral bases could also mediate the stereoselective ROP of *rac*-LA at cryogenic temperatures in toluene. To test this hypothesis, we selected TBD as organic catalyst as it fits the criteria and is highly active for the ROP of LA.<sup>[17,18]</sup> At the outset, the ROP of *rac*-LA was studied in toluene at -75°C for an initial benzyl alcohol (BnOH)-to-TBD molar ratio of 10 and an initial *rac*-LA concentration of 0.08 M ( $[rac\text{-LA}]_0/[BnOH]_0 = 100$ , Table 5.1, entries 1-2).

TBD is uniquely capable of inserting into the ester of the cyclic ester monomer, and subsequent hydrogen bonding of the adjacent nitrogen to an incoming alcohol completes a transesterification cycle to form the polyester (Scheme 5.1).<sup>[18]</sup> Table 5.1 summarizes the results of polymerizations conducted by TBD catalyst.



**Scheme 5.1.** Ring-Opening Polymerization of *rac*-LA through dual activation by TBD

**Table 5.1.** Ring-opening polymerizations of *rac*-LA in toluene at -75°C<sup>a</sup>

<i>Entry</i>	<i>Polym. Time (min)</i>	<i>Conv. (%)<sup>b</sup></i>	<i>M<sub>n,SEC</sub> [g.mol<sup>-1</sup>]<sup>b</sup></i>	<i>Đ<sub>M</sub><sup>b</sup></i>	<i>P<sub>m</sub><sup>c</sup></i>	<i>T<sub>g</sub> [°C]<sup>d</sup></i>	<i>T<sub>m</sub> [°C]<sup>d</sup></i>	<i>ΔH (J.g<sup>-1</sup>)<sup>d</sup></i>
1	50	17	2600	1.09	0.84	44	157	18.9
2	120	30	4200	1.09	0.80	48	155	16.0
3	20	42	7000	1.15	0.85	52	144	26.6
4	30	77	11000	1.25	0.85	51	145	8.5

[a] Entries 1-2 : [*rac*-LA]<sub>0</sub> = 0.08M, [*rac*-LA]<sub>0</sub>/[BnOH]<sub>0</sub>/[TBD]<sub>0</sub> = 100/1/0.1 ; entries 3-4 : [*rac*-LA]<sub>0</sub> = 0.22M, [*rac*-LA]<sub>0</sub>/[BnOH]<sub>0</sub>/[TBD]<sub>0</sub> = 100/1/1 [b] Determined by SEC at 35°C in THF relative to PS standards, using a correcting factor of 0.58.<sup>[19]</sup> [c] Determined by homonuclear decoupled <sup>1</sup>H NMR. [d] Determined by DSC.

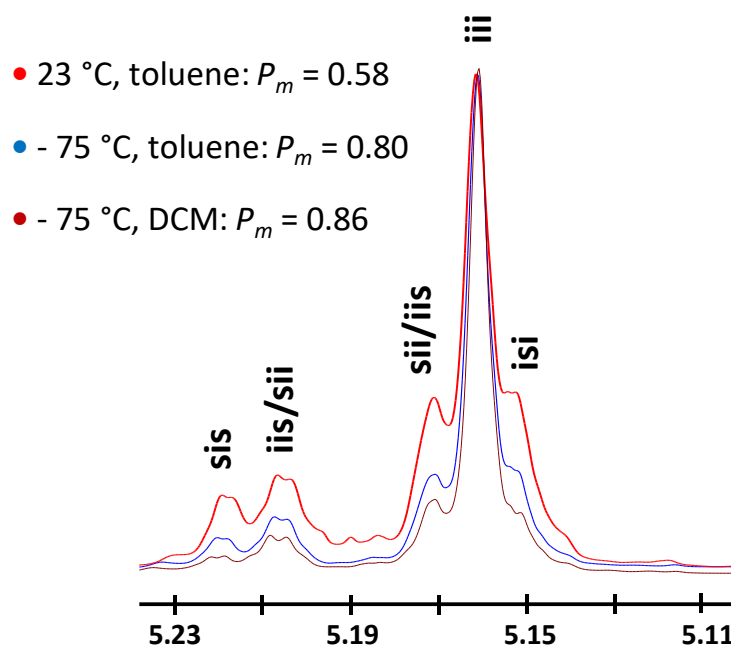
### 5.2.2. Polymer Characterization

The ROP of *rac*-LA was studied in toluene at -75°C for an initial BnOH-to-TBD molar ratio of 10 and an initial *rac*-LA concentration of 0.08M ( $[rac\text{-LA}]_0/[BnOH]_0 = 100$ , Table 5.1, entries 1-2). The chemical structures of the resulting polymers were assigned by  $^1\text{H}$  NMR measurement.  $^1\text{H}$  NMR and homonuclear decoupled  $^1\text{H}$  NMR spectroscopic measurements were performed at room temperature on Bruker Advance instrument at 400 MHz.  $\text{CDCl}_3$  was used as an internal reference ( $\delta = 7.26$ ). The characteristic signals of PLA were observed in the range from 1.53 to 1.61 and from 5.11 to 5.23, which were attributable to the methyl and methine protons, respectively.

Conversion is determined by SEC analysis on the crude medium while  $P_m$ ,  $T_g$  and  $T_m$  values are obtained after precipitation of the crude medium in cold methanol. The ROP of *rac*-LA in such conditions is slow requiring 2 h to reach an overall monomer conversion of 30% (Table 5.1, entry 2). However, the resulting polymerization displays high levels of control with a linear relationship between experimental number-average molar masses ( $M_n$ , SEC) and monomer conversion. The resulting PLAs also display dispersity values ( $D_M = M_w/M_n$ ) less than 1.1.

### 5.2.3. Analysis of the microstructure of PLA derived from achiral TBD

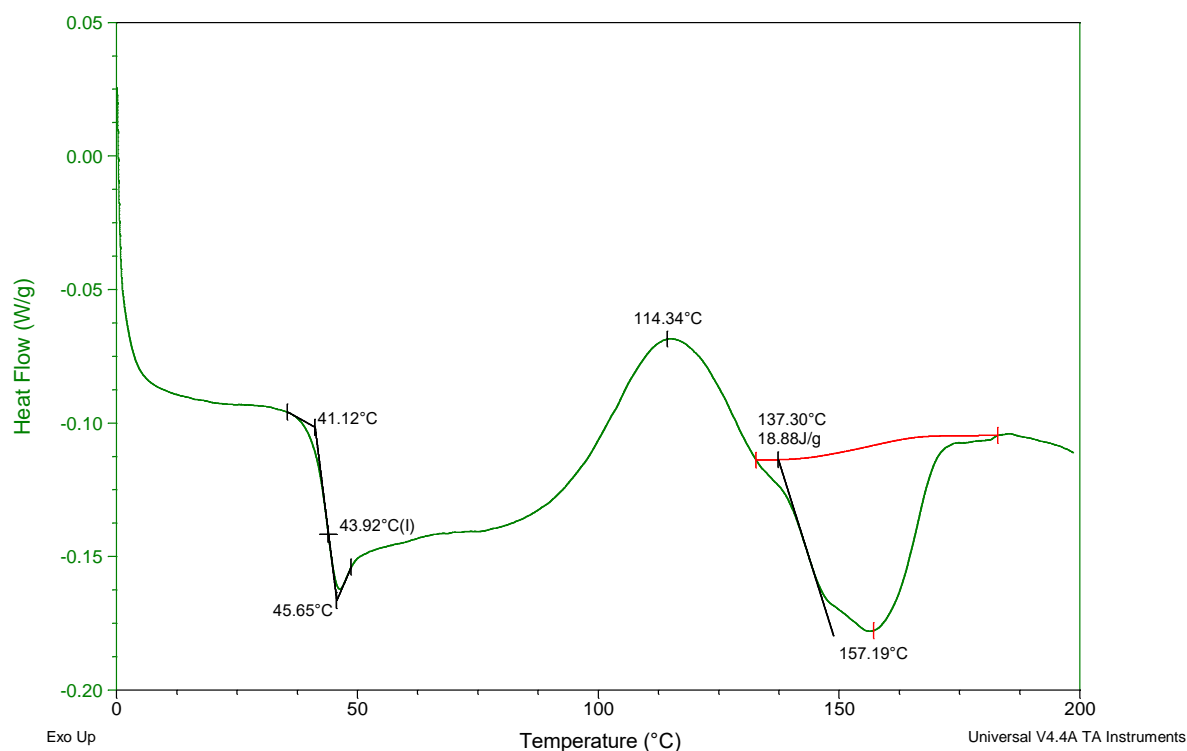
Homonuclear decoupled  $^1\text{H}$  NMR spectroscopy of the resulting materials revealed the formation of isotactic materials presenting  $P_m$  values as high as 0.8 – 0.84 (Figure 5.2). Consistent with the semicrystalline isotactic PLA, the polymers showed a melting transition at *ca.* 155 – 157 °C on their differential scanning calorimetry (DSC) thermograms (Figure 5.3).



**Figure 5.2.** Methine region of homonuclear decoupled  $^1\text{H}$ -NMR spectra of poly(*rac*-LA) obtained at different polymerization temperatures using TBD as catalyst (X-axis in ppm).

As control experiments, the ROP of LA in toluene with TBD as catalyst at 23 °C resulted in a PLA with a  $M_n$  of 4500 g.mol $^{-1}$  and a  $D_M$  of 1.14 at 48% conversion after 20 s. The reaction time was voluntary limited to avoid possible transesterification reactions. As expected,  $P_m$  decreased from 0.80 for PLA prepared at -75 °C (entry 2, Table 5.1) to 0.58 for PLA prepared at 23 °C (Figure 5.2). The low level of isotacticity was further confirmed by DSC with the absence of a melting transition.

In combination with a higher TBD initial content ( $[\text{BnOH}]_0/[\text{TBD}]_0 = 1$ ), the use of a  $[\text{rac-LA}]_0$  of 0.22 M was effective to mediate a faster seteroselective ROP resulting in PLAs of high isotacticity with  $P_m$  values of 0.85 (entries 3-4, Table 1).



**Figure 5.3.** DSC thermogram of the PLA obtained by TBD at  $-75\text{ }^{\circ}\text{C}$  (Table 5.1, entry 1).

Hao et al. reported the solubility and dissolution thermodynamic data of LA in different pure solvents but no accurate solubility data were provided to compare the different LA isomers in toluene at cryogenic temperatures such as  $-70\text{ }^{\circ}\text{C}$ .<sup>[20]</sup> Accepting the idea that the stereocontrolled ROP of *rac*-LA occurs through kinetic resolution relies on the assumption that both *L*- and *D*-isomers dissolve continuously and synchronously during the ROP process. To verify this assumption, we investigated the cryogenic ROP ( $-75\text{ }^{\circ}\text{C}$ ) of both *D*- and *L*-LA using TBD as catalyst in toluene. Polymerizations were initiated from achiral BnOH for a targeted polymerization degree ( $\text{DP} = [\text{LA}]_0/[\text{BnOH}]_0$ ) of 68 ( $[\text{LA}]_0 = 0.11$ ;  $[\text{BnOH}]_0/[\text{TBD}]_0 = 1/0.1$ ). After 10 minutes, the reactions reached conversions of  $77 (\pm 4)\%$  and  $63 (\pm 3)\%$  for *L*- and *D*-LA ROPs, respectively.

#### 5.2.4. Theoretical Investigations

To estimate the relative solubilities of *L*-LA and *D*-LA in toluene, the Cohesive Energy Density (CED) method is used, as implemented in the Materials Studio 6.0 package, which is based on the estimation and comparison of the Hansen solubility parameters of both the solvent and solute.<sup>[21,22]</sup>

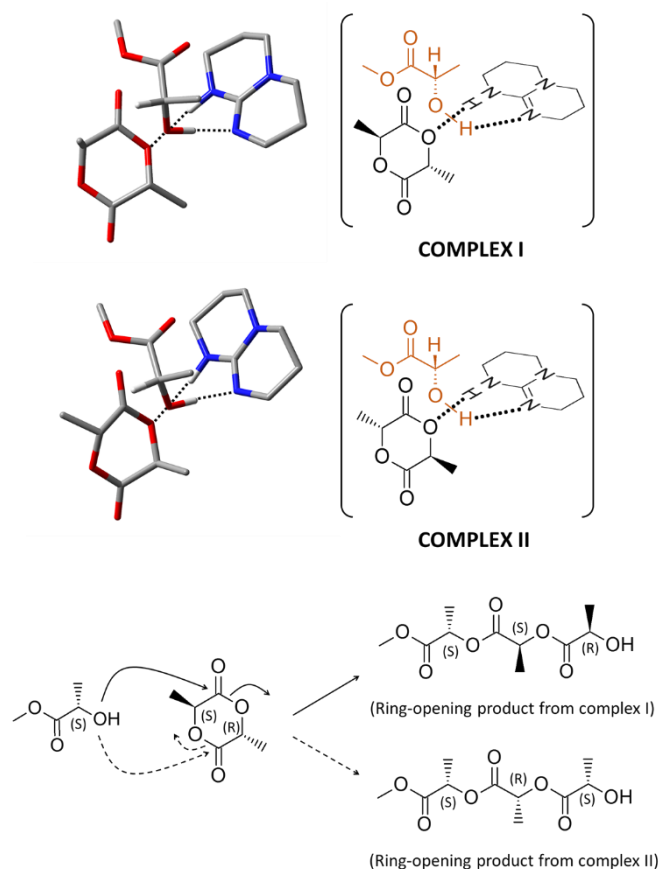
Since both enantiomers should present the same solubility and reactivity towards the catalytic initiating/propagating system, we inspected whether the slight difference in conversion could come from the different solubilities of *L*- and *D*-LA in toluene at -75 °C. Through molecular dynamics simulations, we next evaluated the relative solubilities of *L*-LA and *D*-LA in toluene by computing the Hansen components of the Hildebrand solubility parameter at -75 °C following the Cohesive Energy Density (CED) approach (See Experimental Part).<sup>[21]</sup> These calculations revealed that: (i) both compounds were poorly soluble in toluene, their Relative Energy Difference (RED) parameter being much larger than 1 (complex 1, scheme 5.2); (ii) their (very low) solubility was found basically identical. These results allowed us to rule out a difference in solubility as being the origin of the differences observed in the ROP of *L*- and *D*-LA.

Another explanation for the stereoselectivity related to a difference in reactivity of TBD towards either *L*- or *D*-stereogenic centre. To this end, a cryogenic polymerization of *meso*-lactide in toluene was performed ( $[meso\text{-lactide}]_0/[BnOH]_0/[TBD]_0 = 100/1/1$ ). *Meso*-LA has one *L*- and one *D*-centre and hence both are in equal concentration in the polymerization mixture. The polymer obtained ( $M_{n, SEC} = 17200 \text{ g.mol}^{-1}$ ;  $\bar{D}_M = 1.24$ ) proved to be highly heterotactic ( $P_m = 0.80$ ), supporting that the selectivity during the ROP of *rac*-LA was not due to the enantiomer solubility. In the case of the *meso*-LA, indeed, both the *R* and *S* stereocenters are equally soluble, hence an atactic polymer would have been achieved without any catalyst control.

To further confirm the absence of solubility as a factor that could determine the stereocontrol over the polymerization process, toluene was substituted by DCM in which *rac*-LA is highly soluble. With a ratio of 100 : 1 : 0.1 for  $[rac\text{-LA}]_0/[BnOH]_0/[TBD]_0$  ( $[rac\text{-LA}]_0 = 0.08\text{M}$ ), the monomer was almost quantitatively converted within 1 h at -75 °C (conv.  $\sim 0.9$ ). The produced PLA possessed a  $M_{n, SEC}$  of  $12000 \text{ g.mol}^{-1}$  with a narrow dispersity (1.09). As in the polymerizations carried out in toluene, a high level of isotacticity was confirmed by homonuclear decoupled  $^1\text{H}$  NMR spectroscopy ( $P_m = 0.86$ , Figure 5.2) and DSC analysis ( $T_g = 58.6 \text{ °C}$ ,  $T_m = 158.5 \text{ °C}$ ,  $\Delta H_m = 29.3 \text{ J.g}^{-1}$ ). Such results indicate that the selectivity observed by using TBD as catalyst under cryogenic conditions was not related to the nature of the solvent or any isomer solubility effect. We thus hypothesized that the unexpected stereoselectivity arises from intermolecular interactions between the catalyst, chain end and monomer.



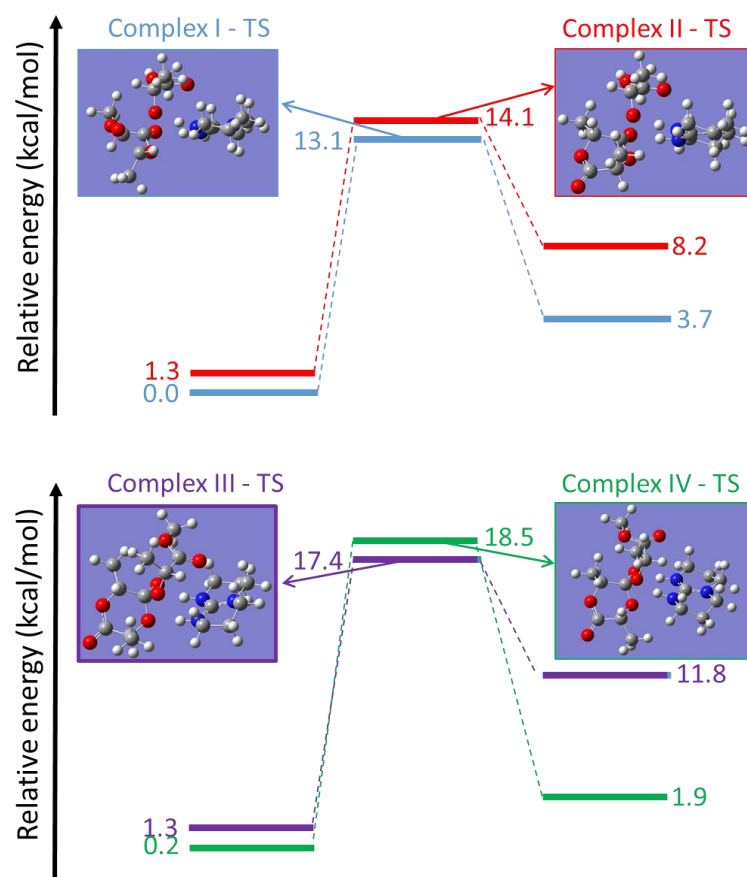
Considering the size and geometry of TBD, along with its mode of action, proceeding through concurrent activation of both monomer and initiating/propagating alcohol,<sup>[23]</sup> we envisioned that the stereocontrol of the cryogenic-based ROP was due to a perfect tetris-based imbrication of both chiral LA and propagating chiral end-group both being in interaction with the TBD catalyst. To confirm this hypothesis, the reaction profiles corresponding to the first step of the ROP process have been simulated at the Density Functional Theory (DFT) level using the  $\omega$ B97XD functional and the 6-31G\*\* basis set (see experimental part for the details). The simulations were performed by using the methyl (*L*)-lactate as (*S*) chiral initiator and considering two possible complexes formed between the *meso*-lactide, the TBD and the (*S*) chiral alcohol. The complex corresponding to the nucleophilic attack of the (*S*) alcohol on the carbonyl carbon adjacent to the (*S*)-stereocenter of the *meso*-lactide and that will give rise to a (*R*) chiral alcohol after ring-opening is referred as complex I. The complex corresponding to the nucleophilic attack of the (*S*) alcohol on the carbonyl carbon adjacent to the (*R*)-stereocenter of the *meso*-lactide and that will give rise to a (*S*) chiral alcohol after ring-opening is referred as complex II (Scheme 5.2).



**Scheme 5.2.** Ring-opening products obtained from complexes I and II formed between *meso*-LA, methyl (*L*)-lactate and TBD.

Prior to any reaction, both complexes exhibit strong H-bonding between the hydrogen of the alcohol group and the nitrogen of TBD, as well as between the hydrogen of TBD and the oxygen adjacent to the carbonyl group. Complex I is more stable by 1.3 kcal.mol<sup>-1</sup> compared to complex II (Figure S5.6) due to smaller steric constraints between the methyl group in  $\alpha$ -position of the carbonyl function and the alcohol moiety. This allows for stronger stabilizing interactions between the hydrogen of TBD and the oxygen adjacent to the carbonyl group.

The transition states corresponding to the attack of the oxygen of the alcohol on the carbonyl carbon of the *meso*-lactide were then optimized (Figure 5.4) and the energetic barriers estimated to -20.7 kcal/mol and -19.7 kcal/mol for complex I and complex II, respectively. Both transition states correspond to the concomitant attack of the oxygen of the alcohol on the carbonyl carbon, the transfer of the hydrogen atom of the alcohol to the nitrogen of the TBD and the departure of the hydrogen of the TBD to the oxygen atom of the carbonyl function. That the transition state of complex I lies 1 kcal.mol<sup>-1</sup> lower in energy than that of complex II suggest that the nucleophilic attack of a (*S*)-chiral alcohol will lead to a polymer chain bearing a (*R*)-chiral chain end. Note that a 1 kcal.mol<sup>-1</sup> energy difference between two structures at 198K translates, according to a Maxwell-Boltzmann distribution, into a population ratio of 93/7, in good agreement with our experimental results. The increased stability of the transition state of complex I originates from much reduced steric interactions between the attacking oxygen and the closest hydrogen atoms of *meso*-lactide.



**Figure 5.4.** DFT-calculated ( $\omega$ B97XD/6-31G\*\*) energy profiles corresponding to the nucleophilic attack of the oxygen of the alcohol on the carbonyl carbon for complexes I-II (top panel) and III-IV (bottom panel). All the energies (in kcal/mol) are relative to the complex I reactant energy. The optimized transition state geometries of all the complexes are also displayed.

Now, when considering the attack of the latter on another *meso*-lactide, we found similar results. The nucleophilic attack of a (*R*) chiral alcohol will lead preferentially to a new (*S*) chiral chain end; the height of the energetic barrier being 1.1 kcal/mol lower in energy (see Table S5.1). All together, these calculations allow rationalizing the observed heterotacticity of the polymer (resulting from isoselectivity) and therefore suggest that, when applied to *rac*-LA, one of the two isomers will be polymerized predominantly over the other one, consistent with our experimental results.

### 5.3. Conclusions and perspectives

In conclusion, a new means to stereocontrol both *rac*- and *meso*-LA ROPs with achiral TBD under cryogenic conditions is described in this chapter. We showed that an achiral catalyst as simple and readily available as TBD can efficiently induce the stereoselective ring-opening polymerization of *rac*- and *meso*-lactides, achieving a highly iso- and heterotactic

polylactide, respectively. To the best of our knowledge, TBD appears now as being the smallest achiral non-sterically encumbered catalyst for the stereoselective ROP of *rac*- and *meso*-LAs. Despite being studied at room temperature, in which a slight preference for isotacticity was reported ( $P_m = 0.58$ , confirmed through control experiments – Figure 5.2), the ROP of LA using TBD as catalyst has never been previously reported under cryogenic temperatures. Considering the size and geometry of the TBD molecule, we demonstrate that the stereocontrol of the cryogenic-based ROP comes from a perfect imbrication of both chiral LA and the propagating chiral end-group both in interaction with the TBD catalyst. The explanation for such performance, as proposed from combined experimental and computational results, lies in small differences in intermolecular interactions within the intermediate ‘monomer-catalyst-growing chain’ complex.

#### 5.4. Experimental and supporting informations

**Materials:** Benzyl alcohol (BnOH, from Sigma, 97%) was dried over calcium hydride for 48 h at room temperature and distilled under reduced pressure and stored in a glove box. *L*- and *D*-lactide (*L*- & *D*-LA, Purac) were recrystallized three times from dried toluene and stored in a glove box under dry nitrogen atmosphere before use. 1,5,7-Triazabicyclododecene (TBD, Acros) was dried under vacuum at 80°C for 12 hours and stored in a glove box. Toluene solvent was dried using a MBraun Solvent Purification System (model MB-SPS 800) equipped with alumina drying columns.

**Instrumentation:**  $^1\text{H}$  NMR and homonuclear decoupled  $^1\text{H}$  NMR measurements were performed at room temperature on Bruker Avance instrument at 400 MHz.  $\text{CDCl}_3$  was used as an internal reference ( $\delta=7.26$ ) and the relaxation time was fixed to 2 s. For homonuclear decoupled  $^1\text{H}$  NMR analysis, relaxation time was measured and fixed to 2.04 s. Samples were obtained in  $\text{CDCl}_3$  solutions with the decoupling pulse based on the methyl region ( $\sim 1.6$  ppm). In case of the well separation of methine region ( $\sim 5.00$ - $5.20$  ppm) global spectral deconvolution technique was implemented by attribution of five mesodyads based on both non-Bernoullian and Bernoullian statistics in case of the operated combination mechanism.

If the next inserted monomer unit is in the same stereoregularity with the previous one, this explains the term of the mesodyad. The probability value resulting from the ratio of the mesodyads creates the  $P_m$  value. Besides that,  $P_r$  has meaning of racemic enchainment, and  $P_m + P_r = 1$ . While  $P_m = 0.5$  indicates a random insertion pattern,  $P_m = 1.0$  indicates perfect retention. To sum up the mesodyad-referenced peaks (*mmm*, *mmr/rmm*) ratios provides  $P_m$  values of the polymers.

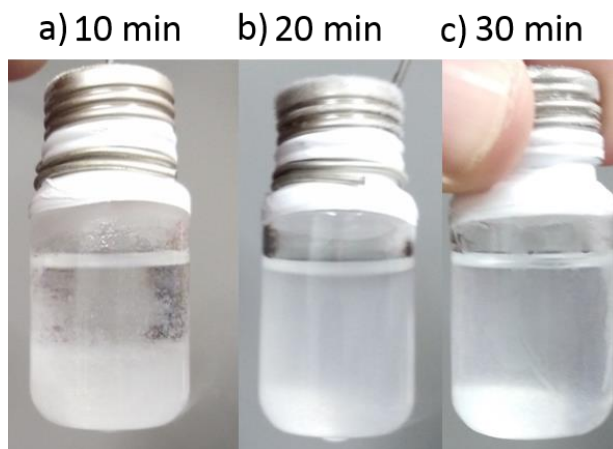
Size-exclusion chromatography (SEC) was performed under room temperature using tetrahydrofuran (THF) as an eluent at a flow rate of 1.0 mL/min. 5 mg/mL sample was used for each analysis. Calibration was performed with polystyrene standard (PS). Differential refractive index (RI) detector was used.  $M_n$  values which were obtained by SEC is multiplied by 0.565 correlation factor for PLA performed with PS standards corresponding to Mark-Houwink equation.

$T_g$ ,  $T_m$  and  $\Delta H_m$  values were analyzed by differential scanning calorimetry (DSC) belongs TA instruments. Polymeric samples were first heated from 25°C to 200°C at 10°C/min. All thermal datas were obtained from the first scan.

**General polymerization methods:** Table 5.1, entry 2: In a glove box ( $\text{H}_2\text{O} < 1\text{ ppm}$ ,  $\text{O}_2 < 0.1\text{ ppm}$ ), a first dried vial was charged by BnOH (7.5 mg, 0.069 mmol), TBD (9.6 mg, 0.069 mmol), 1 mL of dried toluene ( $[\text{BnOH}]_0 = 0.069\text{ M}$ ) and a magnetic bar. In a second dried vial, *L*- and *D*-LA (50 mg each, 34.7 mmol each) were solubilized in 3 mL of dried toluene ( $[\text{rac-LA}]_0 = 0.22\text{ M}$ ) at r.t., in presence of a magnetic bar (Figure S5.1). In a cold room ( $\sim 5^\circ\text{C}$ ), both vials were immersed in a cryogenic bath thermostated at  $-75^\circ\text{C}$ . After 10 minutes under stirring, 100  $\mu\text{L}$  of the alcohol solution ( $6.9 \times 10^{-6}\text{ mol}$ ) was quickly injected on the insoluble monomer medium (Figure S5.2a,  $[\text{rac-LA}]_0/[\text{BnOH}]_0/[\text{TBD}]_0 = 100/1/1$ ). In function of time, the initially insoluble medium becomes more and more soluble at  $-75^\circ\text{C}$ , attesting the good formation of the polymer (Figure S5.2b). After an appropriate reaction time, the medium is quenched by addition of cold heptane allowing both monomer and polymer to precipitate. Conversion is then determined by SEC analysis on the crude medium while  $P_m$ ,  $T_g$  and  $T_m$  values are obtained after precipitation of the crude medium in cold methanol.



**Figure S5.1.** Mixture of *L*- and *D*-LA (1/1 molar ratio) at  $23^\circ\text{C}$  ( $[\text{rac-LA}]_0 = 0.22\text{ M}$ )



**Figure S5.2.** Mixture of *L*- and *D*-LA (1/1 molar ratio) after a) 10 and b) 20 and c) 30 minutes of polymerization at  $-75^\circ\text{C}$

## Theoretical Investigations

### Cohesive Energy Density (CED) method

In practice, we performed molecular mechanics (MM) and molecular dynamics (MD) simulations on a unit cell containing either 66 molecules of toluene or 55 molecules of *L*-LA or *D*-LA that is replicated using periodic boundary conditions to mimic 3D infinite systems. All the MM/MD calculations have been performed with the Materials Studio 6.0 package using a force-field derived from Dreiding in which the default van der Waals parameters of hydrogen have been adjusted to reproduce experimental results.<sup>[24]</sup> We kept all default settings except that partial charges were set by the COMPASS force field, and the electrostatic term follows Coulomb's law ( $r^{-1}$ ) instead of the dressed potential in  $r^{-2}$  defined by default; the dielectric constant is set to 1 (vacuum).

Unit cells were first submitted to a high-temperature MD (NVT, 750 K, 100 ps, 12.5 Å cutoff) to remove any order from the box creation. Then the system was equilibrated for 250 ps at 298 K (NVT, 12.5 Å cutoff) and followed two successive MD in the NPT ensemble to compress and relax the system until densities converged (NPT, 298K 3 GPa and 10-4 GPa, 250 ps, Ewald summation method). In a next step, we lowered the MD temperature to 198 K for 300 ps with the same parameters. A final MD run was performed to analyze the solubility parameters (NPT, 198 K, 10-4 GPa, 300 ps, Ewald summation method) using the Cohesive Energy Density approach.

The Hansen solubility parameters ( $\delta_p$ ,  $\delta_d$ ,  $\delta_h$ ; p, d, and h stand for polar (electrostatic), dispersion (van der Waals) and h-bond, respectively) contributing to the Hildebrand solubility parameter  $\delta$  ( $\delta^2 = \delta_p^2 + \delta_d^2 + \delta_h^2$ ) are then calculated from the 100 snapshots of the last MD runs as follows:

$$\delta_k^2 = \left( \frac{\sum_{i=1}^n \langle E_i^k - E_c^k \rangle}{N_0 \langle V_i / n \rangle} \right)$$

where  $E_c^k$  is the average energy components of the condensed phase simulation unit cell,  $E_i^k$  the energy components of the individual molecules,  $V_c$  the volume of the unit cell,  $n$  the number of molecules,  $N_0$  the Avogadro's number,  $\langle \rangle$  states for time average values over the MD runs and  $k$  runs over coulomb (polar), van der Waals (dispersion) and hydrogen-bond components.

Once the Hansen parameters have been estimated for both toluene and *L*-LA and *D*-LA, the relative energy difference (RED) of the system has been calculated, assuming a radius  $R_0$  for the *L*-LA or *D*-LA monomer of  $\sim 2.7\text{\AA}$ , as follows:

$$RED = \frac{\sqrt{4(\delta_{d1} + \delta_{d2})^2 + (\delta_{p1} + \delta_{p2})^2 + (\delta_{h1} + \delta_{h2})^2}}{R_0}$$

A RED value equal to 1 means that the system will partially dissolve while values smaller [higher] than 1 means that the system will [not] dissolve.

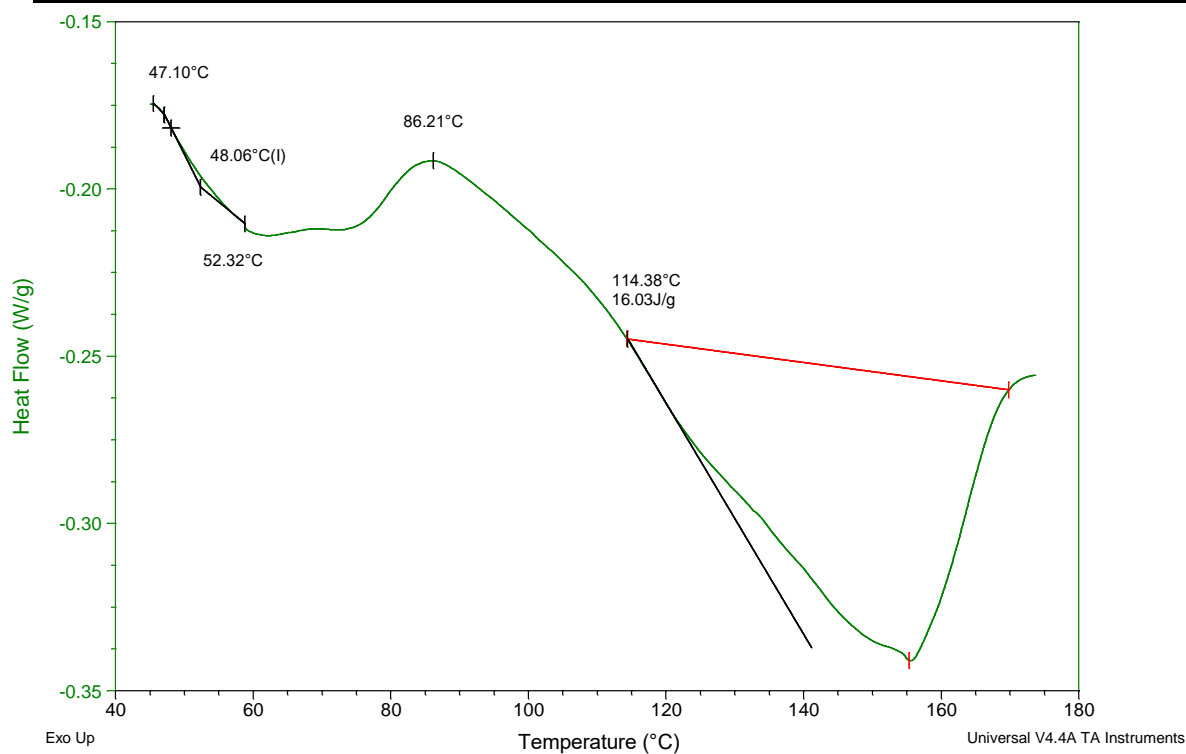
### Density Functional Theory (DFT) method

All the geometries of the reactants, transition states and products have been optimized at the Density Functional Theory (DFT) level using the  $\omega$ B97XD functional and a 6-31G\*\* basis set. Frequency calculations were performed on each optimized structure to confirm that (i) reactants and products correspond to minima on the potential energy surface and (ii) transitions states only have one imaginary frequency. Complex I corresponds to the nucleophilic attack of the methyl (*L*) lactate (referred as the (*S*) alcohol) on the carbonyl carbon of the *meso*-lactide which will give rise to a growing polymer chain bearing a (*R*)-chiral alcohol after ring-opening. Complex II corresponds to the nucleophilic attack of the methyl (*L*) lactate on the carbonyl carbon of the *meso*-lactide which will give rise to a growing polymer chain bearing a (*S*)-chiral alcohol after ring-opening. Complex III corresponds to the nucleophilic attack of the (*R*)-alcohol on the carbonyl carbon of the *meso*-lactide which will give rise to a growing polymer chain bearing a (*S*)-chiral alcohol after ring-opening, while complex IV corresponds to the nucleophilic attack of the (*R*)-alcohol on the carbonyl carbon of the *meso*-lactide which will give rise to a growing polymer chain bearing a (*R*)-chiral alcohol after ring-opening (Table S5.1).

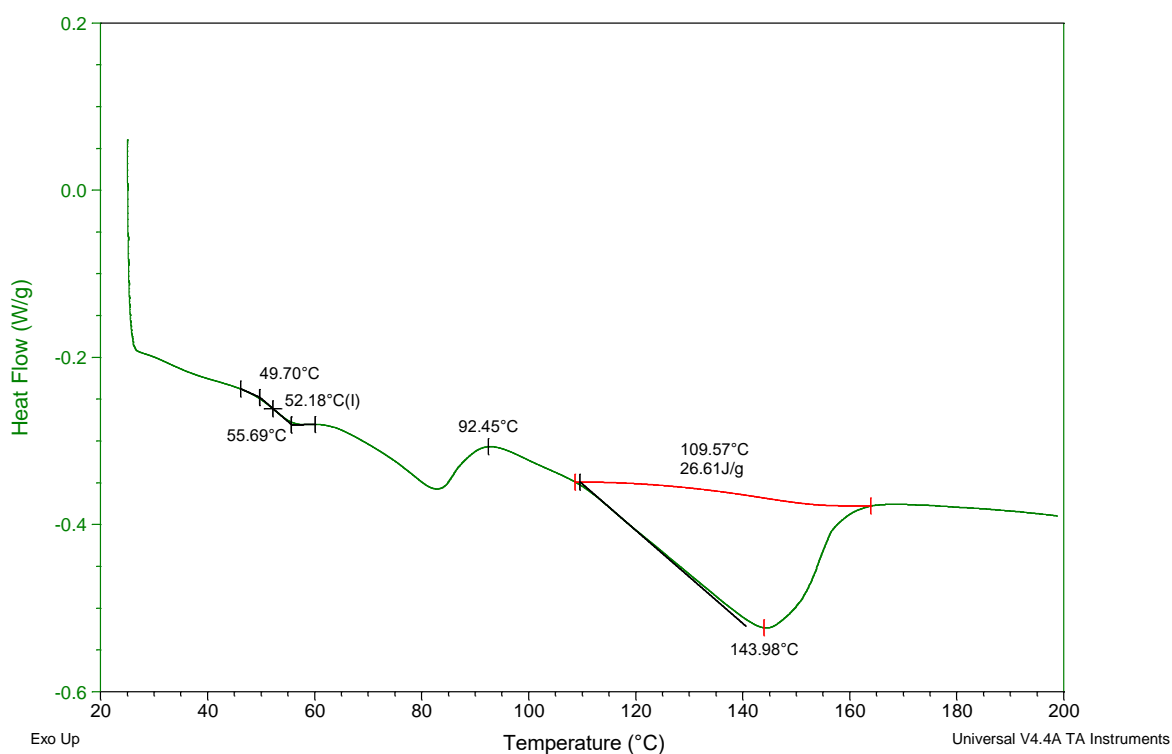


**Table S5.1.** Summary of the chirality of the molecules involved in the simulated ROP processes (column 2 and 3) together with those of the resulting growing polymer chains (column 4). Column 5 corresponds to the DFT-calculated ( $\omega$ B97XD/6-31G\*\*) relative energies (in kcal/mol) of the transition states.

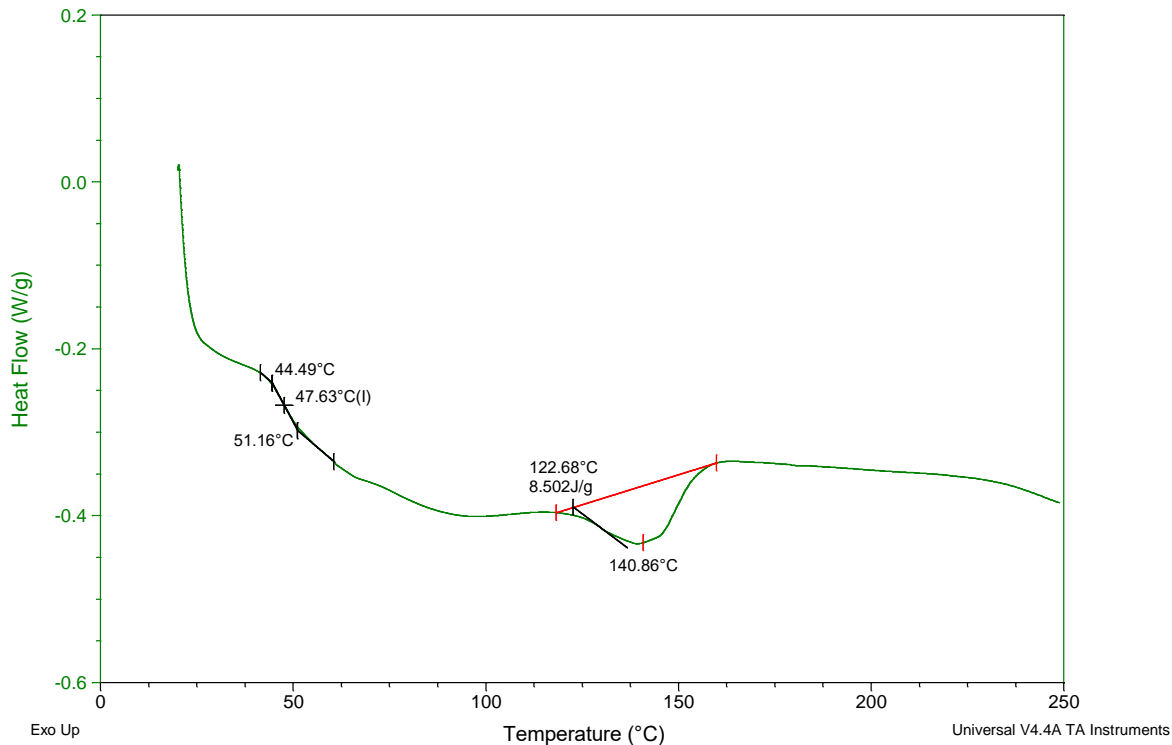
Complex	Alcohol	Meso-LA	Polymer chain	Relative energy of the transition state (kcal/mol)
I	S	(R,S)	S-S-R	-20.7
II	S	(R,S)	S-R-S	-19.7
III	R	(R,S)	R-R-S	17.4
IV	R	(R,S)	R-S-R	18.5



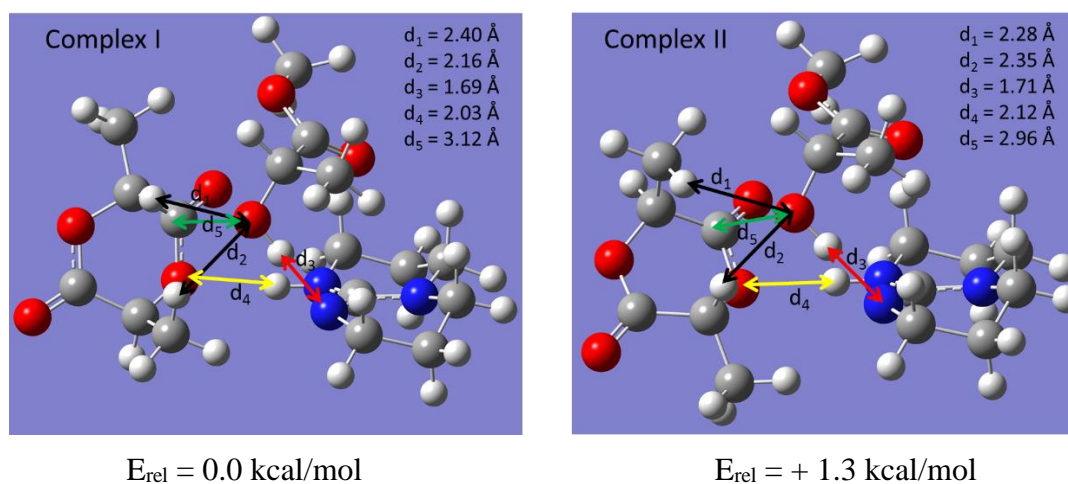
**Figure S5.3.** DSC thermogram of the PLA obtained by TBD at -75 °C (entry 2, Table 5.1)



**Figure S5.4.** DSC thermogram of the PLA obtained by TBD at -75 °C (entry 3, Table 5.1)



**Figure S5.5.** DSC thermogram of the PLA obtained by TBD at -75 °C (entry 4, Table 5.1)



**Figure S5.6.** DFT-calculated ( $\omega$ B97XD/6-31G\*\*) optimized reactant geometries of complex I (left) and complex II (right). The lengths of the H-bonds are listed in  $\text{\AA}$ .

## 5.5. References

- [1] M. Okada, *Prog. Polym. Sci.* **2002**, 27, 87.
- [2] C. M. Thomas, *Chem. Soc. Rev.* **2010**, 39, 165.
- [3] M. J. Stanford, A. P. Dove, *Chem. Soc. Rev.* **2010**, 39, 486.
- [4] P. J. Dijkstra, H. Du, J. Feijen, *Polym. Chem.* **2011**, 2, 520.
- [5] W. N. Ottou, H. Sardon, D. Mecerreyes, J. Vignolle, D. Taton, *Prog. Polym. Sci.* **2016**, 56, 64.
- [6] T. R. Jensen, L. E. Breyfogle, M. a Hillmyer, W. B. Tolman, *Chem. Commun. (Camb).* **2004**, 0135, 2504.
- [7] A. P. Dove, H. Li, R. C. Pratt, B. G. G. Lohmeijer, D. A. Culkin, R. M. Waymouth, J. L. Hedrick, *Chem. Commun.* **2006**, 2881.
- [8] R. C. Pratt, B. G. G. Lohmeijer, D. A. Long, P. N. P. Lundberg, A. P. Dove, H. Li, C. G. Wade, R. M. Waymouth, J. L. Hedrick, *Macromolecules* **2006**, 39, 7863.
- [9] L. Zhang, F. Nederberg, J. M. Messman, R. C. Pratt, J. L. Hedrick, C. G. Wade, *J. Am. Chem. Soc.* **2007**, 129, 12610.
- [10] G. M. Miyake, E. Y. X. Chen, *Macromolecules* **2011**, 44, 4116.
- [11] K. Makiguchi, T. Yamanaka, T. Kakuchi, M. Terada, T. Satoh, *Chem. Commun.* **2014**, 50, 2883.
- [12] J. B. Zhu, E. Y. X. Chen, *J. Am. Chem. Soc.* **2015**, 137, 12506.
- [13] A. Sanchez-Sanchez, I. Rivilla, M. Agirre, A. Basterretxea, A. Etcheberria, A. Veloso, H. Sardon, D. Mecerreyes, F. P. Cossío, *J. Am. Chem. Soc.* **2017**, 139, 4805.
- [14] S. Liu, H. Li, N. Zhao, Z. Li, *ACS Macro Lett.* **2018**, 7, 624.
- [15] B. Orhan, M. J.-L. Tschan, A.-L. Wirotius, A. P. Dove, O. Coulembier, D. Taton, *ACS Macro Lett.* **2018**, 1413.
- [16] R. C. Pratt, B. G. G. Lohmeijer, D. A. Long, P. N. P. Lundberg, A. P. Dove, H. Li, C. G. Wade, R. M. Waymouth, J. L. Hedrick, *Macromolecules* **2006**, 39, 7863.
- [17] B. G. G. Lohmeijer, R. C. Pratt, F. Leibfarth, J. W. Logan, D. A. Long, A. P. Dove, F. Nederberg, J. Choi, C. Wade, R. M. Waymouth, J. L. Hedrick, *Macromolecules* **2006**, 39, 8574.
- [18] R. C. Pratt, B. G. G. Lohmeijer, D. A. Long, R. M. Waymouth, J. L. Hedrick, *J. Am. Chem. Soc.* **2006**, 128, 4556.
- [19] J. Baran, A. Duda, A. Kowalski, R. Szymanski, S. Penczek, *Macromol. Symp.* **1997**, 123, 93.
- [20] Z. Chen, C. Xie, Z. Xu, Y. Wang, H. Zhao, H. Hao, *J. Chem. Eng. Data* **2013**, 58, 143.
- [21] M. Belmares, M. Blanco, W. A. Goddard, R. B. Ross, G. Caldwell, S. H. Chou, J. Pham, P. M. Olofson, C. Thomas, *J. Comput. Chem.* **2004**, 25, 1814.
- [22] HANSEN, CM, *J Paint Technol* **1967**, 39, 511.
- [23] A. Chuma, H. W. Horn, W. C. Swope, R. C. Pratt, L. Zhang, B. G. G. Lohmeijer, C. G. Wade, R. M. Waymouth, J. L. Hedrick, J. E. Rice, *J. Am. Chem. Soc.* **2008**, 130, 6749.
- [24] S. Hoyas, V. Lemaury, Q. Duez, F. Saintmont, E. Halin, J. De Winter, P. Gerbaux, J. Cornil, *Adv. Theory Simulations* **2018**, 1, 1800089.

## **General Conclusion**



As an outstanding alternative to the conventional petroleum-based polymers, the bio-based poly(lactic acid) – or polylactide - (PLA) is one of the most widely used biodegradable and biocompatible polymers in the world. As mentioned throughout this manuscript, the physical properties of PLA make it a viable alternative for highly specialized applications in both pharmaceutical and microelectronics fields. As compared to the traditional and uncontrolled polycondensation of the lactic acid, the ring-opening polymerization (ROP) of lactide (LA, cyclic dimer of the lactic acid) enables a greater level of control over the molecular parameters of the resultant PLA including lower dispersity values, higher molar masses and a high-level of end-group fidelity. One of the other advantages associate to the ROP technics relies on its ability to control the order of insertion of the monomers when conducted in adequate conditions. Due to its unique monomer diversity, a wide range of PLA microstructures can easily be obtained especially from *rac*- or *meso*-LA in the presence of an appropriate chiral or achiral initiators/catalysts. While a variety of active and selective catalysts are available for converting renewable monomers such as LA into well-defined PLAs, data to assess their environmental impacts or sustainability are incomplete. Several attributes of organic catalysts, including their low cost and wide availability, easy removal from polymers, low toxicity, and versatile catalytic mechanisms, make possible a greener and more versatile synthesis of PLA. While metal-based catalysts are in general more competent in tackling the aforementioned challenges, organocatalysts have emerged as an efficient alternative. Surprisingly, the small number of investigated chiral organic small molecules as a stereoselective organocatalyst motivated us to investigate more about them. In the Chapter 2 of this thesis, chiral unimolecular tertiary amine-thiourea catalyst were re-investigated, since the real conducted stereocontrol mechanism was not previously revealed in detail in the state-of-the-art. Both commercially available (*R,R*)- and (*S,S*)-enantiomers of chiral thiourea-amine Takemoto's organocatalysts have been shown to promote efficient control and high isoselectivity at room temperature of the ROP of *rac*-LA. As obtained by a kinetic resolution process, the highly isotactic and semicrystalline PLAs where obtained by a stereocontrol mechanism associating both a chain-end control (CEC) and an enantiomorphous-site control (ESC) processes. Despite some epimerization side reactions, isoselectivity remains high without the need to work at very low temperature. In the presence of concomitant mechanism, the (*R,R*)-TUC organocatalyst preferentially incorporates *L*-LA, whereas the (*S,S*)-catalyst preferentially polymerized the *D*-isomer. The selectivity for one of the other LA enantiomers can thus be switched by changing the configuration of the Takemoto's catalyst.

In the third part of this thesis, novel highly efficient chiral organic *in situ* generated NHC catalysts were investigated for the stereoselective ROP of *rac*-LA. At room temperature, the ROP of *rac*-LA with fast rate has been achieved using *in situ* generated triazolium derivative NHCs by  $K_2CO_3$ . Narrow polymer distributions ( $\bar{D} \sim 1.05$ -1.07) with expected molar mass was achieved and living/control polymerizations were thus confirmed by SEC and  $^1H$  NMR analysis. The structural differences of the NHCs raise the most important effect on their catalytic and stereoselective activity. While less rigid and more stable catalyst structure was showing high catalytic activity, the most sterically hindered ones didn't show any catalytic activity. The semi-crystalline formations of PLAs were confirmed by DSC ( $T_m = 145, 147$  and  $131$  °C). From the structural point of view, NHCs which indicate more stable chiral moiety, was expected to demonstrate higher stereoselectivity, while the stereocontrol was significantly decreased using NHCs with an unstable chiral conformation. To find out the conducted stereocontrol mechanism, kinetic studied were performed. In the light of those investigations, it has been observed that none of the catalysts selectively consumed an enantiopure lactide monomer, and the fastest activation was achieved with the racemic mixture. Thus, the conducted stereocontrol mechanism of NHCs were chain-end activation mechanism. These high performances on catalysis together with the easy *in situ* preparation and stable structures make this protected NHC salt precursors of great potential in practical application. This study expands the use of *in situ* generated NHC catalyst to prepare advanced well-defined polymers.

Although H-bonding (thio)urea catalysts typically suffer from modest activities and limited kinetics, their respective selectivities can be modulated by adjusting their structure and potent acidic behavior. With this idea in mind, in the Chapter 4, corresponding urea counterpart ((*S,S*)-UC) of the chiral unimolecular bifunctional thiourea catalyst investigated in Chapter 2, was studied for the stereoselective ROP of *rac*-LA at various temperatures. We assumed that the stereoselective ROP of *rac*-LA can be achieved with the urea catalyst in which activation is enhanced by increasing basicity, under metal-free conditions and lack of any side reaction risk. As observed, the polymerization time associated to the studied ROPs was found reduced by almost 24 hours, and controlled/living polymerizations were confirmed with the preparation of narrow polymers distribution. As compared to their thiourea congeners, ROPs performed at elevated temperatures with ureas involved low-degree inter-molecular transesterification reactions as monitored by MALDI-ToF analysis. Moreover, as a result of the higher epimerization ratios obtained by (*S,S*)-UC, *meso*-LA was generated during



the ROP process involving stereoerrors in the final PLA material. The semi-crystalline PLA formation at 25 °C was confirmed by both thermal analysis ( $T_m = 138$  °C), and  $^1\text{H}$  { $^1\text{H}$ }NMR analysis ( $P_m = 0.85$ ). Considering the combined kinetic studies and mesotacticity ratios, once again a concomitant mechanism of ESC & CEC was demonstrated.

Finally, it has always been considered that stereoselectivity can only be achieved in the presence of chiral or achiral and sterically hindered catalysts for the ROP of *rac*-LA. However, in the Chapter 5, we investigated achiral and non-sterically hindered organocatalyst, 1,5,7-triazabicyclo-[4.4.0]dec-5-ene (TBD), for the stereoselective ROP of *rac*-LA under cryogenic conditions (at -75 °C). High levels of control with a linear relationship between experimental number-average molar masses ( $M_n$ , SEC) and monomer conversion were obtained with low dispersity values. Isotactic enchainment was confirmed by homonuclear decoupled  $^1\text{H}$  NMR ( $P_m = 0.8 - 0.84$ ) and DSC analysis ( $T_m = 157$  °C). Very interestingly, when applied to the *meso*-LA ROP, heterotactic PLAs were prepared under cryogenic conditions. In accord with the experimental results, DFT investigations conclude that the isoselective ROP of *rac*-LA, under cryogenic conditions, is the result of a game of imbrications toyed between the TBD, the LA isomer and the propagating chain end.

## **Titre: Polymerisations Stéréosélectives par Ouverture de Cycle du Lactide Racémique par Organocatalyse**

**Résumé:** En chimie macromoléculaire, les polymères optiquement actifs, qu'ils soient naturels ou synthétiques, ont fait l'objet de beaucoup d'attention, compte tenu de leurs stéréochimies, du fait que leurs propriétés mécaniques, thermiques et physiques sont fortement affectées par leur stéréorégularité. Parmi ceux-ci, le polylactide (PLA), qui constitue une excellente alternative aux polymères classiques à base de pétrole, est devenu l'un des polymères les plus utilisés, formé à partir de ressources naturelles renouvelables. Il est désormais accepté comme un « polymère d'origine biologique ». En raison de la diversité des structures diastéréoisomères du lactide (LA), de nombreuses chaînes de PLA peuvent être obtenues dans diverses stéréorégularités. Par exemple, des chaînes de PLA isotactiques peuvent être formées à l'aide de *L* ou *D*-LA énantiopures en l'absence de réactions d'épimérisation et montrent une transition vitreuse ( $T_g$ ) à 50 °C et une température de fusion ( $T_m$ ) d'environ 160 à 180 °C. Les propriétés thermiques du PLA peuvent être encore améliorées par la formation de structures de PLA stéréocomplexes à partir de *méso*- et *rac*-LA en présence d'initiateurs/catalyseurs chiraux ou achiraux appropriés dans des conditions appropriées (des conditions cryogéniques peuvent être appliquées) entraînant une augmentation significative de la  $T_m$  autour de 230 - 240 °C. Au cours des deux dernières décennies, de nombreux catalyseurs métalliques ont été signalés dans ce but. Cependant, il n'y a que peu d'organocatalyseurs capables de préparer du PLA stéréorégulier à partir d'une matière première de *rac*-LA. Dans cette thèse, nous avons étudié la (thio) urée organique chirale, les dérivés de carbène *N*-hétérocycliques et le dérivé de guanidine 1,5,7-triazabicyclo [4.4.0] déc-5-ène (TBD) en tant qu'organocatalyseurs pour la ROP stéréosélective *rac*-LA. Les activations catalytiques, les propriétés stéréosélectivités et les mécanismes de stéréocontrôle de ces catalyseurs ont été étudiés. Dans chaque cas, des isosélectivités élevées ont été favorisées même à des températures élevées, ce qui a été prouvé par RMN  $^1\text{H}$  homonucléaire, RMN  $^{13}\text{C}$  quantitative, analyse thermique et études cinétiques.

**Mots clés:** [stéréosélective, lactide, organocatalyse, polymérisation par ouverture de cycle]

---

## **Title: Stereoselective Ring-Opening Polymerizations of Racemic Lactide by Organocatalysis**

**Abstract:** In macromolecular chemistry, both naturally occurring and synthetic, optically active polymers have received great deal of attention considering their stereochemistries due to the fact that their mechanical, thermal and physical properties are strongly affected by their stereoregularity. Among them, polylactide (PLA) as an outstanding alternative to the conventional petroleum-based polymers, has become one of the most widely used polymers, which is formed by renewable natural resources are now being accepted as “bio-based polymer”. Due to the variety of diastereomeric structures of lactide (LA), numerous of PLA chains can be obtained in diverse stereoregularities. As an example, isotactic PLA chains can be formed using enantiopure *L*- or *D*-LA, and show glass transition ( $T_g$ ) at 50 °C, melting temperature ( $T_m$ ) at 160-180 °C. The thermal properties of the PLA can be further enhanced by the formation of stereocomplex PLA from *meso*- or *rac*-LA in the presence of appropriate chiral or achiral initiators/catalysts under appropriate conditions, which displays a significantly increased  $T_m$  around 230–240 °C. Many metal catalysts have been reported to this end. However, there are only few organocatalysts able to prepare stereoregular PLA from *rac*-LA. In this thesis, we studied chiral organic (thio)urea, *N*-heterocyclic carben derivatives, and 1,5,7-triazabicyclo-[4.4.0]dec-5-ene (TBD) organocatalysts for stereoselective ROP of *rac*-LA. Catalytic activations, stereoselectivity properties and stereocontrol mechanisms of these catalysts were investigated. In each case, high isoselectivities were promoted even sometimes at high temperatures, proved by homonuclear decoupled  $^1\text{H}$  NMR, quantitative  $^{13}\text{C}$  NMR, thermal analysis and kinetic studies.

**Keywords:** Stereoselective, lactide, organocatalysis, ring-opening polymerization

---

**Laboratoire de Chimie des Polymères Organiques, UMR 5629**

[16 avenue Pey Berland, 33607 Pessac Cedex, FRANCE]

**Laboratory of Polymeric and Composite Materials**

[23 Avenue Maistriau, 7000 Mons – BELGIUM]